Molecular determinants of alpha-synuclein pathogenicity in Parkinson's Disease

Emily Elizabeth Prescott

Sheffield Institute for Translational Neuroscience

The University of Sheffield

Thesis submitted for the degree of Doctor of Philosophy (PhD)

August 2024

Abstract

Parkinson's Disease is the second most common neurodegenerative disorder currently affecting 6 million people worldwide. While remarkable progress has been made in understanding the molecular basis of Parkinson's Disease, there remains a critical need for the development new therapeutics to alleviate the significant socio-economic burden it imposes. The main hallmark of the disease is the presence of aggregated alpha-synuclein in Lewy body deposits in the central nervous system, accompanied by the death of dopaminergic neurons, resulting in debilitating motor symptoms. The early stages of alpha-synuclein aggregation are not yet fully understood, but it is known that the aggregation of alpha-synuclein and related dysfunctions can occur up to 10 years before symptoms appear. By the time symptoms emerge, it is estimated that between 50-70% of dopaminergic neurons have already been lost, making the development of effective therapeutics particularly challenging. Therefore, detection of the pathogenic αSyn species in the prodromal stages of disease and how they induce dysfunctions could prove critical in the development of early diagnostic tests and more effective disease modifying therapeutics.

This thesis aims to investigate the early dysfunctions induced by alpha-synuclein within cells derived from patients with Parkinson's Disease, in attempt to elucidate the pathogenic mechanisms occurring in both familial and sporadic cases. By combining patient-derived cellular models with high-resolution single-molecule imaging techniques, I identified and characterised pathogenic alpha-synuclein and determined its role in promoting disease. I showed the spontaneous formation of disease specific Lewy body species containing wild-type and phosphorylated alpha-synuclein within the patient cell lines, their presence is largely heterogeneous among Parkinson's Disease patients; with some cell lines exhibiting significantly higher levels of Lewy body-like aggregates, whilst other cell lines show no significant difference compared to healthy controls. However, one phenotype that unifies both familial and sporadic cases of Parkinson's Disease is the elevated levels of extracellular phosphorylated alpha-synuclein. Further probing of these toxic species of alpha-synuclein within the cell media has provided a deeper understanding of how specific compositions and conformations of the alpha-synuclein including both fibrils and oligomers contribute to mitochondrial dysfunction, Lewy body formation, and thus accelerate disease progression. Using this disease specific model, I have investigated the mechanism of alpha-synuclein

aggregation in the disease progression. This data demonstrates that inhibiting a specific microscopic pathway of alpha-synuclein aggregation, specifically the secondary nucleation process, using a chaperone known as BRICHOS R221E, is sufficient to alleviate alpha-synuclein associated pathogenicity in patient-derived cellular models.

In conclusion, this thesis reveals a complex interplay between the composition – wild-type and phosphorylated alpha-synuclein – and the conformation among monomers, oligomers, and fibrils in the pathogenesis of Parkinson's Disease. I have identified how different isoforms of alpha-synuclein induce cellular dysfunctions associated with Parkinson's Disease in patient-derived cellular models and demonstrated these dysfunctions can be inhibited by mechanistically targeting the aggregation pathway. These findings provide a platform for advancing early diagnostic tests to detect specific pathogenic species of alpha-synuclein in human samples, and for developing disease-modifying therapeutics that specifically target their formation.

Dedication

This thesis is dedicated to my Grandad, Eric Ashworth, who suffered with Parkinson's Disease and sadly passed away in July 2023. Your unwavering interest in my research has been a tremendous source of motivation for me.

Acknowledgements

Firstly, I would like to acknowledge and thank the healthy volunteers and patients with Parkinson's Disease who donated skin biopsies. Without your donation this project would not have been possible.

A huge thank you goes to my primary supervisor Dr Suman De, for sharing your immense knowledge with me, your wealth of creative ideas, enthusiasm in the project, and constant belief in me. Thank you to my second supervisor, Professor Heather Mortiboys, for your interest in the project and providing many insightful meetings, your help and advice means a lot to me. Both of your endless support and guidance has contributed to a great research project and allowed me to gain confidence and become a better scientist.

I would like to acknowledge my fellow lab members, Aga, Hollie, and Emma. I am grateful for our chats, both science and non-science related, it has been a pleasure to work alongside you. To Iris, my work bestie. I am lucky to have made such a wonderful friend during my PhD. I will miss our lunch breaks and office chats! Thank you to the SITraN ladies 5-aside, it has been a much-needed relief to play football with you all every Monday evening!

I would like to express my appreciation to several members of the Mortiboys lab who have assisted me in my PhD. Lizzie, for taking the time to teach me iNPC and iDNL culture. Francesco, for all your help with the mitochondrial dysfunction assays, culturing the LRRK2 lines and the SNCA knockdown – your help has been invaluable in this project. To Alex, Niko, and Louise, thank you for your help with culturing Parkin lines and fibroblasts.

I could not have done this without the continuous support of my best friends; Lauren, Aleysha, Georgia, and Eve. Thank you for always listening to me rant, and making sure I still had some fun in my life when work was all consuming!

To my family, I am so grateful for all your love and support. To my mum, for always believing in me and offering kind words of wisdom whenever I needed it. To my dad, for always pushing me to never give up, and reminding me I can do it whenever I doubted myself. I hope I have done you all proud. Finally, to Andre. For being the first friendly face I met at SITraN, and then becoming so much more. Thank you for being my shoulder to cry on in tough times and for making me laugh and smile when I'm stressed out. There is no one I would rather share the ups and downs of a PhD with.

Table of Contents

List of Figures

List of Tables

List of Abbreviations

AD	Alzheimer's Disease
ALS	Amyotrophic Lateral Sclerosis
APS	Ammonium persulphate
APTES	3-Aminopropyltriethoxysilane
Aβ	Amyloid-beta
BCA	Bicinchoninic acid
BDNF	Brain derived neurotrophic factor
BSA	Bovine serum albumin
CL	Cardiolipin
CNS	Central nervous system
CSF	Cerebrospinal fluid
DAPT	N-[N-(3,5-difluorophenacetyl)-l-alanyl]-S-phenylglycine t-butyl ester
DAT	Dopamine transporter
DAT-SPECT	Dopamine transporter single photon emission computed tomography
d-cAMP	d-cyclic adenosine monophosphate
DLB	Dementia with Lewy Bodies
DTT	Dithiothreitol
EDTA	Ethylenediaminetetraacetic acid
EGTA	Ethylene glycol tetraacetic acid
ELISA	Enzyme-linked immunosorbent assay
FGF	Fibroblast growth factor
GDNF	Glial cell line derived neurotrophic factor
HCl	Hydrochloric acid
iDNLs	Induced dopaminergic neuron like cells
IDP	Intrinisically disordered protein
iNPCs	Induced neuronal progenitor cells
iPSCs	Induced pluripotent stem cells
LAMP1	Lysosomal-associated membrane protein 1
LAMP2	Lysosomal-associated membrane protein 2
MAO B	Monoamine oxidase B
MAPS	Misfolding-associated protein secretions
MDS	Movement Disorder Society
MEM	Phenol Red Free Minimum Essential Media
MOI	Multiplicity of infection
MSA	Multiple System Atrophy
NAC	Non amyloid β component
PAGE	Polyacrylamide Gel Electrophoresis
PBS	Phosphate Buffered Saline
PBST	Phosphate Buffered Saline with Tween 20

PD	Parkinson's Disease
PDD	Parkinson's Disease Dementia
PEG	Polyethylene glycol
PFF	Preformed fibril
PLK3	Polo Like Kinase 3
PMCA	Protein misfolding cyclic amplification
PPMI	Parkinson's Progression Markers Initiative
pSer129	Phoshorylated serine 129
p-αSyn	Phosphorylated alpha-synuclein
rAAV	Recombinant adeno-associated viral vector
RBD	REM sleep behaviour disorder
REM	Rapid eye movement
ROS	Reactive oxygen species
RT-QuIC	Real-time quaking induced conversion
SAA	Seed amplification assay
SAG	Smoothened agonist
SD	Standard deviation
SDS	Sodium Dodecyl Sulphate
SiMPull	Single molecule pulldown
SNARE	Soluble N-ethymaleimide-sensitive factor attachment protein receptor
sPD	Sporadic Parkinson's Disease
TBST	Tris Buffered Saline with Tween 20
TDP43	TAR DNA-binding protein 43
TEMED	Tetramethylethyl Enediamine
TGF	Transforming growth factor
TH	Tyrosine hydroxylase
ThT	Thioflavin T
TIRF	Total internal reflection fluorescence
TMRM	Tetramethylrhodamine, methyl ester
TOM20	Translocase of outer mitochondrial membrane 20
Tuj1	Beta-III tubulin
UPDRS	Unified Parkinson's Disease Rating Scale
VDAC1	Voltage dependent anion channel 1
VTA	Ventral Tegmental Area
WT	Wildtype
αSyn	Alpha-synuclein
βSyn	Beta-synuclein
γSyn	Gamma-synuclein

Chapter 1: Introduction

1.1. Protein deposition in neurodegenerative disease

1.1.1 Protein folding and misfolding.

Proteins are the basic building blocks of cells. Proteins are synthesised through a process of transcription and translation to form a polypeptide, and correct folding of the polypeptide chain into its native structure is crucial for the normal functioning of the protein (Alberts *et al.*, 2002; Hoerter and Ellis, 2023). The process of protein folding can be explained by the Gibbs free energy landscape model (Figure 1.1). This model outlines the journey of an unfolded polypeptide chain into a natively folded protein. At high energy states the unfolded polypeptide chain can adopt various conformations, as intramolecular contacts within the protein are increased there is a decrease in free energy and the protein adopts stable low energy state when a native structure is formed (Adamcik and Mezzenga, 2018).

Although this explains the simple protein folding process, in the case of intrinsically disordered proteins (IDP's) this process is much more complex. As IDP's are highly flexible and lack a fixed tertiary structure, they will form various weakly bound partially folded states and fluctuate from different conformations, causing shallow dips in the energy landscape (Strodel, 2021). Intermolecular interactions between partially folded states leads to the formation of amorphous aggregates and amyloid fibrils which are kinetically trapped at a low energy state. This leads to the generation of a rugged energy landscape for IDP's, compared to a smooth energy landscape for native proteins (Mukhtar 2016).

Making up around 33% of the human proteome, IDP's are essential for normal cellular functioning (Ward et al., 2004). They have a unique ability to adopt different conformations depending on their environment, which allows them to carry out distinct biological functions. They have many essential functions within the cell including binding motifs for cell signalling and transcription processes, with high specificity and low affinity, such as alpha-synuclein's (αSyn) 'KTKEGV' membrane binding motif (Zarbiv et al., 2014). However, due to changes in pH, ionic strength, or mutations, IDP's may adopt a partially folded structure that has a higher aggregation propensity (Lindsay et al., 2021). This is supported by the fact that many IDP's are deposited in human tissue in different diseases and cause dysfunctions. These diseases are commonly known as proteinopathies. Neurodegenerative diseases like Alzheimer's Disease (AD), Parkinson's Disease (PD) and Amyotrophic Lateral Sclerosis (ALS) are proteinopathies.

In AD accumulation of amyloid-beta (Aβ) and Tau are commonly observed in patient's brains, whereas αSyn and TDP43 are commonly found in PD and ALS patients central nervous system (CNS), respectively (Uversky, 2015).

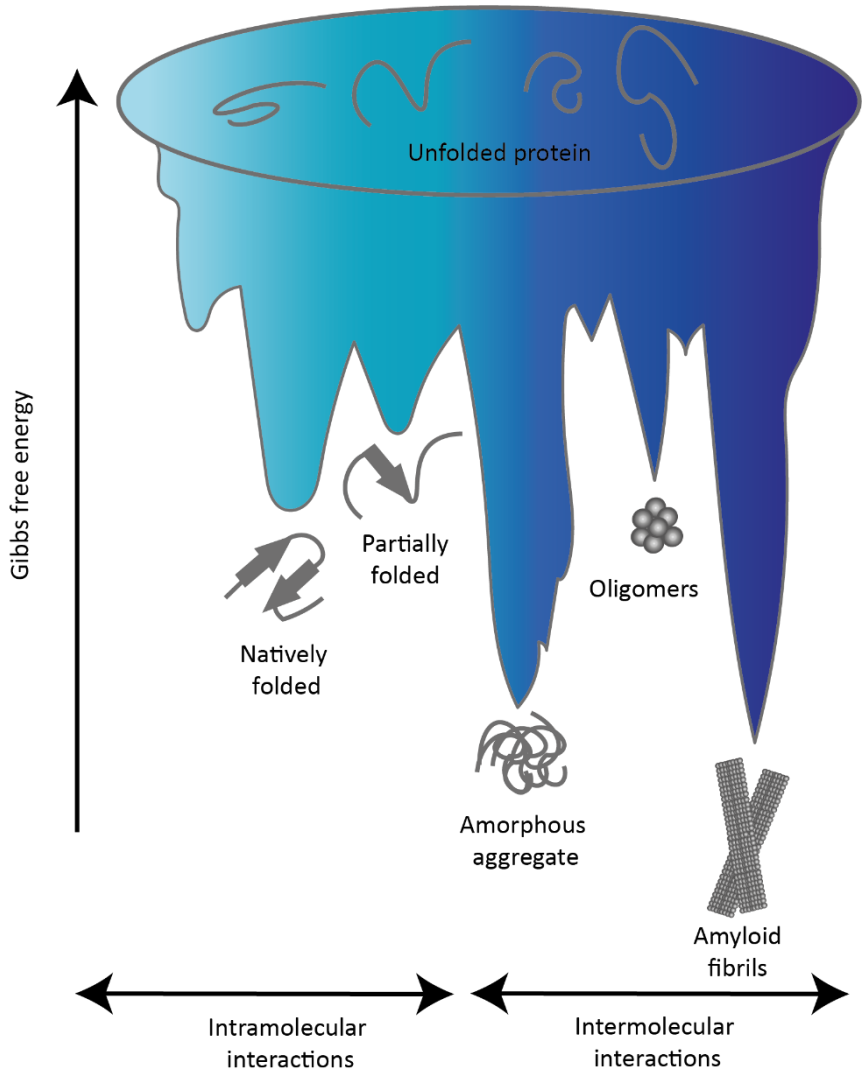

Figure 1.1. Gibbs free energy landscape of protein folding. Intramolecular contacts allow proteins to adopt an energetically favourable partially folded state on their journey to forming a natively folded protein. Intermolecular contacts between different misfolded proteins form kinetically trapped amorphous aggregates and amyloid fibrils with low free energy. Adapted from (Muntau et al., 2014).

1.1.2. Protein aggregation and amyloid formation

Protein deposition is a major hallmark of neurodegenerative diseases, with the gold-standard diagnosis being detection of deposits in postmortem tissue (Baldacci et al., 2020). Protein deposition occurs through a long process of protein misfolding and aggregation. Protein aggregation is a multi-step process, in which monomeric protein misfolds and is then

converted into a highly heterogeneous mixture of higher-order assemblies including oligomers, amorphous aggregates, and fibrils (Figure 1.2). This is a complex process occurring in more than thirty human diseases (Chiti and Dobson, 2017). Protein aggregation begins with a thermodynamically unfavourable conversion of monomeric protein into nuclei, this is known as the lag phase (Wood et al., 1999). Nuclei can then recruit additional monomeric protein to form larger aggregates known as oligomers (Michaels et al., 2020). Subsequently, the rapid exponential growth phase occurs; oligomers may be on-pathway and extend to form protofibrils, or they may lack the ability to elongate and become off-pathway oligomers (Dear et al., 2020). Mature fibrils containing a high level of beta-sheets are formed when many protofibrils are assembled (Khurana et al., 2003). These mature amyloid fibrils get deposited into insoluble amyloid deposits. These amyloid fibril deposits are the major hallmark of many neurodegenerative diseases, and each disease is generally associated with the deposition of one or more proteins. In Alzheimer's Disease Aβ and Tau are deposited, in Parkinson's Disease the main component of Lewy bodies is αSyn, and in Amyotrophic Lateral Sclerosis there are TDP-43 deposits present (Figure 1.2) (Ross and Poirier, 2004).

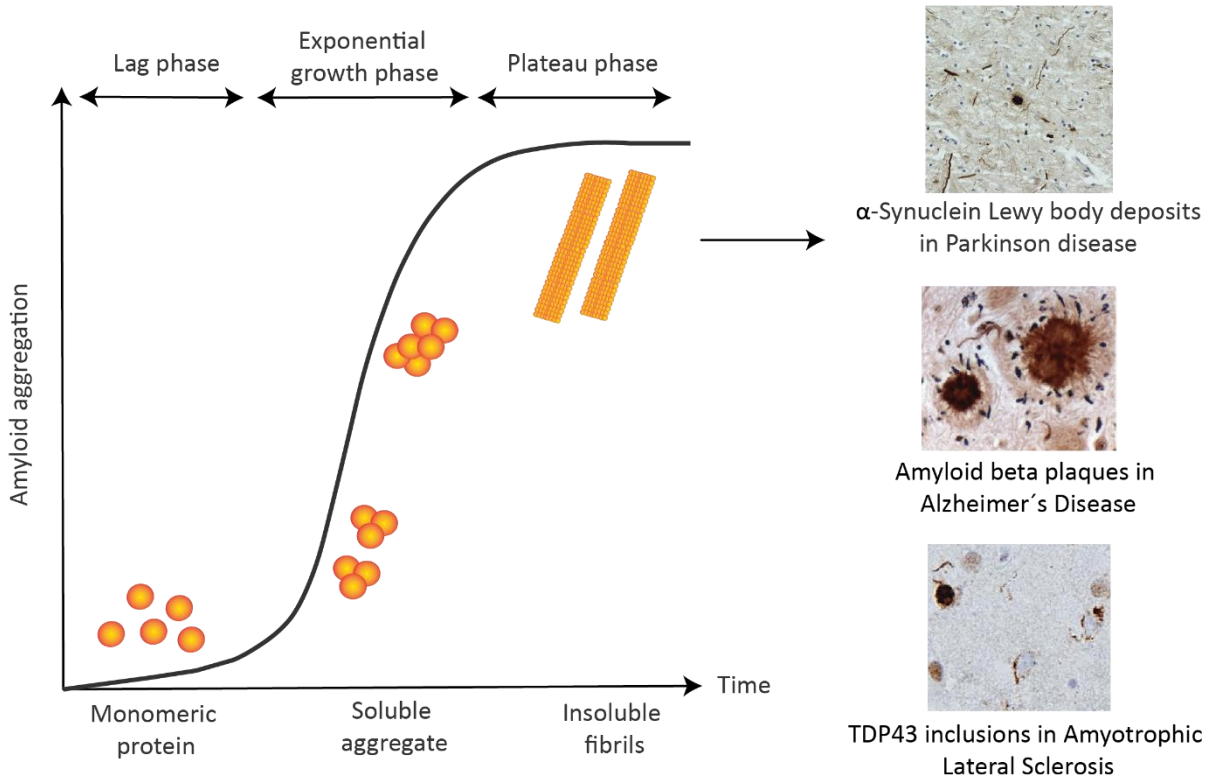

Figure 1.2. Protein aggregation occurs in a multistep process. Schematic of the formation of amyloid deposits from monomeric protein. Monomeric protein forms nuclei within the lag phase of

aggregation reactions, these soluble aggregates are then elongated into larger oligomers and protofibrils in the exponential growth phase. Assembly of protofibrils forms mature fibrils. These insoluble fibrils are the main component of insoluble deposits found in patients CNS, such as αSyn in Lewy Bodies in Parkinson's Disease, amyloid-beta in Alzheimer's Disease, and TDP43 inclusions in Amyotrophic Lateral Sclerosis. PD histopathology was performed in our lab, AD and ALS images taken from (Kumfor, Halliday and Piguet, 2017) and (Cykowski et al., 2017).

This simple three-step outline of aggregation is limiting to the complexities of the aggregation process, there are many additional secondary mechanisms occurring concurrently (Cohen et al., 2012). The process of secondary nucleation was outlined by the addition of fibril seeds to monomeric proteins which led to a change in the aggregation kinetics where the slow primary nucleation phase was shortened or bypassed (Figure 1.3) (Cohen et al., 2013). To understand how the aggregates were forming from the addition of fibrils, an experiment with radioisotope labelled Aβ42 fibrils was performed, when radio-labelled fibrils were incubated with unlabelled monomeric protein, the oligomers and fibrils that formed were not radiolabelled, and therefore not formed due to elongation or fragmentation of existing fibrils (Cohen et al., 2013). As a result, the process of secondary nucleation was uncovered where the monomeric protein is recruited to the fibril surface to form new nuclei, which can aggregate into new oligomeric species and fibrils (Figure 1.3). The fibrils formed through secondary nucleation maintain the structure of the original fibril seed population (Zimmermann et al., 2022). Secondary nucleation has been found to dominate the process of aggregation of αSyn at mildly acidic pH but not at neutral pH, likely due to pH affecting the conformation of intrinsically disordered αSyn (Gaspar et al., 2021).

In addition to secondary nucleation, another secondary process known as fragmentation can also generate new aggregates (Figure 1.3). Fibrils formed in the aggregation pathway can be broken apart to generate a higher number of smaller ´seeds´. This shortens the length of fibrils and provides a higher number of fibrils, leading to increased fibril extension sites, providing a surface for monomeric protein to attach and elongate into longer fibrils (Xue et al., 2009; Cohen et al., 2012). This process continues and allows exponential growth of the amyloid fibrils. Other external factors can influence the rate of aggregation, for example, αSyn primary nucleation happens at an extremely slow rate in quiescent conditions but the addition of agitation lipid membranes, or glass beads act as a catalyst to increase the rate of primary nucleation and speed up aggregation (Galvagnion et al., 2015; Zhou et al., 2020). Additionally, the pH of solution

has a huge effect on aggregation, αSyn aggregates much faster at pHs lower than 6.0 where secondary nucleation dominates, whereas Aβ remains most aggregation prone at pH 6.0 – 8.0 (Khandogin and Brooks, 2007; Buell et al., 2014; Kobayashi et al., 2015).

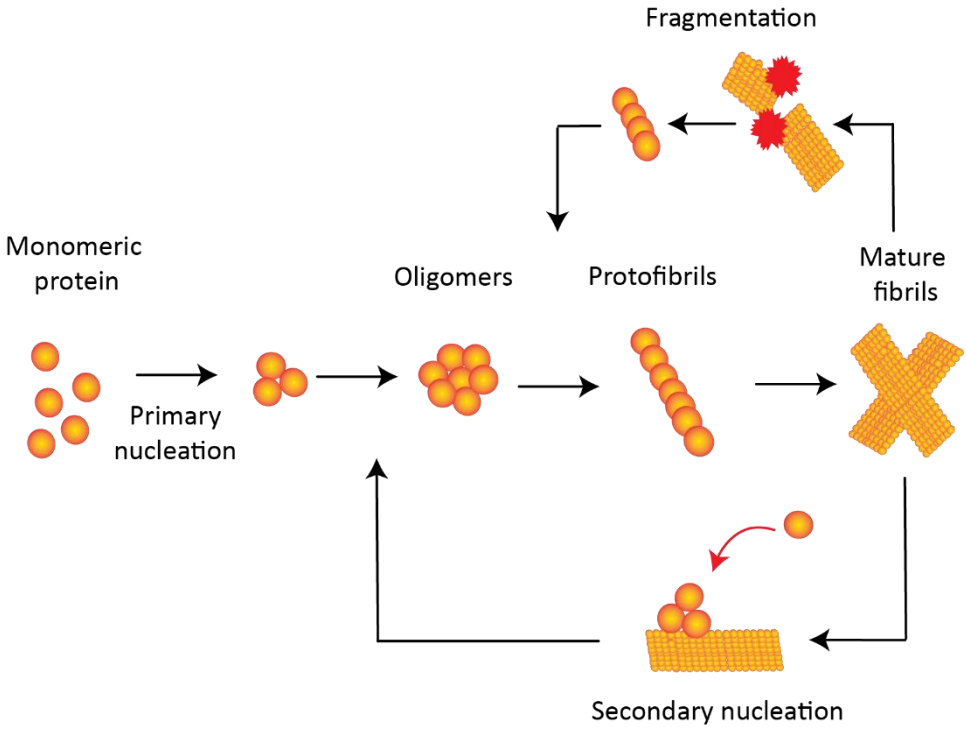

Figure 1.3. Schematic of the secondary processes occurring in aggregation. Schematic depicting how secondary processes of aggregation occur. Secondary nucleation involves fibrils providing a surface for nucleation events and aggregate formation, which occurs at a faster rate than primary nucleation. Fibrils also exponentially increase during fibril fragmentation into smaller species.

1.2. Parkinson's Disease

1.2.1. Epidemiology of Parkinson's Disease

Parkinson's Disease is the second most common neurodegenerative disorder after Alzheimer's Disease, affecting 6 million people worldwide and this is expected to double to 12 million people by 2040 (Dorsey and Bloem, 2018). The disease affects 1% of the population aged 60 and over (Zafar and Yaddanapudi, 2023). The prevalence of PD is higher in men than women, with rates being 1.5 times higher for men aged 50-89 than women (Wooten et al., 2004).

A study into 204 countries between 1990 and 2019 found most countries were experiencing an increase in prevalence e.g., in high income countries such as the United States, Germany

and Norway (Ou *et al.*, 2021). This could be correlated to the growing industrialisation and increased exposure to environmental hazards, but it could also be explained by better access to health care and diagnosis (Vlaar *et al.*, 2018). However, in Italy and Spain a decreasing prevalence is observed, which may be correlated with increased longevity due to a Mediterranean diet (Pérez-López *et al.*, 2009). The largest factor is the growing increase in population and ageing, as patients are living longer with PD this causes an increase in the prevalence. In 1967 average life expectancy for a patient with PD was 10 years, this figure has increased by 55% to 14.5 years from disease onset. Although PD increases the risk of mortality compared to the general population, PD is not typically the underlying cause of death, with most patients suffering from pneumonia or cardiac related deaths (Hobson and Meara, 2018).

There is currently no cure for PD, and with the increasing prevalence it brings a huge economic and social burden on society. The estimated cost of PD in the US is expected to increase from $51.9 billion in 2017 to $79.1 billion in 2037 (Yang *et al.*, 2020). The social burden on both patients suffering with PD and their families is ever-increasing, families often suffering loss of earnings to become full-time care givers, and the expense of implementing specialised equipment and furniture in the home (Whetten-Goldstein *et al.*, 1997).

1.2.2. Clinical symptoms of Parkinson´s Disease

Parkinson's Disease is a progressive neurodegenerative disease characterised by the loss of dopaminergic neurons in the substantia nigra and the presence of Lewy Body plaques in the brain (Beitz, 2014). The result of the loss of dopaminergic neurons is a depletion in total dopamine levels, which is shown to lead to several movement deficiencies associated with PD (Meder *et al.*, 2019).

A huge plethora of clinical symptoms are associated with PD, the main symptoms are slow movement known as bradykinesia, resting tremor, and rigidity (Jankovic, 2008). Postural instability is another common motor symptom of PD which usually manifests in the late stages of disease and has the most impact on patients' day to day living as it causes falls and is responsible for a large amount of healthcare costs due to emergency visits (Palakurthi and Preetham Burugupally, 2019). Patients sometimes also experience a wide range of additional non-motor symptoms including depression, insomnia, rapid eye movement (REM) sleep behaviour disorder (RBD), loss of smell (hyposmia) and constipation. Hyposmia affects up to 95% of individuals with PD and is thought to be one of the earliest signs of disease, occurring

up to 10 years before motor symptoms (Haehner *et al.*, 2009). Additionally, around 38% of RBD patients will develop Parkinsonism within 12 years after RBD diagnosis (Schenck, Bundlie and Mahowald, 1996).

The development of dementia in PD patients or Parkinson's Disease Dementia (PDD) is higher than the general population, around 80% of patients living with PD for over 10 years develop cognitive decline (Aarsland *et al.*, 2003). Individuals with a later age of onset of PD have an increased risk of developing dementia, and the presence of hallucinations and language deficits were also a good predictor for the development of dementia (Hobson and Meara, 2004).

1.2.3. Pathogenesis of Parkinson´s Disease

The causes of dopaminergic neuron death in PD are not fully understood. The pathological hallmark of PD is the presence of abnormal cytoplasmic deposits within neurons known as Lewy Bodies (Gibb and Lees, 1988). Lewy Bodies are generally spherical in shape and located within cell bodies. One of the main components of Lewy Bodies is the protein αSyn, but they also contain various other proteins such as ubiquitin and p62 and are surrounded by lipids and organelles such as mitochondria and lysosomes (Spillantini *et al.*, 1997; Shahmoradian *et al.*, 2019). The presence of Lewy neurites is also identifiable in PD postmortem tissue, which are deposits in diseased neurites containing αSyn and similar components as Lewy Bodies (Braak *et al.*, 1999).

It is not fully understood why specific neuronal cells are more susceptible to damage and death in PD. αSyn is expressed in various cell types within the brain and is highly expressed in areas of the brain affected in PD, for example the olfactory bulb and substantia nigra (Taguchi *et al.*, 2016; Geertsma *et al.*, 2024). However, there is higher expression of αSyn in the ventral tegmental area (VTA), where PD pathology is less observed (Taguchi *et al.*, 2019). Selective vulnerability of dopaminergic neurons in the substantia nigra of PD patients is likely due to a combination of differentially expressed genes compared to dopaminergic neurons in other midbrain areas e.g. (VTA) which are more resistant to degeneration (Brichta and Greengard, 2014).

1.2.4. Genetics of Parkinson´s Disease

Parkinson's Disease is a complex disorder caused by both genetic and environmental influences. Most cases of PD are sporadic (90%) but a relatively smaller number of cases are familial due to inheritance of genetic mutations (10%) (Corti, Lesage and Brice, 2011). The most common genetic causes of monogenic PD are outlined in Table 1.1.

The first identified genetic cause of PD was SNCA, the gene encoding the protein αSyn, and mutations in this gene are linked to early onset PD (Polymeropoulos *et al.*, 1997). The mutation A53T in SNCA was first identified, and since then four other major pathogenic point mutations have been found including A30P, E46K, H50Q and G51D (Krüger *et al.*, 1998; Zarranz *et al.*, 2004; Appel-Cresswell *et al.*, 2013; Lesage *et al.*, 2013). Additionally, gene multiplications of SNCA have been found to be more common than missense mutations (Lesage *et al.*, 2020). Both duplications and triplications were observed across several different families, with triplications causing a more severe phenotype (Olgiati *et al.*, 2015). These findings uncovered the importance of αSyn levels in the development of PD, and the severity of PD correlating with SNCA gene dosage.

The most common known genetic cause of PD is LRRK2, with the most common mutation G2019S accounting for around 4-5% of patients with familial PD and is associated with late onset PD (Brighina *et al.*, 2019). The prevalence of G2019S varies across the globe, causing up to 40% of familial PD cases in North African Arab communities whereas this mutation has not been observed in Asian populations (Lesage *et al.*, 2006; Hu *et al.*, 2011). LRRK2 encodes the leucine rich repeat kinase 2 or PARK8, a large kinase with various domains for several different functions, and the G2019S mutation is responsible for increased kinase activity in PD (West *et al.*, 2005).

Genetic causes of autosomal recessive forms of PD include mutations in the genes PRKN and PINK1. Mutations in the Parkin gene PRKN is the most common genetic cause of early onset PD, a large cohort study found mutations were detected in 67% cases where age of onset was below 20 years, this decreased to only 7% of cases with age of onset after 29 years (Periquet *et al.*, 2003). Interestingly, PARKIN R42P:Exon 3 deletion compound heterozygous patients exhibit benign motor deficits, and present with more severe non-motor symptoms including Parkinson's Disease Dementia and autonomic dysfunctions (Menon et al., 2024).

Mutations in PINK1 which encodes PTEN-induced putative kinase 1 are also associated with early onset PD (Valente *et al.*, 2004). PRKN and PINK1 are known to function in combination in mitochondrial quality control pathways, where PINK1 accumulates on damaged mitochondria and provides a signal for Parkin to target and ubiquitinate the damaged mitochondria for degradation (Pickrell and Youle, 2015). Dysregulation of mitochondrial function has been largely attributed to PD in SNCA, LRRK2, PRKN, PINK1 and sporadic cases (Hattori and Mizuno, 2015).

Sporadic cases account for the majority of all PD cases worldwide, but cases remain extremely heterogeneous. Sporadic PD presents clinically similar to many familial PD cases, and therefore it is likely similar pathogenic mechanisms are occurring. Genome wide association studies into sporadic cases of PD have found common genetic causes including SNCA and LRRK2 (Chai and Lim, 2013). In addition, variations in the SNCA promotor region Rep1 have been established as a causal factor of sporadic PD (Maraganore *et al.*, 2006).

Table 1.1. Genes associated with monogenic Parkinson's Disease. Data taken from (Salles, Tirapegui and Chaná-Cuevas, 2024) and (Day and Mullin, 2021).

Gene	Full name	Inheritance	Function
SNCA	αSynuclein	Dominant	Encodes αSyn
PRKN	Parkin E3 ubiquitin ligase	Recessive	Mitochondrial
PINK1	PTEN-induced kinase 1	Recessive	Mitochondrial
DJ-1	Protein deglycase DJ-1	Recessive	Mitochondrial
LRRK2	Leucine-rich repeat kinase 2	Dominant	Lysosomal, mitochondrial, microtubule
ATP13A2	ATPase 13A2	Recessive	Lysosomal
PLA2G6	Phospholipase A2 group VI	Recessive	Cell membrane
FBXO7	F-box protein 7	Recessive	Mitochondrial
VPS35	VPS35 retromer complex component	Dominant	Endosomal trafficking
DNAJC6	DnaJ heat shock protein family member C6	Recessive	Synaptic vesicle formation and trafficking

SYNJ1	Synaptojanin 1	Recessive	Synaptic vesicle formation and trafficking
VPS13C	Vacuolar protein sorting 13 homolog C	Recessive	Mitochondrial
GBA	Beta-glucocerebrosidase	Dominant	Lysosomal

1.3. Alpha synuclein

1.3.1. Structure of alpha-synuclein

αSyn is an intrinsically disordered protein that lacks a stable secondary structure but can adopt various conformations e.g., an alpha-helical structure in the presence of lipid membranes, and β-sheet structure which is prone to aggregation (Bisi *et al.*, 2021). The protein is composed of 140 amino acids with an N-terminal amphipathic region (residues 1-60) which has an important role in lipid membrane binding, a central non-amyloid-β component (NAC) region (residues 61-95) which is hydrophobic and involved in αSyn aggregation, and a highly disordered acidic C-terminal (residues 96-140) (Figure 1.4) (Gallardo, Escalona-Noguero and Sot, 2020).

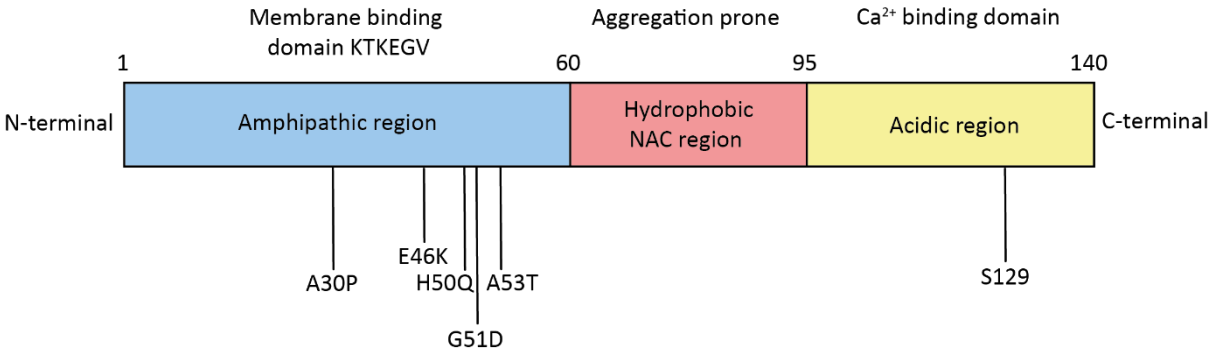

Figure 1.4. Schematic representation of the structure of αSyn. αSyn is an 140 amino acid protein. αSyn has an amphipathic region from residues 1-60 (blue) containing KTKEGV repeats responsible for membrane binding, the amphipathic region also contains the familial PD mutations; A30P, E46K, H50Q, G51D, A53T. Residues 61-95 represent a central hydrophobic NAC region which is aggregation prone (red). Residues 96-140 form an acidic region responsible for calcium binding, and contains serine 129, phosphorylation of serine 129 is associated with PD (yellow).

The native structure of αSyn has caused much controversy within the scientific research field. It has been widely accepted that αSyn exists in the human brain as an unfolded monomer lacking a stable tertiary structure, however some recent publications have challenged this long-standing belief and proposed that αSyn monomer adopts an alpha helical structure and folds as a tetramer (Weinreb *et al.*, 1996; Bartels, Choi and Selkoe, 2011). Despite this

disagreement, it is widely accepted that αSyn can exist in many different structures and conformations depending on the local environment. Many factors including post-translational modifications, pH, interactions with membranes, and protein-protein interactions can influence the intramolecular interactions and alter the conformation of αSyn (Stephens, Zacharopoulou and Kaminski Schierle, 2019).

1.3.2. Function of alpha-synuclein

αSyn function has been widely associated with neurotransmitter release and synaptic regulation. αSyn localises to presynaptic nerve terminals of neurons where it is believed to play a role in neurotransmitter release (Maroteaux, Campanelli and Scheller, 1988). More specifically, αSyn is involved in synaptic vesicle trafficking, docking and fusion of synaptic vesicles at the presynaptic terminal. For neurotransmitter release to take place, synaptic vesicles need to fuse with the presynaptic membrane. SNAREs on the synaptic vesicle must interact with SNAREs on the presynaptic terminal where SNARE complex assembly takes place and allows docking of the synaptic vesicle (Khounlo *et al.*, 2021). αSyn binds to the vesicular SNARE VAMP2 and promotes the assembly of SNARE complexes (Burré *et al.*, 2010). Although the loss of αSyn does not impair synaptic function, triple knockout of three synuclein isoforms; αSyn, βSyn and γSyn, reduces the number of SNARE complexes (Burré *et al.*, 2010). After vesicle docking, a fusion pore is formed, and neurotransmitter is released at the synapse. αSyn's ability to bind to membranes assists with the formation of the fusion pore and allows for expansion of the pore (Khounlo *et al.*, 2021). The mechanism for membrane binding is suggested to be in the highly conserved N-terminal domain present in all synuclein isoforms and explains the need for triple knockout to reduce the synuclein induced SNARE function (Maroteaux and Scheller, 1991; Jao *et al.*, 2004).

Even though αSyn plays an important physiological role, it has been widely reported that it is crucial to maintain a delicate balance of αSyn levels to prevent pathological consequences. Overexpressing αSyn to the levels in a genetic duplication or triplication is sufficient to inhibit neurotransmitter release, by reducing synaptic vesicle reclustering after neurotransmitter release (Nemani *et al.*, 2010). Transgenic mouse models of αSyn showed a change in SNARE protein arrangement and subsequently reduction in neurotransmitter release (Garcia-Reitböck *et al.*, 2010). These findings suggest a link between loss of normal functioning of αSyn and the

dopamine depletion observed in PD. However, a toxic gain of function also contributes to disease, when αSyn misfolds and aggregates are formed.

1.3.3. Alpha-synuclein aggregation in Parkinson´s Disease

αSyn is the one of the main components of Lewy Bodies found in postmortem tissue of PD patients. Since its first discovery, αSyn has been implicated in several other neurodegenerative diseases commonly known as synucleinopathies including Multiple System Atrophy (MSA) and Dementia with Lewy Bodies (DLB) (Galvin, Lee and Trojanowski, 2001). All three diseases share a common feature of the deposition of αSyn in Lewy Body plaques, however their clinical manifestations in patients are distinct.

It is not the physiological form of αSyn that is deposited in human tissue, but αSyn misfolds and aggregates into amyloid fibrils which are the main components of Lewy Bodies (Figure 1.2). Studies determining the structure of αSyn fibrils have outlined the heterogeneity and structural differences of αSyn fibrils in PD and MSA (Shahnawaz *et al.*, 2020). Although insoluble fibrils of αSyn are the major hallmark of PD, it has been shown that earlier aggregation species such as oligomers are more toxic in disrupting cellular processes and causing neuronal death (Emin *et al.*, 2022, Fusco *et al*., 2017, Parres-Gold *et al*., 2020, Verma *et al*., 2015, Winner *et al*., 2015). Oligomers are intermediate species of αSyn's aggregation pathway forming before the insoluble fibrils, their size and solubility means they can move freely within a cell and cause dysfunction. Due to the intrinsically disordered nature of αSyn, the protein can misfold in various conformations depending on the environment, this gives rise to a heterogeneous population of oligomers of different sizes and structures (Cremades, Chen and Dobson, 2017).

Oligomers are shown to induce toxicity in many ways, one major mechanism is through binding to membranes and inducing pore formation (Fusco *et al.*, 2017; Parres-Gold *et al.*, 2020). αSyn's ability to bind membranes allows the oligomeric form to interact with cardiolipin on the mitochondrial membrane, where pore formation leads to disrupted calcium homeostasis and increased cytochrome c release which triggers apoptosis (Luth *et al.*, 2014; Ghio *et al.*, 2019). Primary effects of αSyn oligomers binding to cardiolipin also include mitochondrial fission and implicate αSyn as a huge player in mitochondrial dysfunction (Nakamura et al., 2011). Oligomers exist in various conformations and sizes, it is the smaller oligomeric species of αSyn that exhibit more toxic to membranes than larger oligomers (Emin *et al.*, 2022). These effects have been observed in vivo; oligomer injection into rats caused a reduction in dopaminergic

cells, which was correlated to a higher number of oligomers localised to membranes (Winner *et al.*, 2011).

1.3.4. The role of phosphorylated alpha-synuclein in disease

Importantly, αSyn can undergo several modifications including truncation, phosphorylation, and glycosylation. In particular, αSyn phosphorylated at serine 129 has been predominantly found within Lewy Bodies (Anderson *et al.*, 2006). Due to this it has been widely implicated in the pathogenesis of αSyn. Phosphorylation can induce conformational changes within the disordered protein, and lead to structurally distinct aggregates (Ma *et al.*, 2016).

There is conflicting evidence of pSer129 αSyn's role in PD, with some studies suggesting phosphorylation is a protective mechanism that occurs after protein deposition (Ghanem *et al.*, 2022). However, many studies have implicated the phosphorylated form of αSyn as a key agent in the spread and toxicity associated with PD (Ma *et al.*, 2016). When phosphorylated αSyn fibrils are injected into mice, they induced increased dopaminergic neuron loss and inclusion formation compared to the non-phosphorylated form (Karampetsou *et al.*, 2017). It is not clear why pSer129 αSyn is toxic to cells and present within Lewy Body inclusions, and more research needs to be done to understand its role in disease. Phosphorylated αSyn aggregates, unlike WT αSyn, have been reported to preferentially bind to the mitochondrial membrane, highlighting a close relationship between pathogenic αSyn aggregates and mitochondrial dysfunction (Wang et al., 2019). This is supported by PD patients exhibiting higher accumulation of αSyn at the mitochondria than healthy controls (Devi *et al.*, 2008).

1.3.5. A link between genetics of Parkinson´s Disease and alpha-synuclein

αSyn pathology is implicated in both familial and sporadic forms of PD. In SNCA multiplications, a higher expression of αSyn leads to increased αSyn aggregates present leading to elevated dysfunction (Byers, Cord, Nguyen, Schü Le 5, et al., 2011; Mohamed et al., 2021). Similarly, SNCA missense mutants alter the αSyn dysfunction, three of the mutations; A53T, E46K and H50Q are suggested to speed up the aggregation of αSyn (Flagmeier *et al.*, 2016). Whereas G51D is thought to slow down the aggregation of αSyn (Flagmeier *et al.*, 2016). There are conflicting studies surrounding the aggregation kinetics of A30P.

However, there are other PD causative genes that are not directly linked to αSyn including LRRK2 and Parkin. In LRRK2, it has been questioned whether there is an interaction between

LRRK2 protein and αSyn, but ultimately there is not enough evidence to draw a strong conclusion (O'Hara *et al.*, 2020). Some studies suggest LRRK2 proteins are present within Lewy Bodies, however many LRRK2 patients do not display the typical Lewy Body phenotype of PD (O'Hara *et al.*, 2020). Similarly, Parkin mutants are not consistently associated with Lewy Body pathology, but they were more likely to be present in patients with a later onset of disease (Madsen *et al.*, 2021). Due to the complexity of sporadic PD, a link between sporadic PD and αSyn is not fully understood. Although sporadic patients usually present with typical PD pathology including Lewy Body inclusions in postmortem tissue, this could be linked with SNCA being the biggest genetic risk factor of sporadic PD (Mezey et al., 1998).

1.3.6. Cell to cell transmission of alpha-synuclein during disease progression

Postmortem brain studies of patients with PD have highlighted in the early stages of disease pathology is only present in the dorsal vagus nucleus and olfactory bulb, spreading to the midbrain, and in the later stages of disease pathology is more widespread within the cortex and prefrontal areas (Braak *et al.*, 2003). This led to the understanding that αSyn pathology spreads throughout the brain via anatomical connection and is related to disease progression.

The transmission of disease within the central nervous system, via anatomical connections, occurs due to the cell-to-cell spread of pathogenic αSyn aggregates in a process known as seeding. A cell with αSyn dysfunction can release pathogenic seeds of αSyn which are taken up by a neighbouring cell (Figure 1.5). These pathological seeds act as a template and promote the misfolding of endogenous αSyn. Monomeric αSyn can use the surface of the seed to aggregate into higher order structures (Karpowicz *et al.*, 2017). The introduction of a pathological seed is sufficient to recruit endogenous αSyn and facilitate the production of Lewy Bodies in primary neurons (Volpicelli-Daley *et al.*, 2011). The uptake of pathogenic seeds into primary neurons is sufficient to decrease endogenous αSyn localising to VAMP2 in the SNARE complex (Volpicelli-Daley *et al.*, 2011). The seeding process continues as the new fibrils generated fragment and produce more pathological seeds which are then released from the cell. This allows the αSyn pathology to spread from one area of the brain to another via anatomical connection (Figure 1.6). The spreading of αSyn throughout the brain was recapitulated in a rat model injected with αSyn preformed fibrils, where Lewy Body pathology was developed distal to the inoculation site (Luk, V. Kehm, *et al.*, 2012).

The exact mechanisms of how αSyn is being released and taken up by a neighbouring cell is still under investigation. There is evidence of αSyn secreted from the cell in both free and membrane bound forms (Emmanouilidou *et al.*, 2010; Danzer *et al.*, 2012). αSyn is suggested to be released by exocytosis, studies measuring the release of αSyn into cell culture medium found that low temperature, a classical blocker of exocytosis, is sufficient to cause a reduction in the release of αSyn (Lee, Patel and Lee, 2005). Another pathway has been discovered known as the misfolding-associated protein secretions (MAPS), where misfolded proteins are packaged into late endosomes and released into the extracellular space (Lee *et al.*, 2016). The chaperone DNAJC5 and ubiquitin specific peptidase USP19 facilitate the release of αSyn by the MAPS pathway (Xu *et al.*, 2018). A small amount of αSyn is released and contained within exosomes, and this is supported by the presence of αSyn in exosomes in the cerebrospinal fluid (CSF) of PD patients (Emmanouilidou *et al.*, 2010; Stuendl *et al.*, 2016). The majority of αSyn was found attached to the outer membrane of vesicles, with a small proportion being contained within the vesicle lumen (Danzer *et al.*, 2012; Gustafsson *et al.*, 2018).

With regards to the entry of αSyn into a neighbouring cell, monomeric αSyn can interact with cellular membranes and translocate into the cell via passive diffusion (Steiner, Angot and Brundin, 2011). However, for larger oligomers and aggregates active diffusion via endocytosis is more likely. A blocker of endocytosis led to the accumulation of αSyn on the cell surface, whereas untreated cells contained αSyn diffuse within the cytoplasm (Lee *et al.*, 2008).

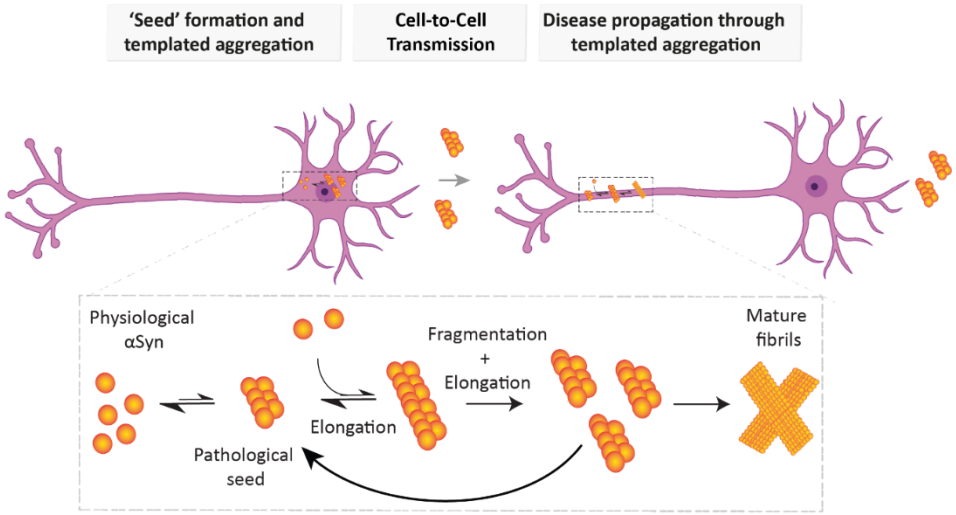

Figure 1.5. Spreading of pathological αSyn occurs through cell-to-cell transmission. The spreading of pathology in PD is associated with the spreading of αSyn pathological seeds from one cell to

another. The seeds act as a surface for endogenous αSyn to misfold and aggregate on. This causes the spread of αSyn dysfunction between cells.

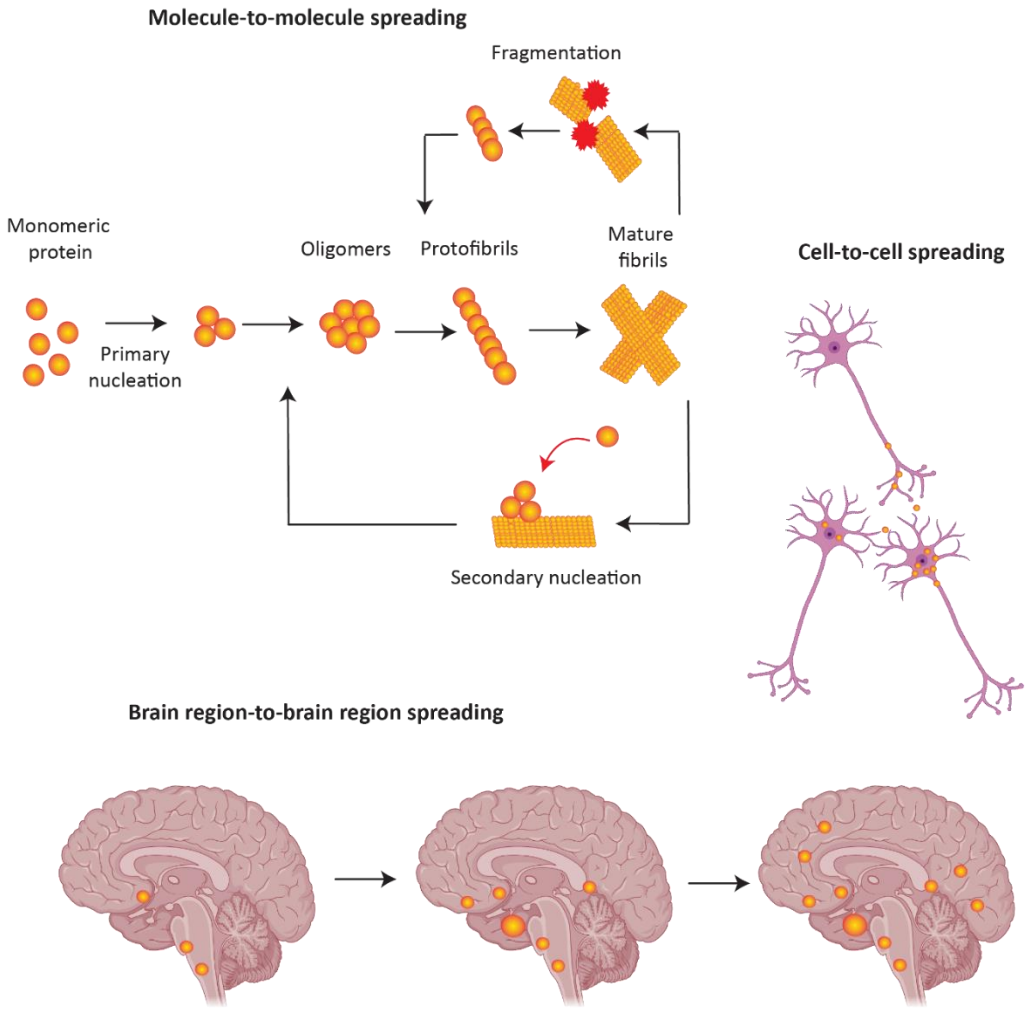

Figure 1.6. Summary of pathological spreading of αSyn. Pathology spreads from molecule-to-molecule, cell-to-cell and brain region-to-brain region.

1.4. Diagnosis of PD

1.4.1. Diagnosis of PD

There is currently no test for the early diagnosis of PD before significant damage has occurred, leading to difficulties in treating the disease. An early diagnostic test would be helpful to delay disease progression, improve patient management and the implementation of early disease modifying therapy.

The gold standard diagnostic test is the presence of αSyn positive Lewy body deposits within postmortem tissue (Gibb and Lees, 1988). But for individuals to be diagnosed with PD, the

practitioner takes into consideration symptoms, physical examination, and the patient's medical history. Medical history evaluation includes but is not limited to, depression, anxiety, sleep disturbances and constipation (*Diagnosing Parkinson's: Medical History & Physical Exam*, 2017). When Parkinson's is suspected, a physical examination of symptoms will be undertaken including assessing the patient's ability to complete several motor symptoms to determine the presence of bradykinesia, resting tremor and rigidity (Massano and Bhatia, 2012; Koller, 2018). Additionally, smell tests can be done as this is a common symptom of early Parkinson's. However, it is not completely reliable, as not all patients with Parkinson's will develop hyposmia (Sui *et al.*, 2019).

The Unified Parkinson's Disease Rating Scale (UPDRS) is a commonly used clinical rating scale of PD which was first established in the 1980s and revised in 2008 by the Movement Disorder Society (MDS) to form the MDS-UPDRS (Goetz *et al.*, 2008). It has been widely used to study the progression of PD and allows assessment of disability and impairment. The MDS-UPDRS includes 4 components; part I includes non-motor experiences in daily life, part II includes motor experiences in daily life, part III refers to the motor examination, and part IV includes motor complications. Longitudinal studies of patients diagnosed with PD shows a progression of UPDRS scores (average 4.68 points annually) from initial diagnosis to 5 years later (Holden *et al.*, 2018).

Even with a full assessment of clinical symptoms, physical examination and medical history, patients are still often misdiagnosed. To reduce this misdiagnosis, a Levodopa challenge test can be carried out. Levodopa is a dopamine replacement used to treat the motor symptoms associated with PD, patients are given an MDS-UPDRS score before and after levodopa treatment, to examine if symptoms improve with treatment (Rossi *et al.*, 2000; Gandhi and Saadabadi, 2023). If patients' symptoms do not improve after a high dose of Levodopa, then a PD diagnosis is unlikely. It is recommended to use the Levodopa challenge test alongside a clinical assessment for accurate diagnosis (Schade *et al.*, 2017). A combination of the Levodopa challenge and a hyposmia test increased the sensitivity for an early PD diagnosis (Terroba Chambi *et al.*, 2017).

Additionally, neuroimaging of dopamine dysfunction can also be used as a diagnostic biomarker. DAT-SPECT or dopamine transporter single-photon emission computed tomography, assesses the functioning of dopamine transporters, with the aim to detect any

abnormalities in PD patients (Akdemır, Bora Tokçaer and Atay, 2021). However, they may not rule out other disorders as dopamine reduction is also common in MSA (Bajaj, Hauser and Grachev, 2013).

However, the limitation with current diagnosis of PD is symptoms emerge at the later stages of disease when most of the dopaminergic neurons (~70%) are already damaged irreversibly (Wong *et al.*, 2019). The delayed onset of clinical symptoms prevents early diagnosis when treatment is most effective. There is a growing need to detect PD at the early stages. One of the earliest dysfunctions of Parkinson's Disease is the misfolding of αSyn, as this is shown to happen up to 10 years before symptoms arise (Lansbury and Lashuel, 2006; Kluge *et al.*, 2024). Therefore, detection of misfolded αSyn in accessible human samples could be a potential pathway for the early diagnosis of PD.

1.4.2. αSyn as a potential biomarker for PD

αSyn is considered a potential biomarker for PD due to its critical role in the disease's pathology (Stefanis, 2012). The protein is ubiquitously present in nearly all PD cases, predominantly within Lewy bodies in affected brain regions (Gibb and Lees, 1988; Spillantini *et al.*, 1997). αSyn aggregates begin forming long before the appearance of clinical symptoms, suggesting that early detection could lead to pre-symptomatic diagnosis (Lansbury and Lashuel, 2006). The progression of αSyn aggregation correlates with disease severity, and it can be detected in bodily fluids like CSF, blood, and saliva, offering for minimally invasive testing (Shahnawaz *et al.*, 2017; Angius *et al.*, 2023). Additionally, the specific patterns of αSyn aggregates can help distinguish PD from other neurodegenerative disorders known as synucleinopathies, enhancing its diagnostic specificity (Shahnawaz *et al.*, 2020). These attributes make αSyn a promising marker for early diagnosis and monitoring of PD.

To address the need for early diagnostic markers of PD, the Michael J Fox Foundation have recently created the Parkinson's Progression Markers Initiative (PPMI), which is a large research collaboration to uncover early biomarkers of disease. Recently the development of αSyn as a biomarker has shown promising results. Misfolded αSyn aggregates are present in the biofluids of PD patients such as CSF, however they are present at such low concentrations it is difficult to detect. Researchers have developed assays to amplify αSyn species present in the biofluids. The αSyn seed amplification assay (SAA) was developed following the work of two groups reporting a protein misfolding cyclic amplification (PMCA) and real-time quaking-

induced conversion (RT-QuIC) (Shi *et al.*, 2013; Shahnawaz *et al.*, 2017). The term SAA allows for standardisation of the method to amplify seeding-relevant αSyn, which works on the same principles as both PMCA and RT-QuIC.

The SAA assay works on the basis that αSyn aggregates will act as a template for monomeric protein and speed up the normally slow nucleation phase of αSyn aggregation pathway, whilst maintaining structural properties of the initial αSyn seeds (Yamaguchi *et al.*, 2005; Buell *et al.*, 2014). In the first step of the assay, biofluid collected from the patients is incubated with excess monomeric αSyn, if αSyn seeds are present in biofluid then secondary nucleation occurs, more aggregates form and fibril elongation happens (Figure 1.5) (Concha-Marambio, Shahnawaz and Soto, 2019). The newly formed fibrils are then fragmented by mechanical force typically sonication, resulting in an exponential increase in αSyn seeds (Concha-Marambio *et al.*, 2023). After several cycles αSyn species are amplified to a level where they are detectable. If there is absence or low amounts of αSyn seeds in the biofluids, i.e., in healthy individuals, no or significantly low amplification will occur compared to the biofluids collected from patients. The SAA was tested on a large cohort of PD patients, healthy individuals, and those at risk for PD (Siderowf *et al.*, 2023). The SAA results showed that 87.7% PD patients received a positive result compared to only 3.6% of healthy individuals. Interestingly, the test showed increased accuracy for patients with a common early dysfunction of PD, loss of smell, with 97% of patients gaining a positive result. This test could be a promising breakthrough in the early diagnostics of PD, as 86% of those at risk of the disease gained a positive result. Using this technique, researchers have also shown a distinction between the αSyn aggregates observed in PD CSF compared to MSA CSF and could be a promising opportunity for distinguishing between synucleinopathies (Shahnawaz *et al.*, 2020).

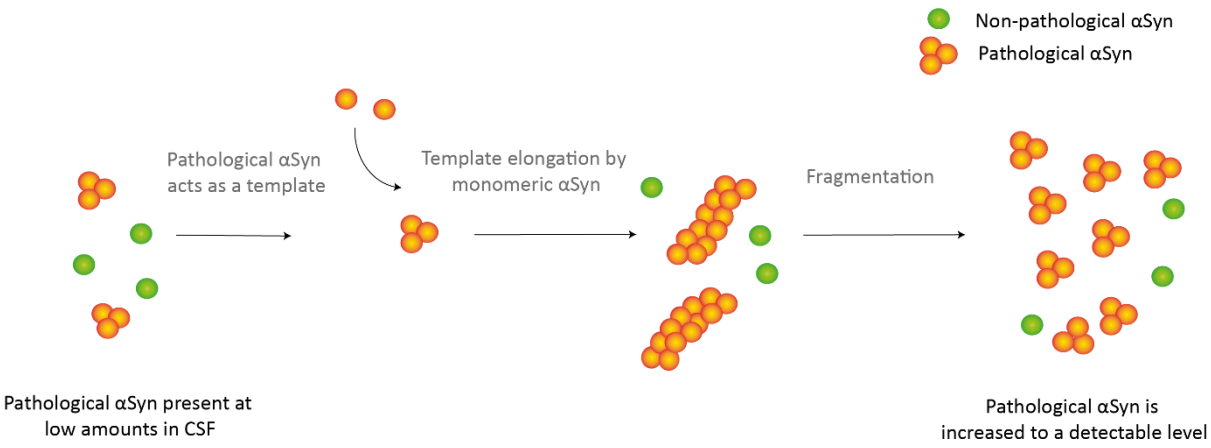

Figure 1.7. αSyn-SAA amplifies pathological αSyn in CSF and is a promising diagnostic test for PD. CSF containing pathological αSyn is incubated with recombinant αSyn. The pathological αSyn acts as a template for recombinant αSyn to elongate. Elongated αSyn are then fragmented by mechanical force to generate an increased number of pathogenic αSyn. Many cycles occur until pathological αSyn is increased to a detectable level.

A limitation of the αSyn-SAA method is the reliance on lumbar puncture to retrieve CSF samples from patients and healthy individuals which is an invasive process with side effects often lasting weeks and potential complications (Kim, 2022). A recent study has outlined the potential of αSyn-SAA using a less invasive procedure of skin biopsies, with 92% of PD patients showing a positive result and 93% of healthy individuals showing a negative result (Kuang *et al.*, 2024).

Additionally, other studies have investigated the detection of αSyn species for diagnosis in a more accessible manner, including saliva and blood samples (Angius *et al.*, 2023). PD patients were successfully distinguished from healthy individuals by using an ELISA assay to detect altered ratios of phosphorylated αSyn / total αSyn and oligomeric αSyn (Vivacqua *et al.*, 2016; Angius *et al.*, 2023).

Although a promising development in the field, more research needs to be done to make the αSyn diagnostic test more accessible to facilitate early diagnosis of PD in clinical settings.

1.5. Therapies of PD

1.5.1. Current treatment of PD

There are currently no disease modifying therapies for PD, and medication aims to alleviate symptoms. Levodopa is the main treatment for PD. Levodopa is a precursor of dopamine and

is converted to dopamine within the brain (Gandhi and Saadabadi, 2023). It works by alleviating Parkinson's motor symptoms that are caused by a reduction in dopamine. The drug appears less effective over time, this is due to the increased loss of neuronal cells later in the disease and additional dopamine cannot compensate for the loss. Side effects associated with Levodopa include nausea, drowsiness, dizziness and confusion (Gandhi and Saadabadi, 2023).

Monoamine oxidase B (MAO B) inhibitors are another treatment option for individuals with PD. MAO B enzyme breaks down dopamine within the brain, so inhibitors of MAO B can be used to maintain dopamine levels (Tan, Jenner and Chen, 2022). Similar to Levodopa, MAO B inhibitors help alleviate motor symptoms of PD. In the later stages of disease when symptoms become more severe, Levodopa and MAO B can be used in combination (Dezsi and Vecsei, 2017).

All current medications for PD only work by symptom management, and there is a growing need for treatments to slow or halt progression of the disease (McFarthing *et al.*, 2022).

1.5.2. Targeting αSyn as a therapy for PD

Due to αSyn's deposition in Lewy Bodies, toxicity to cells, and spreading throughout the brain, targeting pathological αSyn to stop the spread of pathology throughout the PD brain has been investigated as a potential therapy for PD (Fields, Bengoa-Vergniory and Wade-Martins, 2019).

Immunotherapy to target aggregated αSyn has shown huge promise and led to the use of αSyn targeting antibodies in clinical trials. Prasinezumab is a monoclonal antibody, directly targeting the aggregated form of αSyn, showing efficacy in mouse models, and safety in humans (Masliah *et al.*, 2011; Jankovic *et al.*, 2018). A 2-year phase 2 trial, PASADENA, was conducted with 316 individuals recently diagnosed with PD. The primary outcome was to reduce MDS-UPDRS scores, and secondary outcomes were changes in DAT scan measurements, however the results found there was no overall difference between the treatment group and those receiving the placebo (Pagano *et al.*, 2022). The drug did slow progression of the motor symptoms associated with MDS-UPDRS III scores compared to placebo receiving participants, and this effect was heightened in individuals with rapidly progressing symptoms (Pagano *et al.*, 2024). Following on from PASADENA, a phase 2b trial was started called PADOVA, using the same drug Prasinezumab including advanced patients who

are receiving treatment of dopamine replacement (Nikolcheva *et al.*, 2023). The primary endpoint of the trial will focus on the progression of motor symptoms in MDS-UPDRS III.

Another immunotherapy, Cinpanemab interacts directly with αSyn, and shows an 800-fold higher affinity to aggregated αSyn compared to monomeric αSyn (Weihofen *et al.*, 2019). The antibody showed promise in reducing the pathological spreading of αSyn and alleviating motor symptoms in mouse models (Weihofen *et al.*, 2019). However, in phase 2 trials the drug failed to report any change in MDS-UPDRS scores and DAT-SPECT imaging, and development of Cinpanemab has been stopped (Lang *et al.*, 2022).

More recently, a new antibody trial for Exidavnemab, a monoclonal antibody that targets aggregated αSyn with high affinity, has shown promising results (Boström *et al.*, 2024). The drugs phase I trial showed the safety and efficacy, where a dose dependent reduction in αSyn was observed. Following on from this, the drug will be tested for its effects in PD patients.

Many small molecules have been investigated as PD therapies to target αSyn. Emrusolmin or Anle138b works by binding to pathological αSyn aggregates and preventing oligomer formation, and in a mouse model of PD treatment reduced αSyn deposition and rescued dopaminergic neuron dysfunction (Wagner *et al.*, 2013; Wegrzynowicz *et al.*, 2019). Phase I clinical trials confirmed safety of the drug in addition to high plasma concentrations (Levin *et al.*, 2022). Phase II clinical trials are planned for 2024, with a focus on MSA patients rather than PD, as Anle138b has shown efficacy in mouse models of MSA (Heras-Garvin *et al.*, 2019).

Additionally, the chaperone domain Bri2 BRICHOS has been investigated in both AD and PD as it harbours the ability to bind to both oligomeric and fibrillar species and modulate the aggregation process (Biverstål et al., 2020). The binding inhibits secondary nucleation on the surface of fibrils thereby preventing formation of toxic oligomers (Adam et al., 2024). The use of BRICHOS has been widely investigated *in vitro* and *in vivo* mouse models, leading to decreased Aβ burden in AD mice, and suppression of αSyn neurotoxicity in mouse hippocampal tissue (Manchanda et al., 2023, Adam et al., 2024). This novel approach of developing therapeutics against key pathological mechanisms is important for future advancements, however the use of BRICHOS in human models is limited, and therefore the efficacy of BRICHOS as a treatment for neurodegenerative diseases is unknown.

These therapy approaches are crucial because αSyn not only aggregates to form Lewy bodies but also plays a role in normal synaptic functions. Therefore, therapies need to be designed carefully to target the pathological aspects of αSyn without disrupting its normal physiological functions. The development of treatments that specifically target pathological forms of αSyn while preserving its normal function could provide disease-modifying effects without significant side effects.

1.6. Cellular models of PD

In order to understand the pathogenesis of PD, and to develop new therapeutics, it is essential to model Parkinson's Disease. An effective model of PD will contain the key aspects of PD; the degeneration of dopaminergic neurons and the aggregation of αSyn. Animal models effectively show PD pathology, however they are expensive and take a long time to develop pathology. In this way, cellular models may be more beneficial to understanding specific microscopic events leading up to pathology.

1.6.1. Over expression models of alpha-synuclein

Overexpression models of αSyn are an invaluable tool for studying the effects of αSyn on the cell. The development of recombinant adeno-associated viral vector (rAAV) αSyn models has allowed the study of αSyn in PD in rodents where behavioural phenotypes and Lewy Body pathology can be studied. rAAV studies report the expression of αSyn in dopaminergic neurons in the substantia nigra, leading to the specific loss of dopaminergic neurons and subsequent motor symptoms occurring after 50% dopaminergic neuron loss (Kirik *et al.*, 2002; St Martin *et al.*, 2007; Theodore *et al.*, 2008). rAAV αSyn models also show an increase in p-αSyn deposition which is correlated to neurodegeneration, as when animals were injected with empty vectors there was an absence of p-αSyn aggregates and neurodegeneration (Ip *et al.*, 2017).

Although a great tool to study αSyn pathology and correlate to behaviour deficits, some studies report overexpression of 4-5-fold increase of αSyn. Although this allows us to observe αSyn induced dysfunction, it is not physiologically representative (Decressac *et al.*, 2012; Volpicelli-Daley *et al.*, 2016; Duffy *et al.*, 2018).

1.6.2. Alpha-synuclein seeding based models of PD

Although SNCA multiplication cases of PD are associated with increased αSyn expression levels, most sporadic cases do not show a higher expression of αSyn. Therefore, overexpression models cannot always recapitulate sporadic forms of disease.

The development of αSyn preformed fibril (PFF) models involves injection of toxic forms of αSyn leads to Lewy Body pathology in a model expressing normal levels of αSyn. The model relies on the generation of αSyn fibrils formed *in vitro* from recombinant monomeric αSyn. The *in vitro* fibrils are then applied to either cells or injected into animal models and PD pathology is initiated. It was utilized in primary neuronal cell-based models, where αSyn fibrils were introduced to the cell media and taken up by neurons (Volpicelli-Daley *et al.*, 2011). After treatment, inclusions were present within neurons. Inclusion formation was due to the recruitment of endogenous αSyn onto PFFs to promote aggregation. This was confirmed in a mouse model, as when mice lacking endogenous αSyn were treated with PFFs, Lewy Bodies were not present (Volpicelli-Daley *et al.*, 2011).

PFF modelling has been extensively studied in mouse models. Mice injected with PFFs have developed Lewy Body pathology in the form of p-αSyn insoluble inclusions associated with ubiquitin (Luk, V. Kehm, *et al.*, 2012; Luk, V. M. Kehm, *et al.*, 2012). Mice injected with phosphorylated αSyn PFFs exhibited increased Lewy Body inclusions compared to mice injected with WT αSyn PFFs (Karampetsou et al., 2017). These models have been invaluable for understanding the spread of αSyn in disease and supports the principle that PD pathology is driven by the cell-to-cell transmission and seeding of αSyn. One single intrastriatal injection of αSyn is sufficient to promote the spread of αSyn inclusions to distal areas including amygdala and frontal cortex (Luk, V. Kehm, et al., 2012). Although most αSyn PFF models display αSyn deposition and neurodegeneration, there is huge variability in behavioural phenotypes including motor deficits between studies (Polinski, 2021).

A drawback of this model is that the pathology is induced by the addition of an *in vitro* formed fibril. The pathology observed is not endogenous, natural disease progression and does not completely recapitulate disease mechanisms in patients.

1.6.3. Induced pluripotent stem cell models of Parkinson's Disease

One of the major drawbacks of cell models in studying disease is they do not directly recapitulate the disease environment observed in patient cells. A huge breakthrough in the field occurred when the Yamanaka lab pioneered the development of induced pluripotent stem cells (iPSCs) (Takahashi and Yamanaka, 2006). They generated a protocol that utilises transcription factors (Oct3/4, Sox2, c-Myc and KLf4) to transform human fibroblasts into embryonic cells capable of generating various cell types, including neuronal cells such as dopaminergic neurons (Takahashi et al., 2007). Many researchers have utilized this model to generate dopaminergic neurons from PD patients carrying PD genetic mutations and healthy controls (Devine et al., 2011; Jiang et al., 2012; Sánchez-Danés et al., 2012).

Using iPSCs, researchers have determined many different PD disease mechanisms including changes in neuronal morphology and networks, mitochondrial function, ER stress and the unfolded protein response in PD dopaminergic neurons (Baena-Montes, Avazzadeh and Quinlan, 2021). Fibroblasts from patients carrying SNCA multiplications showed that once differentiated into dopaminergic neurons, the neurons produce double the amount of αSyn compared to healthy individuals (Devine et al., 2011). Similarly, other iPSC multiplication studies report that endogenous αSyn aggregates were present within the cell body without the addition of stressors, and the number of aggregates correlated to copy number of SNCA (Iannielli et al., 2022). The aggregates were found to have an interaction with mitochondrial protein TOM20. SNCA multiplication cell lines also appeared to have a distinct fragmented mitochondrial network, and a reduced basal membrane potential compared to isogenic controls (Iannielli et al., 2022). iPSCs can recapitulate the formation of toxic species within PD, cell lines with SNCA multiplications have been reported to have significant accumulation of p-αSyn, Parkin mutant iPSCs showing p-αSyn accumulation to a lesser extent, and LRRK2 exhibits slight increase in p-αSyn compared to healthy controls (Lin et al., 2016). Studies into αSyn in iPSCs mainly focus on genetic variants namely SNCA multiplications and mutations, and an advantage of this approach is the ability to develop isogenic controls that lack the disease mutation (Natalwala et al., 2022). However, familial mutations only accounts for a small subset of patients as most PD patients present with idiopathic disease.

A drawback of iPSC models is their lack of ageing phenotype. Due to the transcriptional and epigenetic mark being removed during the conversion to pluripotent stem cells, these cells

lack some characteristics of ageing cells (Lapasset et al., 2011). For example, these models restore mitochondrial quality control and function, a process that is compromised in ageing cells and contributes to disease mechanisms in PD (Lin and Beal, 2006; Suhr et al., 2010).

1.6.4. Induced neuronal progenitor cell models of Parkinson´s Disease

To overcome this issue, researchers developed a method of direct conversion of adult human fibroblasts to tripotent induced neuronal progenitor cells (iNPCs) which can be differentiated into oligodendrocytes, astrocytes and neurons (Meyer et al., 2014). More specialised neuronal populations can be generated, for example researchers have differentiated iNPCs into a dopaminergic neuronal model to study PD (Pfisterer et al., 2011; Shrigley et al., 2018; Schwartzentruber et al., 2020; Drouin-Ouellet et al., 2022).

The advantage of direct conversion is the generation of cell lines that retain both the genetic background and features of ageing and therefore provide a more relevant model to study neurodegenerative disease (Gatto et al., 2021). Directly converted dopaminergic neurons derived from PD patients showed age-related phenotypes including a reduction in chaperone-mediated autophagy compared to healthy control dopaminergic neurons (Drouin-Ouellet et al., 2022). Stress induced autophagy also led to the formation of αSyn pathology in the PD lines but not healthy controls. This phenotype was not observed in iPSCs derived from the same patients; this highlights the importance of maintaining ageing properties when studying neurodegenerative disease (Drouin-Ouellet et al., 2022).

The use of direct conversion is invaluable in the investigation of αSyn dysfunction within sporadic PD, where ageing features of the cell may be crucial in disease progression. In this way, direct conversion of fibroblasts can provide a model to study the early dysfunctions that occur within PD αSyn deposition, in a disease relevant aged cell model. The early stages of αSyn dysfunction and aggregation have not yet been investigated in patient derived models of dopaminergic neurons from iNPCs.

1.7. Motivation for this thesis

PD is the second most prevalent neurodegenerative disorder globally, with its incidence expected to rise sharply in the aging population. Despite significant advancements in understanding PD, the precise causes and mechanisms driving the disease remain largely unknown. This gap in mechanistic insight represents a formidable barrier to developing

definitive, disease-modifying treatments, which, if unresolved, threatens to impose overwhelming burdens on society, healthcare systems, and economies worldwide.

PD is mainly characterized by the progressive degeneration of dopaminergic neurons in the substantia nigra, a vital brain region for movement control. Notably, clinical symptoms manifest predominantly at advanced stages of disease when irreversible loss of 50-70% of dopaminergic neurons has already occurred. Thus, whilst dopamine depletion correlates closely with PD symptoms, an urgent need exists for early biomarkers that can detect the disease before substantial neuronal loss.

In this context, αSyn emerges as a pivotal biomarker and therapeutic target due to three key observations:

1. Detectability of αSyn in human biofluids: αSyn holds significant potential as a diagnostic biomarker for PD due to its key role in pathology of the disease and presence in biofluids.

2. Ubiquitous presence: αSyn accumulates abnormally in the dopaminergic neurons of almost all PD patients.

3. Early onset of dysfunction: αSyn deposition and associated dysfunctions commence decades before clinical symptoms appear.

These attributes make αSyn an ideal candidate for probing the early mechanisms of PD and potentially developing a biomarker for early diagnosis. Furthermore, targeting these early αSyn dysfunctions may offer new avenues for therapeutic intervention.

A major challenge in using αSyn for PD pathology studies is the absence of models that can reliably replicate the disease's heterogeneity without external perturbations. PD's variability - stemming from both genetic and sporadic origins - manifests as diverse pathophysiology's, complicating the establishment of a consistent pathology across models based on αSyn. Additionally, despite the potential for early detection, the lack of ultra-sensitive methods to quantitatively assess these dysfunctions hinders progress, as αSyn's complex behaviour and conformational flexibility define its precise role in the disease.

Addressing these gaps in knowledge, my thesis introduces a novel approach using patient-derived cellular models tailored to both sporadic and various genetic forms of PD. Coupled with high-resolution single-molecule imaging-based ELISA techniques, this study aims to

pinpoint specific αSyn conformations and compositions that play a central role in the disease. These cellular models have been validated through the spontaneous formation of hallmark Lewy body deposits, facilitating a more nuanced exploration of αSyn's pathogenic roles without external interference.

Aims of the thesis

My thesis addresses significant gaps in the understanding of molecular drivers behind αSyn dysfunction and aggregation in PD, using innovative patient-derived cellular models. The specific objectives are outlined as follows:

1. Characterization and validation of cellular models: To characterize the cellular models of dopaminergic neurons derived from PD patients, focusing on the role of αSyn in disease pathogenesis, including its aggregation patterns and effects on neuronal health.

2. Identification and analysis of toxic αSyn species at the single-molecule level: To identify and analyse the conformationally distinct αSyn species that contribute to neurotoxicity, utilizing advanced single-molecule imaging techniques to quantify their presence and impact in cellular models.

3. Elucidation of the mechanisms of αSyn associated pathogenic pathways: To elucidate the molecular pathways through which αSyn contributes to cellular dysfunction, focusing on its interactions with cellular components and the resulting disruptions to cellular homeostasis.

4. Development of therapeutic strategies: To explore potential diagnostic markers based on specific αSyn conformations and to evaluate potential therapeutic strategies aimed at mitigating αSyn-induced toxicity, thereby rescuing the disease phenotype in patient-derived models.

By achieving these aims, this thesis seeks to provide a comprehensive understanding of αSyn's role in PD and to identify actionable targets for the development of disease-modifying therapies.

Chapter 2: Materials and Methods

2.1 Materials

Table 2.1. General Reagents

Reagent	Company	Catalogue Number
Acetic acid, glacial	Fisher Scientific	10171460
Acetone	VWR Chemicals	20066.330
Acrylamide 30% (v/v)	Geneflow	A2-0072
(3-Aminopropyltriethoxysilane) APTES	Thermofisher	80370
Ammonium persulphate (APS)	Sigma	A3678-25G
Beta-mercaptoethanol	Sigma	516732
Biotinylated PEG	Laysan Bio	BIO-PEG-SVA-5K
Bovine Serum Albumin	Thermofisher	B14
Bromophenol blue	Thermofisher	A18469-18
Ca^{+} buffer	Thermofisher	21083027
Cardiolipin (CL)	Avanti Lipids	710335
Dithiothreitol (DTT)	Sigma	1019777001
EDTA	Thermofisher	1861274
EGTA	Bioworld	40121266
Glycerol	Thermofisher	A16205-AP
Halt™ Protease & Phosphatase Inhibitor Cocktail	Thermofisher	1861281
Horse serum	Thermofisher	26050088
Hydrochloric acid (HCl)	VWR Chemicals	20252.335
Ionomycin	Cambridge Bioscience	1565-5
Isopropanol	Thermofisher	P/7500/17
Lightning-Link Alexa Fluor 488 conjugation kit	Abcam	ab236553
Lightning-Link Alexa Fluor 594 conjugation kit	Abcam	ab269822
Lightning-Link Alexa Fluor 647 conjugation kit	Abcam	ab269823
Lightning-Link Biotinylation kit	Abcam	ab201795
Methanol	Millipore	32213

Magnesium Chloride ($MgCl_2$)	Melford	M24000-1000
Mg-ATP	Sigma	A9187
mPEG	Laysan Bio	MPEG-SVA-5000
$MS(PEG)_4$ Methyl-PEG-NHS-Ester	Thermofisher	22341
Neutravidin	Thermofisher	31000
Paraformaldehyde	Thermofisher	28908
Phosphatidylcholine Biotinylated (PC)	Avanti Lipids	860563C
Phosphatidylcholine (PC)	Avanti Lipids	850457C
Phosphatidylethanolamine (PE)	Avanti Lipids	850757
Phosphatidylinositol (PI)	Avanti Lipids	850142
Phosphatidylserine (PS)	Avanti Lipids	840034
Pierce BCA Protein Assay Kit	Thermofisher	23225
PLK3	Life Technologies	PV3812
PMSF	Thermofisher	36978
Potassium Hydroxide	Millipore	1310-58-3
Precision Plus Protein™ Dual Color Standards	Bio-Rad	1610394
Skim milk powder	Millipore	70166-500G
Sodium azide	Sigma	S2002-100G
Sodium bicarbonate	Thermofisher	424270010
Sodium chloride (NaCl)	Thermofisher	S/3161/65
Sodium dodecyl sulfate (SDS)	Thermofisher	S/5200/53
TEMED	Thermofisher	T18000-0.1
Tris	Melford	T60040-5000
Triton X-100	Thermofisher	A16046-AE
Tween-20	Sigma	P1379-1L

Table 2.2. Materials

Incubators	**Company**
Innova44 Shaking Incubator	New Brunswick Scientific
Midi Oven Dual 14 Incubator	Akribis Scientific

Clifton Unstirred Digital Waterbath	Fisher Scientific
Tissue Culture CO_2 37°C incubator	Akribis Scientific
Microplate readers and plates	
CLARIOstar Plus Microplate Reader	BMG Labtech
96-well half area plates	Corning
Nunc 96-well immunoplate	Thermofisher
Immunoblotting	
Criterion blotter	Bio-Rad
LI-COR Odyssey Fc Imaging system	LI-COR
Mini-PROTEAN tetra vertical electrophoresis cell	Bio-Rad
Nitrocellulose blotting membranes	Cytiva
Whatman blotting paper	Sigma
Single molecule pulldown coverslip preparation	
Coverslips 26 x 76 mm	Epredia
CultureWell chambered coverglass	Millipore
Plasma system Zepto One	Deiner Electronic GmbH
Ultrasonic cleaning bath	Fisher Scientific
Single molecule microscope setup	
100x Plan Apo TIRF NA 1.49 oil immersion objective lens	Nikon
Beam shaper	Asphericon
Beam splitter	Laser 2000
sCMOS Camera Prime 95b	Teledyne Photometrics
LightHub 405 nm laser	Omicron
LightHub 488 nm laser	Omicron
LightHub 637 nm laser	Omicron
Nikon Ti2 Eclipse	Nikon
OBIS 561 nm laser	Coherent
Quarter-wave plate	Thorlabs
High-content confocal imaging	

Opera Phenix	Perkin Elmer
96-well flat bottom plates	Agilent

Table 2.3. Primary Antibodies

Primary antibody	Company and Catalogue Number	Approaches and Concentration	Isotype
Anti-Alpha-synuclein [syn211]	Abcam ab206675	SiMPull 10 nM WB 1:1000	Mouse IgG1
Anti-Alpha-synuclein [MJFR1]	Abcam ab209420	SiMPull 5 nM WB 1:1000	Rabbit IgG
Anti-Alpha-synuclein	Sigma AB5038	ICC 1:1000	Polyclonal
Alexa Fluor 594 Anti-alpha-Synuclein Phospho (Ser129)	Biolegend 825708	SiMPull 5 nM	Mouse IgG2a, κ
Anti-Alpha-synuclein (phospho S129) [MJF-R13]	Abcam ab168381	SiMPull 5 nM ICC 1:500	Rabbit IgG
Alexa Fluor 647 Anti-Alpha-synuclein aggregate [MJFR-14-6-4-2]	Abcam ab216309	SiMPull 5 nM	Rabbit IgG
Anti-Alpha-synuclein aggregate [MJFR-14-6-4-2]	Abcam ab209538	ICC 1:1000	Rabbit IgG
Coralite Plus 488-conjugated TOM20	Proteintech CL488-11802	SiMPull 10 nM ICC 1:500	Rabbit IgG
Coralite Plus 488-conjugated VDAC1/Porin	Proteintech CL488-55259	SiMPull 10 nM	Rabbit IgG
Coralite Plus 488-conjugated Ubiquitin	Proteintech CL488-10201	SiMPull 10 nM	Rabbit IgG
Alexa Fluor 488 anti-Ubiquitin	Biolegend	SiMPull 10 nM	Mouse IgG1, κ
Coralite Plus 488-conjugated P62/SQSTM1	Proteintech CL488-66184	SiMPull 10 nM ICC 1:500	Mouse IgG2a
Alexa Fluor 647 Anti-βIII Tubulin	Abcam ab190575	ICC 1:1000	Rabbit IgG
Alexa Fluor 488 Anti-Tyrosine Hydroxylase	Biolegend 818006	ICC 1:200	Mouse IgG2a
Anti-Dopamine Transporter	Invitrogen PA5-78382	ICC 1:500	Rabbit IgG
Anti-PAX6	Abcam ab18102	ICC 1:200	Mouse IgG1
Anti-Nestin	Abcam ab5790	ICC 1:200	Rabbit IgG

Table 2.4. Secondary Antibodies

Antibody	Company and Catalogue Number	Approaches and Concentration	Isotype
Anti-mouse Alexa Fluor 790	Jackson Immunoresearch	WB 1:50,000	Donkey IgG
Anti-rabbit Alexa Fluor 680	Jackson Immunoresearch	WB 1:50,000	Donkey IgG
Anti-mouse Alexa Fluor 488	Invitrogen A11001	ICC 1:1000	Goat IgG
Anti-mouse Alexa Fluor 647	Invitrogen A31571	ICC 1:1000	Donkey IgG
Anti-rabbit Alexa Fluor 488	Invitrogen A11008	ICC 1:1000	Goat IgG
Anti-rabbit Alexa Fluor 647	Invitrogen A31573	ICC 1:1000	Donkey IgG

Table 2.5. Dyes

Dye	Company	Catalogue number	Approaches and concentration
Cal-520 AM	Stratech	21130-AAT	Vesicle preparation 100 µM
Hoechst 33258	Sigma	B2883	IF 1:10,000 Live imaging 1:250
LysoTracker™ Deep Red	Invitrogen	L12492	Live imaging 1:20,000
MitoTracker™ Green FM	Invitrogen	M7514	Live imaging 1:1,000
Thioflavin T (ThT)	AAT Bioquest	23060	Kinetics assay 25 µM
Tetramethylrhodamine methyl ester perchlorate (TMRM)	Sigma	T5428	Live imaging 1:1000
Vibrant™ DiO cell labelling solution	Invitrogen	V22889	SiMPull 1 µM

Table 2.6. Cell culture reagents

Reagent	Purpose	Company	Catalogue Number
DMEM/F12 Glutamax	Media base	Gibco	31331-028
B-27 supplement	Media supplement	Gibco	11530536
N-2 supplement	Media supplement	Gibco	15410294
Penicillin/Streptomycin (P/S)	Media supplement	Lonza	DE17-603E
Basic fibroblast growth factor (FGF basic)	iNPC factor	Peprotech	100-18B
Accutase	Passaging	Sigma	A6964-100ML
Fibronectin	Coating dishes	Millipore	FC010-10MG
N-[N-(3,5-difluorophenacetyl)-l-alanyl]-S-phenylglycine t-butyl ester (DAPT)	iDNL factor	Sigma	D5942-5MG
Fibroblast growth factor 8 (FGF8)	iDNL factor	Peprotech	100-25A
Smoothened agonist (SAG)	iDNL factor	Millipore	566660-1MG
Brain derived neurotrophic factor (BDNF)	iDNL factor	Peprotech	450-02
Glial cell line derived neurotrophic factor (GDNF)	iDNL factor	Peprotech	450-10
Transforming growth factor beta (TGF)	iDNL factor	Peprotech	100-36E
d-cyclic adenosine monophosphate (d-cAMP)	iDNL factor	Sigma	D0627-250MG
Ciprofloxacin	iDNL factor	Sigma	PHR1044

2.2 Cell culture methods

Cell culture media and reagents used were all sterile and filtered using 0.2 µm filters. All cell culture work was carried out in a laminar flow cabinet to ensure sterile conditions.

2.2.1 Cell lines

The cell lines used within this thesis have been obtained from control and patient fibroblasts (Table 2.7.). Briefly, skin biopsies were collected from the forearm of the donor, and

fibroblasts were cultured according to a previously published protocol (Carling et al., 2020). The OB lines were biopsied in Sheffield under the ethics mentioned in Carling et al,. 2020. The ND lines were obtained from the NINDS collection under MTA. GM13335 was obtained from Coriell cell repository under MTA.

We acknowledge that for cell line SNCA and LRRK2, the gene name has been used. This is for ease of reference and within this thesis, as outlined by Table 2.7, does not refer to the gene.

Table 2.7. Cell line information

Cell line	Disease mutation	Sex	Age at biopsy
SNCA (ND27760)	SNCA triplication	F	55
sPD1 (OB209)	Sporadic PD	F	56
sPD2 (OB182)	Sporadic PD	F	51
LRRK2 (ND34198)	LRRK2 G2019S	M	57
Parkin (ND30171)	Parkin R42P;EX3 Del	M	54
Control 1 (ND29510)	Healthy control	F	55
Control 2 (OB247)	Healthy control	M	58
Control 3 (OB248)	Healthy control	M	55
Control 4 (GM13335)	Healthy control	M	58
Control 5 (GM13335)	Healthy control	M	58

2.2.2 Induced neuronal progenitor cell culture

Induced neuronal progenitor cells (iNPCs) were generated previously by direct conversion of fibroblasts, according to a published protocol (Meyer et al., 2014). OB lines were reprogrammed by Professor Heather Mortiboys and Professor Laura Ferraiuolo (Carling et al., 2020). ND27760, ND34198, ND29510 and GM13335 were reprogrammed by Professor Heather Mortiboys (Schwartzentruber et al., 2020; Rusilowicz-Jones et al., 2021). ND30171 was reprogrammed by Professor Heather Mortiboys, Professor Laura Ferraiuolo and Dr Monika Myszczynska (Schwartzentruber et al., 2020; Rusilowicz-Jones et al., 2021).

Reprogramming involved treating fibroblasts with retroviral vectors OCT3, c-Myc, SOX2 and KLF4 for 48 hours. Following this treatment, the cells were maintained in DMEM/F12

Glutamax supplemented with 1% N2, 1% B27, 20 ng/mL FGF-2 and 20 ng/mL EGF until the morphology changed and the cells were positive for iNPC markers Pax6 and Nestin.

Once iNPCs were generated, the cells were cultured in DMEM/F12 Glutamax supplemented with 1% N2, 1% B27, 1% Penicillin/Streptomycin (P/S) and 40ng/mL basic fibroblast growth factor. Cells were fed every 2 days and passaged twice a week when they reached around 80% confluency. Briefly, cell media was removed, and cells were washed with PBS and then incubated with accutase for 5 minutes at 37°C to lift the cells. Accutase was then diluted with PBS, and the cell suspension was centrifuged at 200 g for 4 minutes. The supernatant was discarded, and the cell pellet was resuspended in iNPC media. Cells were then replated at a lower density in a 10cm dish coated with 2.5 µg/mL Fibronectin diluted in PBS. Cells were incubated at 37°C with 5% CO_2. Cell culture of LRRK2 and Control 4 iNPCs was done by Dr Francesco Capriglia, and Parkin and Control 5 iNPCs were cultured by Dr Alexander Bury and Nikolaos Stefanidis.

2.2.3 Induced dopaminergic neuron-like cell culture

The differentiation of iNPCs into induced dopaminergic neuron-like cells (iDNLs) was performed following a protocol from previously published papers (Carling et al., 2020; Schwartzentruber et al., 2020; Rusilowicz-Jones et al., 2021).

iNPCs were plated into a 6-well plate coated with fibronectin, at a density of approximately 70,000 – 100,000 cells per well. Differentiation of iNPCs to iDNLs was initiated when the cells reached ~90% confluency. The neuron media used throughout differentiation remained the same (DMEM/F12 Glutamax) however was supplemented with different factors depending on the stage of differentiation (Table 2.8.). Briefly, to begin differentiation the cells were cultured with neuron media supplemented with 2.5 µM DAPT for 2 days to enhance neuronal differentiation. DAPT was then removed and replaced with neuron media supplemented with SAG and FGF8 in order to generate neurons with a midbrain lineage. Cells were fed every day for 10 days. For control 3 and sPD2 this stage only lasted 4 days due to excessive cell death in this stage. After 10 days, cells were replated into fibronectin coated plates, according to the endpoint assay. For SiMPull and western blot experiments, cells were replated into 6 well plates at a density of 500,000 cells per well. For ICC experiments, cells were replated into black clear bottom 96 well plates at a density of 10,000 cells per well. For replating, cells were washed with PBS and then lifted using accutase incubation for 4 minutes at 37°C, before

quenching with PBS. Cell suspension was centrifuged at 200 rpm for 4 minutes. Cell pellets were resuspended in SAG/FGF8 media and cells were counted using a haemocytometer (0.1 mm depth, Marienfeld). The day after replating, cells were transferred into neuron media to generate dopaminergic neurons, the media contained 30 ng/mL brain derived neurotrophic factor (BDNF), 30 ng/mL glial cell line derived neurotrophic factor (GDNF), 75 ng/mL transforming growth factor β (TGFβ), 2 mM d-cyclic adenosine monophosphate (dcAMP) and 1 µg/mL ciproflaxin to prevent mycoplasma infections. The cells were fed daily and maintained in this media for a following 15 days or until the cell morphology changed to exhibit long projections, and then cells were assayed.

Differentiation of LRRK2 and Control 4 iNPCs was done by Dr Francesco Capriglia, and Parkin and Control 5 iNPCs were differntiated by Dr Alexander Bury and Nikolaos Stefanidis.

Table 2.8. iDNLs differentiation media composition

Day of Differentiation	Factors	Concentration
1-2	DAPT	2.5 µM
3-10	SAG FGF8	0.5 µM 16.5 ng/mL
11-27	BDNF GDNF TGF dcAMP Ciprofloxacin	30 ng/mL 30 ng/mL 75 ng/mL 2 mM 1 µg/mL

2.3 Molecular Biology Techniques

2.3.1 Phosphorylation of alpha-synuclein

Phosphorylation of alpha-synuclein (αSyn) was carried out according to a published protocol (Fauvet and Lashuel, 2015). This method uses the polo like family of kinases, PLK3, which specifically phosphorylates αSyn at S129 (Mbefo et al., 2010). Recombinant αSyn protein was obtained from our collaborator Professor Michele Vendruscolo from University of Cambridge. In summary, phosphorylation buffer (50 mM HEPES, 1 mM $MgCl_2$, 1 mM EGTA, 1 mM DTT) was freshly prepared and combined with 230 µM αSyn along with 2 mM Mg-ATP and 1µL PLK3. The solution was thoroughly mixed by pipetting and incubated at 30°C for 12 hours without agitation. Phosphorylation of αSyn at S129 (P-αSyn) was confirmed by western

blotting using MJF-R13 alpha-synuclein phospho S129 antibody (ab168381). In the future, to assess the success of the phosphorylation reaction, mass spectrometry could be performed.

2.3.2 αSyn and p-αSyn in vitro aggregation

For aggregation assays, 70 µM αSyn or p-αSyn was incubated in Tris NaCl buffer (25 mM Tris, 0.1 M NaCl, pH 7.4) supplemented with 0.01% NaN_3 and 25 µM Thioflavin T (ThT) dye in a LoBind® Eppendorf tube. The samples were incubated at 37°C under constant agitation at 200 rpm (New Brunswick incubator) for up to 7 days. Aliquots were taken at regular time points and aggregation was measured by ThT fluorescence at 482 nm using the CLARIOstar Plus microplate reader. For aggregation of 488-αSyn (Anaspec) and 488-P-αSyn, a mixture of 10% 488-labelled protein and 90% unlabelled protein was prepared and incubated in aggregation buffer without ThT. The 488-αSyn conjugation process is random but is performed through conjugation to amines of lysines within the protein.

Aggregates taken at 48 hours and 7 days were visualised using SiMPull. For any functional assays, aggregates were made up following the same protocol without the addition of ThT dye.

2.3.3 αSyn and p-αSyn seeding in iDNLs

iDNLs were differentiated as previously described. At the end of differentiation, αSyn and p-αSyn aggregates taken at 48 hours and 7 days (prepared without ThT dye) were applied onto the cells at a final concentration of 1 µM. For 96-well plates, the aggregates were made up in PBS at a concentration of 10 µM, 10 µL of aggregate was then added to 90 µL of cell media. For 6-well plates, aggregate was directly added to the cell media to a final concentration of 1 µM. After 24 hours, the cell media was aspirated and replaced with fresh media. After a further 24 hours the cells were assayed.

2.3.4 SNCA Knockdown

iDNL's were differentiated in a 6-well plate. At the end of differentiation, cells were treated with a short hairpin RNA (shRNA) virus at multiplicity of infection (MOI) 20. The shRNA was designed to target SNCA and reduce expression of αSyn. The shRNA sequence contained 48 bp: ACCAAAGAGCAAGTGACAAATCTCGAGATTTGTCACTTGCTCTTTGGT (21 bp target sequence, 6bp loop sequence, 21 bp guide sequence). Once inside the cell, shRNA triggers RNA interference and degradation of SNCA mRNA, to reduce gene expression. After 24 hours, the

media containing virus was removed and replaced with viral-free neuron media. 5 days post-shRNA treatment, cells were used for further analysis. Transductions were performed by Dr Francesco Capriglia.

2.3.5. Meso Scale Discovery assay

Meso Scale Discovery (MSD) ELISA was carried out in collaboration with the University of Cambridge. Briefly, MJFR1 capture antibody was immobilized on the surface of the plate overnight. Plates were then blocked with blocking solution for one hour at room temperature with shaking. Blocking solution was then removed and samples were added for at least one hour at room temperature with shaking. After one hour, samples were washed three times with PBST before adding biotin anti-human-synuclein antibody for detection of total αSyn, and biotin EP1536Y for detection of phosphorylated serine 129 αSyn, mixed with SULFO-TAG streptavidin. After one hour incubation with shaking, the plate was washed three times with PBST, before MSD read buffer was applied and the signals were detected using a MESO QuickPlex SQ 120 multiplexing imager.

2.4 Biochemical Techniques

2.4.1 Cell lysis

For SiMPull assays and Western blotting, iDNLs were lysed at the end of differentiation and after treatment. Cell media was removed from 6-well plates containing neurons and subsequently washed with PBS to remove serum. Then ice-cold lysis buffer (20 mM Tris-HCl pH 7.4, 150 mM NaCl, 1% TritonX-100, 10% glycerol, supplemented with 1mM EDTA, 1mM PMSF, 1 mM PIC) was applied to each well and cells were scraped and collected into 1.5 mL LoBind Eppendorf tubes. Each sample was needled 10 times using 25-gauge needles, and then incubated on ice for 10 minutes. Cell lysates were then centrifuged at 14,000 g for 5 minutes at 4°C. The resulting supernatant containing soluble proteins was transferred into a new tube, and the pellet was discarded. Total protein concentration of the cell lysate was determined using the Pierce™ BCA Protein Assay Kit.

2.4.2 Bicinchoninic acid (BCA) Protein Assay

To determine total protein concentration of cell lysates, the Pierce™ BCA Protein Assay was used. This was carried out according to manufacturer's instructions. Briefly, BSA standards were prepared in PBS to generate a standard curve, and samples were diluted to an

appropriate concentration (1:10). 25 µL of standard or sample was applied to each well, in triplicate, of a clear 96-well microplate, and 200 µL working reagent (BCA reagent A and BCA reagent, B 50:1) was added to each well. The plate was placed on a shaker for 30 seconds to induce mixing, and then incubated at 37°C for 30 minutes. The microplate was then cooled to room temperature and absorbance of cell lysates and BSA standards were measured at 562 nm using the CLARIOstar Plus microplate reader. The BSA standard curve generated was used to determine the protein concentration of unknown cell lysates.

2.4.3 Sodium dodecyl sulfate polyacrylamide gel electrophoresis (SDS-PAGE)

SDS-PAGE gels were prepared using resolving and stacking gel (Table 2.9.) in a mini-PROTEAN Tetra Vertical Electrophoresis Cell (BioRad). APS and TEMED were added directly before pouring into a sealed casting chamber. Resolving gel was first poured into the casting chamber and isopropanol was added on top to prevent formation of bubbles. After the resolving gel had set, isopropanol was drained off, the stacking gel was added, and a 10-well or 15-well Mini-PROTEAN combs were inserted. Once the whole gel had set, the comb was removed, and wells were washed out with ddH_2O to prevent bubble formation. The gel was then transferred into the tank and the tank was filled with running buffer (50 mM Tris HCl, 1% SDS). Samples were then prepared for loading, at least 20 µg of protein was mixed with 4x Lamelli buffer (250 mM Tris-HCl pH 6.8, 8% SDS, 40% glycerol, 0.02% bromophenol blue, 5% beta-mercaptoethanol) and boiled at 95°C for 5 minutes to denature the proteins. The boiled samples were centrifuged to retain the sample at the bottom of the tube, and then loaded onto the gel along with 6 µL protein ladder in a single well. The electrodes of the tank were connected to a power pack and ran at 50 V for 30 minutes to pass through the stacking gel, and 150 V for 1 hour 30 minutes or until the dye front had reached the bottom of the gel. The gel was removed from the casting chamber and then prepared for immunoblotting.

Table 2.9. SDS-PAGE gel solutions

Reagent	**10% Resolving Gel**	**12% Resolving Gel**	**5% Stacking Gel**
H_2O	5.9 mL	5 mL	3.4 mL
30% Acrylamide mix	5 mL	6 mL	830 µL
1.5 M Tris (pH 8.8)	3.8 mL	3.8 mL	-
1 M Tris (pH 6.8)	-	-	630 µL

10% SDS	150 µL	150 µL	50 µL
10% APS	150 µL	150 µL	50 µL
TEMED	6 µL	6 µL	5 µL

2.4.4 Immunoblotting

Following protein resolution via SDS-PAGE, proteins on the gel were transferred to a nitrocellulose membrane. The gel was assembled into a sandwich with Whatman filter paper and a nitrocellulose membrane, which were all soaked in transfer buffer (50 mM Tris HCl, 20% methanol). The sandwich was then transferred into the Criterion Blotter and filled with transfer buffer. The transfer was run at 100 V for 30 minutes with an ice pack. After the transfer, the membrane was fixed for 30 minutes with agitation using 2% formaldehyde, and then blocked for 1 hour using blocking buffer (5% milk in TBST) with agitation. The membranes were then incubated with primary antibody in blocking buffer and incubated at 4°C overnight on a roller. The membranes were then washed 3 times for 10 minutes each in TBST. Fluorescent secondary antibodies (Table 2.4.) were diluted in TBST and incubated onto the membranes for 1 hour at RT, the membranes were protected from light. The membranes were then washed 3 times for 10 minutes each in TBST. Following the washes, the membranes were then imaged using the LI-COR Odyssey Fc imaging system.

2.5 Immunofluorescence and conventional microscopy

2.5.1 Immunocytochemistry

Cells plated in 96-well plates for immunofluorescence were fixed with 3.7% paraformaldehyde at the end of neuron differentiation. Cells were then permeabilized using 0.2% Triton-X 100 in PBS for 10 minutes. The cells were washed 3 times with PBS to remove any excess Triton-X 100. The cells were then blocked using blocking buffer (3% Horse serum in PBS with 0.1% Triton-X 100) at room temperature on a plate rocker for 1 hour. During blocking, primary antibodies were made up at the appropriate concentrations in blocking buffer (Table 2.3.), after the 1 hour incubation the blocking buffer was removed and primary antibody solutions were applied to the cells. The plate was then incubated at 4°C overnight on a plate rocker. The following day, the primary antibody solutions were removed, and cells were washed 3 times with PBS, with each wash being incubated for 10 minutes on a plate rocker. Then secondary antibodies were made up in blocking buffer at the appropriate

concentrations and applied to the cells (Table 2.4.). The plate was incubated at room temperature for 1 hour in the dark on a plate rocker. After the incubation, the cells were washed 3 times with PBS, each for 10 minutes, and then were incubated with nuclear counterstain Hoechst 33258 diluted in PBS. Finally, the cells were washed again 3 times with PBS and then stored in PBS at 4°C until imaging.

2.5.2 Mitochondrial dysfunction assays

For mitochondrial dysfunction assays, live imaging of cells stained with mitochondrial and lysosomal dyes (TMRM 80 nM, MitoTracker™ Green 1 µM, LysoTracker™ Deep Red 50 nM and Hoechst 33258 40 µM) determined mitophagy, the number of mitochondria and lysosomes. Media of live cells was removed, and dyes were applied. Mitochondrial and lysosomal dyes were made up in clear MEM without phenol red and incubated onto the cells for 1 hour at 37°C and 5% CO_2. After 1 hour, dyes were removed and clear MEM was added, the cells were imaged using the Opera Phenix High Content Screening System using the 40x water objective, at 37°C and 5% CO_2. At least 9 fields of view were captured per well.

2.5.3 Imaging of fixed and live cells

Imaging of fixed and live cells in 96-well plates was performed using the Opera Phenix High Content Screening System using a 40x water objective. For live imaging experiments, temperature was set to 37°C and CO_2 5%. For image acquisition, 4 different excitation lasers were used depending on the antibodies and dyes in the assay, including 488 nm, 561 nm, 647 nm, and 405 nm. Each technical replicate includes three different wells imaged in at least 10 different fields of view per well, and each field of view contains a Z-stack of at least 5 planes.

2.4.4 Analysis of cell imaging data

All images taken on the Opera Phenix Imaging System were analysed using Harmony image analysis software. Analysis sequences were made based on the experiment. Briefly, Z-stacks were combined to generate a maximum projection of the cells and a basic flatfield correction was applied. Nuclei were detected and selected based on size, intensity, and morphology, to exclude dead cells. Next the cytoplasm was detected using either cytoplasm detection or whole image region detection.

For detecting the percentage of cells positive for iNPC or iDNL markers, the intensity of staining in the cytoplasm was detected and a threshold was established based on background

staining from secondary antibody-only controls. Cells with higher intensity staining than the threshold, were positive for the marker.

For quantifying αSyn spots within cells, spots within the αSyn channel were detected and selected for based on size, morphology, and intensity to eliminate any artefacts or background staining. The number of spots was then normalised to either image region or number of cells (based on nuclei staining).

For live imaging with mitochondrial and lysosomal dyes, the mitochondria and lysosomes were segmented based on MitoTracker™ Green/TMRM and LysoTracker™ Deep Red. The segmented mitochondria and lysosomes were then selected based on size and intensity to eliminate any artefacts and background staining. The selected staining was then used to quantify the number of mitochondria and lysosomes per cell. To calculate mitophagy, the colocalization of MitoTracker™ Green and LysoTracker™ Deep Red was used as a proxy for mitophagy measurement. These methods of measuring mitochondrial dysfunction have previously been published (Carling et al., 2020; Schwartzentruber et al., 2020; Rusilowicz-Jones et al., 2021).

2.5 Single Molecule Imaging

2.5.1 Coverslip Preparation for Single Molecule Pulldown assay

The single molecule pulldown coverslip preparation is outlined in Figure 2.1. First, coverslips were placed into a coverslip rack inside a glass beaker, and the coverslips were cleaned. The glass beaker was filled with Milli-Q H_2O and then placed into a water bath sonicator, where the slides were sonicated for 10 minutes. Milli-Q was removed and replaced with acetone before sonicating for a further 10 minutes. Finally, the slides were washed in methanol and sonicated for 10 minutes. Next, sonication with 1 M KOH for 20 minutes allows for etching and exposing hydroxyl groups for salinization. To remove traces of KOH, slides were then rinsed with milli-Q H_2O then methanol, before drying with N_2 flow. Slides were further cleaned of impurities by 30 minutes of argon plasma cleaning. The coverslip surface was then functionalized by amino-silanization chemistry; a mixture of (1.5:2.5:50) APTES (3-aminopropyl trimethoxysilane), acetic acid (acts as a catalyst for the reaction) and methanol (used as a solvent) was incubated onto the coverslips for 20 minutes with a 1-minute sonication every 10 minutes. Slides were then rinsed with methanol and Milli-Q H_2O, and

finally dried with N_2 flow. The cover slides were then transferred into a humid chamber, and a PDMS chamber integrated onto the surface of each slide. The next step involved passivating the amine-coated cover slide with mPEG-Succinimidyl Valterate to reduce any non-specific binding and biotinylated PEG to promote binding of target molecules. mPEG was dissolved in Milli-Q H_2O at 110 mg/mL and biotin-PEG was dissolved in Milli-Q H_2O at 100 mg/mL. mPEG and biotin-PEG are mixed in a 99:1 ratio, respectively. 9 µL of PEG mixture was added to each well, and an additional 1 µL of 1 M $NaHCO_3$ was added to each well to speed up the reaction. The incubation was run at 4°C overnight in a humid chamber. The next day, the slides were dried with N_2 flow, and the second round of surface passivation took place. $MS(PEG)_4$ Methyl-PEG-NHS-Ester was dissolved in Milli-Q H_2O at 10 mg/mL, and 9 µL applied to each well. To speed up the reaction, 1 µL of 1 M $NaHCO_3$ was added to each well. The incubation was run overnight at 4°C in a humid chamber. The next day, the slides were dried with N_2 flow and put in vacuum containers in -20°C freezer for long-term storage.

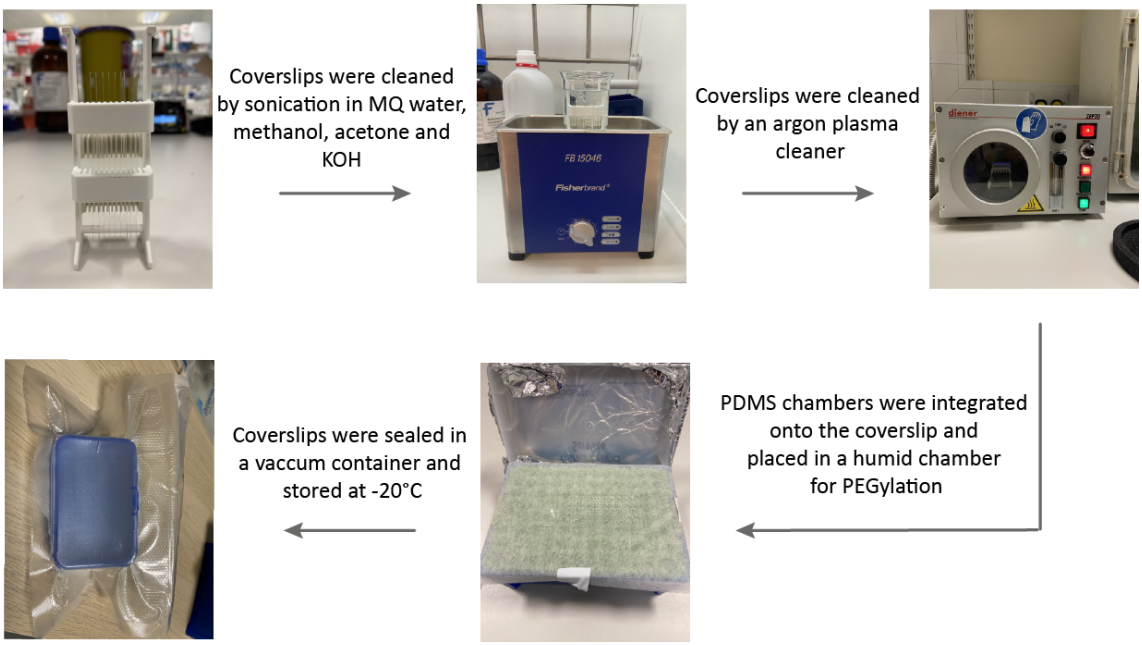

Figure 2.1. Outline of SiMPull coverslip preparation. Coverslips were placed into a rack inside a glass beaker and cleaned by sonication in MQ-water, methanol, acetone and KOH. Slides were dried and then cleaned in an argon plasma cleaner. After functionalization with APTES, the coverslips were placed in a humid chamber with a PDMS chamber for coating with PEG, Biotin-PEG and MS-PEG. After coating, the coverslips were placed in a vacuum sealed container and stored at -20°C.

2.5.2 Antibody conjugation for Single Molecule Pulldown assay

Unlabelled antibodies were modified for use in the SiMPull assay using the Lightning-Link conjugation kits (Abcam). Antibodies were conjugated with either Biotin, Alexa Fluor 488,

Alexa Fluor 568, or Alexa Fluor 637, according to the manufacturer's instructions. Briefly, 1 µL of modifier reagent was added to 10 µL of unlabelled antibody and mixed gently. The antibody-modifier mix was then pipetted onto the lyophilized conjugation mix and gently mixed. This mixture was then incubated in the dark overnight to facilitate conjugation. After incubation, 1 µL of quencher was added to deactivate any unbound label and gently mixed. The labelled antibodies were then ready to use after 5 minutes. The labelled antibody was then stored at 4°C for up to 18 months.

2.5.3 Single molecule pulldown assay

Prepared coverslips were taken out of the -20°C freezer 1 hour prior to starting. After the coverslip had reached room temperature, it was transferred into a humid chamber. For biotin-neutravidin linkage, neutravidin was diluted in PBST (0.05% Tween in PBS) at 0.2 mg/mL and added to each well for 5 minutes (Figure 2.2.). The wells were then washed twice with PBST and once with 1% Tween in PBS. The biotin capture antibody (syn211 biotin-conjugated) was immobilised onto the coverslip surface through biotin-neutravidin linkage, the antibody was diluted to 10 nM in PBS-BSA (0.5% BSA in PBS) and incubated on each well for 10 minutes. Each well was then washed twice with PBST and once with 1% Tween in PBS. Samples (diluted cell lysate, in vitro aggregates) at the appropriate dilution were then applied to the wells and incubated in the humid chamber for at least 1 hour. During incubation, imaging antibodies (Table 2.3.) were diluted to either 5 nM or 10 nM in PBS-BSA. After sample incubation, each well was washed twice with PBST and once with 1% Tween in PBS. Imaging antibodies were then applied onto the wells and incubated for 30 minutes protected from light. During incubation, a fresh coverslip was cleaned of impurities by plasma argon cleaning for 20 minutes. After incubation with imaging antibody, each well was washed twice with PBST. A fresh gasket was placed onto the top of the coverslip, and 8 µL of PBS was pipetted into each well. The coverslip was sealed with the second argon cleaned coverslip, and then imaged using the Nikon Ti2 TIRF microscope.

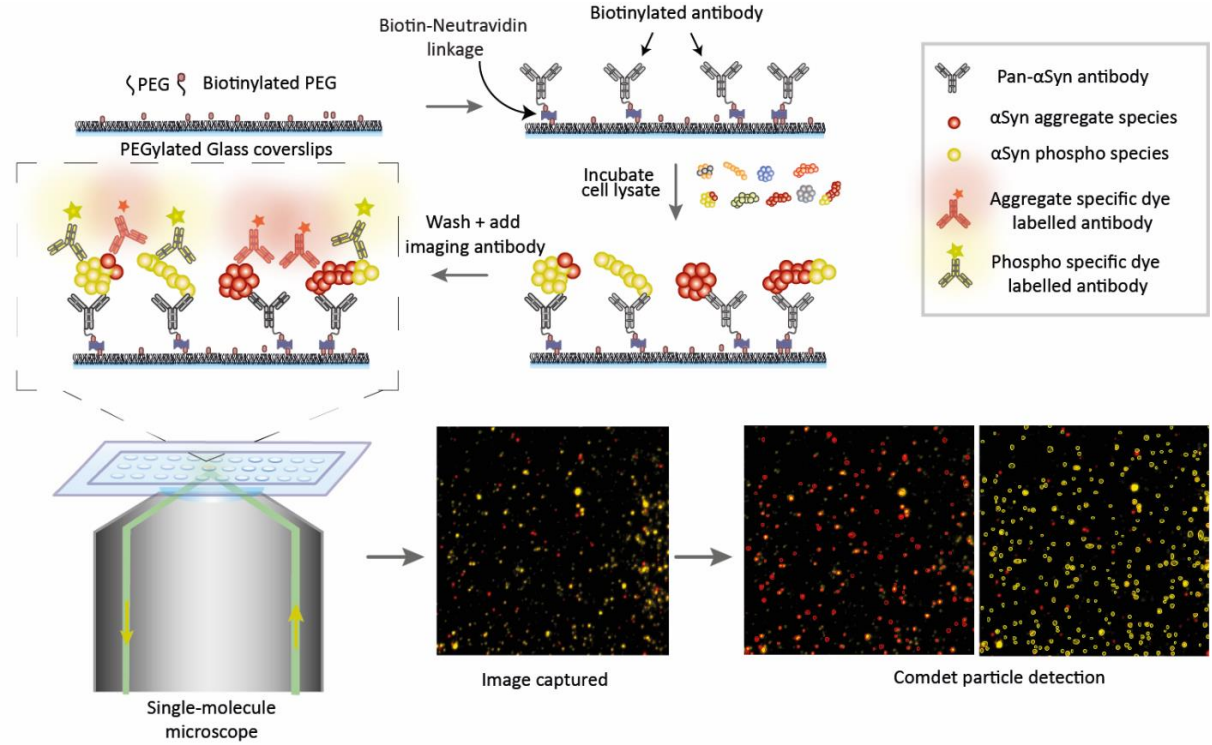

Figure 2.2. Schematic of Single Molecule Pulldown assay (SiMPull). Biotinylated antibodies are immobilized on PEGylated glass coverslips using a biotin-neutravidin linkage. Cell lysate is then incubated onto the coverslip, and αSyn captured through binding to the immobilized antibody, excess lysate is washed away. Any αSyn captured is then imaged using specific dye-labelled antibodies. Images are acquired using a single-molecule microscope and then analysed using ComDet Fiji Plugin.

2.5.4 Membrane permeabilization assay

Vesicle preparation and the membrane permeabilization assay were carried out according to a previously published protocol (Flagmeier et al., 2017). Vesicles were prepared by ten freeze-thaw cycles using a mixture of various phospholipids: phosphatidylcholine and biotinylated phosphatidylcholine (100:1), phosphatidylethanolamine, phosphatidylinositol, phosphatidylserine and cardiolipin. They were combined in different ratios to increase the cardiolipin content and mimic the mitochondrial membrane (Table 2.10.).

Table 2.10. Lipid composition for vesicles

Lipid	0% CL vesicles	10% CL vesicles	20% CL vesicles
Phosphatidylcholine (PC)	50%	45%	40%
Phosphatidylethanolamine (PE)	40%	35%	30%
Phosphatidylinositol (PI)	5%	5%	5%
Phosphatidylserine (PS)	5%	5%	5%

Cardiolipin (CL)	0%	5%	10%

The lipid mixture was then hydrated in HEPES buffer containing Cal-520 dye. The Cal-520 filled vesicles were then immobilised onto SiMPull coverslips using neutravidin-biotin linkage, as previously described. Imaging was carried out using the home-built TIRF microscope. Firstly, the immobilised vesicles were incubated in Ca^{2+} buffer, excitation of Cal-520 was at 488 nm and fluorescence was captured, this is the negative control blank fluorescence (Figure 2). Then the immobilised vesicles were incubated with sample (αSyn aggregate) for 20 minutes and then fluorescence was imaged again. The samples were then removed, and Ionomycin was added as a positive control to observe complete vesicle permeabilization. For the negative control, sample and positive control, the exact same areas were imaged for direct comparison. The calcium influx caused by αSyn aggregate was calculated using the following equation;

$$Calcium\ influx = \frac{\text{Sample fluorescence} - \text{Blank fluorescence}}{\text{Ionomycin fluorescence} - \text{Blank fluorescence}}$$

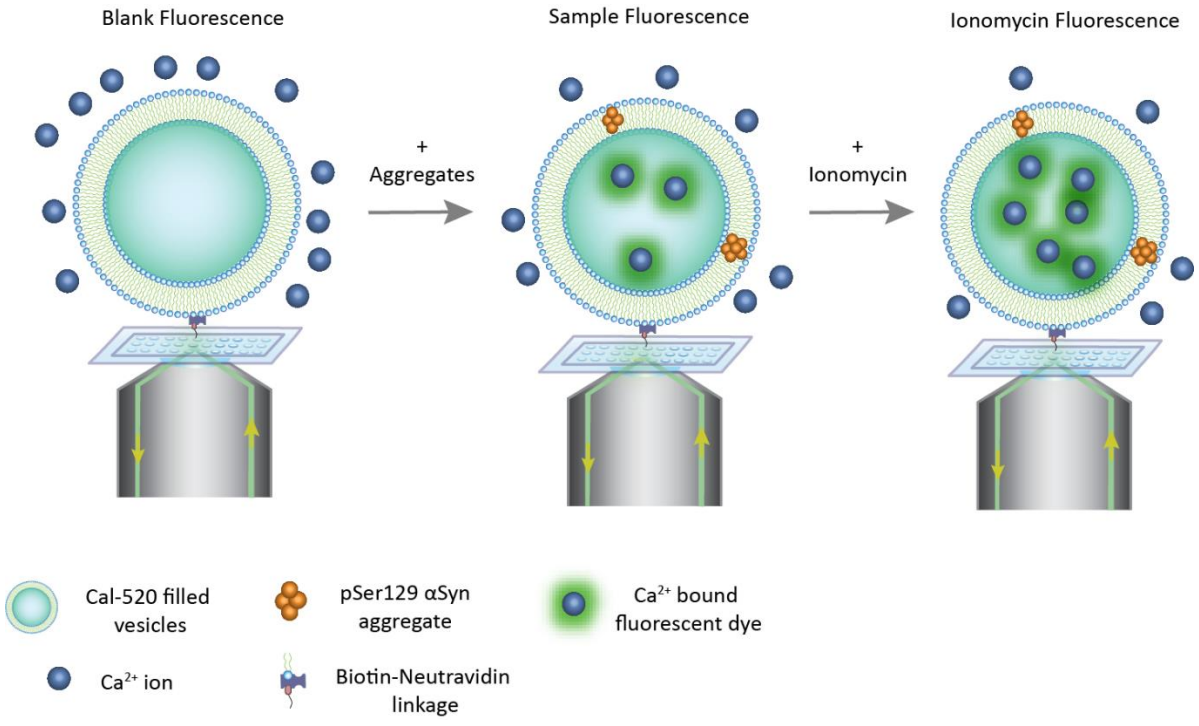

Figure 2.3. Schematic of the membrane permeabilization assay. Vesicles containing Cal-520 dye were immobilised onto PEGylated coverslips through biotin-neutravidin linkage. A Ca^{+} buffer was added to the vesicles and a blank fluorescence was measured using a 488 nm laser. Sample was then added and fluorescence of the same field of view was measured. Finally, positive control ionomycin was added to measure maximum fluorescence.

2.5.5. Fluorescent nanosphere generation

For fluorescent nanosphere experiments, 30 nm nanospheres were resuspended in 50 mM MES buffer pH 6.0 with gentle pipetting and 30 minutes of sonication to remove clumping. Monomeric αSyn and p-αSyn were diluted in the correct ratios in MES buffer to a final concentration of 5 µM and added to the nanospheres on ice. The amount of protein required to ensure a complete covering of the nanosphere was determined. The protein and nanospheres were incubated for 15 minutes on ice, and then EDC solution was added to a final concentration of 1 mg/mL. The pH of the solution was adjusted to 6.5, and samples were incubated overnight at 4°C. Glycine was then added to a final concentration of 0.1 M to quench the reaction. The mixture was then sonicated for 15 minutes on an ice slurry. The nanosphere-protein mixtures were then centrifuged at 10,000 g, followed by a PBS wash and a 15-minute sonication on ice, the PBS wash and sonication was repeated three times. Finally, the protein-conjugated nanospheres were resuspended in PBS and stored at 4°C.

The nanospheres were sonicated on ice for 30 minutes before resuspending in PBS. Then five times excess monomeric αSyn or p-αSyn or their ratios, to induce aggregate formation overnight at 4°C quiescent conditions. The aggregate-nanosphere mixtures were stored at 4°C protected from light and used within 36 hours.

To ensure nanospheres have uniform protein coating, BCA assays were carried out. All fluorescent nanosphere synthesis was carried out by other members of the lab.

2.5.6. Total internal reflection fluorescence (TIRF) microscopy

Imaging was carried out on a custom-built total internal fluorescence (TIRF) microscope based on a Nikon Ti2 Eclipse platform (Figure 2.4. A), which included a perfect focus unit. The microscope setup is depicted in Figure 2.4. B. In summary, laser beams at wavelengths of 405 nm, 488 nm, 561 nm, and 638 nm were filtered through a neutral density filter to adjust the power of the lasers, expanded with lenses and circularly polarised using a ¼ wave plate. A beam shaper was employed to transform the gaussian beam into a top-hat beam to allow even illumination. The lasers were then focused onto the back focal plane of a 100x TIRF NA 1.49 oil-immersion objective lens. Laser emission was passed back through the objective and separated from the excitation light by a beam splitter. The laser emission was then passed through a bandpass filter and imaged using a sCMOS camera. All images were captured using the open-source software Micro-Manager. For each biological replicate, at least 9 fields of

view were imaged, with 50 frames collected per field of view each with an exposure time of 50 ms.

TIRF microscopy relies on the angle of the incident light to visualise single molecules at a higher resolution than conventional microscopy. The incident light can be adjusted so that it either refracts through the second medium or reflects at the interface back into the first medium. The critical angle (θc) is the point at which lights refraction direction becomes parallel to the interface. At angles larger than the critical angle, the light is reflected into the first medium causing total internal reflection (Figure 2.4. C). This means no light is being passed through the second medium, however the reflected light generates an electromagnetic field adjacent to the interface known as the evanescent field. This field decays in intensity with distance from the interface, allowing selective excitation of fluorophores at the surface. This results in a higher signal-to-noise ratio than conventional microscopy and allows for single molecules to be visualised.

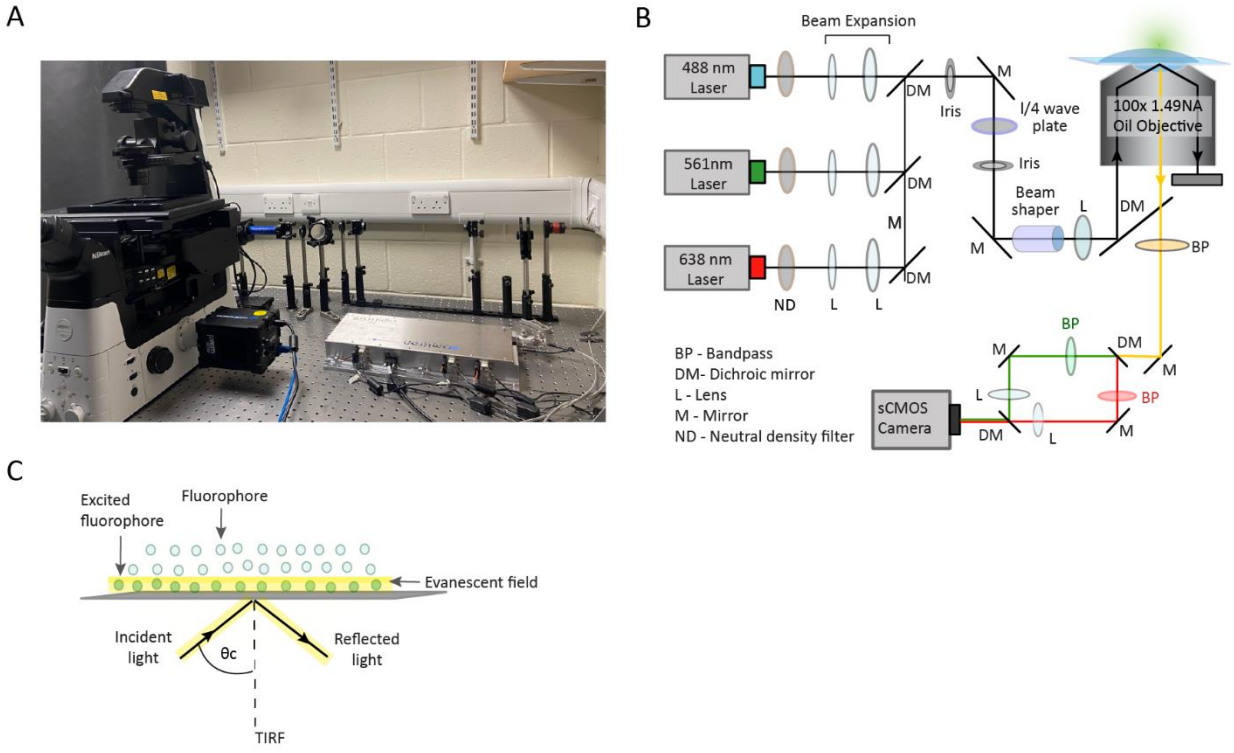

Figure 2.4. Total Internal Fluorescence (TIRF) Microscopy was used to visualise single molecules. A. Image of the TIRF microscope. **B**. Schematic of TIRF microscope setup, outlining the pathway of lasers through the objective to the specimen and back to the camera. **C**. The principles of TIRF microscopy. The incident light angle must be larger than the critical angle to allow for total internal reflection, creating an evanescent wave that travels through the specimen, causing only fluorophores at the surface to illuminate (green fluorophores), and fluorophores further away will not be excited. This produces a higher resolution image than conventional microscopy.

2.5.7. Analysis of SiMPull data

Each image acquisition comprised of 50 frames per field of view, firstly the 50 frames were averaged using an Image J macro. Averaged images were then merged if two-colour or three-colour imaging was performed, this created a composite image incorporating all three laser emissions. The number of fluorescent spots was then detected using a Fiji Plugin ComDet. For colocalization analysis, two spots in different channels were considered colocalised if their centre of mass was less than 3 pixels apart. Each pixel is 111 nm in size. The number of spots in each channel and number of colocalised spots was then normalised to total protein concentration if imaging cell lysate.

2.6 Statistical Analysis

Statistical analysis was conducted in Origin 9.0 (OriginLab). Data is displayed as the mean and error bars represent the standard deviation across biological replicates. To assess the significance between two data sets, an unpaired two-sample T test was used. To assess the significance between two data sets showing fold change, a paired T test was used. Values of statistical significance were defined as follows, $p < 0.05$ = *, $p < 0.01$ = **, $p < 0.001$ = *** and $p < 0.000$

Chapter 3. Unravelling endogenous αSyn dysfunction and aggregation in PD patient cells

3.1. Introduction

The aggregated and phosphorylated form of αSyn in postmortem tissue of patient brains is a hallmark of PD (Spillantini et al, 1997). However, understanding the complete aggregation pathway of αSyn is challenging due to its complexity. The aggregation pathway is a multistep process and involves the formation of highly heterogeneous species. These species differ in size, shape, aggregation state and post-translational modifications. Since these molecular features drive their biological functions, it is important to understand which species are most toxic to cells and how they drive toxicity. This complex, dynamic pathway provides only a limited view, solely studying postmortem human tissue provides a snapshot of the aggregation pathway, typically capturing the end stages of aggregation. This snapshot does not reveal the dynamic process of aggregation or how different αSyn species contribute to toxicity during the disease progression. To overcome these limitations, cell-based disease models are generally employed. These models offer a dynamic and controllable environment to study how different structural and molecular features of αSyn aggregates form and function, providing insights into their specific roles in PD pathology. This approach facilitates a deeper understanding of the toxic species and their mechanism of action, which are crucial for developing targeted interventions in PD.

Many studies have aimed to recapitulate disease phenotypes at a cellular level, with particular focus on αSyn pathology. The αSyn gene SNCA has been linked to both familial and sporadic PD, with point mutations and gene triplications being responsible for early onset and more severe course of disease. iPSCs carrying SNCA multiplications have been shown to contain double SNCA mRNA and αSyn protein which is maintained when generating several iPSC lines from the same patient (Devine et al., 2011). A triplication of the SNCA gene has been associated with αSyn dysfunction including increased oligomerization of αSyn, increased phosphorylated αSyn, and increased deposition of αSyn aggregates within the brain (Singleton et al., 2003; Miller et al., 2004; Lin et al., 2016). Less research has been done into αSyn dysfunction within sporadic disease. Although the etiology of sporadic PD remains largely unidentified, there have been many attempts to attribute sporadic cases to specific genetic factors. Studies have implicated variability in a major promotor (REP1) of the SNCA gene leading to increased

susceptibility of PD (Maraganore et al., 2006; Kay et al., 2008). These findings indicate a significant connection between αSyn and the pathogenesis of sporadic PD, further highlighting the importance of understanding αSyn's role in both sporadic and familial forms of disease.

Despite the phosphorylation of αSyn at serine 129 having huge pathological importance being a critical component of Lewy Bodies, and the formation of Lewy Bodies is a major hallmark of PD, the precise mechanisms by which pSer129 contributes to αSyn aggregation and Lewy body formation remain poorly understood. Phosphorylated αSyn aggregates are conformationally distinct from WT αSyn aggregates leading to functional differences (Ma et al., 2016, Parra-Rivas et al., 2023). Studies have shown that levels of pSer129 αSyn are significantly higher in PD neurons, including those with Parkin and LRRK2 mutations, sporadic PD cases, and SNCA triplications, compared to wildtype neurons (Lin et al., 2016). However, the process through which these aggregates form and contribute to disease progression is not fully elucidated.

Many studies have mimicked αSyn pathology within cells by inducing αSyn aggregation by the addition of preformed fibrils of αSyn. The addition of fibrils leads to the formation of Lewy Body-like aggregates within the cells, characterised by insoluble pSer129 αSyn and Lewy Body markers such as p62 and ubiquitin (Mahul-Mellier et al., 2020; Tanudjojo et al., 2021). The Lewy Body-like inclusions also sequester organelles including mitochondria and lysosomes (Mahul-Mellier et al., 2020). However, a spontaneous model of Lewy body formation – one that does not rely on external stressors or preformed fibrils – has not yet been developed. This represents a significant gap in understanding of the early stages of αSyn dysfunction, especially differentiating between sporadic and familial forms of PD.

iPSCs are an invaluable tool for investigating disease specific mechanisms within patient cells and have provided advances in understanding αSyn dysfunction in patients with distinct familial mutations. However, due to their pluripotent nature they do not retain key ageing features present within PD such as oxidative stress and mitochondrial dysfunction. The direct conversion method of generating from patient fibroblasts retain the ageing phenotype of the fibroblasts and can be used as a model to study neurodegenerative diseases (Gatto et al., 2021).

3.2 Aims and objectives.

The aims of this chapter were to develop a robust cell-based model of PD that enables the detailed investigation of αSyn aggregation, dysfunction, and associated toxicity. The specific objectives to achieve this aim are as follows:

1. Characterise the iNPC and iDNL cellular model.
2. Quantify the endogenous αSyn levels within cell lines with different disease mutations.
3. Characterise αSyn aggregates present within the cells to identify protein-protein interactions and the formation of Lewy Body-like aggregates.
4. Investigate mitochondrial function within the model.

3.3 Results

3.3.1. Characterising induced dopaminergic neuron-like cells.

To investigate αSyn within a human derived cellular model I have adopted the use of induced dopaminergic neuron-like cells (iDNLs). This model utilises fibroblasts taken from either PD patients or healthy controls, the fibroblasts have been directly reprogrammed into iNPCs and then differentiated into iDNLs. Within this study I have used a series of cell lines outlined in Table 2.6. Each PD cell line was paired with a matched control, these pairings were maintained as cell differentiation was carried out in a pairwise manner.

To confirm successful conversion of fibroblasts to iNPCs, the expression of two NPC markers Pax6 and Nestin was assessed within 6 of the lines used (Figure 3.1). Pax6 and Nestin are markers for CNS progenitor cells, that are reduced in expression when cells are differentiated into neuronal cells and have been widely used to characterise iNPCs (Dahlstrand, Lardelli and Lendahl, 1995; Zhang et al., 2010; Tian et al., 2013; Meyer et al., 2014). All lines showed over 85% positive cells for Nestin (Figure 3.1 B) and over 95% positive cells Pax6 (Figure 3.1 C).

Once the iNPCs were confirmed to express iNPC markers, I started differentiating the iNPCs into iDNLs. The protocol for generating dopaminergic iNeurons from iNPCs has previously been published, and within this study the cells expressed dopaminergic neuron markers and were functionally active, releasing dopamine and possessing an expected neuronal membrane potential (Schwartzentruber et al., 2020). At the end of the differentiation process each cell line used was probed for both pan-neuronal; Beta-III Tubulin (Tuj1) and

dopaminergic neuron markers; Tyrosine Hydroxylase (TH) and Dopamine Transporter (DAT) before use in any assays. There were no functional assays carried out in this thesis to characterise these specific cell lines, and therefore they are referred to as induced dopaminergic neuron like cells (iDNLs) instead of dopaminergic iNeurons. Immunostaining with antibodies for Tuj1, TH and DAT was carried out and the percentage of cells positive for the markers was calculated (Figure 3.2). All cell lines showed over 85% of cells positive for Tuj1 (Figure 3.2B). With the exception of Control 3, all cell lines were over 85% positive for TH (Figure 3.2C) and over 85% positive for DAT (Figure 3.2D). As shown in Figure 3.2A, Control 3 has a distinct morphology and grows in clusters of cells. This could explain the lower percentage of positive cells for both TH and DAT.

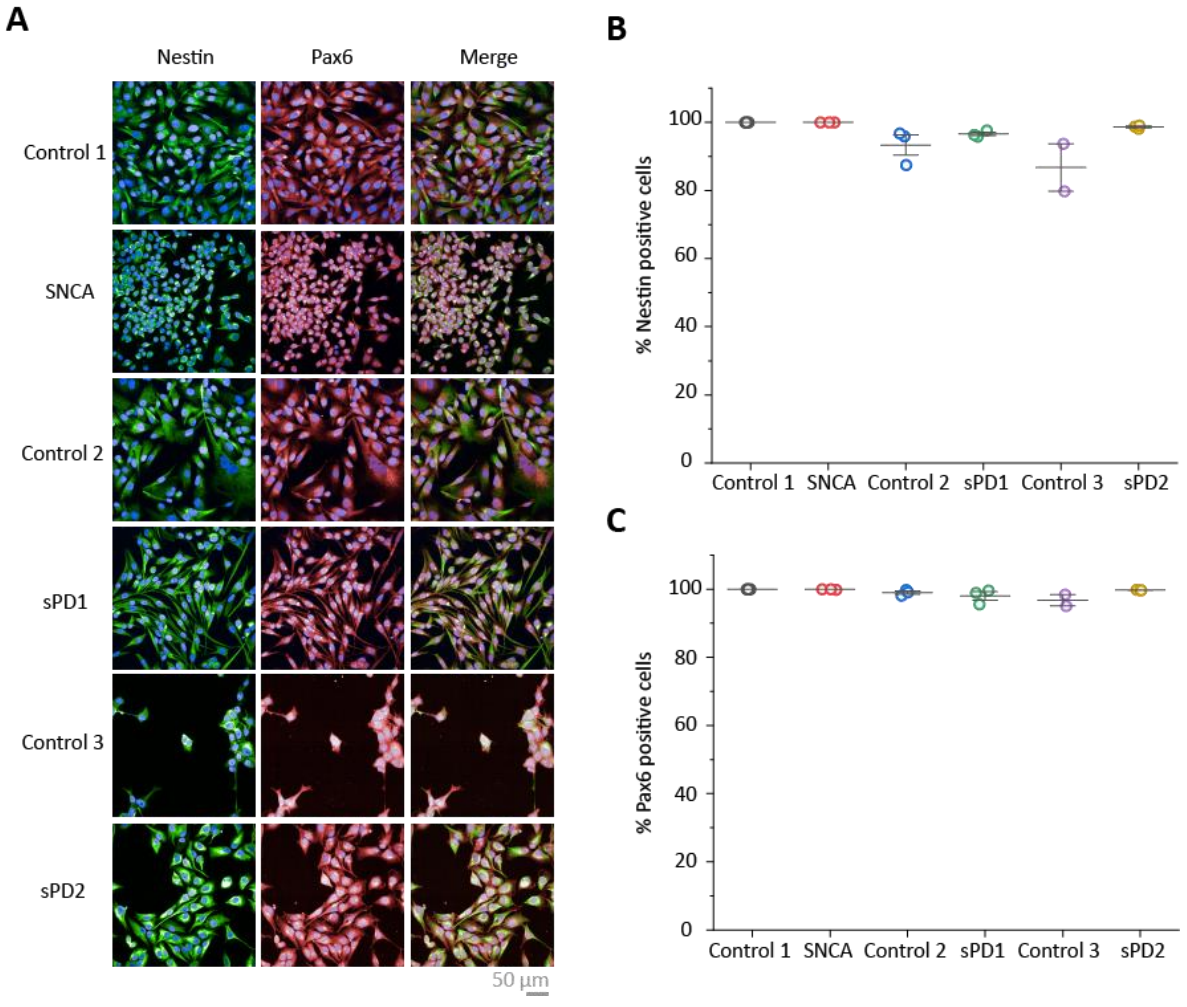

Figure 3.1. Characterisation of induced neuronal progenitor cells (iNPCs). A. Representative images from 3 PD cell lines and 3 healthy control cell lines, stained for Nestin (green) and Pax6 (red). **B**. Percentage of cells positive for Nestin. **C**. Percentage of cells positive for Pax6. Scale bar shows 50

µm. Graphs show three biological replicates for all lines except Control 3 which only contains two biological replicates. Bars represent mean ±SD.

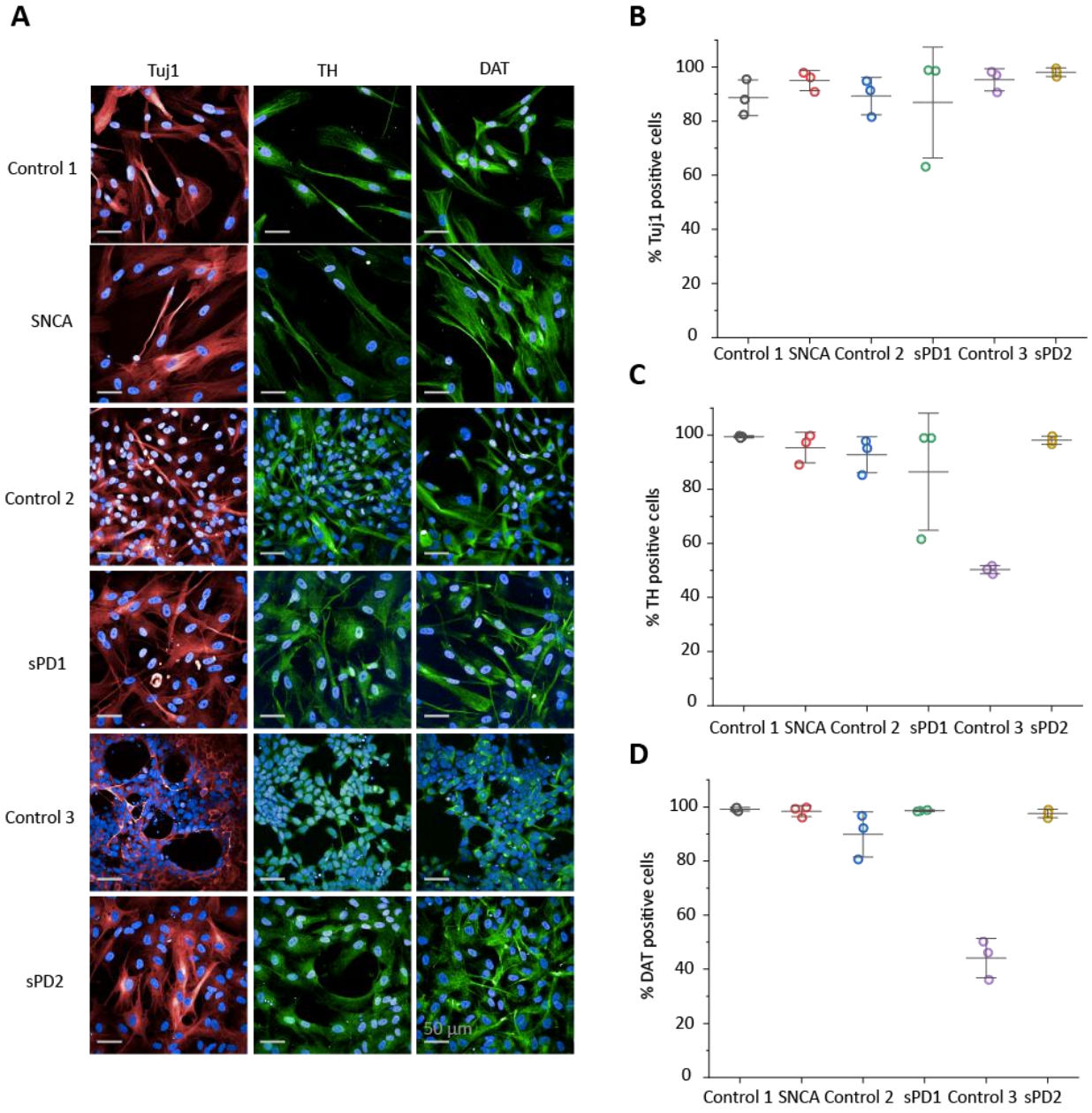

Figure 3.2 Characterisation of induced dopaminergic neuron like cells (iDNLs). A. Representative images of 3 Control lines and 3 PD lines at the end of differentiation into iDNLs, stained for pan-neuronal marker Tuj1, and dopaminergic neuron markers TH and DAT. **B.** Percentage of Tuj1 positive cell. **C.** Percentage of TH positive cells. **D.** Percentage of DAT positive cells. Scale bars show 50 µm. Graphs show three biological replicates, bars represent mean ± SD.

3.3.2. Quantifying endogenous αSyn in iDNLs

To determine the endogenous levels of αSyn within this model, the SNCA line and Control 1 line were differentiated from iNPCs into iDNLs, and immunocytochemistry was carried out with antibodies against total αSyn and pSer129 αSyn (Figure 3.3). For quantification of total αSyn, the total αSyn spots were counted and the sum of the total αSyn intensity calculated and normalised to the number of cells (Figure 3.3 A-C). The total αSyn staining was diffuse within the cell and there was no significant difference between the amount of αSyn spots per cell in Control 1 and SNCA lines. Additionally, SNCA had a higher mean αSyn intensity per cell than Control 1, although this increase was not statistically significant. Next, the amount of pSer129 αSyn was quantified in the two lines (Figure 3.3 D-E). SNCA exhibited a significant increase in pSer129 αSyn spots compared to Control 1. Additionally, there was significantly higher total pSer129 intensity per cell in SNCA compared to Control 1. This data shows that there may be no difference between total αSyn levels within the cells using this methodology, however there is an increase in specific conformations of αSyn (pSer129) which are related to pathology.

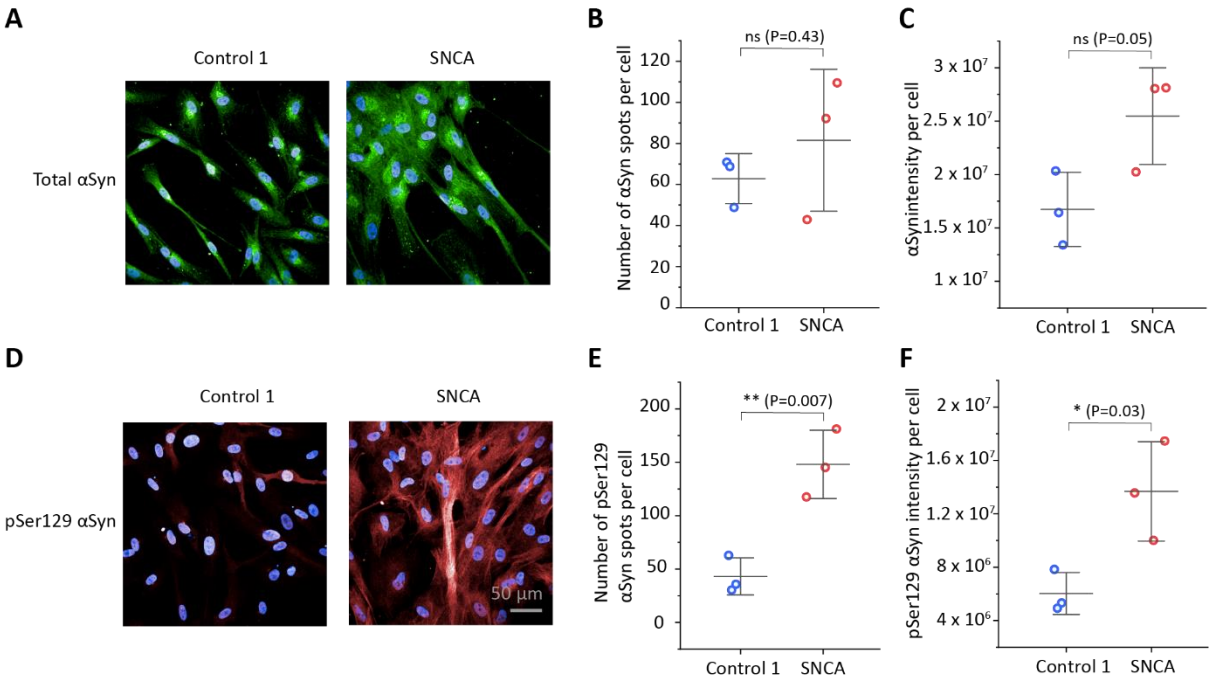

Figure 3.3. SNCA iDNLs contain a higher amount of phosphorylated αSyn than Control 1. Quantification of αSyn and pSer129 αSyn in iDNLs by immunocytochemistry. **A.** Representative images of Control 1 and SNCA stained with total αSyn antibody. **B.** The number of αSyn spots per cell in Control 1 (blue) and SNCA (red). **C.** Total αSyn intensity per cell. **D.** Representative images of Control 1 and SNCA stained with pSer129 αSyn antibody. **E.** Number of pSer129 αSyn spots per cell. F. Total pSer129 αSyn intensity per cell. Scale bar shows 50 µm. Each data point represents one biological repeat, the mean of three technical replicates. Bars represent the mean ± SD.

However, the limitations of immunocytochemistry, such as its qualitative nature and the diffuse staining pattern observed, it is difficult to accurately quantify αSyn levels within the cells. To gain an accurate understanding of the amount of αSyn and p-αSyn within the cells an electrochemiluminescence-based multiplex immunoassay (MSD) was carried out. A pan-αSyn capture antibody MJFR1 was used to capture all species of αSyn in the lysate, and detection antibodies anti-alpha synuclein (MSD) and anti-alpha-synuclein phospho S129 were used separately. Due to differences in antibody binding affinity, αSyn was quantified using count rather than concentration, for future studies it would be interesting to quantify ng/ml. The levels of αSyn in all iDNL lines were assessed (Figure 3.4). SNCA contained a significantly higher number of αSyn compared to Control 1 (223% increase), a difference not detected by immunocytochemistry as it provides mostly qualitative data (Figure 3.4 A). For the other cell lines, sPD1, sPD2, LRRK2 and the associated controls, there was no difference in levels of αSyn within the cells from corresponding matched controls (Figure 3.4 B-D). Parkin had reduced intracellular αSyn compared to its corresponding control (Figure 3.4 E). When the levels of p-αSyn within the cells were assessed, there was a significant increase of p-αSyn in SNCA compared to Control 1 (313% increase), as well as a slight increase in the mean number of p-αSyn in sPD1 compared to Control 2, however this was not significant when t-tests were used (Figure 3.4 F-G). For sPD2, LRRK2 and Parkin there was no increase in p-αSyn levels compared to Control 3, Control 4, and Control 5 respectively (Figure 3.4 H-J).

Next, the cell culture media was tested for the presence of both αSyn and p-αSyn secreted into the media (Figure 3.5). There is a consistent trend of higher levels of αSyn in the media in the PD cells compared to controls, however not significant in every line (Figure 3.4 A-E) Importantly, the levels of p-αSyn in the media are significantly increased in SNCA, sPD2, LRRK2 and Parkin, compared to their respective controls (SNCA: 168% increase, sPD2: 159% increase, LRRK2: 167% increase, Parkin: 115% increase) (Figure 3.5 F-J). The levels of p-αSyn still remain higher in sPD1 but a third biological repeat would need to be done to determine if the result is significant. These results show, even if there is no difference in the amount of intracellular αSyn, the PD cells consistently have an elevated amount of phosphorylated αSyn released into the media.

Finally, to reinforce the validity of using iDNLs as a model for PD, the levels of αSyn and p-αSyn were assessed in fibroblasts. All fibroblasts were cultured by Louise Heywood. iDNLs are

favoured as a model to investigate PD as they express significantly higher levels of αSyn compared to fibroblasts (Figure 3.6). Levels of αSyn and p-αSyn were tested in fibroblast media, but levels were too low for any detection. This highlights the advantage of using iDNLs for studying PD-related αSyn dysfunction.

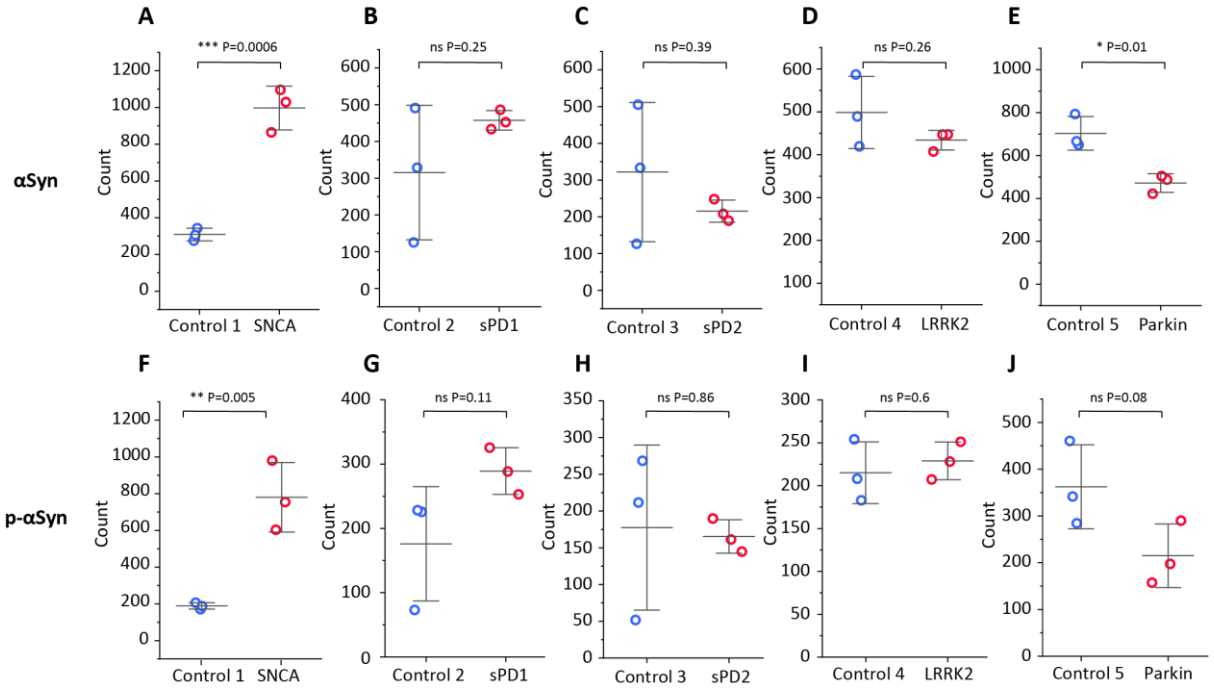

Figure 3.4. Measurement of intracellular αSyn and pSer129 αSyn levels by MSD assay. A-E. The levels of αSyn were quantified in all PD cells and corresponding healthy controls including SNCA (**A**), sPD1 (**B**), sPD2 (**C**), LRRK2 (**D**) and Parkin (**E**). **F-J**. The levels of pSer129 αSyn were quantified in all PD cells and corresponding healthy controls including SNCA (**F**), sPD1 (**G**), sPD2 (**H**), LRRK2 (**I**) and Parkin (**J**). Graphs show three biological replicates, bars represent mean ± SD. Paired cell lines were differentiated at the same time.Two-sample T tests were used to determine significance.

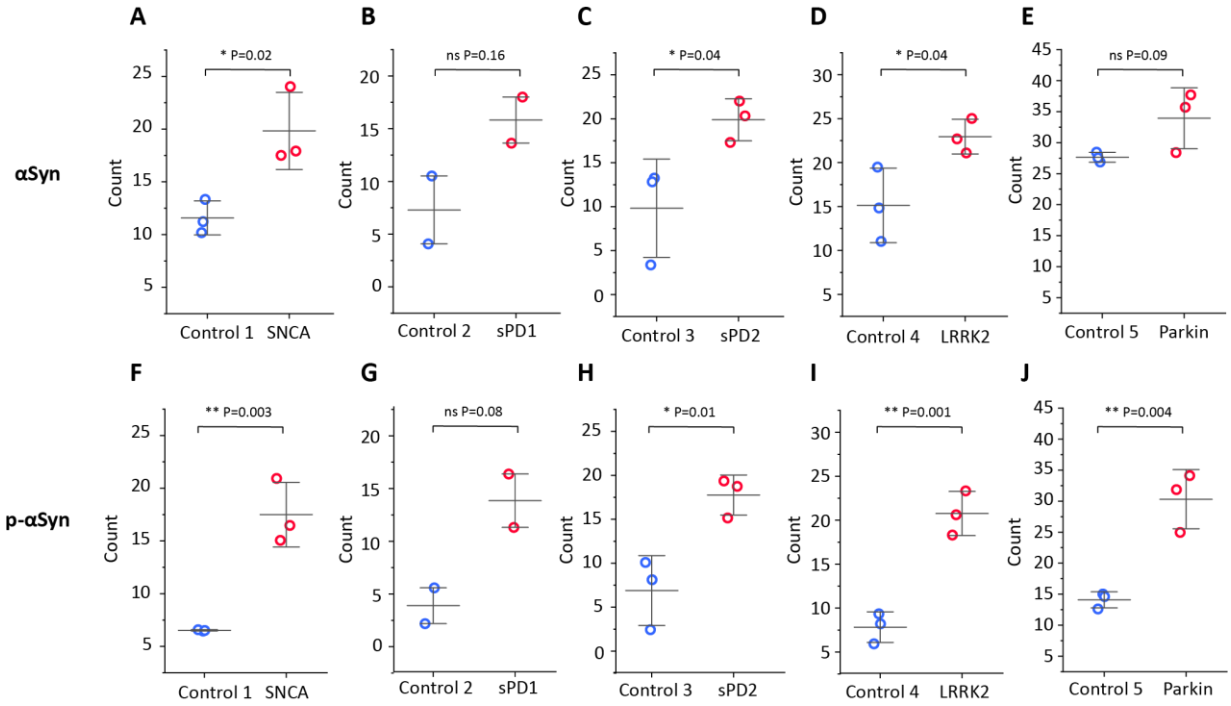

Figure 3.5 Measurement of extracellular αSyn and pSer129 αSyn levels by MSD assay. A-E. The levels of αSyn were quantified in all PD cell media and corresponding healthy controls including SNCA (**A**), sPD1 (**B**), sPD2 (**C**), LRRK2 (**D**) and Parkin (**E**). The levels of pSer129 αSyn were quantified in all PD cell media and corresponding healthy controls including SNCA (**F**), sPD1 (**G**), sPD2 (**H**), LRRK2 (**I**) and Parkin (**J**). Graphs show three biological replicates excluding B and G with only two biological replicates, bars represent mean ± SD. Two-sample T tests were used to determine significance.

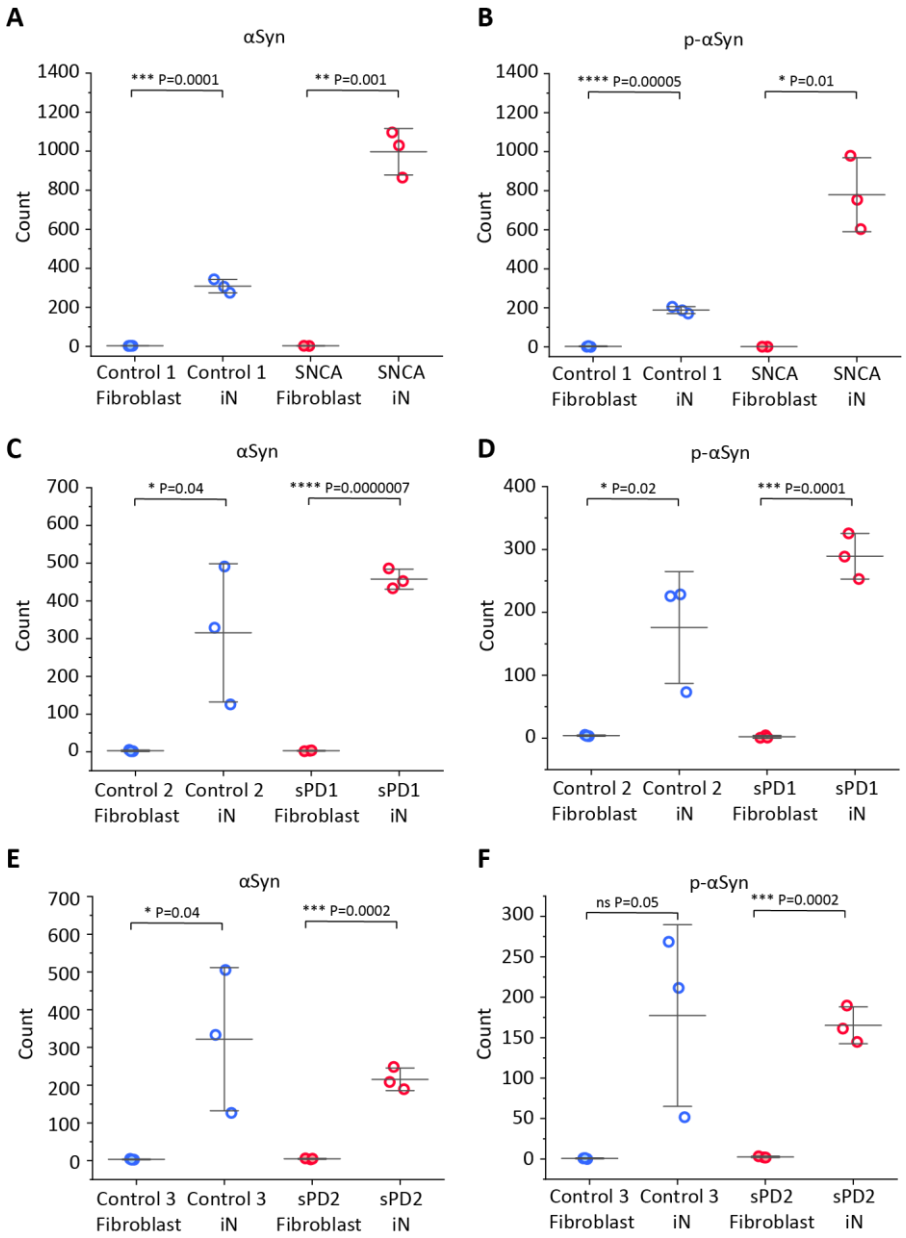

Figure 3.6. Quantifying the levels of αSyn and pSer129 αSyn in iDNLs and fibroblasts by MSD ELISA. The levels of αSyn and pSer129 αSyn were quantified by MSD ELISA for fibroblasts and iDNLs in Control 1 and SNCA (**A-B**), Control 2 and sPD1 (**C-D**), and Control 3 and sPD2 (**E-F**). Graphs represent three biological replicates excluding SNCA fibroblasts which show only two replications. Bars represent the mean ±SD, statistical significance was determined using two-sample T test. Fibroblasts were cultured by Louise Heywood.

3.3.3. Detection of single αSyn aggregates within PD iDNLs

The MSD results provide reliable quantification of the total αSyn and p-αSyn present in the cells. However, this method does not distinguish between different conformations of αSyn, such as monomers or aggregates, which are critical to understanding the diseases pathology. Since αSyn aggregates are known to be more toxic than monomeric protein, and aggregated phosphorylated αSyn is pathologically relevant as it is deposited in Lewy Bodies. It is not known whether an aggregated and phosphorylated form of αSyn may be better at differentiating disease and control lines. Given the importance of these aggregates in PD, it is crucial to detect which conformations of αSyn exist within the model. To achieve this, single molecule pulldown (SiMPull) was employed. This technique allows for the visualisation and characterisation of individual αSyn aggregates at the single molecule level.

To gain more information about the number of intracellular aggregated and phosphorylated αSyn, SiMPull was used to quantify individual aggregates of αSyn. At the end of iDNL differentiation the cells were lysed, and total protein concentration was determined using BCA. A pan-αSyn capture antibody (syn211) was immobilised onto the SiMPull coverslip surface, since this antibody detects all species of αSyn (Kumar et al., 2020). I used the pan-αSyn antibody to capture all αSyn containing species, regardless of their molecular features. This approach allows us to measure the full spectrum of αSyn forms that are present within cells, including different sizes, shapes, aggregation states and post-translational modifications. By using this broad spectrum pan-αSyn antibody, I ensure that I am not selectively capturing only specific conformations or states of αSyn, but rather getting a comprehensive view of all αSyn-related species in the model.

Then cell lysates were applied to the SiMPull slide and all αSyn present in the sample is captured. For detection of αSyn aggregates present within cell lysate two different antibodies were used in combination; αSyn aggregate antibody (Alexa Fluor 647) and pSer129 αSyn antibody (Alexa Fluor 594) and two-colour imaging was carried out using the single-molecule microscope. It is important to note, although the αSyn aggregate antibody is extensively shown to preferentially bind to specific aggregated conformations of αSyn by the scientific community (Sampson et al., 2016; Ludtmann et al., 2018; Elfarrash et al., 2019; Guo et al., 2020), it has been found to display some low binding affinity towards monomeric protein (Kumar et al., 2020).

The number of endogenous αSyn aggregates and pSer129 αSyn was first determined in Control 1 and SNCA iDNLs (Figure 3.7). For each well imaged, at least 9 fields of view were captured, and the number of spots in each field of view was detected using ImageJ macro ComDet3 and normalised to total protein concentration. SNCA displayed a significant increase in αSyn aggregates compared to Control 1 (Figure 3.7 C). There was also a higher of pSer129 αSyn in SNCA compared to Control 1 (Figure 3.7 D). To determine the number of aggregates that were also phosphorylated, colocalization analysis using a ComDet3 plugin (Fiji) was performed to detect colocalised spots from αSyn aggregate 647 nm channel and pSer129 594 nm channel. A higher number of these phosphorylated αSyn aggregates were present in SNCA compared to Control 1 (Figure 3.7 E). These findings suggest that SNCA triplication not only leads to an overall increase in αSyn aggregation, but also results in a higher proportion of pathogenic phosphorylated αSyn aggregates.

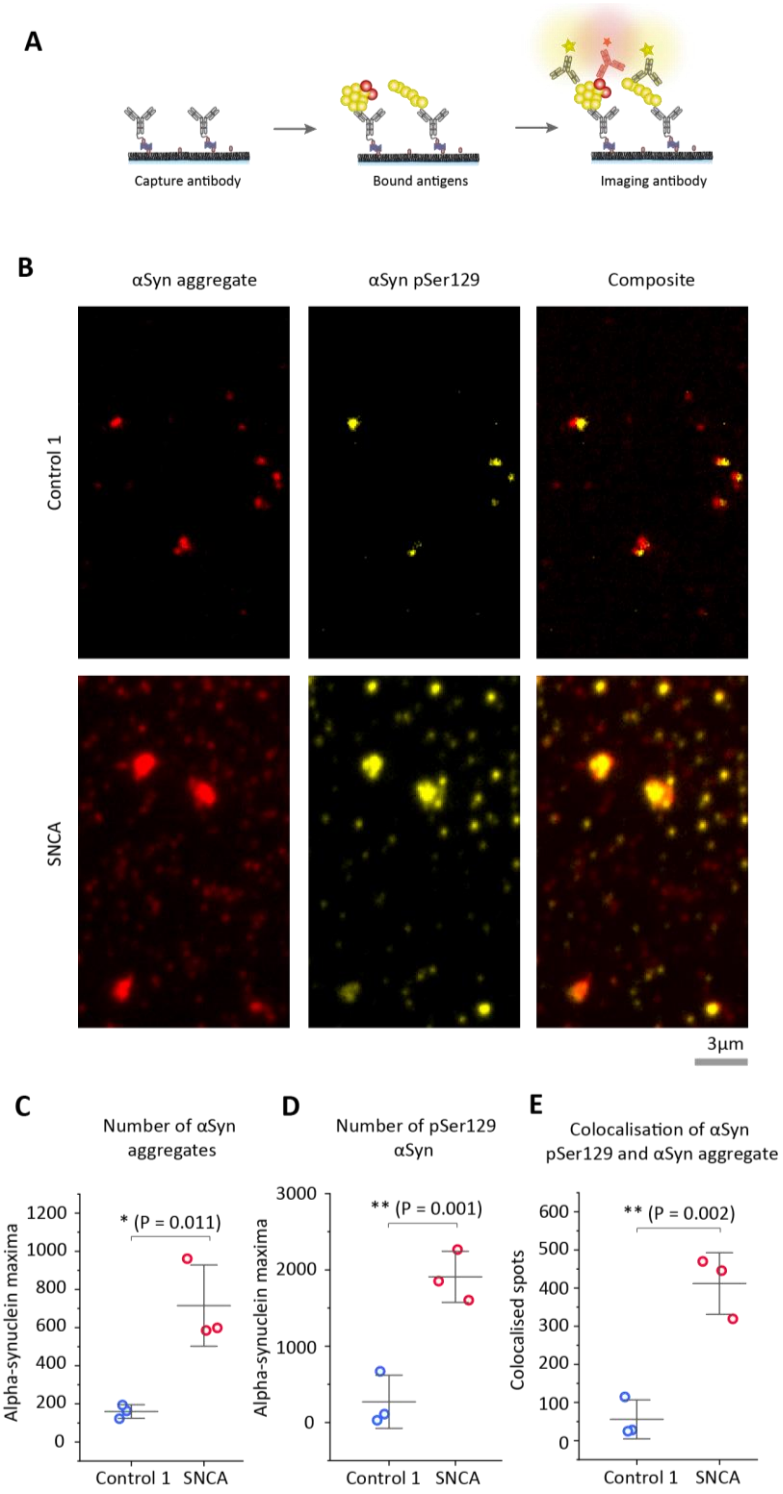

Figure 3.7. SNCA triplication iDNLs have increased aggregated and phosphorylated αSyn compared to healthy control iDNLs. A. Schematic of SiMPull assay. **B**. Representative SiMPull images of αSyn aggregate (red) and αSyn pSer129 (yellow) spots in Control 1 and SNCA. **C**. Quantification of αSyn aggregates in Control 1 (blue) and SNCA (red). **D**. Quantification of αSyn pSer129 in Control 1 (blue) and SNCA (red). **E**. Number of colocalised spots in Control 1 (blue) and SNCA (red). Data is normalised to total protein concentration. Graphs show three biological replicates, bars represent mean ± SD. Two-sample T tests were used to determine significance.

The αSyn phenotype was investigated in sporadic PD iDNLs to determine if they shared the same phenotype as SNCA, an enhanced number of αSyn aggregates and phosphorylated αSyn. The number of αSyn aggregates and pSer129 αSyn was assessed using SiMPull of sPD1 and Control 2 lysates (Figure 3.8 A). Although there was no difference in αSyn aggregate levels between Control 2 and sPD1, there was a large amount of variability particularly in Control 2 (Figure 3.8 B). There was significantly more of the pathogenic form of αSyn present in the sporadic line, shown by an increase in the number of pSer129 αSyn spots in sPD1 compared to Control 2 (Figure 3.8 C). Additionally, there was an increased amount of colocalised spots of αSyn which were aggregated and phosphorylated in sPD1 (Figure 3.8 D).

To confirm if these findings are replicated in multiple sporadic cells, two-colour SiMPull was carried out with Control 3 and sPD2 (Figure 3.9 A). There was no difference observed in the amount of αSyn aggregate, pSer129 αSyn and colocalised aggregate and pSer129, between Control 3 and sPD2 (Figure 3.9 B-D). This suggests the elevated phosphorylated αSyn levels found in SNCA and sPD1 are not maintained in every case of sporadic PD. This variability observed was expected between only two sporadic lines, and a larger number of sporadic lines would need to be investigated to draw strong conclusions.

Finally, the levels of αSyn aggregate were assessed in two more PD mutation lines. The number of αSyn aggregate and pSer129 αSyn was determined in LRRK2 and Control 4 iDNLs, and no difference was observed (Figure 3.10). Another PD line, Parkin, was investigated for the presence of pathological αSyn. Parkin and Control 5 were compared and the number of αSyn aggregate and pSer129 αSyn was determined (Figure 3.11). No difference was observed in the number of αSyn species between Parkin and Control 5.

This data indicates that the presence of elevated phosphorylated αSyn aggregates seen in SNCA and some sporadic lines like sPD1, might be specific to certain mutations or specific sporadic cases and not a universal feature of all PD based cellular models. These findings illustrate the complexity and heterogeneity of PD pathology, especially concerning αSyn aggregation and phosphorylation at the cellular level. They underscore the need for detailed investigations to fully understand the implications of αSyn pathology in PD.

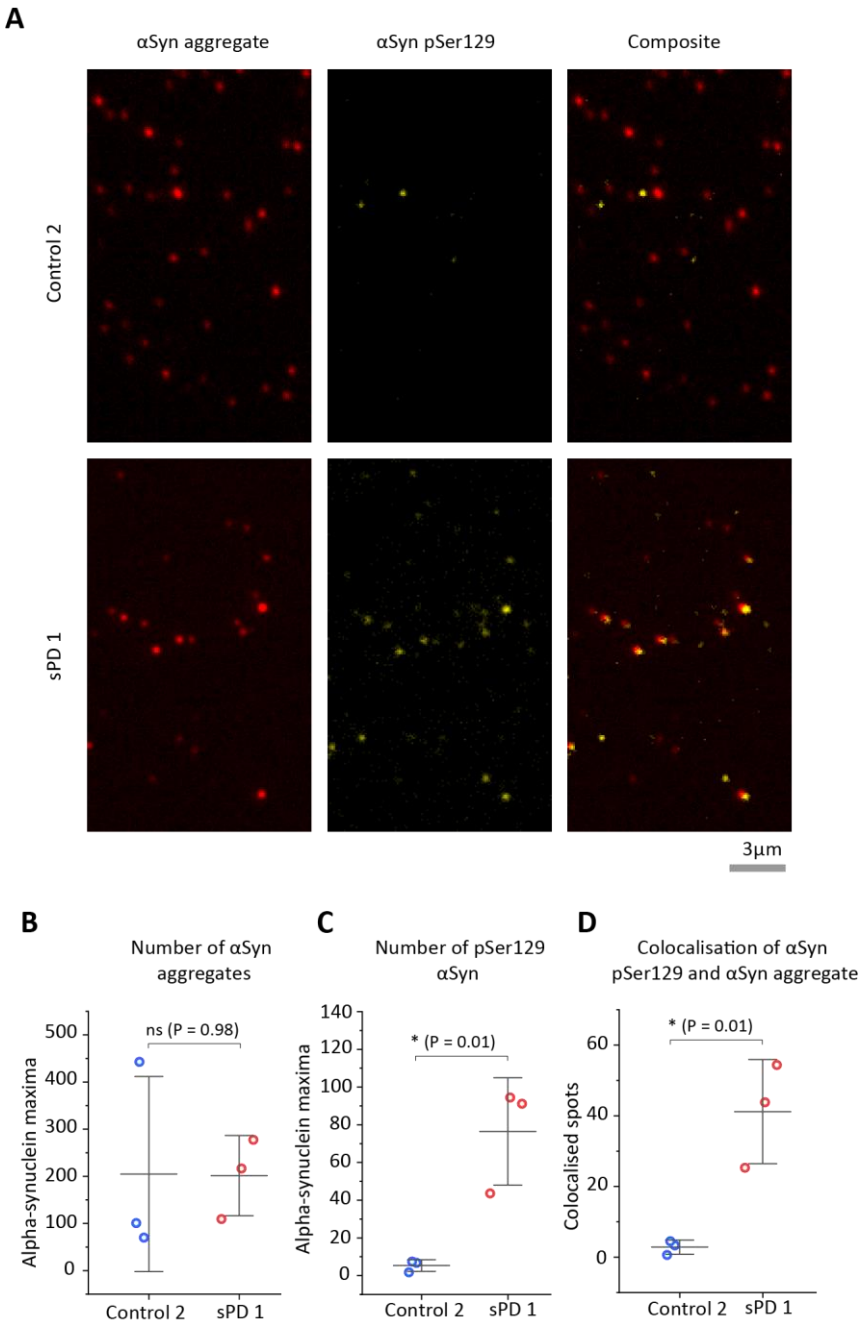

Figure 3.8. sPD1 iDNLs have increased phosphorylated αSyn and increased phosphorylated aggregates compared to healthy control iDNLs. A. Representative SiMPull images of αSyn aggregate (red) and αSyn pSer129 (yellow) spots. **B**. Quantification of αSyn aggregates, αSyn pSer129 and colocalised spots in healthy control (blue) and sPD (red). Data is normalised to total protein concentration. Graphs show three biological replicates, bars represent mean ± SD. Two-sample T tests were used to determine significance.

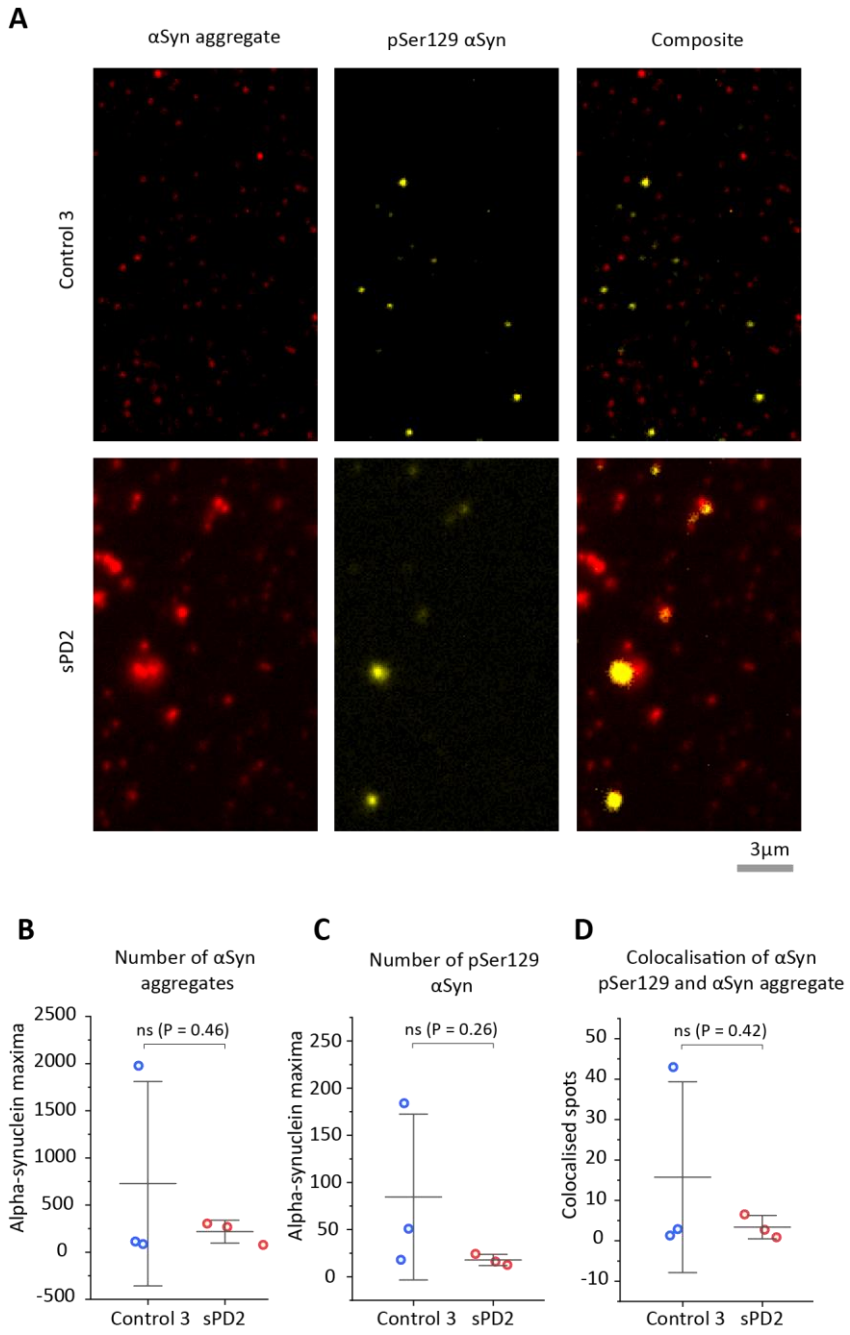

Figure 3.9. αSyn aggregates and phosphorylated αSyn levels are not significantly different in sPD2 and Control 3 iDNLs. A. Representative images of aggregated αSyn (red) and phosphorylated αSyn (yellow) in Control 3 and sPD2 iDNLs. **B.** Quantification of the number of αSyn aggregates in Control 3 (blue) and sPD2 (red). **C.** Quantification of the number of pSer129 αSyn in Control 3 and sPD2. **D.** Colocalization of αSyn aggregate and pSer129 αSyn in Control 3 and sPD2. Data is normalised to total protein concentration. Graphs show three biological replicates, bars represent mean ± SD. Two-sample T tests were used to determine significance.

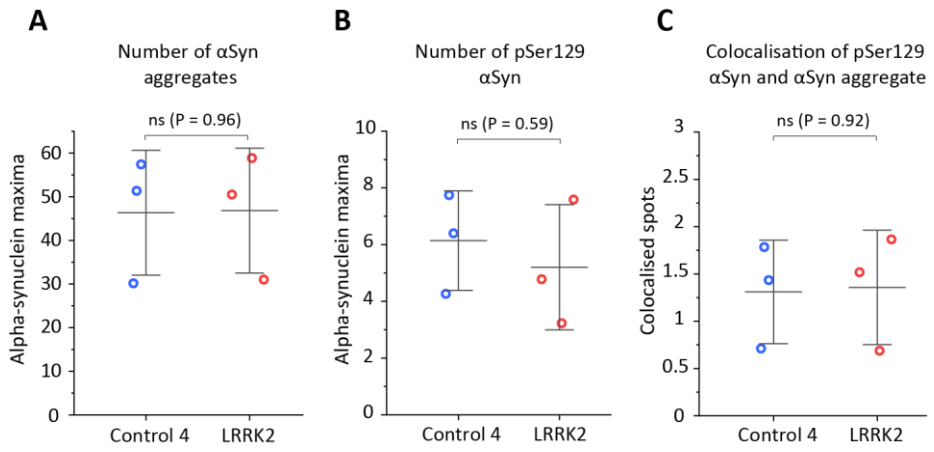

Figure 3.10. There is no significant difference in the number of αSyn aggregates and pSer129 αSyn in Control 4 and LRRK2. A. Number of αSyn aggregates in Control 4 and LRRK2. **B.** Number of pSer129 αSyn. **C.** Number of colocalised spots of pSer129 αSyn and αSyn aggregate. Graphs show three biological replicates, bars represent mean ± SD. Two-sample T tests were used to determine significance.

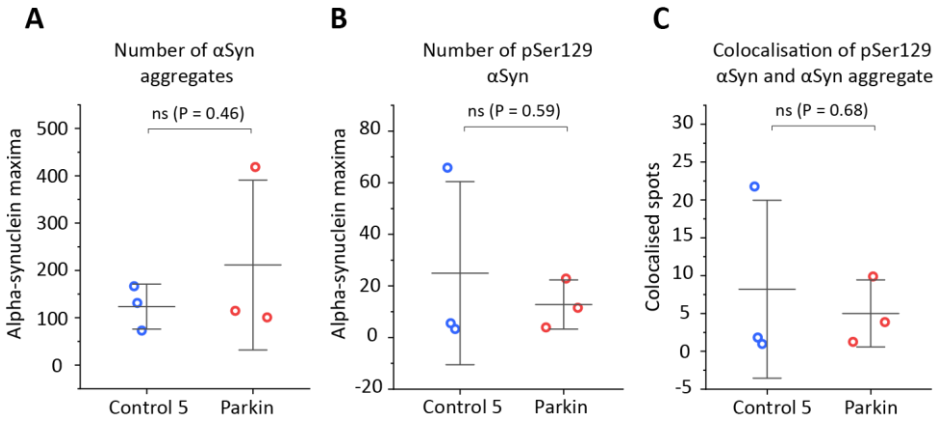

Figure 3.11. αSyn aggregate and pSer129 αSyn levels are not significantly different between Control 5 and Parkin. A. Number of αSyn aggregates in Control 5 and Parkin. **B.** Number of pSer129 αSyn. **C.** Number of colocalised spots containing both αSyn aggregate and pSer129 αSyn. Graphs show three biological replicates, bars represent mean ± SD. Two-sample T tests were used to determine significance.

3.3.4. αSyn spontaneously forms Lewy Body-like aggregates within cells.

The process of Lewy Body formation is a major hallmark of PD, and the main component of Lewy Bodies is aggregated αSyn and phosphorylated αSyn. Lewy Bodies from post-mortem tissue have shown to also contain many cellular proteins including mitochondrial proteins, lysosomal proteins, p62 and ubiquitin (Gai et al., 2000; Kuusisto, Parkkinen and Alafuzoff, 2003). Although studies have shown the formation of Lewy Body-like aggregates after addition of αSyn PFFs, the spontaneous Lewy Body formation has not yet been recapitulated in a cell model (Mahul-Mellier et al., 2020).

As this model displayed increased αSyn aggregates and phosphorylated αSyn within PD-derived cells, the aggregates were characterised further to detect the presence of Lewy Body-like aggregates by probing other protein interactions. To do this, tri-colour imaging was performed using the single molecule microscope. The same antibodies previously used were used (pan-αSyn to capture and αSyn aggregate and pSer129 αSyn for imaging) in addition to a 'Lewy body marker' antibody which was labelled with either CoraLite 488 or Alexa Fluor 488. Imaging was carried out the same as previously, however colocalisation was measured using either just two channels, or all three channels together.

Firstly, αSyn's interaction with mitochondrial proteins were measured in SNCA and Control 1. The presence of TOM20 within the αSyn aggregates was assessed (Figure 3.12 A-D). There were significantly more αSyn aggregates containing TOM20 in the SNCA iDNLs compared to Control 1. However, due to sample variability, there was no significant difference in pSer129 αSyn containing TOM20. The number of αSyn aggregates containing pSer129 αSyn and TOM20 were then quantified, and there was an increased number in SNCA iDNLs compared to Control 1. A second mitochondrial protein was also investigated for its interaction with αSyn, VDAC1 (Figure 3.12 E-H). There was a significant increase of αSyn aggregates containing VDAC1 in SNCA compared to Control 1. However, there was no statistically significant difference between phosphorylated αSyn-VDAC1 spots, and 3-colour colocalized aggregated phosphorylated αSyn-VDAC1 spots, although the trend suggests there are more of these αSyn species present within SNCA iDNLs.

Next, αSyn's interaction with lysosomal markers were investigated in SNCA and Control 1 iDNLs (Figure 3.13). The presence of LAMP1 within αSyn aggregates and pSer129 αSyn was investigated (Figure 3.13 A-D). SNCA showed increased αSyn aggregate colocalised with

LAMP1 compared to Control 1, and increased αSyn containing aggregate, phosphorylated αSyn and LAMP1. However, there was no significant difference between SNCA and Control 1 in the amount of pSer129 αSyn colocalised with LAMP1. Another lysosomal protein, LAMP2 was investigated for its interaction with αSyn (Figure 3.13 E-H). There was no difference in the number of αSyn aggregates containing LAMP2 and the number of pSer129 αSyn containing LAMP2 between SNCA and Control 1. However, there was significantly more αSyn aggregates that were phosphorylated and contained LAMP2 in SNCA compared to Control 1.

Finally, two major Lewy Body marker proteins were assessed for their presence within αSyn aggregates and pSer129 αSyn (Figure 3.14). I investigated the presence of αSyn in combination with ubiquitin (Figure 3.14 A-D). SNCA shows a trend of containing a higher number of αSyn colocalised with ubiquitin, both the aggregated and phosphorylated form. Finally, I found a significantly higher number of αSyn interacting with p62 in both aggregates and pSer129 αSyn in SNCA compared to Control 1 (Figure 3.14 E-H).

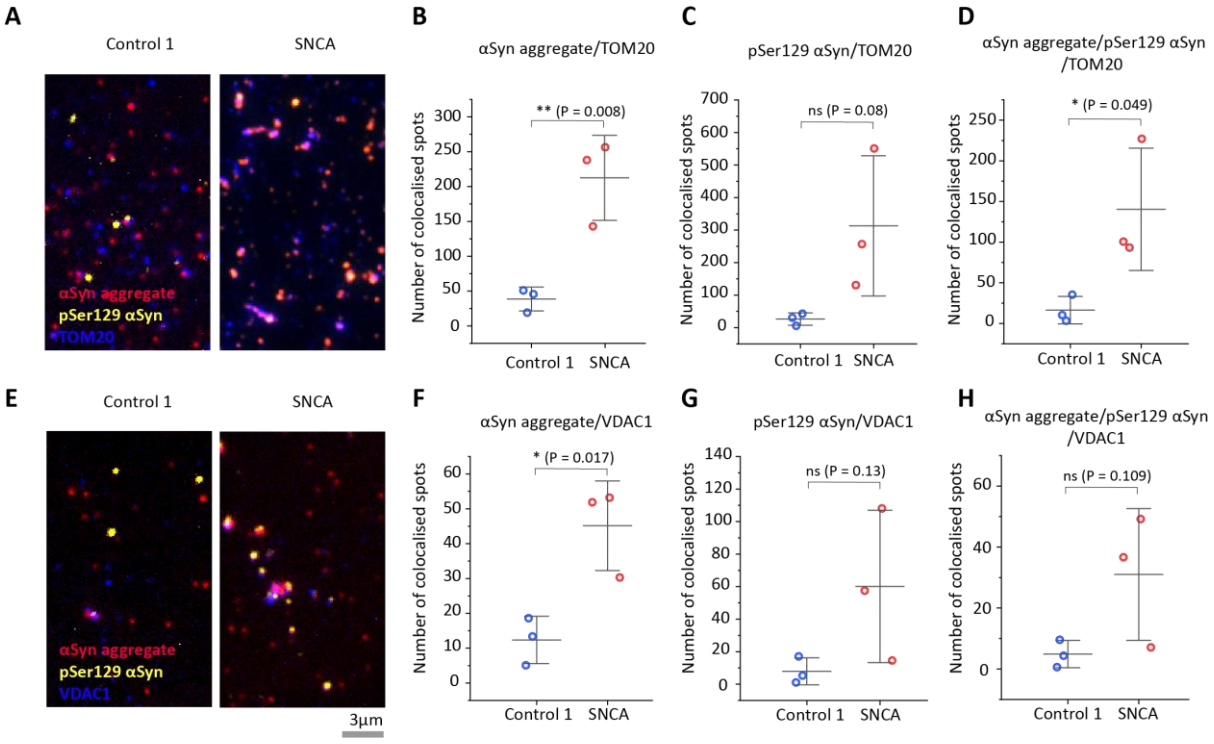

Figure 3.12. αSyn aggregates colocalise with mitochondrial proteins in SNCA iDNL's. A. Representative images of αSyn aggregate (red), pSer129 (yellow) and TOM20 (blue) in Control 1 and SNCA. **B-D.** The presence of αSyn colocalised with TOM20 was assessed and compared between SNCA and Control 1, including αSyn aggregate with TOM20 (**B**), pSer129 αSyn with TOM20 (**C**) and αSyn aggregate, pSer129 αSyn and TOM20 colocalised (**D**). **E**. Representative images of αSyn aggregate (red), pSer129 (yellow) and VDAC1 (blue) in Control 1 and SNCA. **F-H.** The presence of αSyn colocalised with VDAC1 was investigated, including αSyn aggregate colocalised to VDAC1 (**F**), pSer129 αSyn colocalised with VDAC1 (**G**) and αSyn aggregates that are phosphorylated and contain VDAC1 (**H**). Data is normalised to total protein concentration determined by BCA. Graphs show three biological replicates, bars represent mean ± SD. Two-sample T tests were used to determine significance.

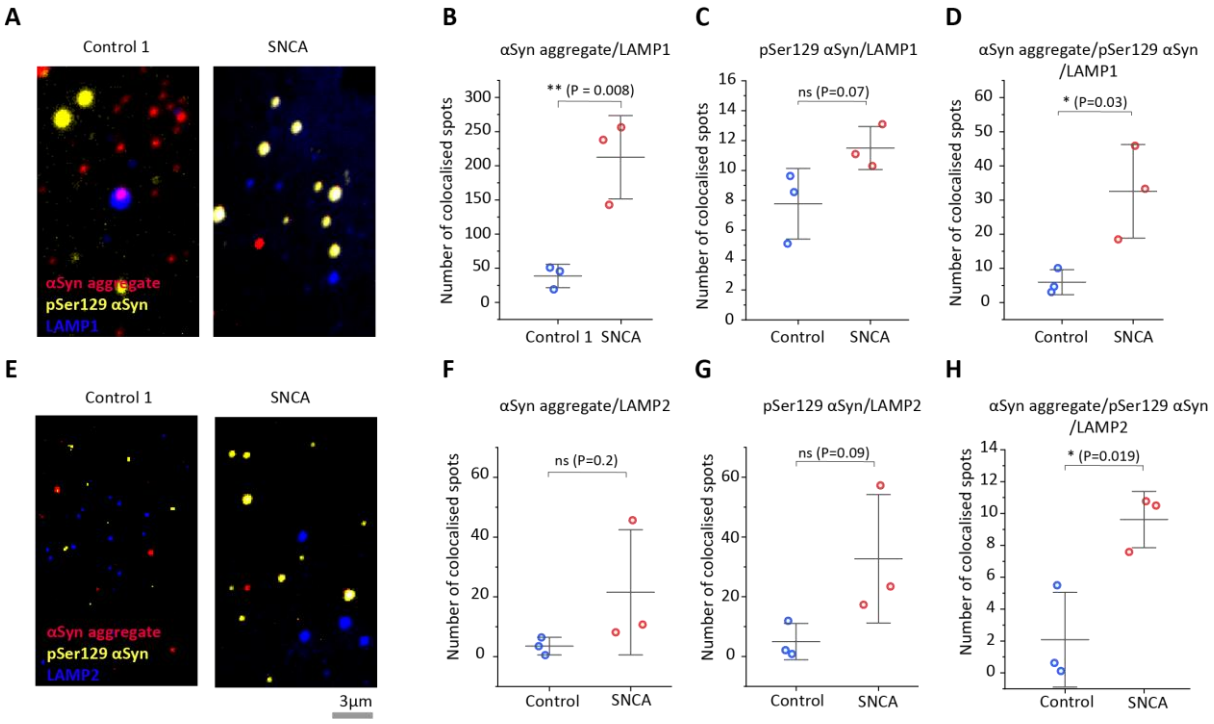

Figure 3.13. αSyn aggregates colocalise with lysosomal proteins in SNCA iDNL's. A. Representative images of αSyn aggregates, pSer129 αSyn and LAMP1 colocalised in Control 1 and SNCA **B-D.** αSyn interaction with LAMP1 was quantified and compared between SNCA and Control 1, in aggregated form (**B**), phosphorylated form (**C**), and aggregates that are phosphorylated (**D**). **E**. Representative images of αSyn aggregates, pSer129 αSyn and LAMP2 in Control 2 and SNCA. **F-G**. αSyn's interaction with LAMP2 was quantified in aggregated form (**F**), phosphorylated form (**G**), and aggregate, phosphorylated αSyn colocalised with LAMP2 (**G**). Raw data was normalised to total protein concentration. Graphs show three biological replicates, bars represent mean ± SD. Two-sample T tests were used to determine significance.

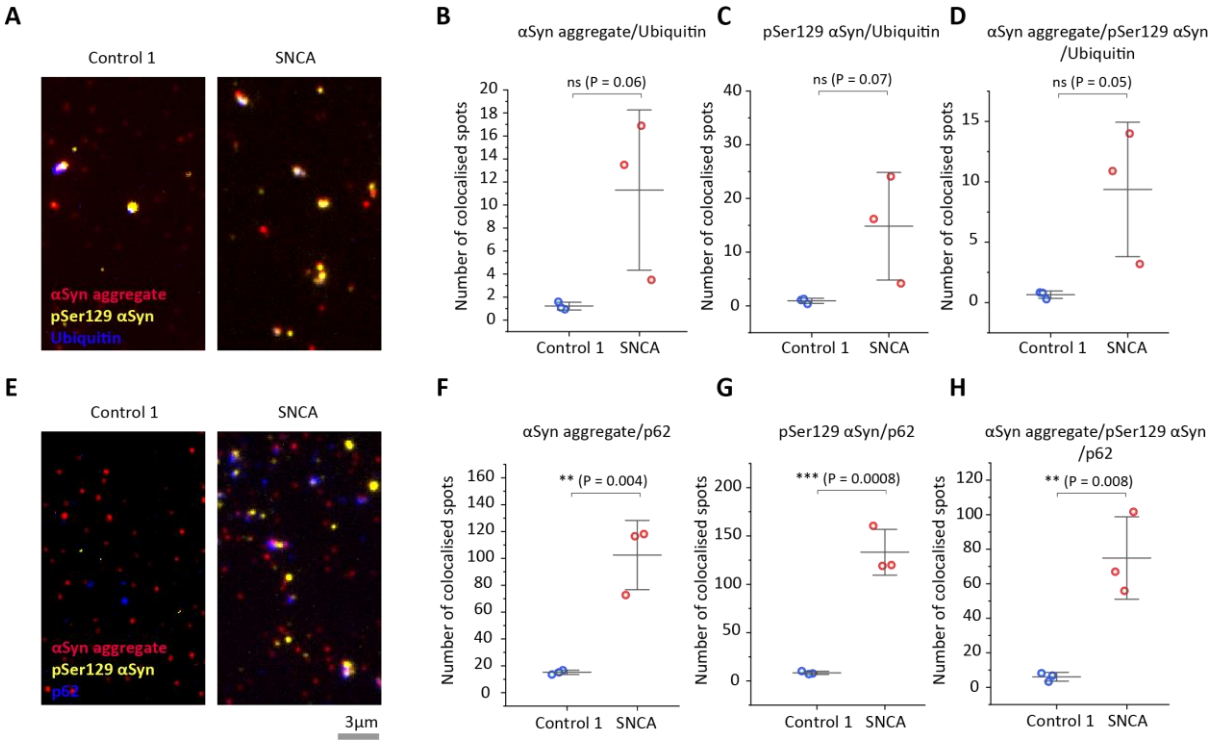

Figure 3.14. Phosphorylated αSyn aggregates colocalise with ubiquitin and p62 in SNCA iDNLs. A. Representative images of colocalised spots of αSyn aggregate, pSer129 αSyn and ubiquitin in Control 1 and SNCA. **B-D.** The presence of ubiquitin within αSyn species was compared in SNCA and Control 1, including colocalisation with aggregated αSyn (**B**), phosphorylated αSyn (**C**), and aggregates that are also phosphorylated (**D**). **E**. Representative images of colocalised spots of αSyn aggregate, pSer129 αSyn and ubiquitin in Control 1 and SNCA. **F-G**. The presence of p62 within αSyn species was compared in SNCA and Control 1, the number of αSyn aggregates containing p62 (**F**), the number of pSer129 αSyn containing p62 (**G**), and the number of aggregated, phosphorylated αSyn containing p62 (**H**) was quantified. Graphs show three biological replicates, bars represent mean ± SD. Two-sample T tests were used to determine significance.

After probing αSyn interactions with other Lewy Body associated proteins, it was clear that the SNCA line contained a higher amount of intracellular αSyn colocalised with Lewy Body markers. Next, sporadic PD lines were investigated to determine if they also formed Lewy Body-like aggregates. Firstly, sPD1 and Control 2 were probed for αSyn colocalising with mitochondrial markers (Figure 3.15). The presence of TOM20 within αSyn aggregates was investigated (Figure 3.15 A-D). There was interaction of TOM20 and αSyn in both the sPD1 cells and the Control 2 cells, with no significant difference between the two. As previously shown, there's a higher number of pSer129 αSyn within sPD1 but not αSyn aggregate, so the number of Lewy Bodies present was normalised to the total αSyn present (using αSyn aggregate as the total) (Figure 3.15 E-G).

There was no significant difference between the amount of αSyn aggregates containing TOM20, but there was a trend towards a higher number of pSer129 containing TOM20 in sPD1 compared to Control 2. A second mitochondrial protein was probed for its interaction with αSyn in sPD1 and Control 2, VDAC1 (Figure 3.15 H-K). There was no significant difference between the number of αSyn species interacting with VDAC1 between the PD and healthy control line. As these graphs show a trend towards higher levels of these Lewy Body-like aggregates in sPD1, the number of Lewy Body aggregates were normalised to total αSyn aggregates (Figure 3.15 L-N). This showed that in sPD1 there was a significantly higher amount of pSer129 αSyn that contained Lewy Body markers compared to Control 2. This data suggests that in sporadic cells there is a higher proportion of the total αSyn forming Lewy Body-like aggregates than in Control 2 cells.

Next, lysosomal proteins were assessed for their interaction with αSyn in sPD1 and Control 2 (Figure 3.16). αSyn aggregates and pSer129 were probed for the presence of LAMP1 (Figure 3.16 A-D). There was no significant difference between the total number of αSyn aggregates and pSer129 αSyn colocalised to LAMP1. However, when the data was normalised to total αSyn aggregate, there was a higher number of pSer129 colocalised with LAMP1 (Figure 3.16 E-G). This data suggests that although there may not be a difference between the actual number of αSyn interacting with LAMP1, there is a higher percentage of αSyn that is forming Lewy Body-like aggregates in sPD1 than in Control 1. To confirm if this is true for other lysosomal proteins, the presence of LAMP2 in αSyn species was investigated (Figure 3.16 H-K). This follows the same trend as LAMP1, there is no significant difference in total number of

Lewy Body like aggregates. However, when normalised to total αSyn aggregate, there is a higher number of pSer129 αSyn colocalised with LAMP2 in sPD1 compared to Control 1 (Figure 3.16 L-N).

Lastly, Lewy Body markers ubiquitin and p62 were assessed for their colocalisation to αSyn aggregates and pSer129 αSyn in sPD1 and Control 2 (Figure 3.17). There is no difference between the αSyn aggregates and pSer129 αSyn colocalised with p62 (Figure 3.17 A-C). Out of the αSyn aggregates present in the sample, more of them were forming Lewy Body-like aggregates in sPD1, this was significant in the phosphorylated αSyn but not the aggregated αSyn (Figure 3.17 D-F). Ubiquitin containing aggregates were then probed in both sPD1 cells and Control 2 (Figure 3.17 G-I). There was no significant difference observed between ubiquitin colocalised aggregates in sPD1 and Control 2. Due to the variability between biological replicates, there was still no significant difference in the number of Lewy Body-like aggregates when normalised to total αSyn levels (Figure 3.17 J-L). Overall, I found that there is no difference between the amount of aggregated αSyn colocalising with Lewy Body markers in sPD1 and Control 2, however there is significantly more pSer129 αSyn containing Lewy Body markers in sPD1 compared to Control 2.

To determine whether this phenotype is replicated in other sporadic PD cells, the presence of Lewy Body-like aggregates was investigated in sPD2 and Control 3 iDNLs (Figure 3.18). I observed no difference in the presence of Lewy Body-like aggregates between sPD2 and Control 3 when probing various proteins, TOM20 (Figure 3.18 A-C), p62 (Figure 3.18 D-F) and ubiquitin (Figure 3.18 G-I). This is not surprising as there was no difference in the total number of αSyn aggregate and pSer129 αSyn when previously investigated (Figure 3.9). Due to these results, I did not probe for any other Lewy Body markers as I did not expect to see a difference between sPD2 and Control 3.

Finally, two more PD mutations were assessed for their ability to form αSyn Lewy Body-like aggregates. The presence of Lewy Body-like aggregates was determined in LRRK2 (Figure 3.19). There was no difference between LRRK2 and Control 4 for αSyn colocalised with 3 different Lewy Body markers; TOM20, LAMP1 and p62. Parkin and Control 5 were then probed for the presence of Lewy Body-like aggregates, and there was no difference between the two lines (Figure 3.20).

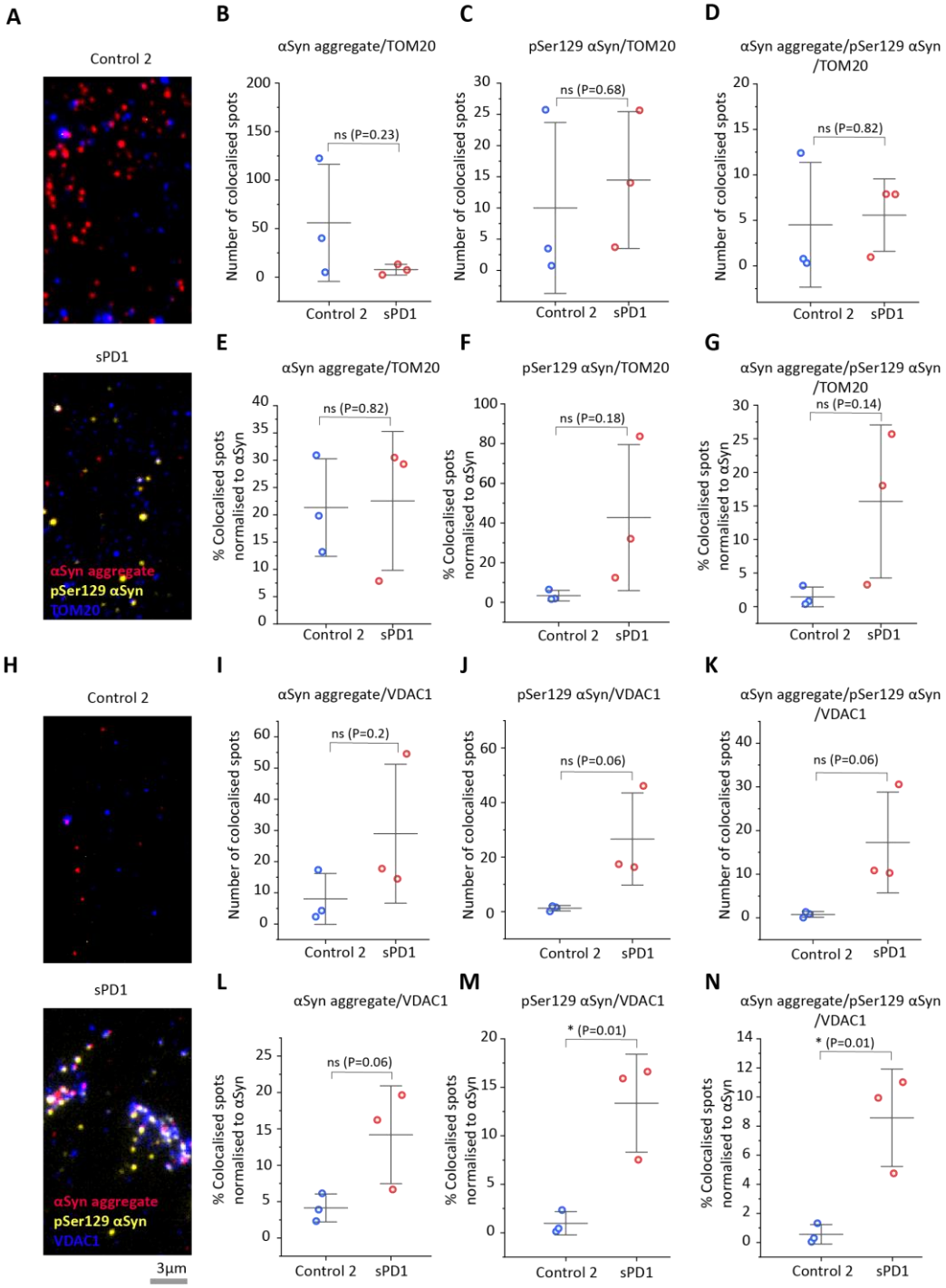

Figure 3.15 sPD1 and Control 2 both contain αSyn colocalised to mitochondrial markers, but VDAC1 is significantly higher in sPD1. A. Representative images of αSyn aggregate (red), pSer129 αSyn (yellow) and TOM20 (blue) in Control 2 and sPD1. **B-D**. Number of TOM20 spots colocalised to αSyn aggregate (**B**), pSer129 αSyn (**C**) and aggregated pSer129 αSyn (**D**). **E-G**. Percentage of αSyn colocalised with TOM20 normalised to total αSyn. **H**. Representative images of αSyn aggregate, pSer129 αSyn and VDAC1 in Control 2 and sPD1. **I-K** Number of VDAC1 spots colocalised to αSyn aggregate (**I**), pSer129 αSyn (**J**) and aggregated pSer129 (**K**). **L-M**. Percentage of αSyn forming Lewy Bodies normalised to total αSyn levels. Graphs show three biological replicates, bars represent mean ± SD. Two-sample T tests were used to determine significance.

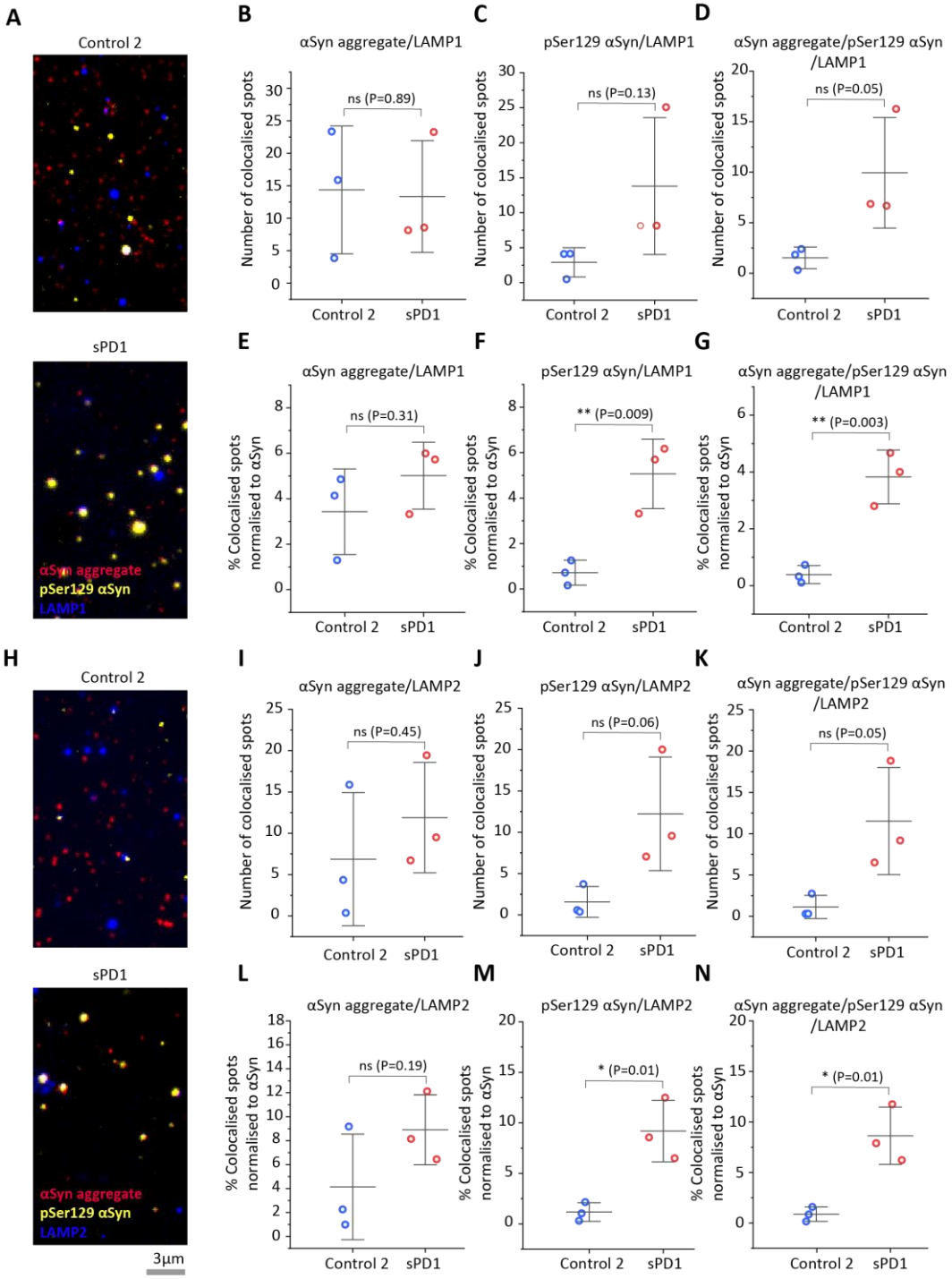

Figure 3.16. sPD1 contains a higher number of Lewy Body-like aggregates containing lysosomal proteins than Control 2. A. Representative images of αSyn aggregate, pSer129 and LAMP1 from Control 2 and sPD1 iDNLs. **B-D.** Number of LAMP1 spots colocalised with αSyn aggregate (**B**), pSer129 αSyn (**C**), and phosphorylated αSyn aggregate (**D**). **E-G.** The percentage of αSyn forming Lewy Body-like aggregates, normalised to total αSyn number. **H.** Representative images of αSyn aggregate, pSer129 αSyn and LAMP1. **I-J.** Number of LAMP2 spots colocalised to αSyn aggregate (**I**), pSer129 αSyn (**J**) and αSyn aggregate and pSer129 αSyn (**K**). **L-N.** Percentage of αSyn that is forming Lewy Body-like aggregates containing LAMP2. Graphs show three biological replicates, bars represent mean ± SD. Two-sample T tests were used to determine significance.

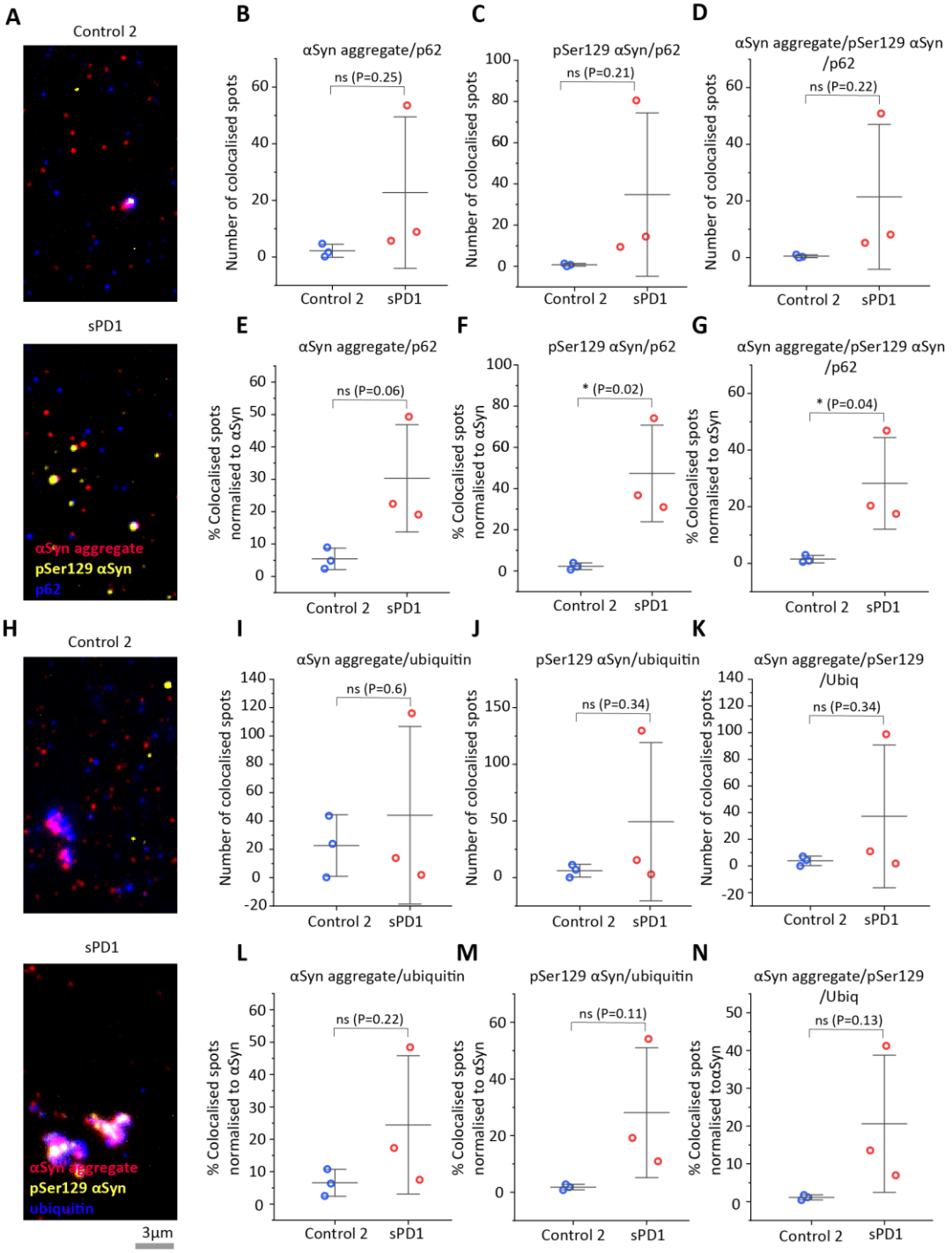

Figure 3.17 sPD1 contains significantly more pSer129 αSyn aggregates with p62 than Control 2. A. Representative images of αSyn aggregate, pSer129 αSyn and p62 in Control 2 and sPD1. **B-D.** Number of p62 spots colocalised with αSyn aggregate (**B**), pSer129 αSyn (**C**), pSer129 αSyn and αSyn aggregate (**D**). **E-G** Number of Lewy Body aggregates normalised to total αSyn levels, for p62 αSyn aggregate (**E**), pSer129 αSyn and p62 (**F**), and 3-colour aggregates (**G**). **H.** Representative images of Lewy Body-like aggregates containing ubiquitin. **I-K.** Number of ubiquitin spots colocalised with αSyn aggregate (**I**), pSer129 αSyn (**J**) and aggregate and pSer129 αSyn (**K**). **L-N.** Percentage of total αSyn aggregates forming Lewy Body-like aggregates. Graphs show three biological replicates, bars represent mean ± SD. Two-sample T tests were used to determine significance.

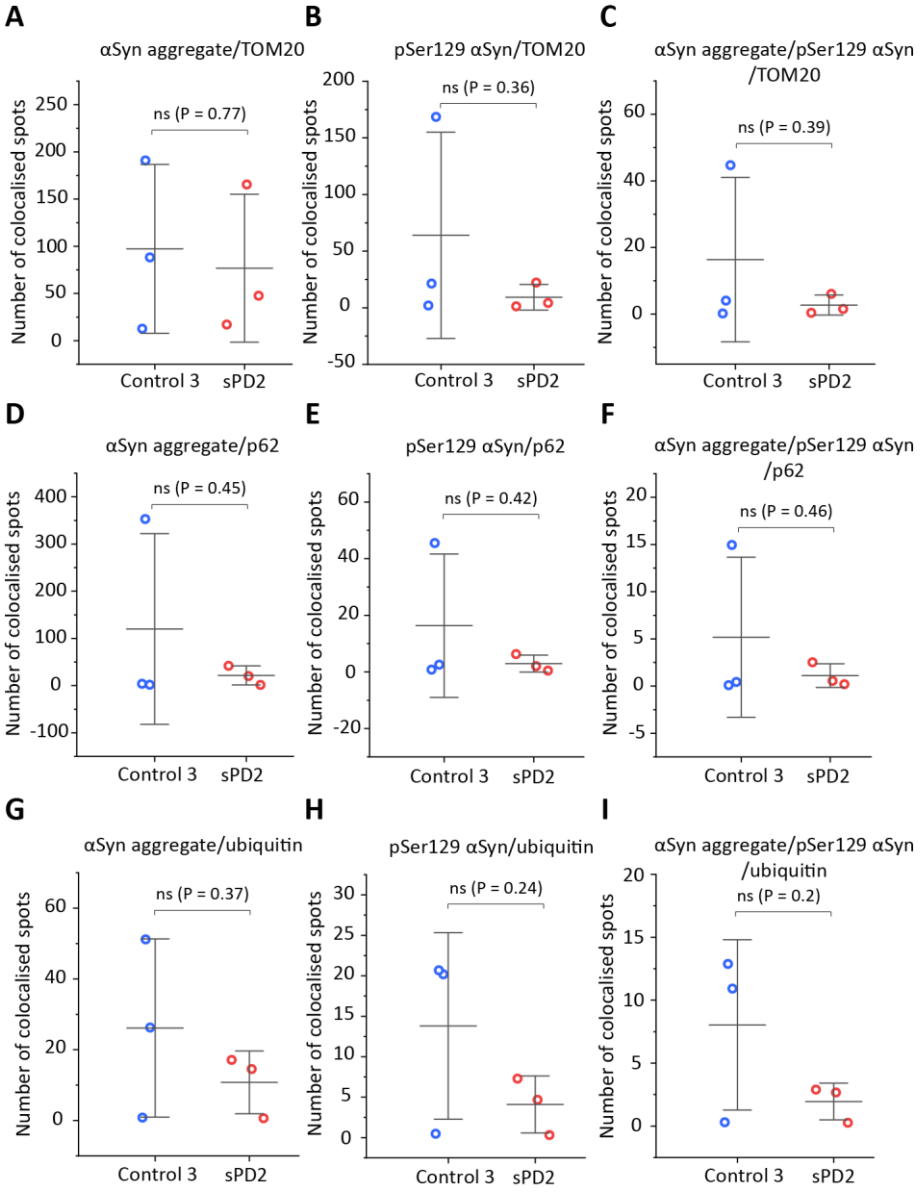

Figure 3.18 There is no significant difference in the presence of Lewy Body-like aggregates between sPD2 and Control 3. A-C. Number of Lewy Body-like aggregates containing TOM20 and αSyn aggregate (**A**), pSer129 αSyn (**B**), and both αSyn aggregate and pSer129 αSyn (**C**). **D-F.** Number of Lewy Body-like aggregates containing p62 and αSyn aggregate (**D**), pSer129 αSyn (**E**), and both αSyn aggregate and pSer129 αSyn (**F**). **G-I.** Number of Lewy Body-like aggregates containing ubiquitin and αSyn aggregate (**G**), pSer129 αSyn (**H**), and both αSyn aggregate and pSer129 αSyn (**I**). Graphs show three biological replicates, bars represent mean ± SD. Two-sample T tests were used to determine significance.

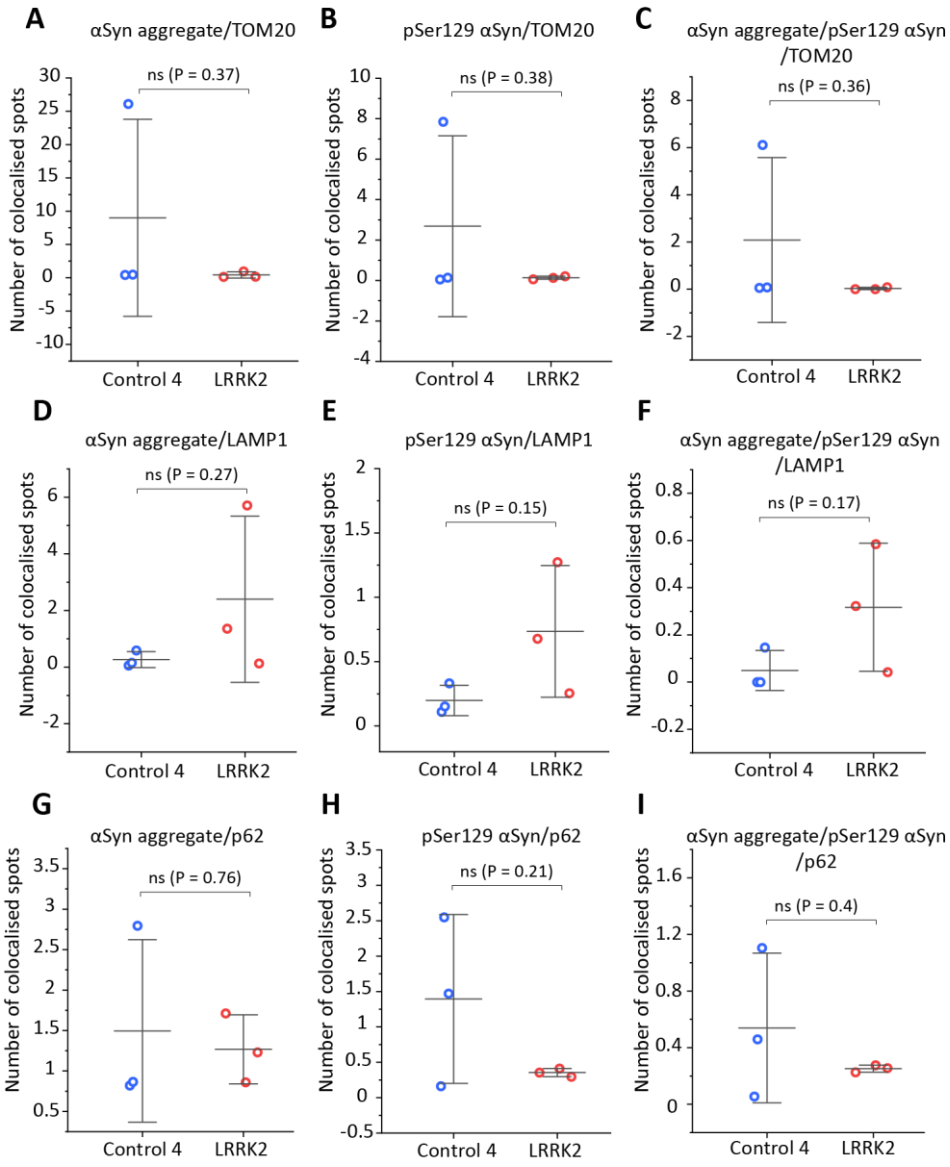

Figure 3.19. There is no difference between the number of Lewy Body like aggregates in Control 4 and LRRK2. A-C. Number of Lewy Body-like aggregates in Control 4 and LRRK2 containing TOM20 and αSyn aggregate (**A**), pSer129 αSyn (**B**) and αSyn aggregate and pSer129 (**C**). **D-F.** Number of Lewy Body-like aggregates containing LAMP1 and αSyn aggregate (**D**), pSer129 αSyn (**E**), and αSyn aggregate and pSer129 (**F**). **G-I.** Number of Lewy Body-like aggregates containing p62 spots colocalised with αSyn aggregates (**G**), pSer129 αSyn (**H**), and αSyn aggregate and pSer129 αSyn (**I**). Graphs show three biological replicates, bars represent mean ± SD. Two-sample T tests were used to determine significance.

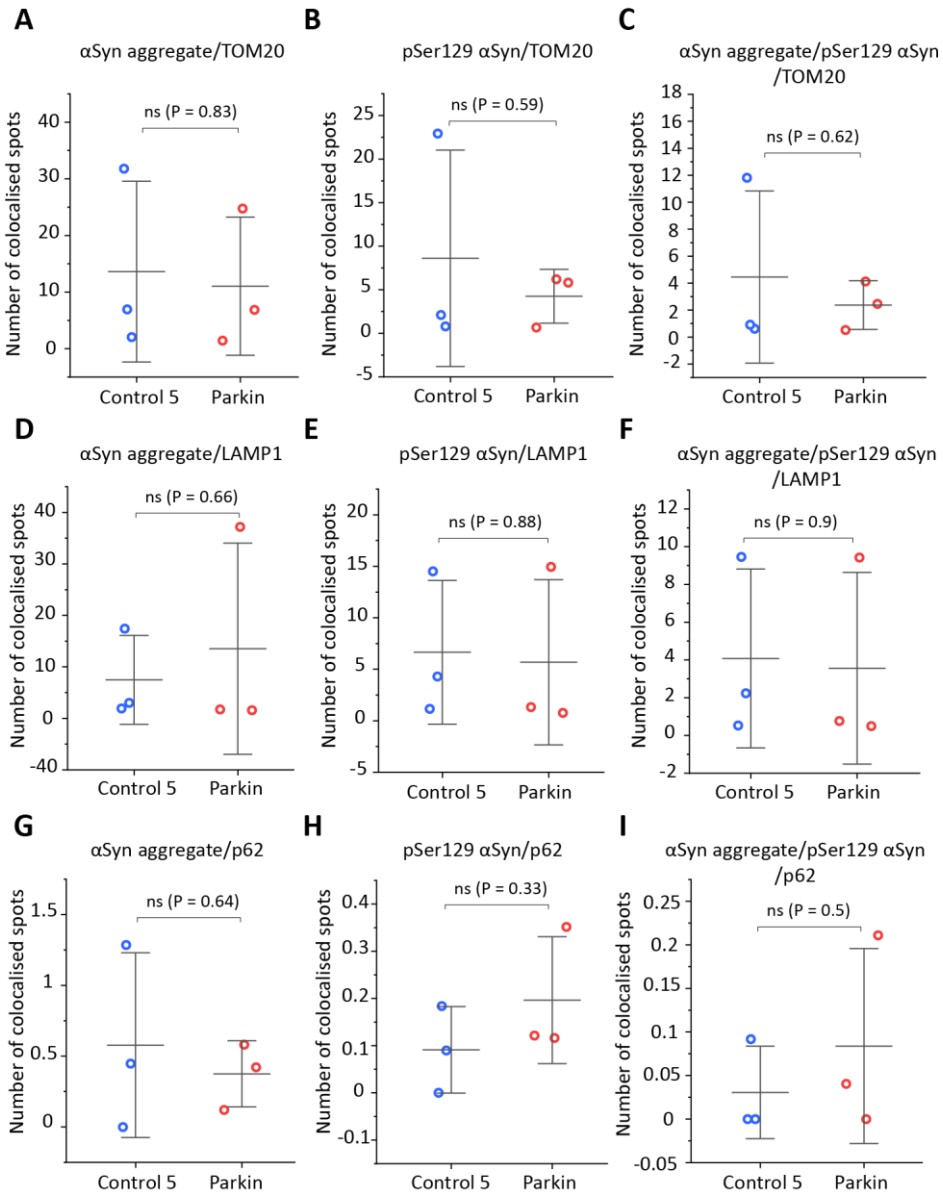

Figure 3.20. There is no difference in the number of Lewy Body like aggregates in Control 5 and Parkin. A-C. Number of Lewy Body-like aggregates in Control 5 and Parkin containing TOM20 and αSyn aggregate (**A**), pSer129 αSyn (**B**), αSyn aggregate and pSer129 αSyn (**C**). **D-F.** Number of Lewy Body-like aggregates containing αSyn aggregate (**D**), pSer129 αSyn (**E**), and αSyn aggregate and pSer129 αSyn (**F**). **G-I.** Number of Lewy Body-like aggregates containing p62 and αSyn aggregate (G), pSer129 αSyn (**H**), and αSyn aggregate and pSer129 αSyn (**I**). Graphs show three biological replicates, bars represent mean ± SD. Two-sample T tests were used to determine significance.

3.3.5. PD iDNLs show impairment in mitochondrial and lysosomal function.

A large body of literature implicates both αSyn aggregation and mitochondrial dysfunction as closely related with PD, however their complex interplay remains to be elucidated. Several studies report αSyn aggregates causing mitochondrial dysfunction in PD; αSyn oligomers interact with TOM20 and impair mitochondrial protein import, and αSyn interactions with VDAC1 cause increased mitochondrial permeabilization (Di Maio et al., 2016; Risiglione et al., 2021). I have shown αSyn aggregates present within this model are interacting with both TOM20 and VDAC1 when forming Lewy Body-like aggregates, therefore the mitochondrial function of the cells was investigated.

To determine mitochondrial function of the cells, live imaging was performed on the Opera Phenix using dyes to detect mitochondrial and lysosomes (MitoTracker™ Green, TMRM, LysoTracker™ Deep Red). From this imaging, the total number of mitochondria was calculated by using the MitoTracker™ green signal, signal was segmented, and mitochondria were selected based on their size and intensity. This process was carried out for TMRM staining of active mitochondria, and LysoTracker™ staining of lysosomes. The total number of mitochondria and lysosomes was quantified and normalised based on the number of cells. The amount of mitophagy was calculated based on the number of mitochondria colocalised to lysosomes and normalised to the image region area.

Mitochondrial dysfunction in SNCA and Control 1 was investigated (Figure 3.21). It was found that SNCA had a significantly higher number of mitochondria (Figure 3.21 B) and a higher number of lysosomes (Figure 3.21 C) compared to Control 1. SNCA also had decreased mitophagy compared to Control 1 (Figure 3.21 D). This data largely replicates the phenotypes measured in these cells by other Mortiboys lab members in unpublished data.

To understand if this phenotype was specific to SNCA or not, the mitochondrial dysfunction assays were performed on sporadic PD lines (Figure 3.22). sPD1 showed a higher number of mitochondria and lysosomes per cell compared to Control 2 (Figure 3.22 B-C). There was a reduction in mitophagy in sPD1 however it was not statistically significant (Figure 3.22 D).

Another PD sporadic cell line was used to understand if mitochondrial dysfunction is preserved across different PD patients (Figure 3.23). sPD2 has significantly more mitochondria and lysosomes per cell than Control 3 (Figure 3.23 B-C). There was no difference in mitophagy

within sPD2 and Control 3 (Figure 3.23 D). This is not surprising, as I did not observe any elevated αSyn phenotypes in sPD2.

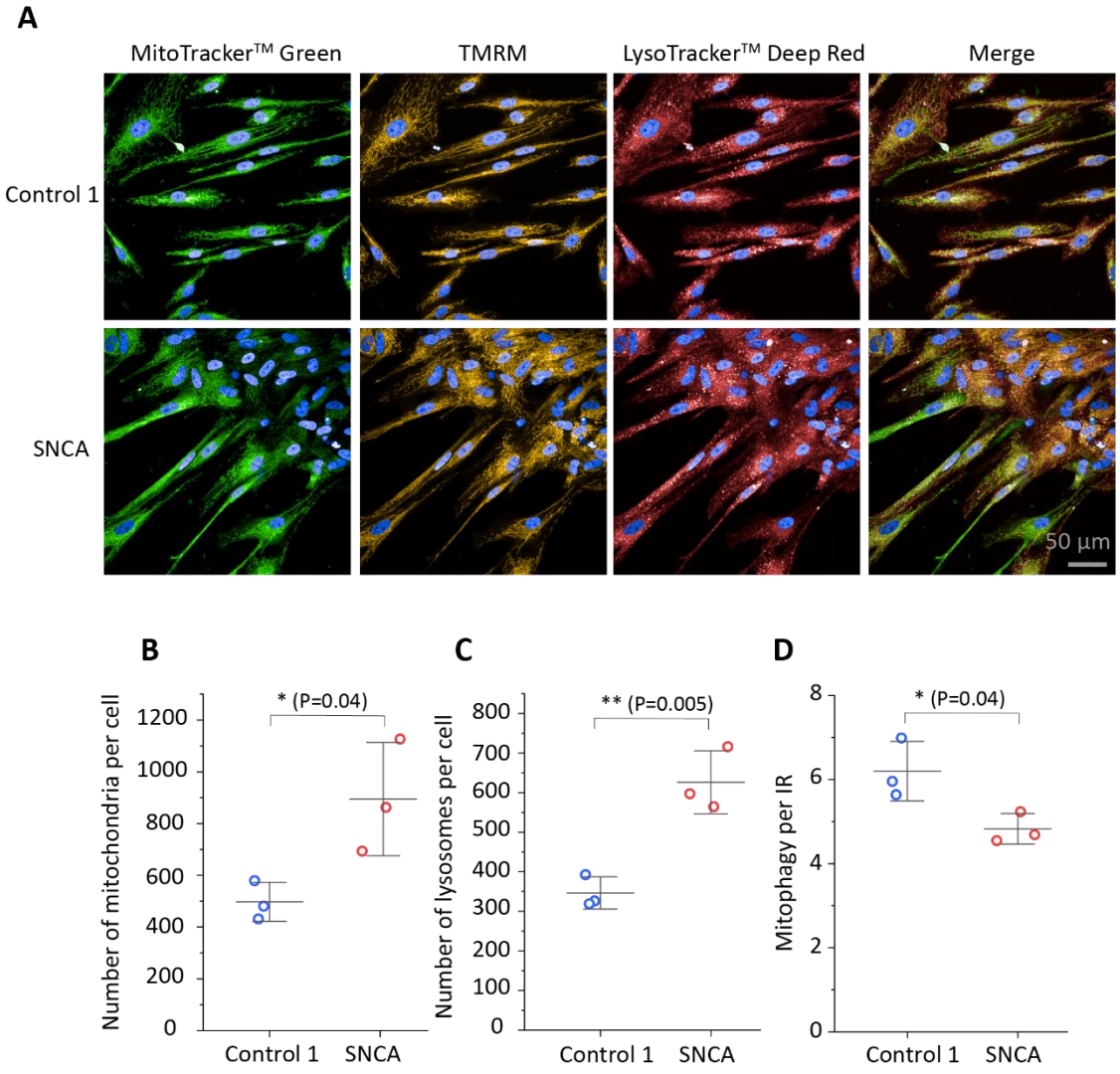

Figure 3.21 SNCA iDNLs have increased mitochondrial dysfunction compared to Control 1. A. Representative images of Control 1 and SNCA iDNLs stained with MitoTracker™ Green, TMRM, LysoTracker™ Deep Red and Hoechst. **B.** The number of mitochondria per cell, quantified by segmented MitoTracker™ Green signal. **C.** The number of lysosomes per cell, quantified by segmented LysoTracker™ Deep Red signal. **D.** The amount of mitophagy determined by colocalisation of mitochondria and lysosomes, normalised to image region. Graphs show three biological replicates, bars represent mean ± SD. Two-sample T tests were used to determine significance.

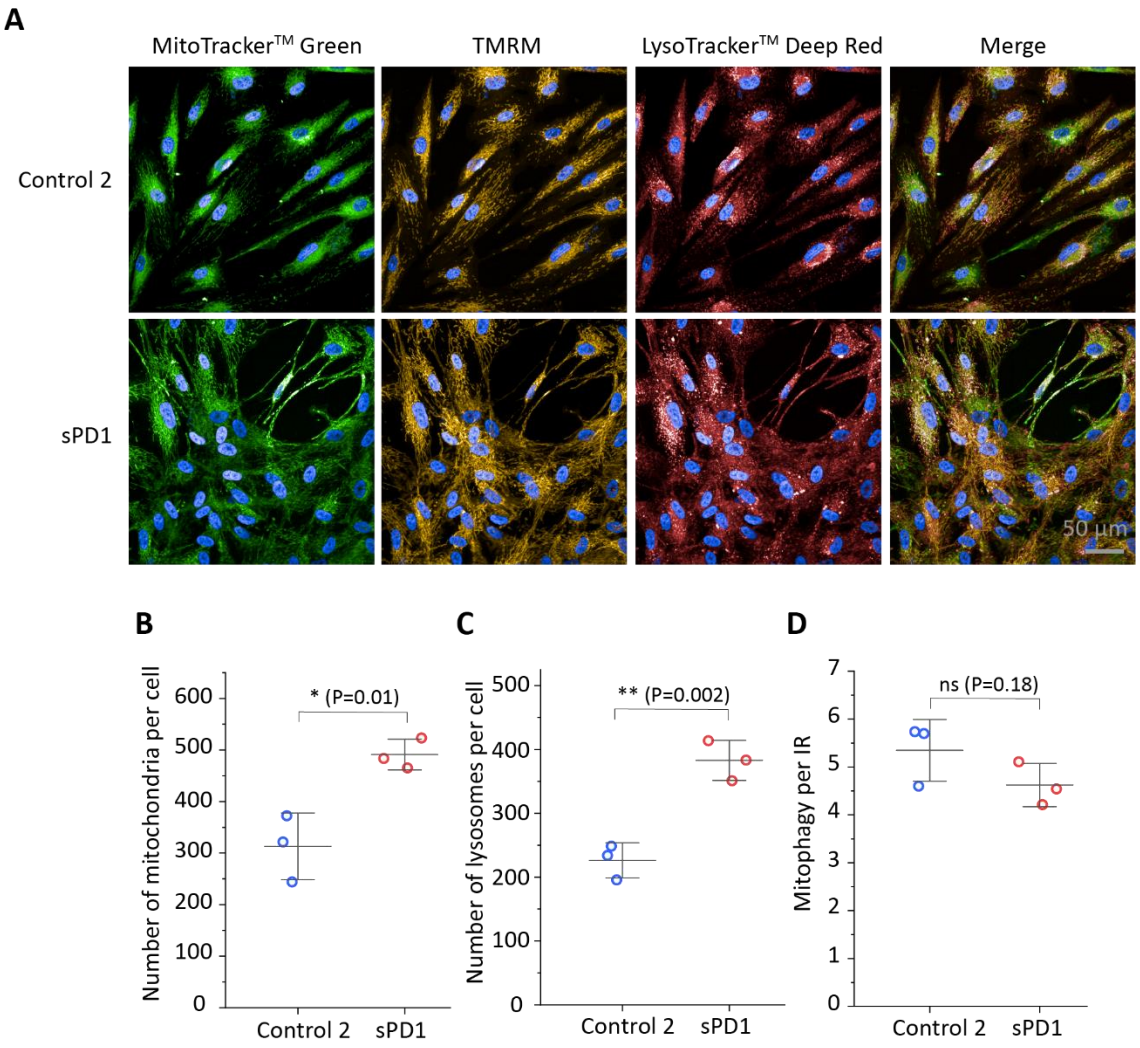

Figure 3.22. sPD1 has increased mitochondria and lysosomes compared to Control 2. A. Representative images of Control 2 and sPD1 stained for mitochondria (MitoTracker™ Green, TMRM) and lysosomes (LysoTracker™ Deep Red). **B.** Number of mitochondria per cell in Control 2 (blue) and sPD1 (red), quantified by segmented MitoTracker™ Green signal. **C.** Number of lysosomes per cell, quantified by segmented LysoTracker™ Deep Red signal. **D.** Amount of mitophagy in Control 2 and sPD1, calculated by mitochondria and lysosome colocalisation, normalised to image region area. Graphs show three biological replicates, bars represent mean ± SD. Two-sample T tests were used to determine significance.

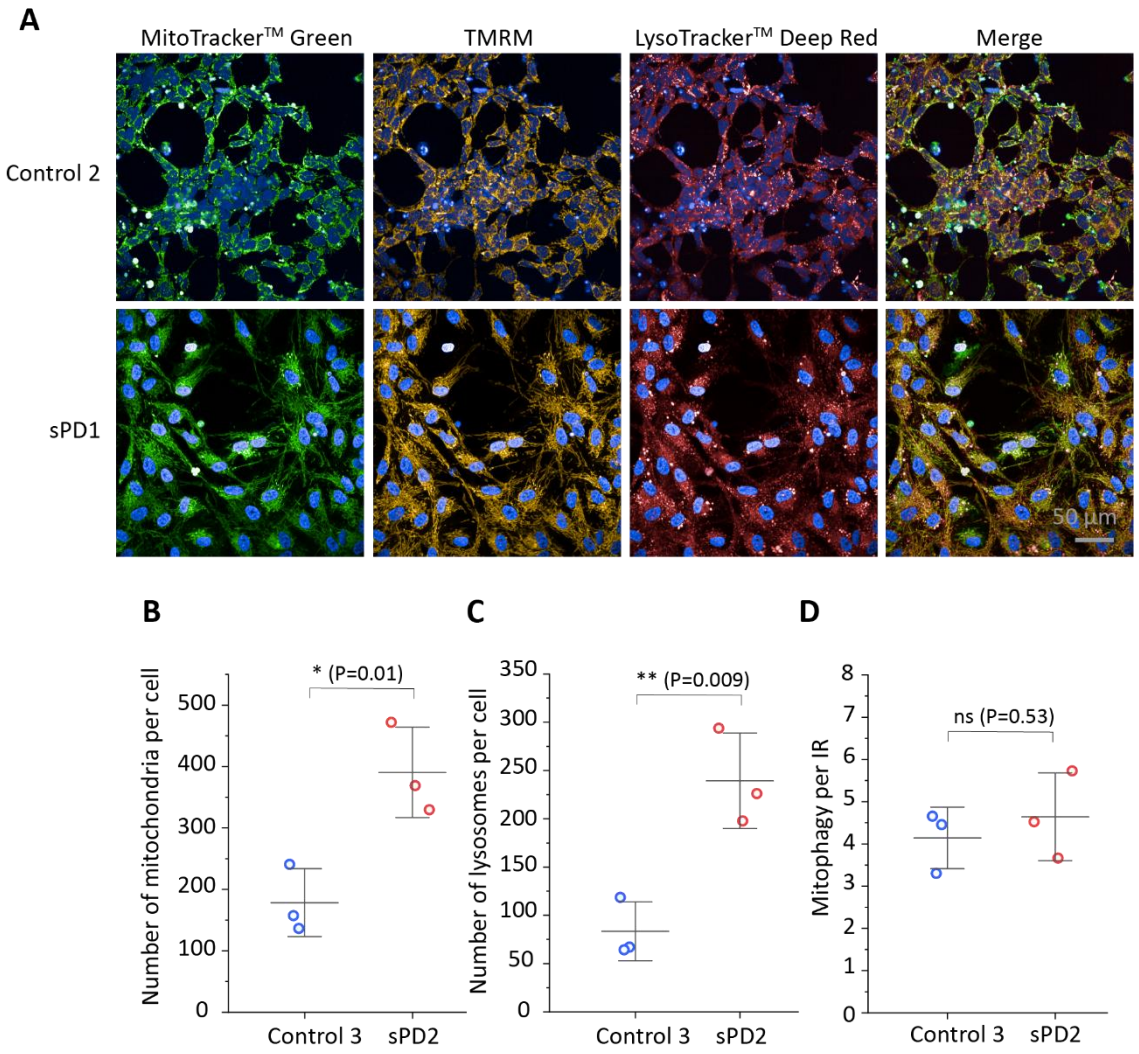

Figure 3.23. sPD2 has increased mitochondria and lysosomes compared to Control 3. A. Representative images of Control 3 and sPD2 stained for MitoTracker™ Green (mitochondria), TMRM (active mitochondria), LysoTracker™ Deep Red (lysosomes) and Hoechst (nuclei). **B.** Number of mitochondria per cell, quantified by segmented MitoTracker™ Green signal. **C.** Number of lysosomes per cell quantified by segmented LysoTracker™ Deep Red signal. **D.** Amount of mitophagy, detected by mitochondria and lysosome colocalisation, in Control 3 and sPD2 normalised to image region area. Graphs show three biological replicates, bars represent mean ± SD. Two-sample T tests were used to determine significance.

3.4. Discussion

This chapter focused on characterising the iDNL model of PD and healthy controls, to understand the intrinsic dysfunction within these models. The study focused on several key aspects of PD pathology: the levels of αSyn, the amount of aggregated and phosphorylated αSyn, the number of Lewy Body-like aggregates present and signs of mitochondrial dysfunction. The overall results and p-values are shown in Table 3.1. Phenotypic variations in αSyn and p-αSyn levels was evident among cell lines, indicating that not all PD mutations manifest with the same intensity or form of αSyn pathology. Interestingly, the extent of the formation of Lewy body-like aggregates was not uniformly observed across all PD models, suggesting that this pathological feature may be specific to certain genetic backgrounds or mutations within the PD spectrum. Mitochondrial dysfunction, a well-known aspect of PD pathology was observed within the cell lines and has been previously shown by other Mortiboys lab members, outlining the importance of mitochondrial involvement in PD across different genetic and environmental contexts.

However, a notable and consistent finding across all PD cell models was the presence of extracellular secreted p-αSyn in the cell media, suggesting a common pathogenic mechanism among sporadic and mutant lines. This finding is critical as it points to potential biomarkers and therapeutic targets for PD, emphasising the role of extracellular αSyn in disease mechanisms.

Table 3.1. Statistical significance and p-values of results in Chapter 3. Statistical tests were two-sample T tests. Significance indicates an increase compared to the corresponding control. Red values indicate a significant decrease compared to control. Yellow represents significant difference and blue represents no significant difference.

	SNCA	sPD1	sPD2	LRRK2	Parkin
Total intracellular αSyn	***P=0.0006	ns P=0.25	ns P=0.39	ns P=0.26	*P=0.01
Total extracellular αSyn	*P=0.02	ns P=0.16	*P=0.04	*P=0.04	ns P=0.09
Total intracellular p-αSyn	**P=0.005	ns P=0.11	ns P=0.86	ns P=0.6	ns P=0.08
Total extracellular p-αSyn	**P=0.003	ns P=0.08	*P=0.01	**P=0.001	**P=0.004
αSyn aggregates	*P=0.01	ns P=0.98	ns P=0.46	ns P=0.96	ns P=0.46
p-αSyn aggregates	**P=0.001	*P=0.01	ns P=0.26	ns P=0.59	ns P=0.68
TOM20 Lewy Bodies	*P=0.04	ns P=0.14	ns P=0.39	ns P=0.36	ns P=0.62
VDAC1 Lewy Bodies	ns P=0.1	*P=0.01	N/A	N/A	N/A
LAMP1 Lewy Bodies	*P=0.03	**P=0.003	N/A	ns P=0.17	ns P=0.9
LAMP2 Lewy Bodies	*P=0.01	*P=0.01	N/A	N/A	N/A
P62 Lewy Bodies	**P=0.008	*P=0.04	ns P=0.46	ns P=0.4	ns P=0.9
Ubiquitin Lewy Bodies	ns P=0.05	ns P=0.13	ns P=0.2	N/A	N/A
Number of mitochondria	*P=0.04	*P=0.01	*P=0.01	N/A	N/A
Number of lysosomes	**P=0.005	**P=0.002	**P=0.009	N/A	N/A
Mitophagy	*P=0.04	ns P=0.18	ns P=0.53	N/A	N/A
MMP	ns P=0.29	ns P=0.72	ns P=0.57	N/A	N/A

3.4.1. Heterogeneity of endogenous αSyn levels within sporadic and familial PD

Although there is some controversy as to whether fibroblasts express αSyn, most studies show no expression of αSyn in fibroblasts (Devine et al., 2011). In this work, I found that fibroblasts express αSyn significantly lower than corresponding iDNLs. This observation reinforces the validity of using reprogrammed fibroblasts to generate iDNLs as a model system for investigating αSyn dysfunction in. Quantifying endogenous levels of αSyn determined that the iDNLs are highly heterogenous across different cell lines, with SNCA showing higher levels of αSyn and phosphorylated αSyn, and sPD1 showing higher levels of phosphorylated αSyn compared to Control 1 and Control 2, respectively. However, sPD2 and

the other disease mutations LRRK2 and Parkin did not show a difference in the amount of αSyn and p-αSyn within the cells.

Several models have investigated endogenous αSyn in a patient derived cell model with PD causing mutations. Studies have shown SNCA triplication cells have elevated mRNA compared to controls and doubling of αSyn protein (Byers, Cord, Nguyen, Schü Le 5, et al., 2011; Devine et al., 2011). These results support the data presented in this chapter, where SNCA has increased αSyn and p-αSyn confirmed by MSD ELISA and SiMPull. Although many studies do observe an increase in αSyn protein levels in LRRK2 lines (Sánchez-Danés et al., 2012), other studies have observed no difference in SNCA expression with LRRK2 mutants (Reinhardt et al., 2013; Marrone et al., 2018; Bose, Petsko and Studer, 2022). I did not observe any difference in αSyn protein levels within LRRK2 cells, which could be due to the heterogeneity within the cell lines, and additional LRRK2 cell lines would need to be assessed to confirm this.

Sporadic cases of PD present an even more complex scenario, as they arise from a huge spectrum of environmental and genetic factors. GWAS has reported the most common genetic cause of sporadic PD is mutations within the SNCA and LRRK2 genes (Chai and Lim, 2013). But importantly there is huge variability in the genetic causes of sporadic PD and population specific differences, for example, regions on the MAPT gene have been associated with PD in European cohorts, but this association was absent within an Asian population (Satake et al., 2009). Besides the genetic variability, the total αSyn levels in PD compared to controls generally remain unchanged. One study comparing seven sporadic lines, four LRRK2 mutants, and four healthy controls, showed there was no difference in intracellular levels of αSyn in sporadic cases and healthy controls (Sánchez-Danés et al., 2012). The variability of αSyn endogenous levels across different familial and sporadic cases show that the absolute levels of αSyn within the cell may not be a determinant for the development or diagnosis of PD.

In summary, the heterogeneity observed in αSyn expression among different PD models highlights the complexity of the disease and suggests that factors beyond total αSyn levels, such as the formation of specific pathological aggregates, may play a more critical role in disease progression and diagnosis.

3.4.2. Lewy Body pathology within sporadic and familial PD

The total levels of αSyn have shown not to be correlated with PD risk, leading to the hypothesis that specific conformations such as aggregated αSyn and phosphorylated within Lewy bodies may serve as a better marker for determining risk and progression of PD. To date, the formation of Lewy Bodies within neuronal cells has been limited to models where αSyn PFFs have been added. Spontaneous formation of αSyn Lewy bodies in a cellular model without external stressors and PFF addition has not yet been consistently reported. The major hallmark of PD is the formation of Lewy Bodies, and the gold standard of diagnosis is the presence of Lewy Bodies in postmortem tissue. Therefore, most sporadic cases of PD present with Lewy Bodies in postmortem tissue, however there is some variability in their presence and abundance in familial PD cases.

Within this work, I identified that in SNCA triplication and in one sporadic case there is increased formation of Lewy Body-like aggregates compared to controls. This is supported by various studies within the literature whereby SNCA duplications and triplications lead to increased phosphorylated αSyn, and increased Lewy Body formation in postmortem tissue (Miller et al., 2004). Additionally, brain organoid models of SNCA triplication have increased phosphorylated and aggregated αSyn that is correlated to the loss of dopaminergic neurons (Mohamed et al., 2021). Most LRRK2 cases present pathology similar to what is observed in sporadic PD cases, however some LRRK2 mutations do lack Lewy Body pathology. A comparative study of thirty-seven LRRK2 PD cases show that G2019S mutation gives rise to a higher number of Lewy Body cases than other mutations, however still 35% of G2019S cases did not show Lewy Body pathology (Kalia et al., 2015). This data supports the results within this chapter, where LRRK2 iDNLs show no difference in Lewy Body-like aggregate formation compared to Control 4. Similarly, no difference in the number of Lewy Body-like aggregates were found between Parkin and Control 5. These results are in line with previous studies that PD cases involving Parkin mutants although they often present with neuronal loss specifically in the substantia nigra, they tend to stray from the standard pathology of idiopathic PD with cases usually showing no Lewy Bodies present at post-mortem (Takahashi et al., 1994; Van De Warrenburg et al., 2001; Cornejo-Olivas et al., 2015). However, a few studies report cases showing Lewy Body pathology, but when they are present, they are described as sparse (Farrer et al., 2001; Doherty et al., 2013).

The heterogeneity observed in Lewy body pathology across different PD cases at the postmortem level is reflected in the variability seen in the patient-derived cellular models of iDNLs. This variability underscores the complexity of PD and suggests that while Lewy body formation is a hallmark of the disease, their presence and abundance are not consistent across all PD subtypes. Crucially, understanding the specific conditions that lead to Lewy body formation – such as the aggregation of αSyn and its PTMs – is essential for developing more accurate diagnostic tools and targeted therapies for PD. Identifying these conditions will provide deeper insights into why certain cases develop more Lewy bodies while others do not, potentially revealing critical pathways that could be exploited to treat or prevent PD.

3.4.3. Phosphorylated αSyn as a biomarker for PD

The pathological forms of αSyn play a critical role in the prion like spreading from cell-to-cell. This spreading occurs through a seeding process, where cells release toxic αSyn aggregates that can be taken up by a neighboring cell. Once αSyn seeds are taken up by a new cell they promote rapid aggregation by secondary nucleation, leading to the cellular dysfunction and spreading of disease. A striking finding within this chapter was the increased presence of p-αSyn within the media of all PD derived iDNLs, compared to their respective controls, regardless of whether the PD was of sporadic or familial in origin. This consistent finding across all PD cell lines suggests that PD cells are releasing an increased amount of p-αSyn compared to the controls, regardless of the intracellular levels of αSyn. This supports the idea that enhanced αSyn seeding and spreading of disease occurs within the PD iDNLs.

This finding is particularly important within the field, as αSyn has been largely investigated as a biomarker for PD specifically αSyn presence within CSF or serum. The correlation between αSyn in CSF and PD has varied between studies, but most studies find CSF from PD patients have reduced αSyn levels compared to healthy controls (Wang et al., 2015; Ganguly et al., 2021). However, when studying disease specific αSyn e.g. aggregated and phosphorylated αSyn, there is an increase within these species in PD CSF compared to healthy controls (Zhou et al., 2015; Eusebi et al., 2017). A major challenge in using αSyn as a biomarker has been the low concentration of αSyn in CSF and the lack of sufficiently sensitive detection methods, leading to variability and potential inaccuracies in test results. This challenge has spurred the development of the α-synuclein seeding amplification assay (αSyn-SAA), which is designed to detect toxic forms of αSyn in biofluids with high sensitivity and specificity (Siderowf et al., 2023).

This test can discriminate individuals with PD compared to healthy controls and is being developed as a diagnostic test. The assay mimics the self-propagation and seeding behaviour of αSyn in vitro, allowing for the differentiation of toxic, seeding-competent αSyn from non-toxic forms that do not promote aggregation. The findings of increased p-αSyn in the media of all PD iDNLs used in this thesis strongly supports the fact that diseased cells release αSyn from within the cell and this contributes to disease propagation. The consistent findings of increased p-αSyn in the media across all PD lines I have studied, support that p-αSyn may be a better biomarker for PD, and αSyn-SAA could be used to detect p-αSyn in human biofluids. In the next chapter, the seeding ability of both p-αSyn and αSyn will be further investigated to better understand their roles in disease and progression and their potential as biomarkers for early diagnosis and treatment strategies.

3.4.4. Mitochondrial dysfunction within PD cells

Mitochondrial dysfunction was assessed by live high-content confocal imaging using mitochondrial and lysosomal dyes. It was found that SNCA triplication and sporadic iDNLs displayed distinct mitochondrial phenotypes compared to control iDNLs. This is supported by extensive research in iDNLs by other Mortiboys lab members, showing sporadic PD cells display mitochondrial dysfunctions including increased mitochondrial number, increased ROS and additionally lower mitochondrial membrane potential and reduced bioenergetics (Carling et al., 2020., R Hughes PhD thesis). Mitochondrial dysfunction in the SNCA triplication cells has been extensively measured by Dr Lizzie Stephen and Dr Francesco Capriglia, showing a consistent increased mitochondrial number, reduced mitophagy and reduced mitochondrial membrane potential compared to the control. The increased mitochondria and lysosomes but decreased mitophagy observed in PD cells could represent an accumulation of damaged and dysfunctional mitochondria, as mitochondrial quality control pathways are known to be reduced in PD patient neurons (Chen et al., 2023). The accumulation of dysfunctional mitochondrial can contribute to cellular stress and neurodegeneration, which are key features of PD pathology.

Additionally, the observed increase in mitochondria in PD cells could represent increased mitochondrial fragmentation. *In vitro* studies show that transfection of αSyn into cells leads to mitochondrial fragmentation (Nakamura et al., 2011). Using artificial membranes, this was suggested to be a due to direct interaction with αSyn aggregates and mitochondrial

membranes. This study also found no correlation between αSyn and mitochondrial membrane potential, in line with the results presented here. Similar results are observed *in vivo*, in a *Drosophila* model, overexpression of αSyn but not aggregated αSyn causes the fragmentation of mitochondria (Krzystek et al., 2021).

Although not investigated in this study, Parkin and LRRK2 iDNLs exhibit mitochondrial dysfunction – these studies have been done by other Mortiboys lab members. Parkin iDNLs used within this study have previously been shown to exhibit mitochondrial dysfunctions, including increased mitochondria, reduced bioenergetics and mitochondrial membrane potential, and increased ROS (Schwartzentruber et al., 2020). LRRK2 iDNLs exhibit increased mitochondrial number, increased ROS, and a reduction in mitochondrial membrane potential and mitophagy (Capriglia Unpublished).

Although I observed this mitochondrial dysfunction within SNCA and both sPD cell lines, it is important to note that due to the distinct morphology of Control 3, the cells grow in clumps and are smaller in size compared to the other iDNL lines used in this study. This means they may have less mitochondria and lysosome per cell compared to sPD2 due to their altered cellular morphology.

3.5. Conclusions

I have used the iDNL model to investigate αSyn accumulation and mitochondrial dysfunction in PD. When determining the total levels of αSyn, aggregated αSyn and p-αSyn, within the cells, there was considerable heterogeneity across the cell lines. Importantly, this work reports the formation of spontaneously formed Lewy Bodies within a patient derived cell model with no overexpression or addition of αSyn PFFs and proves further validity of the model. SNCA triplication line and both sporadic PD lines all displayed a level of mitochondrial dysfunction compared to healthy controls, and mitochondrial dysfunctions have previously been observed in the other disease mutations LRRK2 and Parkin. Despite the variability in αSyn and Lewy Body-like aggregates levels across the different PD cell lines, one phenotype that is maintained is the elevated level of p-αSyn within the cell media compared to the corresponding healthy controls. This consistent release of p-αSyn into the extracellular environment across both sporadic and familial forms of PD, regardless of genetic background, serves as a unifying feature of PD pathology. This shared characteristic emphasises the potential of p-αSyn as a valuable biomarker for early diagnosis and as a therapeutic for

interventions aimed at halting or slowing the progression of PD, applicable to patients across diverse origins.

Chapter 4: Phosphorylated αSyn plays a critical role in promoting mitochondrial dysfunction and the formation of Lewy Bodies in PD.

4.1. Introduction

Deposition of αSyn aggregates in brain tissue is a key hallmark of PD, but very little is known about the exact toxic mechanisms leading to pathology. There has been much debate about what forms of αSyn are inducing toxicity, with evidence for both fibrillar and oligomeric αSyn in dysfunction, including inducing membrane dysfunction, caspase activation and inclusion formation (Verma et al., 2015). Structural and conformational differences, such as aggregation state and morphology, of αSyn aggregates are likely to play a role in distinct pathogenic mechanisms (Shahnawaz et al., 2020). Phosphorylated αSyn also plays a crucial role in the deposition pathways of aggregates and formation of Lewy Bodies, but the exact role of pSer129 αSyn in pathogenesis remains unknown. Mutation of serine 129 to an alanine residue abolishes the possibility of phosphorylation and leads to a reduction in the formation of Lewy Body inclusions (Smith et al., 2005). *In vitro* fibrils generated from pSer129 αSyn have a distinct structure to wildtype αSyn fibrils, and application onto cells results in higher cytotoxicity, higher apoptosis, and increased ROS production as a result of the phosphorylated form (Ma et al., 2016).

One of the major mechanisms involved in the spread of PD pathology throughout the brain is αSyn seeding. This process involves pathogenic αSyn seeds being released from a diseased cell and the seeds are taken up by a neighbouring cell not yet exhibiting αSyn dysfunction. Once taken up, the seeds provide a scaffold that prompts the aggregation of endogenous αSyn, prompting rapid seed multiplication (Volpicelli-Daley et al., 2011). This speeds up the aggregation process and spreads the αSyn pathology across neural networks. Due to the inherent heterogeneity of αSyn, numerous conformations variants of seeds exist within cells, each with different capacities to induce further αSyn seeding. The structure of αSyn has been shown to influence their ability to induce αSyn seeding (Candelise et al., 2019). The results from Chapter 3 suggest that phosphorylated αSyn is implicated in cell to cell seeding. Specifically, cell culture media from PD patient-derived cellular models exhibited elevated levels of extracellular phosphorylated αSyn compared to samples from healthy control cells, highlighting its potential role in the disease's progression.

Conflicting studies on the role of pSer129 αSyn in PD have raised important questions about its function in both physiological and pathological contexts. Some studies suggest that pSer129 αSyn might be neuroprotective. It has been shown that there is a lower aggregation propensity of pSer129 αSyn compared to wildtype αSyn, and reduced ability to seed brain homogenates than wildtype αSyn (Ghanem et al., 2022). The researchers observed the large presence of pSer129 αSyn aggregates in PD pathology and attributed this to a secondary effect after αSyn aggregation, acting to reduce the toxicity of these aggregates rather than contributing to it. Similar findings were reported in Yeast, where prevention of phosphorylation of αSyn induced toxicity, suggesting a link between phosphorylation and clearance of αSyn (Tenreiro et al., 2014).

These contrasting studies pose questions about the role of phosphorylated αSyn role in physiological and disease conditions. Phosphorylated αSyn has an important physiological function of assisting αSyn regulated neurotransmission, by increasing αSyn interactions with VAMP2 for SNARE complex assembly (Parra-Rivas et al., 2023). Overall, these results suggest the loss of physiological pSer129 αSyn impairs neuronal functions, however a change in conformation and aggregation state can induce pathology (Ramalingam et al., 2023).

In contrast, other studies have linked pathological pSer129 αSyn to mitochondria dysfunction. Phosphorylated αSyn has a higher propensity to bind mitochondrial membranes compared to non-phosphorylated αSyn (Wang et al., 2019). The accumulation of aggregated phosphorylated αSyn at the mitochondria observed in neuronal cells, mouse models and postmortem tissue, is linked to mitochondrial dysfunction, and potentially contributes to neurodegeneration (Wang et al., 2019). Given these conflicting roles of pSer129 αSyn, I aim to clarify whether the increased pSer129 αSyn observed in PD patient cells is causing toxicity and uncover the underlying pathological mechanisms.

To achieve this, I plan to use established PD models where preformed fibrils or PD brain homogenates are introduced into healthy cells. Several studies have modelled PD pathology by the addition of preformed fibrils or PD brain homogenates into cells (Luk et al., 2009; Mahul-Mellier et al., 2020; Volpicelli-Daley et al., 2011). These models have shown the induction of toxicity and the formation of intracellular Lewy bodies. I will utilise this model to determine which species of αSyn promote toxicity in the cellular model. Healthy control cells which display no αSyn dysfunction or mitochondrial dysfunction will be treated with different

species of αSyn including distinct conformations: αSyn and pSer129 αSyn, and distinct aggregation states: 48 h (oligomeric) and 7 d (fibrillar).

By investigating the specific roles and mechanisms of different αSyn species, including their distinct conformations, aggregation states and post-translational modification, I aim to determine whether each contributes to neurotoxicity in similar or distinct ways. Understanding whether each species has a unique pathway in promoting cell-to-cell propagation of PD will help us depict the pathways of αSyn-induced neurotoxicity. Throughout this study, I intend to identify key aspects of the αSyn seeding mechanism and uncover potential therapeutic targets that could help halt the progression of PD.

4.2. Aims and Objectives

The aims of this chapter are to understand which species of αSyn are the most toxic and the mechanisms of toxicity. The objectives are:

- To seed healthy control iDNLs with different αSyn species, including oligomer and fibrils of wildtype and phosphorylated αSyn, and measure mitochondrial dysfunction and αSyn associated dysfunctions.
- To investigate which αSyn species are the most potent in inducing dysfunctions in healthy control iDNLs.
- To uncover the potential mechanisms of how αSyn exert their toxic effects and induces dysfunctions.

4.3. Results

4.3.1. Seeding healthy control iDNLs with αSyn species and measuring dysfunction

In order to investigate which species of αSyn present within the iDNLs are toxic, these species were generated in vitro. Recombinant monomeric αSyn was provided by our collaborators Professor Michele Vendruscolo from University of Cambridge, and phosphorylated αSyn was generated using a published protocol (Fauvet & Lashuel, 2015). Validation of the generation of pSer129 αSyn was done by western blot (Figure 4.1).

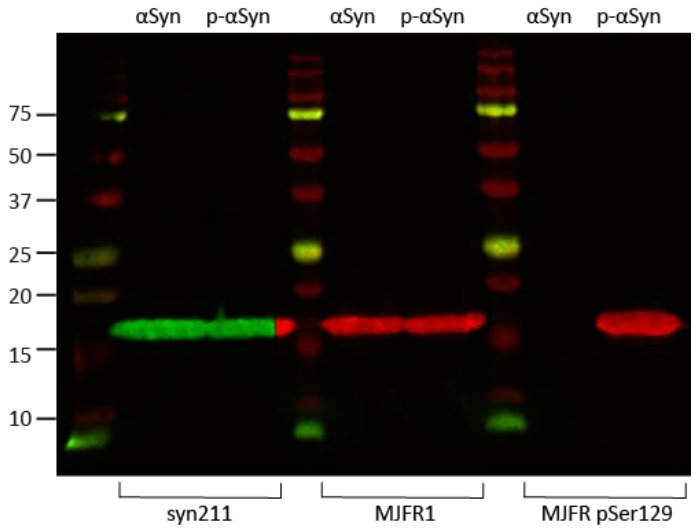

Figure 4.1. Validation of the generation of pSer129 αSyn. Western blot using αSyn recombinant αSyn protein and lab generated pSer129 αSyn. The proteins were detected with two pan-αSyn antibodies; syn211 and MJFR1, and an antibody specific to pSer129 αSyn; MJFR pSer129.

As I observed αSyn aggregates of varying sizes present in the iDNLs, in vitro aggregation of αSyn and p-αSyn was carried out and aggregate morphology was observed over 7 days (Figure 4.2, Supplementary Figure 2). Short fibril structures were present after only 24 hours in p-αSyn compared to αSyn which takes 3 days to form short fibrils. By 7 days, p-αSyn has formed large aggregate clumps, whereas αSyn has a clear fibril structure. In order to assess the toxicity of αSyn and p-αSyn aggregates, aliquots were taken at both 48h and 7d.

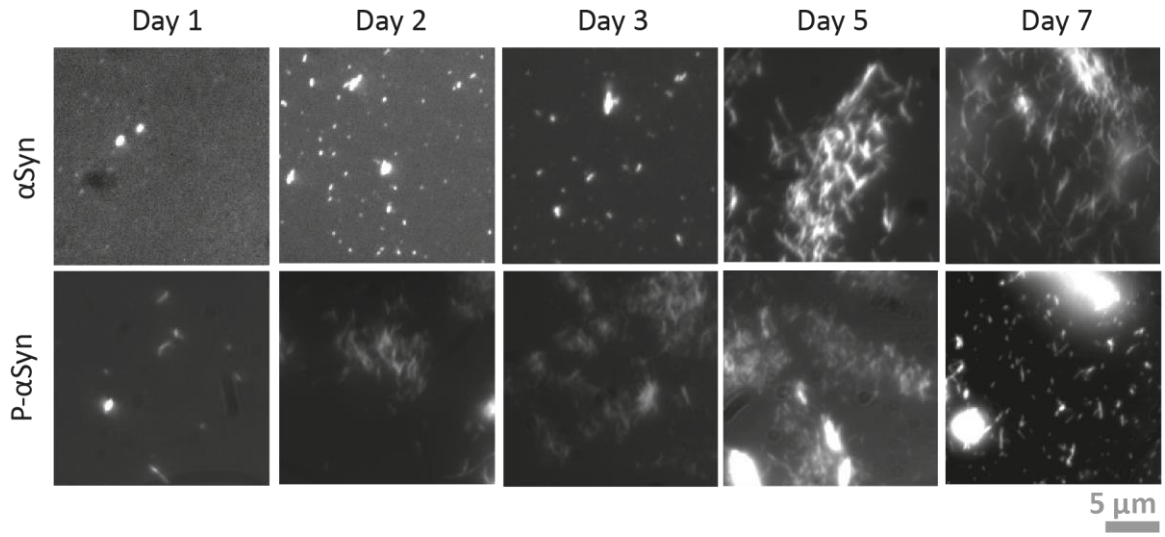

Figure 4.2. Aggregation of αSyn and p-αSyn. Representative images αSyn and p-αSyn aggregates at D1-D7. Aggregates are made up with ThT and imaged using the single molecule microscope at 405 nm wavelength.

All seeding studies in this chapter used Control 1 iDNLs, iDNLs were differentiated as previously described (Chapter 2). At the end of differentiation, αSyn aggregate species including oligomers (αSyn 48h and p-αSyn 48h) and fibrils (αSyn 7d and p-αSyn 7d) were added to the cell media to a final concentration of 1 µM. The aggregates were incubated on the cells for 24 hours and then media was removed, and fresh media was placed for another 24 hours (Figure 4.3) After a total of 48 hours the cells were then assayed.

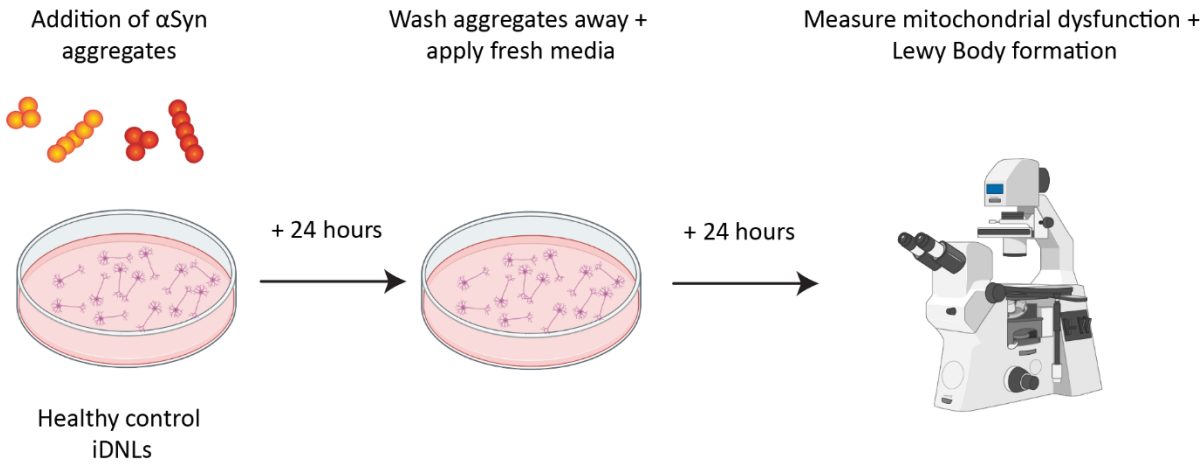

Figure 4.3. Schematic showing the seeding protocol. Aggregates are added to the iDNLs at the end of differentiation and incubated for 24 hours. After 24 hours aggregates are removed, cells are washed with PBS and fresh media is applied. After a further 24 hours cells are ready to assay.

Firstly, αSyn species ability to induce mitochondrial dysfunction in a healthy control model was tested by using TMRM, which accumulates and fluoresces in active mitochondria with intact membrane potential, and LysoTracker™ Deep Red to detect acidic organelles including lysosomes (Figure 4.4 A). TMRM and LysoTracker™ Deep Red have previously been used to detect dysfunctions in PD cells (Kim et al., 2021; Payne et al., 2024). As shown previously, Control 1 does not exhibit mitochondrial dysfunction (Figure 3.21). After adding the αSyn aggregates, the mitochondrial function was assessed. p-αSyn fibrils (7d) seeding induced a higher number of both mitochondria and lysosomes in the control iDNLs (Figure 4.4 B-C). Additionally, there was an increased amount of mitophagy after adding p-αSyn fibrils (7d) compared to the non-treated cells (Figure 4.4 D). There was a trend towards higher mitochondrial dysfunction after adding αSyn fibrils (7d) however it was not significantly different to PBS only treatment. Both oligomeric aggregates of αSyn and p-αSyn (48h) do not induce mitochondrial dysfunction in

Control 1 iDNLs. This data suggests that the most toxic species to cause mitochondrial dysfunction in iDNLs was p-αSyn fibrillar (7d) aggregates.

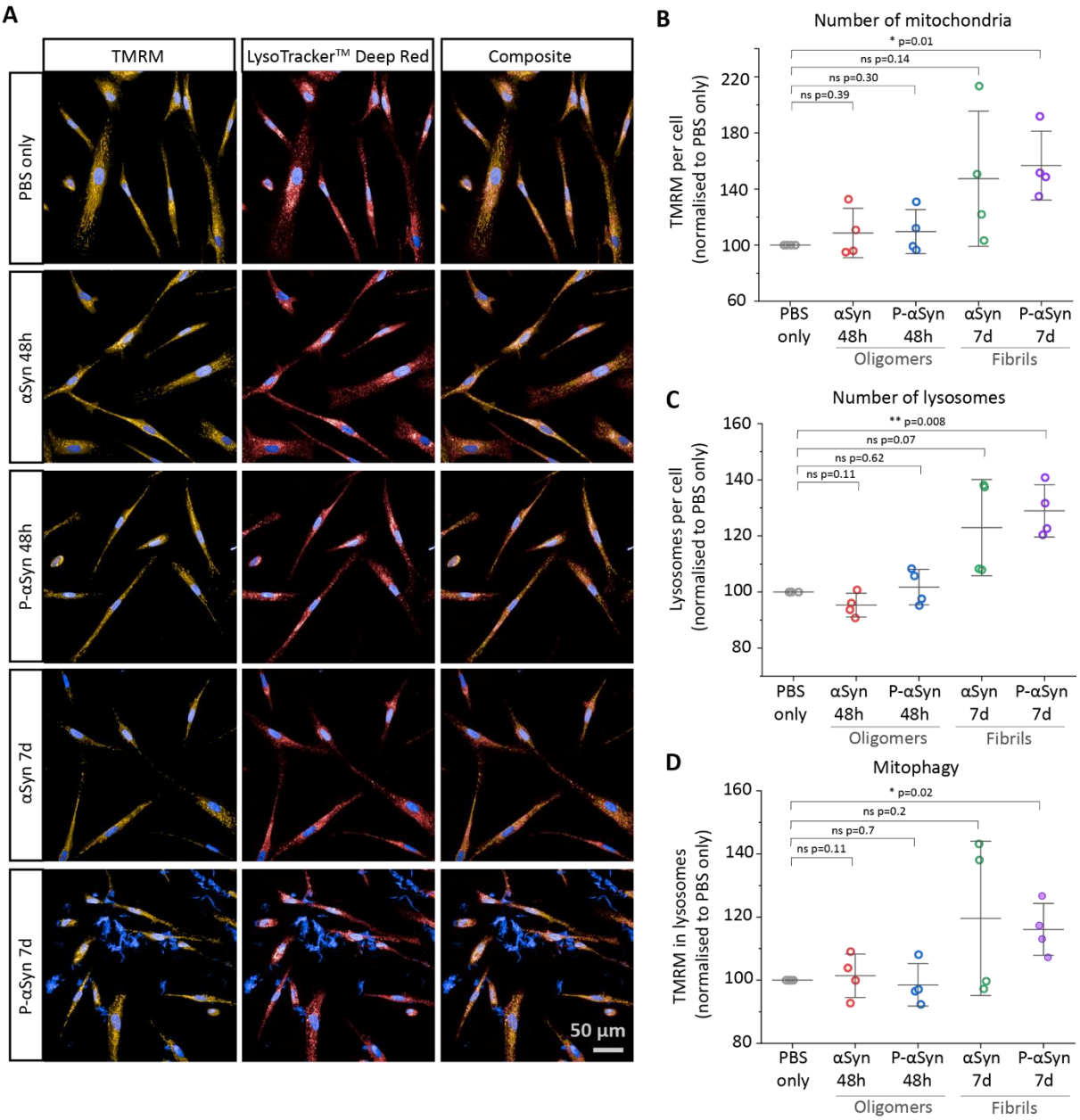

Figure 4.4. Seeding control iDNLs with αSyn species induces mitochondrial dysfunction. (**A**) Control 1 iDNLs treated with αSyn were incubated with MitoTracker™ Green, TMRM, LysoTracker™ Deep Red and Hoechst and imaged using the Opera Phenix. (**B**) Number of mitochondria per cell was calculated using TMRM. (**C**) Number of lysosomes per cell was calculated using LysoTracker™ Deep Red. (**D**) Mitophagy was calculated by the colocalization of TMRM Mitochondria in LysoTracker™ red spots. Graphs show four biological repeats, bars represent the mean ± SD. Statistical significance was determined using a paired sample t-test.

It was shown previously that PD patient iDNLs exhibit both mitochondrial dysfunction and the production of Lewy Body-like aggregates (Chapter 3). Seeding healthy iDNLs with species of αSyn is sufficient to induce mitochondrial dysfunction, and so next it was investigated whether the addition of αSyn aggregates could induce Lewy Body-like aggregates within a healthy control model.

For Lewy Body-like aggregate detection, the cells were lysed after treatment and cell lysates were probed for different Lewy Body markers in the presence of αSyn using SiMPull. The presence of mitochondrial proteins in αSyn aggregates was investigated (Figure 4.5). A higher number of Lewy Body-like aggregates containing αSyn aggregate, pSer129 αSyn and TOM20 formed after treatment with p-αSyn fibrils (7d) compared to the other αSyn species added, however due to the variability in single aggregate number, the difference is not significant (Figure 4.5 A-C).

Another mitochondrial marker VDAC1, was tested for its interaction with both αSyn aggregate and pSer129 αSyn after αSyn seeding in healthy controls (Figure 4.5 D-F). After treatment with p-αSyn fibrils (7d) there was a significantly higher number of αSyn aggregates colocalised with VDAC1 (Figure 4.5 D) and phosphorylated αSyn colocalised with VDAC1 (Figure 4.5 E). Lewy Body-like aggregates containing all three markers; aggregated αSyn, phosphorylated αSyn and VDAC1 was increased after treatment with p-αSyn fibrils (7d) (Figure 4.5 F). Interestingly, after treatment with αSyn oligomers (48h) there was also a significant increase in αSyn aggregates colocalised with VDAC1, and a significant reduction in phosphorylated αSyn colocalised Lewy Body-like aggregates compared to iDNLs treated with PBS only.

Next, the formation of Lewy Body-like aggregates containing p62 and ubiquitin was investigated after seeding iDNLs with αSyn (Figure 4.6). There was a significantly higher number of αSyn aggregates colocalised to p62, pSer129 αSyn colocalised to p62 and Lewy Body-like aggregates containing αSyn aggregate, pSer129 αSyn and p62 when Control 1 iDNLs were treated with p-αSyn fibrils (7d) (Figure 4.6 A-C). There was no significant difference in the formation of p62 Lewy Body-like aggregates when treated with either oligomeric (48h) aggregates of both αSyn and p-αSyn or αSyn fibrillar (7d) aggregates.

The presence of ubiquitin containing Lewy Bodies was assessed after αSyn seeding (Figure 4.6 D-F). Although there was a trend of a higher number of Lewy Body-like aggregates after

treatment with p-αSyn fibrils (7d), due to the variability in the number of single aggregates between repeats the difference was not significant. No difference was observed in the other conditions. This data suggests that p-αSyn fibrils (7d) are more toxic to iDNLs than other species, as it induces a large amount of Lewy Body-like aggregate formation.

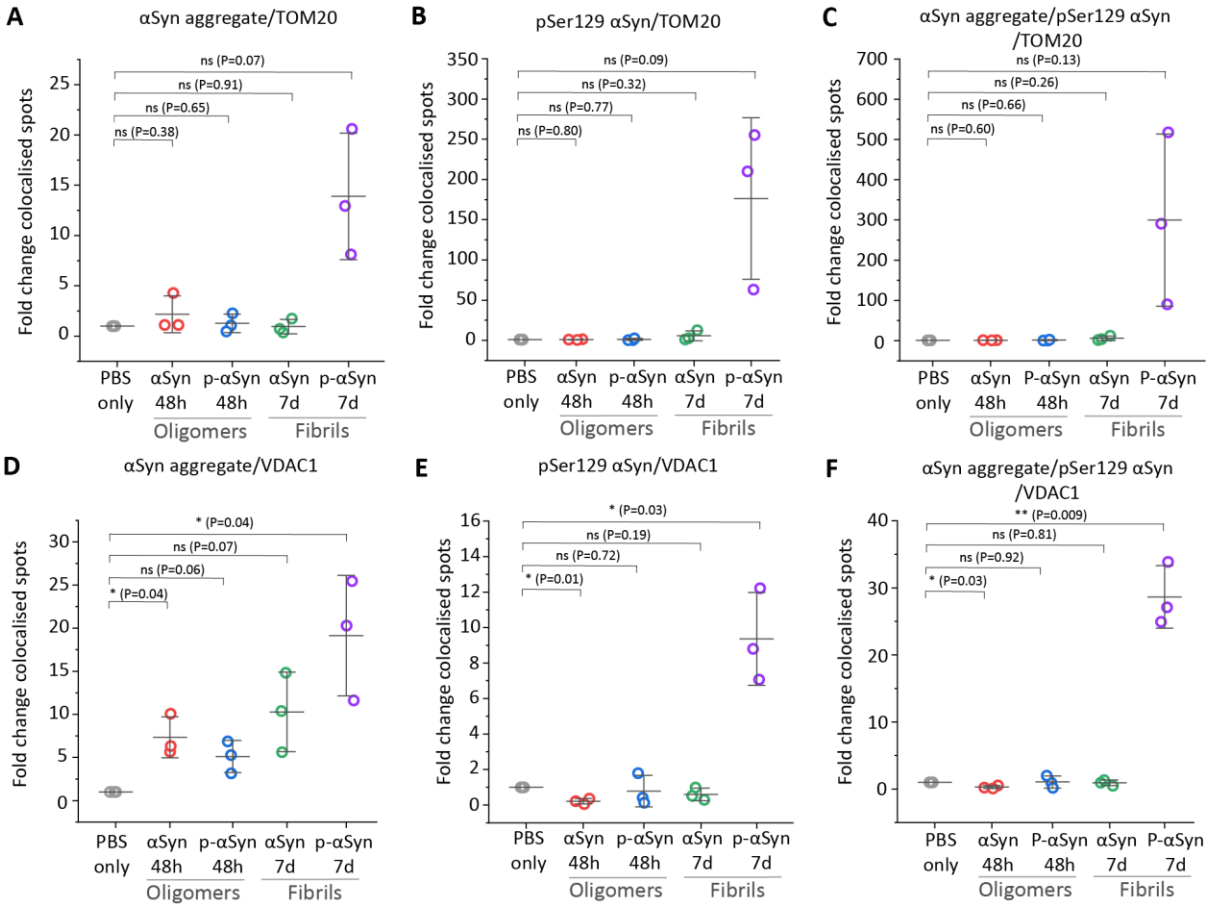

Figure 4.5. p-αSyn fibrils (7d) induces the formation of Lewy Body-like aggregates containing VDAC1 in iDNLs. After 48h of seeding with αSyn species, cells were lysed and Lewy body species were quantified using SiMPull, Lewy body species containing TOM20 (**A-C**) and VDAC1 (**D-F**) were investigated. Graphs show three biological repeats, bars represent the mean ± SD. Statistical significance was determined by a paired sample t-test.

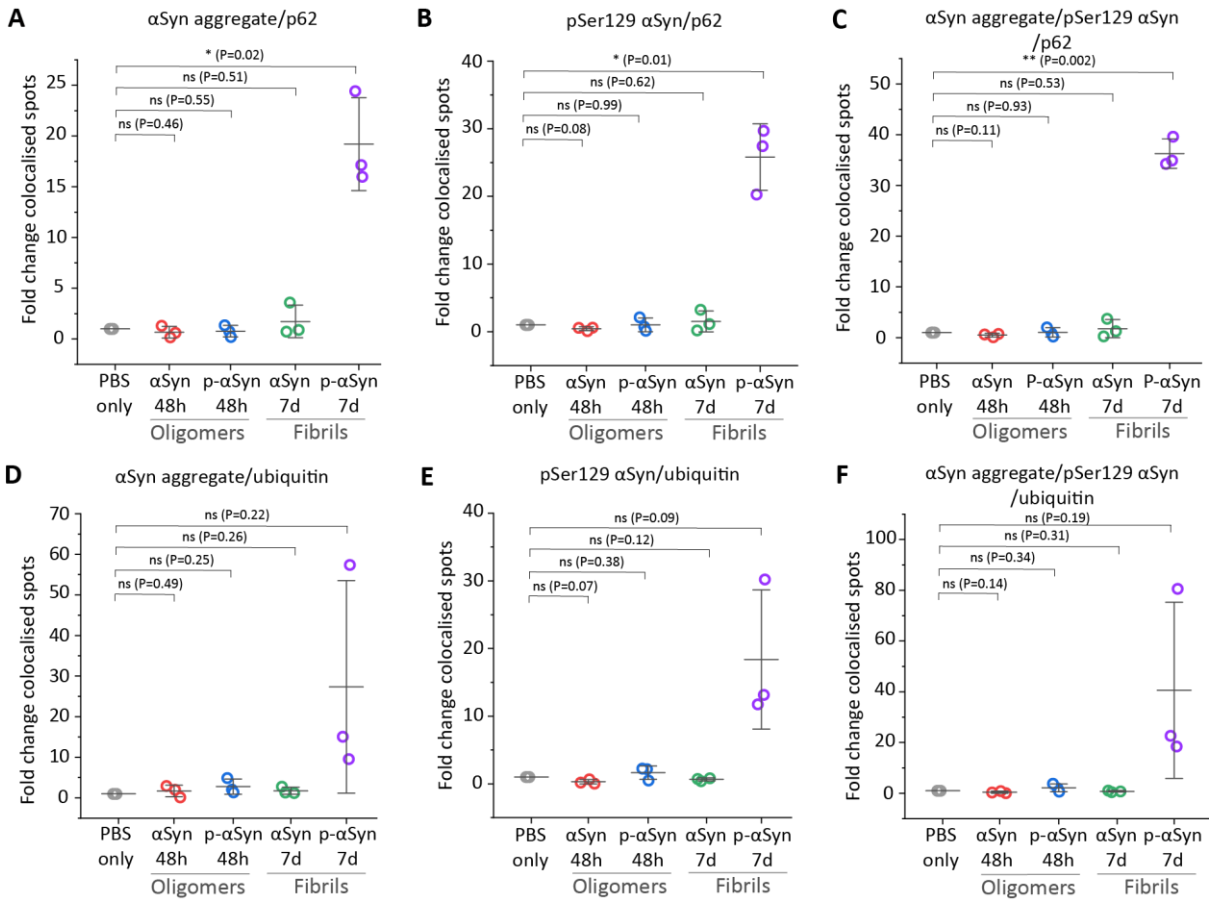

Figure 4.6. p-αSyn fibrils (7d) induces the formation of Lewy Body-like aggregates containing p62 in iDNLs. After 48h of seeding with αSyn species, cells were lysed and Lewy body species were quantified using SiMPull, the colocalisation of αSyn aggregate and pSer129 αSyn with p62 (**A-C**) and ubiquitin (**D-F**) were investigated. Graphs show three biological repeats, bars represent the mean ± SD. Statistical significance was determined by a paired sample t-test.

4.3.2. Probing the mechanism of mitochondrial dysfunction and Lewy body-like aggregate formation

To understand why only phosphorylated αSyn fibrils (7d) aggregates can induce mitochondrial dysfunction and Lewy body-like species formation within iDNLs, I deconstructed the specific pathway involved in the seeding mechanism. This pathway involves the following steps:

- The uptake of αSyn species by cells: I compared the efficacy of cellular internalisation of different types of αSyn aggregates.
- Processing of αSyn species: I assessed how quickly the internalised αSyn seeds reached the lysosome machinery for degradation.
- Recruitment of endogenous αSyn monomer to form more 'seeds': I tracked the ability of the αSyn seeds to recruit endogenous αSyn monomers and form aggregates by mimicking in vitro aggregation.
- Mitochondrial damage induced by αSyn aggregates: I studied the interaction between the αSyn and p-αSyn aggregates and mitochondrial membranes to understand αSyn-mediated mitochondrial damage.

Each of these steps provides insight into the specific behaviours and characteristics of αSyn and p-αSyn aggregates, including both oligomers and fibrils, that make them particularly potent in inducing PD pathology in cellular models.

4.3.3. The uptake of αSyn species by cells

It is important to understand if there is a difference in uptake of different species into iDNLs, as increased uptake of specific forms of αSyn could lead to more seeding and greater toxicity. To measure the uptake, I used 488-labelled αSyn in order to differentiate in vitro aggregates from endogenous αSyn within the cells. 488-labelled αSyn was bought and phosphorylated in the lab as previously outlined in Chapter 2. To confirm phosphorylation, a western blot was carried out using pan-αSyn antibody and pSer129 αSyn antibody (Figure 4.7).

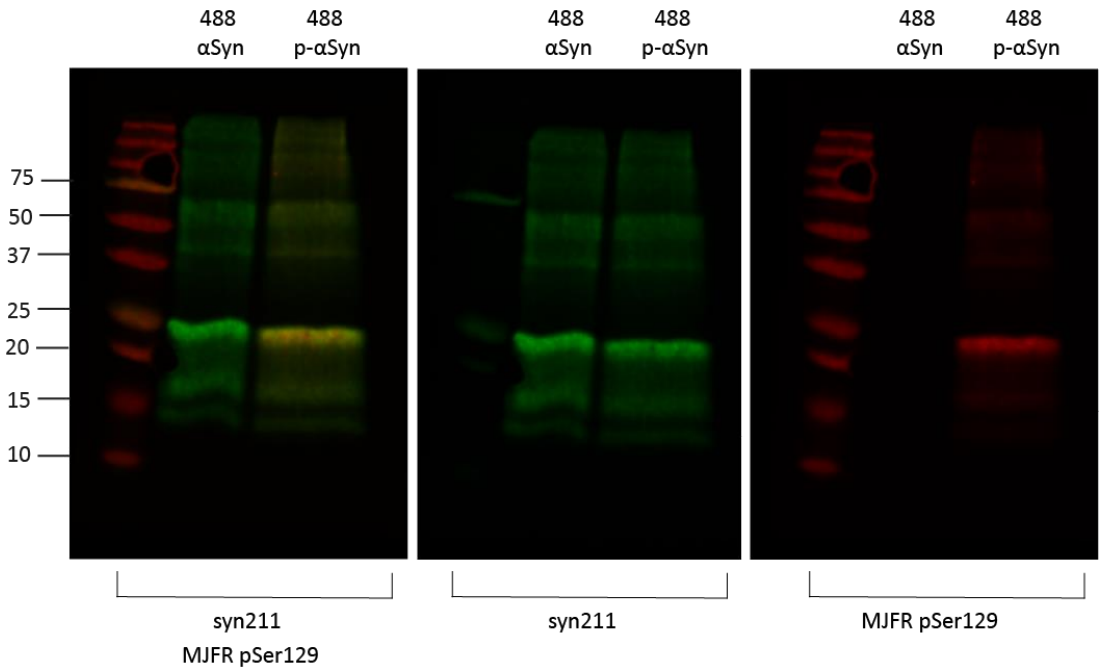

Figure 4.7. Validation of the phosphorylation of 488-labelled αSyn. 488-labelled αSyn was phosphorylated according to protocol, and the phosphorylation was validated by probing both proteins on a western blot for pan-αSyn antibody syn211 (green) and pSer129 αSyn antibody (red).

Once 488-labelled αSyn and 488-labelled p-αSyn monomeric proteins were prepared, aggregates were generated in the same way as previously shown. Aggregates were added to iDNLs media to a final concentration of 1 µM, incubated for 24 hours and uptake was measured by the 488 fluorescence within the iDNLs (Figure 4.8). TMRM was used as a cellular mask and then Alexa Fluor 488 fluorescence within the cellular mask was measured. The uptake of 1 µM αSyn and p-αSyn oligomers (48h) and fibrils (7d) was measured. Emission using 488 nm excitation was observed in all conditions except the PBS only control (Figure 4.8 A). However, there was no difference in the number of αSyn spots (Figure 4.8 B), the spot intensity (Figure 4.8 C) and the spot area (Figure 4.8 D) after addition of any of the αSyn species.

Next, the uptake after 48 hours was assessed. αSyn aggregates were added to cell media and incubated for 24 hours, after 24 hours the media was changed and incubated for a further 24 hours. After 48 hours in total, the cells were imaged using the Opera Phenix (Figure 4.9 A). Upon addition of 1 µM aggregate there was no difference between number of αSyn spots, intensity of αSyn spots and area of αSyn spots after 48 hours (Figure 4.9 B-D). This data shows

only two repeats so a third repeat would be necessary to conclude a significant difference, however it seems there is no difference in αSyn uptake after both 24 hours and 48 hours.

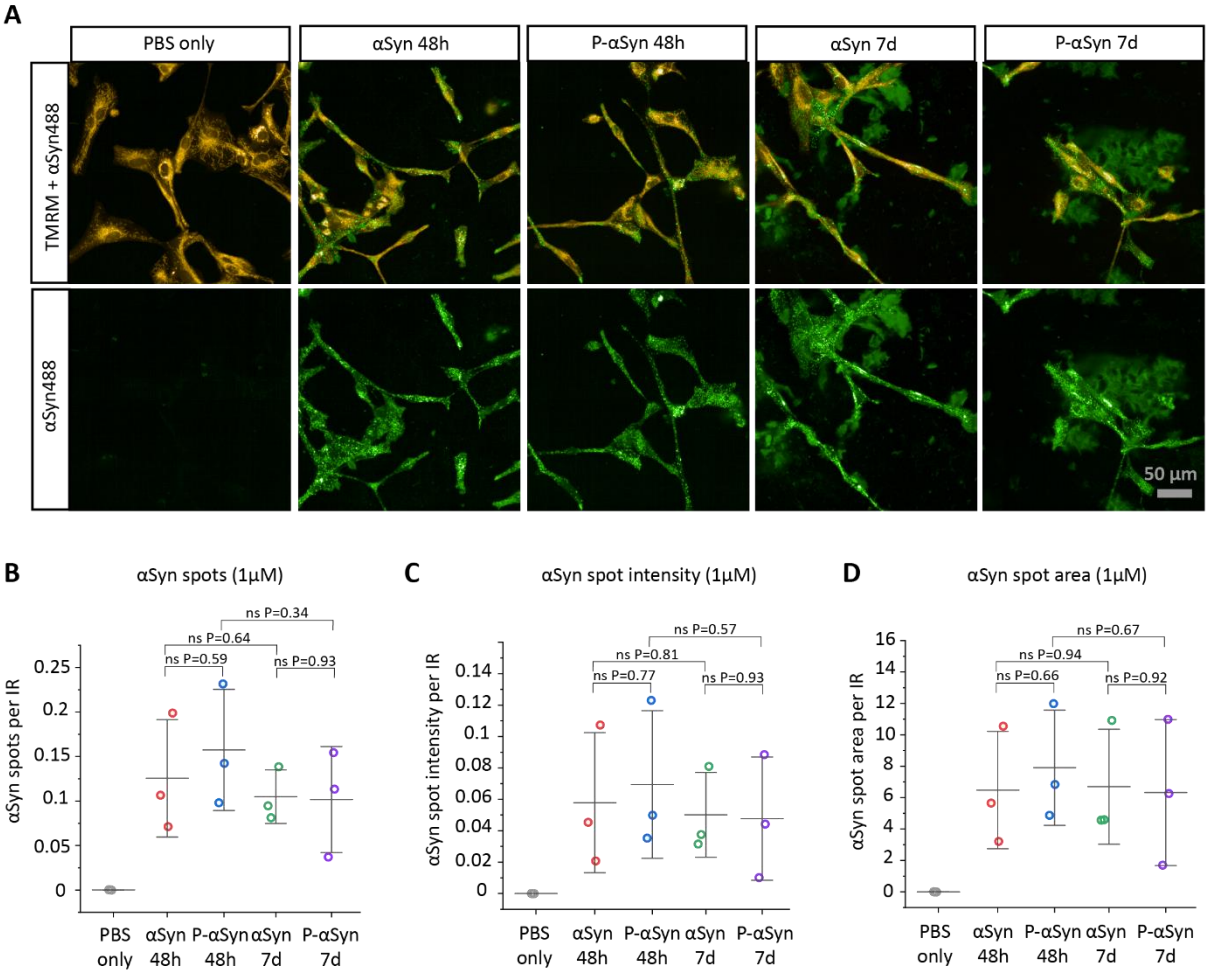

Figure 4.8. There is no difference in uptake between different aggregation states and conformations of αSyn after 24 hours. A. Representative images of iDNLs after 24-hour treatment with PBS only, or 1 µM of αSyn or p-αSyn oligomer (48h) or fibrils (7d). TMRM dye was used to calculate the cell area, and 488 nm laser detected any 488-labelled αSyn uptake. **B.** The number of αSyn spots per image region was calculated after addition of aggregates. **C.** αSyn fluorescence intensity per image region after addition of aggregates. **D.** αSyn spot area in pixels normalised to total image region after addition of aggregates. Graphs show 3 biological repeats per condition, bars represent mean ± SD. Statistical significance was determined by a two sample t-test.

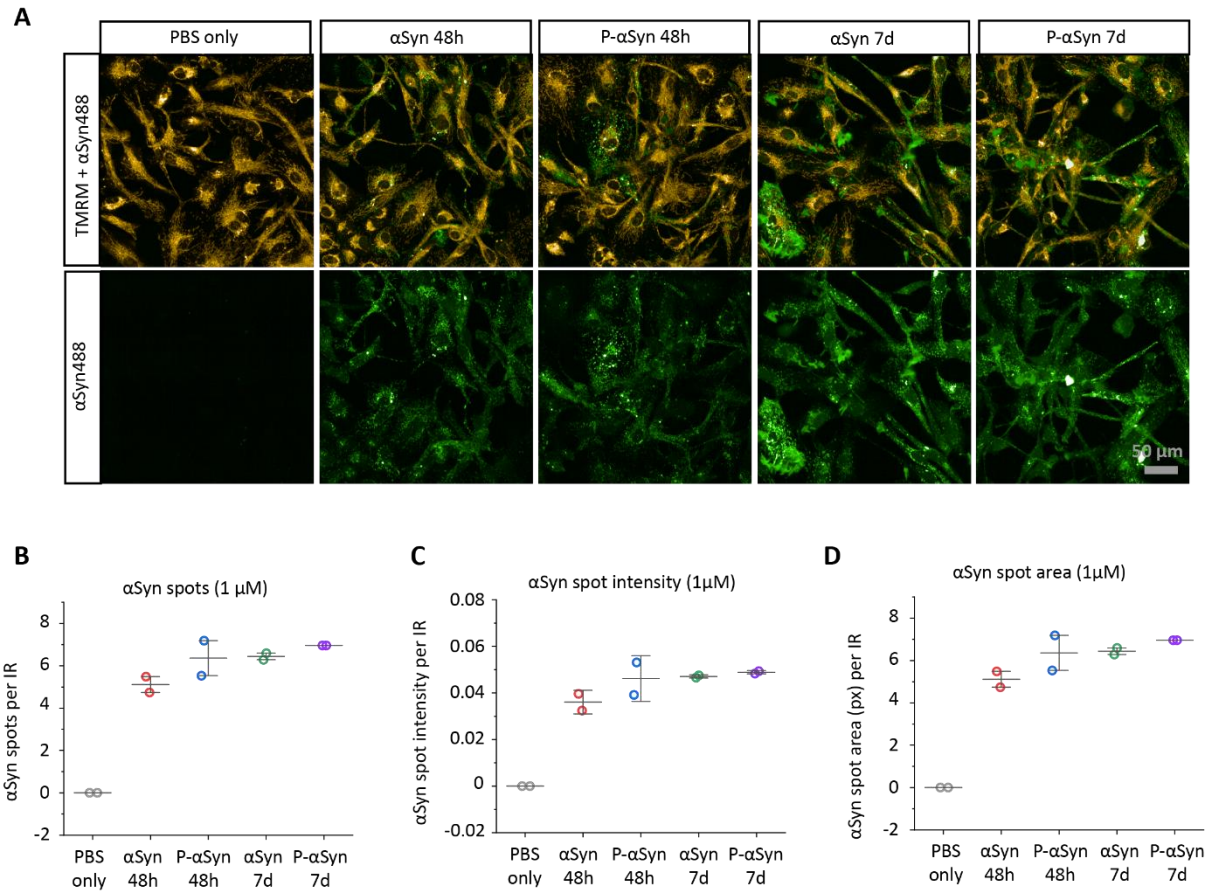

Figure 4.9. There is no difference in uptake of αSyn 48 hours after treatment. (A) Representative images of iDNLs after treatment with either PBS, αSyn 48h, p-αSyn 48h, αSyn 7d or p-αSyn 7d. Cells were imaged with 488 to detect αSyn-488, and TMRM to detect the cell area. (B) The number of αSyn spots in the cells normalised to image region. (C) The intensity of αSyn spots in the cells normalised to image region. (D) The area of αSyn spots in the cells normalised to image region. Graphs show two biological repeats, bars represent mean ± SD. Statistical test was not performed due to only two repeats.

4.3.4. Processing of αSyn species

Once the αSyn aggregates were taken up, I sought to understand if there was a difference in how fast the aggregates were being processed by the degradation machinery of the cells. To do this, aggregates were added for 1 hour before removal and fluorescence of 488 nm dye was measured at regular intervals from 2 hours to 8 hours post-treatment (Figure 4.10). There was a significantly higher number of αSyn-488 spots, the intensity of αSyn spots and the area of αSyn spots in αSyn fibrils (7d) treated cells compared to the phosphorylated form (Figure 4.10 B-D). This difference was not observed in the oligomeric (48h) aggregates of αSyn and p-αSyn, and the intensity of oligomers was lower than fibrillar (7d) aggregates. Despite the aggregates being removed from the cells, fluorescence intensity significantly increased over time for both αSyn and p-αSyn fibril (7d) treated cells. It was surprising why fluorescence signal arising from dye labelled αSyn aggregates within the cells was increasing once aggregates had been removed, as no aggregate remained in the media to be taken up by the cells. To confirm this, the assay was repeated with two extra PBS washes after removing the aggregates, to ensure that no aggregates remain on the plate (Figure 4.11). After PBS washes, an increase in number of αSyn spots, intensity of αSyn spots and area of αSyn spots was still observed over time (Figure 4.11 A-C).

To explain this unexpected finding, I first hypothesised that 488-αSyn seeds may recruit endogenous unlabeled monomeric αSyn present within the cells, and the rearrangement into new aggregate structures may increase the fluorescence intensity of peptide bound dyes. To test this hypothesis, an in vitro assay was performed whereby 488-labelled aggregates were incubated with non-labelled αSyn monomer at 37°C. There was no increase in fluorescence observed over time for both αSyn and p-αSyn aggregates (Figure 4.11 D). Next, it was investigated whether 488-labelled dye was pH sensitive and fluorescence intensity depends on the cellular location. To test this hypothesis, 488-labelled αSyn aggregates were incubated in buffer with varying pH values (7.5-4.5) and the fluorescence was measured. It was found that both 488 labelled αSyn and p-αSyn exhibit a lower fluorescence at higher pH's such as pH 7.5, and the fluorescence increases at lower pH's such as pH 4.5 (Figure 4.11 E). This result suggests that when αSyn is trafficked to any cellular organelle with low pH such as lysosome (pH 4.5-5), it will have increased fluorescence compared to in the cytosol (pH 7.5). This was verified within iDNLs by measuring colocalisation of αSyn-488 and lysosomes using

LysoTracker™ Deep Red in a time dependent manner (Figure 4.12 A). It was found that αSyn colocalisation with lysosomes increased over time; there was an increase in the number of αSyn spots colocalised to lysosomes over time, an increase in the fluorescence of αSyn spots in lysosomes over time, and increased area of αSyn spots in lysosomes over time (Figure 4.12 B-D). The increase was much larger in the αSyn fibril (7d) treated cells, whereas p-αSyn fibrils (7d) plateaus after 4 hours.

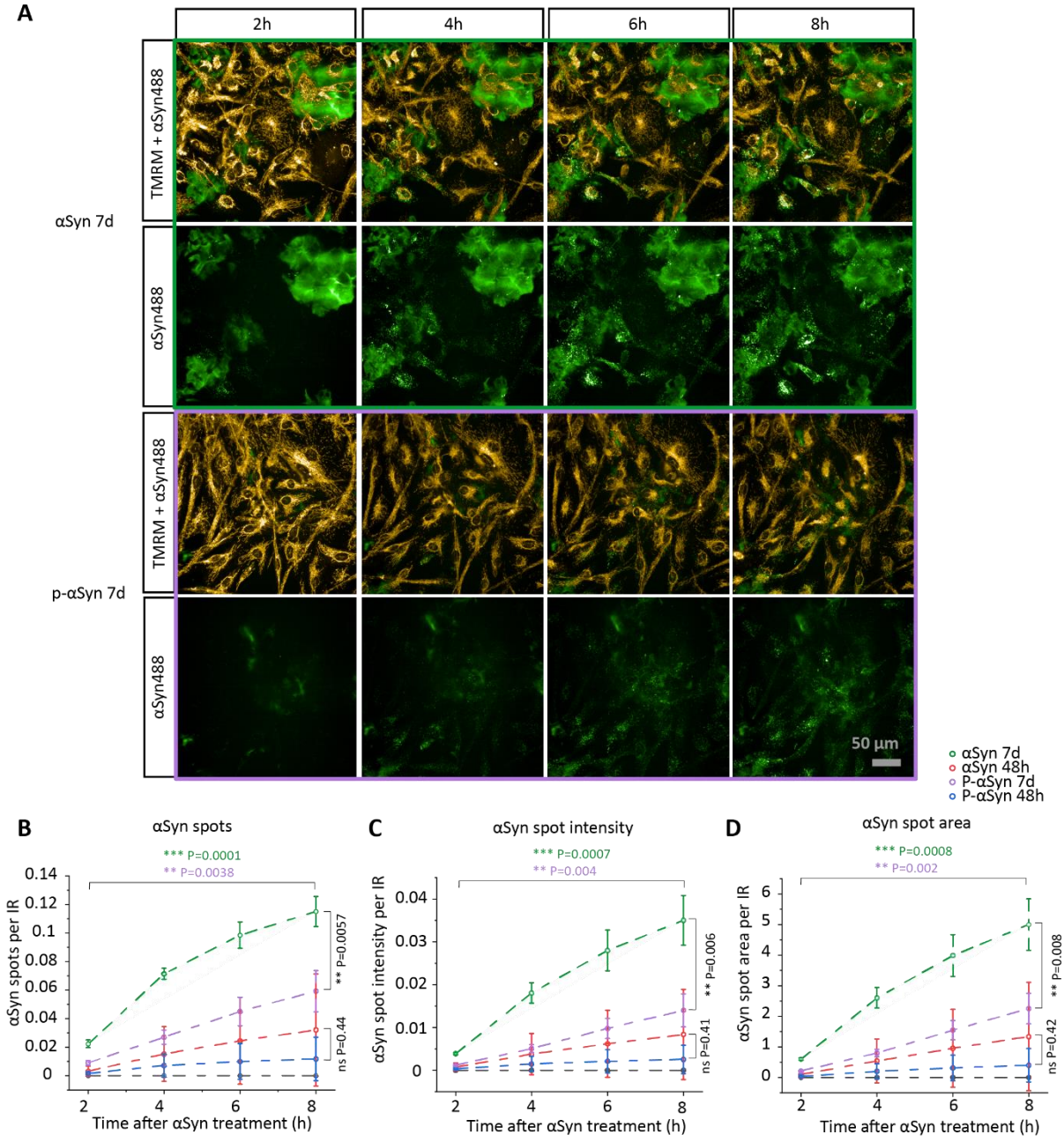

Figure 4.10. αSyn-488 fluorescence increases over time from 2 hours to 8 hours. A. Representative images of iDNLs after treatment with 1 µM 488-labelled αSyn and p-αSyn fibrils (7d) over time. **B-D.** Cells were treated with 1 µM either αSyn or p-αSyn oligomers (48h) or fibrils (7d), the number of αSyn spots was determined (**B**), the αSyn spot intensity determined (**C**), and the αSyn spot area in

pixels was calculated (**D**). Each readout was normalized to total image region. Error bars represent the mean ± SD of three replicates. Statistical tests included two sample t-test.

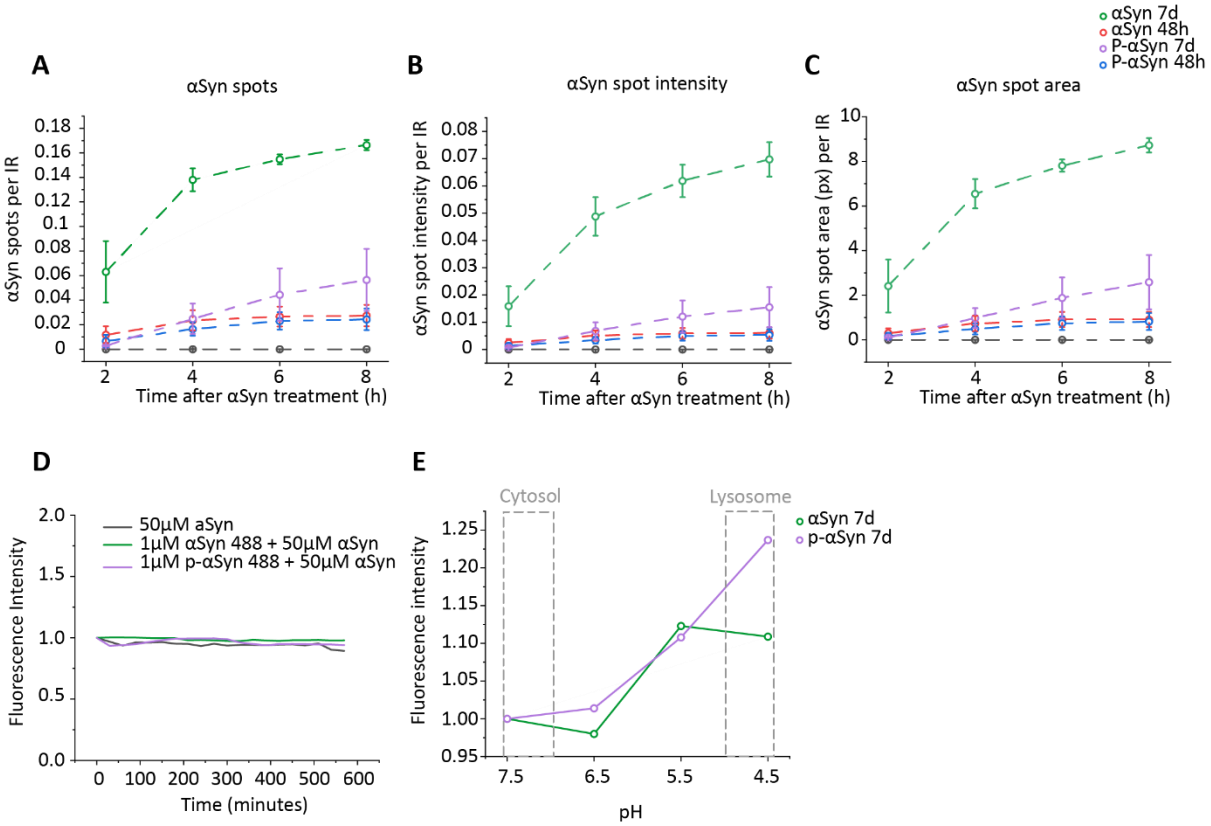

Figure 4.11. Investigating the increase of αSyn 488 fluorescence once within the cell. To understand why αSyn-488 fluorescence increases when no more αSyn-488 is taken up by the cells, several assays were performed. **A-C.** αSyn aggregates were added for 1 hour, and then removed and two extra PBS washes were performed. The uptake was then measured at 2 hours, 4 hours, 6 hours and 8 hours post-treatment. Uptake was determined in the form of: number of αSyn spots (**A**), αSyn spot intensity (**B**), and αSyn spot area (**C**). **D.** 488-labelled αSyn and p-αSyn fibrils (7d) were incubated with monomeric αSyn and their fluorescence intensity measured over time, normalised to fluorescence value at 0 minutes. **E.** The pH sensitivity of αSyn and p-αSyn fibrils (7d) were measured, data normalised to fluorescence at pH 7.5. Data points in A-C represent two biological replicates, and bars represent the mean and SD. Data points in D-E represent one biological replicate.

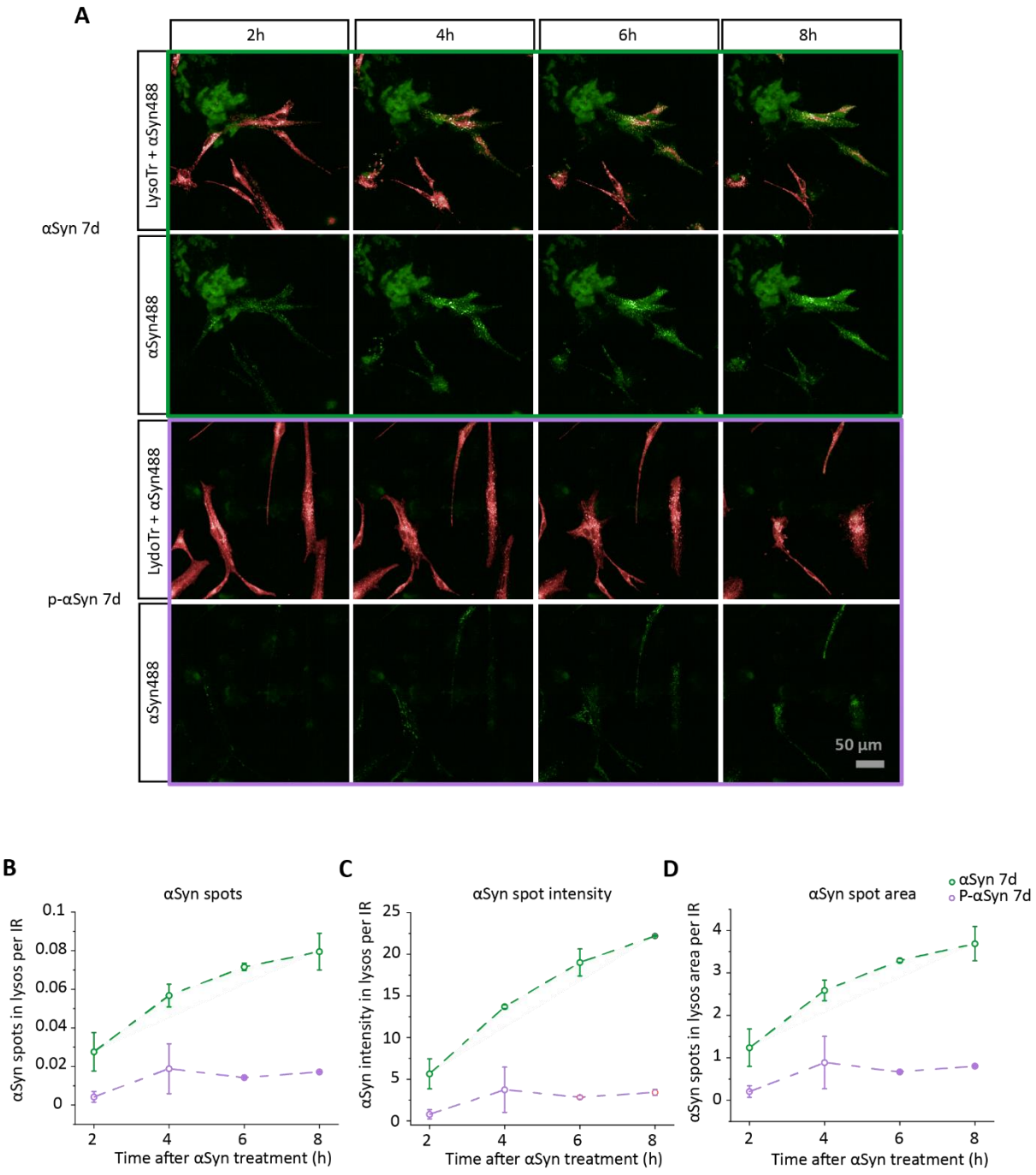

Figure 4.12. αSyn 7d colocalises with lysosomes over time. (**A**) Representative images of Control 1 iDNLs after treatment with 488 labelled αSyn and p-αSyn fibrils (7d) at 2 hours, 4 hours, 6 hours and 8 hours post-treatment. (**B**) The number of αSyn spots colocalised with lysosomes normalised to image region. (**C**) The intensity of αSyn spots that are colocalised in lysosomes, normalised to image region. (**D**) αSyn spot area of spots colocalised with lysosomes, normalised to image region. Bars represent the mean and SD of 2 biological repeats.

4.3.5. Recruitment of endogenous αSyn monomer to form more 'seeds'

Variability in the structural conformation of αSyn strains contributes to differential abilities in recruiting monomeric αSyn and inducing seeding, therefore these strains have varying capacities to spread αSyn aggregates and promote disease progression (Candelise et al., 2019; Froula et al., 2019). To determine whether αSyn and p-αSyn fibrils (7d) have different seeding propensities which lead to their differential toxicity, in vitro seeding experiments were performed. The process of seeding has been largely recapitulated in vitro, where αSyn fibrils are added to monomeric αSyn and they can act as templates to allow further aggregation. The aggregation is monitored and determines the seeding ability of the fibril.

αSyn and p-αSyn fibrils (7d) acted as seeds for monomeric αSyn, and the aggregation was measured by ThT fluorescence over time, in quiescent conditions (Figure 4.13). Various concentrations of seeds were added to 50 µM monomeric protein from 0% seeds to 10% seeds. Without any seeds, no aggregation of either αSyn or p-αSyn was observed (Figure 4.13 A-B). In the presence of 0.2% seeds, p-αSyn aggregates at a faster rate than αSyn as shown by an increased ThT fluorescence (Figure 4.13 C-D). A similar trend is shown in the presence of 0.5% seeds and 1% seeds, the images show fibrils are starting to form clumps together (Figure 4.13 E-H). When monomeric αSyn is incubated with 5% seeds and 10% seeds, aggregation happens very quickly for both αSyn and p-αSyn, as they both reach a plateau by 10 hours (Figure 4.13 I-L). However, the plateau for p-αSyn is a much higher fluorescence value of 2.5 x 10^7, compared to αSyn´s fluorescence value of 5 x 10^6. This could be due to more p-αSyn aggregates forming, or a different conformation of aggregate being generated.

As 0% seeds to 1% seeds do not reach plateau by 45 hours it is not possible to calculate the half time or t_{50} (time at which fluorescence is 50% of the plateau fluorescence). At 5% seeds, the half-time for αSyn is 5.08 hours, whereas the half-time for p-αSyn is 0.58 hours (Figure 4.14). Aggregation occurs much quicker with the addition of 10% seeds, shown by the half-time of αSyn at 2.4 hours compared to 0.25 hours for p-αSyn (Figure 4.14). Overall, this suggests that p-αSyn can recruit monomeric αSyn more effectively and allow for rapid seeding and explains why p-αSyn is more toxic to iDNLs than αSyn.

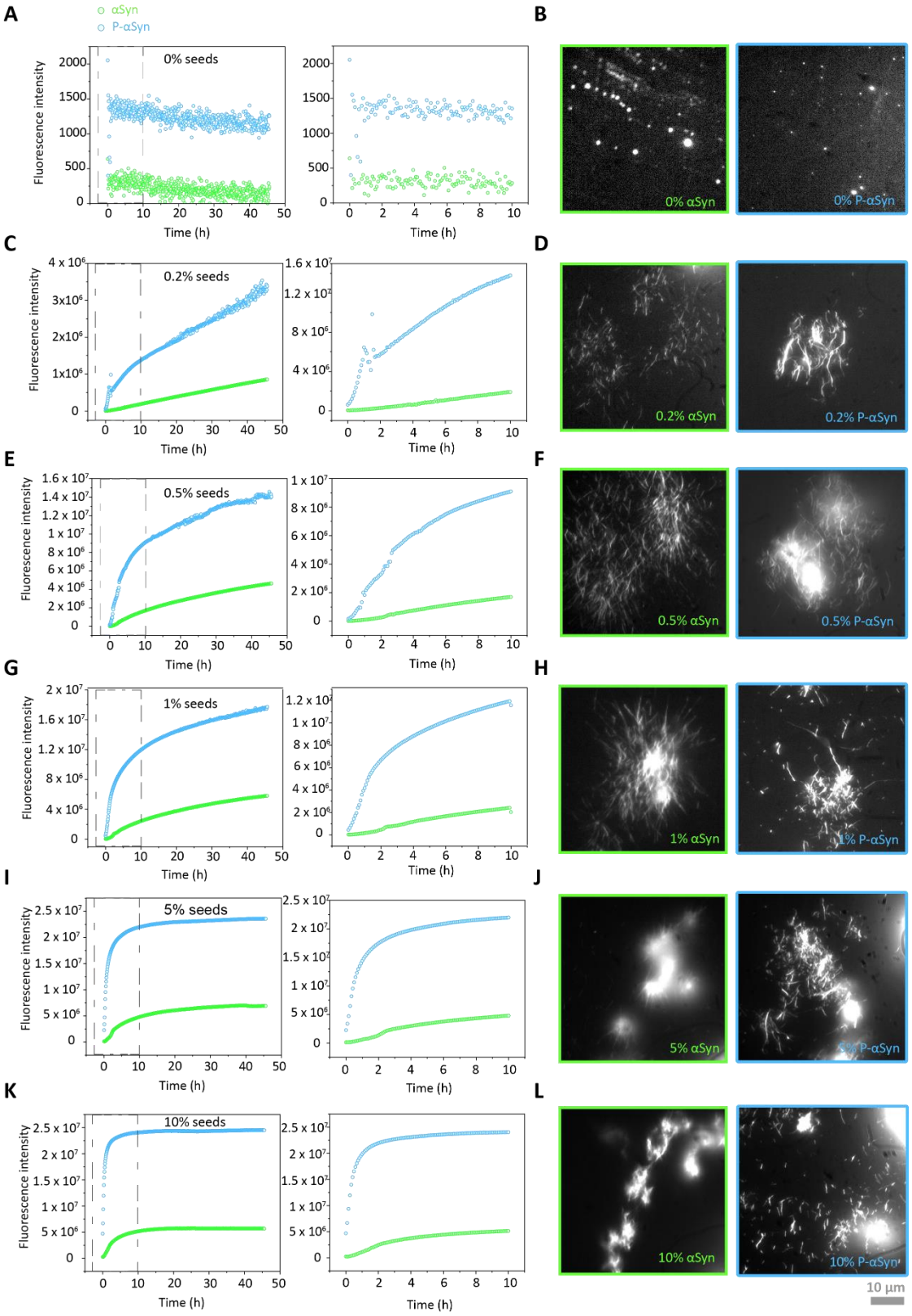

Figure 4.13. In vitro seeding of αSyn using αSyn and p-αSyn seeds. Aggregation of αSyn was measured in the presence of different percentages of seeds of αSyn and p-αSyn by ThT fluorescence, and representative images are shown, for 0% seeds (A-B), 0.2% seeds (C-D), 0.5% seeds (E-F), 1% seeds (G-H), 5% seeds (I-J) and 10% seeds (K-L). Graphs show 0-50 hours and 0-10 hours. Results are taken from one biological replicate.

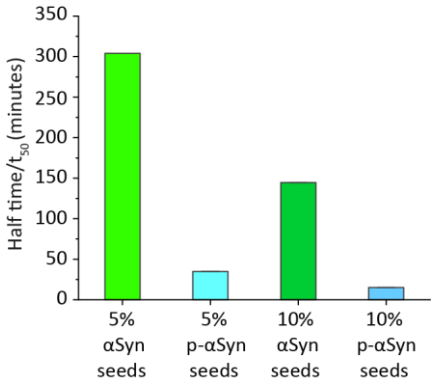

Figure 4.14. Half time plots of 5% and 10% seeded aggregation for αSyn and p-αSyn. The time taken to for fluorescence to reach the maximum plateau fluorescence was plotted for the presence of 5% and 10% seeds of αSyn (green) and p-αSyn seeds (blue). Graph shows one biological replicate.

4.3.6. Mitochondrial damage induced by αSyn aggregates.

The data within this chapter suggests that p-αSyn fibrils are more potent seeds to induce mitochondrial toxicity to control iDNLs than its non-phosphorylated wildtype counterpart (Figure 4.4). Here I propose a mechanism of how the p-αSyn isoform is more toxic to cells, by focusing on mitochondrial dysfunction.

αSyn aggregates are known to interact with and disrupt lipid membranes, in particular smaller αSyn aggregates, similar to oligomers, are reported to be more toxic than larger αSyn species (Emin et al., 2022; Fusco et al., 2017). I investigated the ability of αSyn species, that were either phosphorylated or non-phosphorylated, to disrupt lipid membranes. Vesicles were created with varying phospholipids, and filled with calcium sensitive dye, so that membrane permeabilization by αSyn species could be measured based on the influx of calcium ions into the vesicle (Figure 4.15. A). This method was previously used to analyse αSyn aggregate toxicity using recombinant proteins and those isolated from postmortem tissue, CSF and PD patient derived stem cell models (Choi et al., 2022; Rodrigues et al., 2022; Sanderson et al., 2020; Varela et al., 2018). The ability of monomeric αSyn, αSyn oligomers (48h) and αSyn fibrils (7d) aggregates to disrupt lipid membranes was assessed (Figure 4.15 B). It was found that the oligomeric (48h) aggregates induced higher calcium ion influx compared to both αSyn monomer and αSyn fibrils (7d). Fibrillar aggregates of αSyn also had an increased ability to disrupt membranes compared to αSyn monomer. Phosphorylated αSyn was then tested for its ability to permeabilize membranes, similarly the p-αSyn oligomeric aggregates were the

most damaging, followed by p-αSyn fibrils, and p-αSyn monomer did not induce membrane damage (Figure 4.15 C).

Since I have observed that p-αSyn aggregates interact with mitochondrial proteins and induce mitochondrial dysfunction, vesicles that mimic the mitochondrial membrane were generated. A mitochondrial exclusive phospholipid, cardiolipin, comprises around 20% of total phospholipids within the mitochondrial membrane (Hryc et al., 2023). The ability of αSyn species to disrupt the membranes was assessed again when the vesicles contained 10% and 20% cardiolipin (Figure 4.15 D). Upon increasing the percentage of cardiolipin in the membrane from 0% to 20%, the calcium influx induced by p-αSyn oligomers increased significantly (** P=0.0032), whereas αSyn oligomers showed no difference in calcium ion influx (ns P=0.19). When vesicles were incubated with p-αSyn fibrils there was increase in calcium influx from 0% cardiolipin to 20% cardiolipin (* P=0.01), whereas αSyn fibrils showed no difference in calcium influx after increasing cardiolipin (ns P=0.37). This suggests that phosphorylated αSyn aggregates are more toxic to mitochondrial membranes than non-phosphorylated αSyn, and their propensity to damage the mitochondrial membrane increased with cardiolipin content.

To investigate within a cellular model, the ability to disrupt membranes was assessed using cell lysate of Control 1 and SNCA (Figure 4.15 E). There was a trend towards higher calcium influx in SNCA compared to Control 1, however due to the variability in samples this was not significant. Then αSyn pulldown was used to remove any αSyn species within the lysate, and the ability to disrupt membranes was measured again. There was significantly less calcium influx in Control 1 after removal of αSyn, however there was no significant difference in SNCA after αSyn pulldown, but the trend suggests there was less membrane damage after removing αSyn.

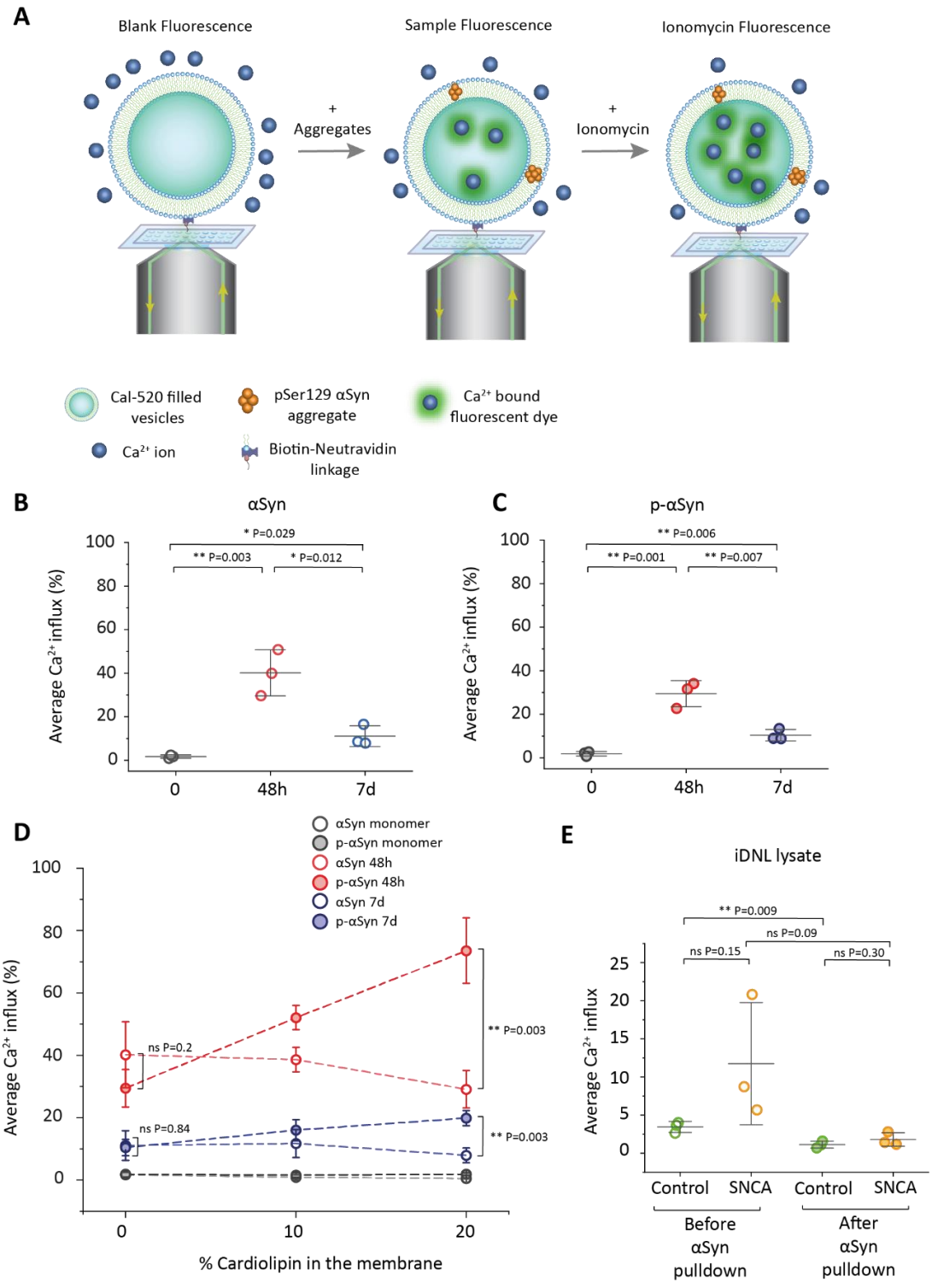

Figure 4.15. P-αSyn aggregates are more damaging to mitochondrial membranes than αSyn aggregates. The ability of αSyn species to disrupt membranes was assessed a membrane permeabilization assay. (**A**) Schematic of the membrane permeabilization assay to measure Ca^{2+} influx after incubation with αSyn and p-αSyn aggregates. (**B**) Average Ca^{2+} influx of liposomes after incubation with αSyn monomer, αSyn oligomers (48h) and αSyn fibrils (7d). (**C**) Average Ca^{2+} influx of liposomes after incubation with p-αSyn monomer, p-αSyn oligomers (48h) and p-αSyn fibrils (7d). (**D**) Measurement of membrane permeabilization of αSyn species upon increasing concentration of

cardiolipin in the membrane to mimic a mitochondrial membrane (0%, 10%, 20%). (**E**) Membrane permeabilization of iDNL lysate of Control 1 and SNCA, before and after pulldown to remove αSyn species. Each data point represents one biological repeat, bars represent mean and SD of three biological repeats.

αSyn aggregates that are present within human cells and living organisms are comprised of various conformations of αSyn, containing both phosphorylated and non-phosphorylated αSyn. Due to their structural similarities, these isoforms are likely to co-aggregate during the aggregation process. However, the complex nature of aggregation processes suggests that the proportion of these isoforms within co-aggregates can vary, potentially leading to differing characteristics in the aggregates formed. This variation in composition may influence the biological properties of the aggregates, such as toxicity, or interaction with cellular components. I sought to understand in a controlled way, how much p-αSyn needs to be present within an αSyn p-αSyn co-aggregate to deem it more toxic to mitochondria than pure αSyn aggregate. To do this, fluorescent nanosphere were coated in different ratios of αSyn and p-αSyn aggregates (αSyn: p-αSyn 100:0, 75:25, 50:50, 25:75, 0:100) (Figure 5.16 A). This method, recently developed in our lab, allows for the creation of homogenous aggregates of known size and composition, enabling precise measurement of their functional impacts. By precisely controlling the proportion of phosphorylation at a single-particle level, I dissected the effects of these key molecular drivers on the overall disease-related functions of the αSyn containing aggregates. Once the coated nanospheres were engineered, total protein concentration was assessed to confirm the amount of protein was the same across different ratios (Figure 4.16 B), and colocalisation to confirm the beads contained both αSyn and p-αSyn (Figure 4.16 C).

The ability of the coated beads to disrupt membranes was then assessed. First, vesicles without cardiolipin were incubated with each type of nanosphere (Figure 4.16 D). There was no difference in calcium ion influx between the different ratios of αSyn and p-αSyn. This data supports previous observation where phosphorylation at Ser129 does not change the ability of αSyn to disrupt cardiolipin free membranes (Figure 4.15). As I previously showed p-αSyn is more toxic to mitochondrial mimicking membranes, nanospheres containing different ratios of αSyn and p-αSyn were incubated with a mitochondrial like membrane (20% cardiolipin) and calcium ion influx was assessed (Figure 4.16 E). Introducing 25% phosphorylated αSyn

into the nanosphere was sufficient to cause a significant increase in membrane damage, compared to pure wildtype αSyn coated nanospheres. These results show that just 25% of phosphorylation within αSyn aggregates render them more damaging towards mitochondrial mimicking membranes. When the phosphorylated αSyn content was increased to 50%, there was a significant increase in calcium influx compared to 25% p-αSyn and made them as damaging as pure p-αSyn coated nanospheres. This data clearly shows that p-αSyn are more damaging towards cardiolipin rich mitochondrial membranes and the proportion of p-αSyn within αSyn aggregates is correlated with their mitochondrial damaging property.

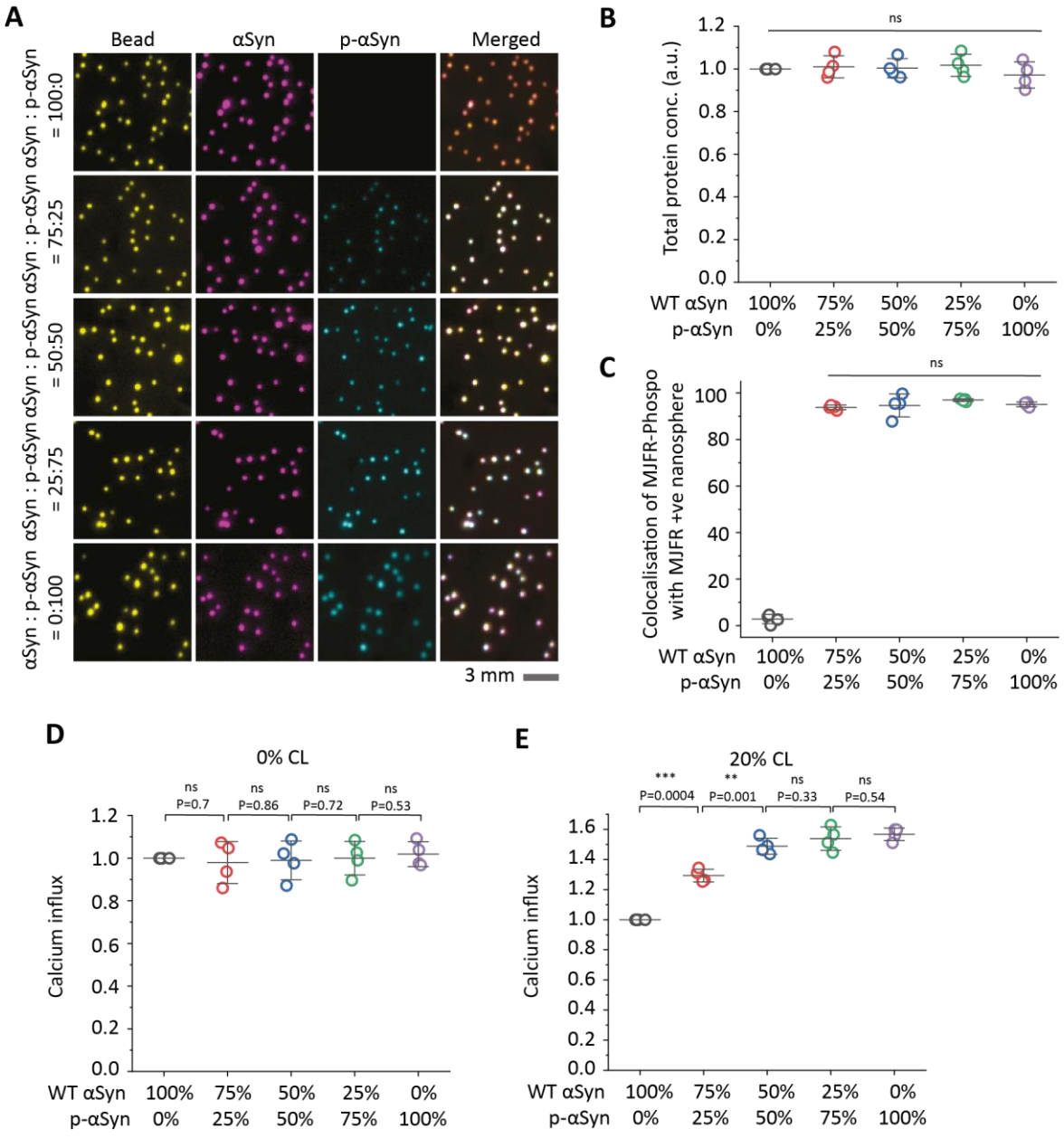

Figure 4.16. Increasing the amount of phosphorylated αSyn within an aggregate increases its ability to damage mitochondrial membranes. (**A**) Representative images of beads coated with both αSyn and p-αSyn at varying concentrations. (**B**) Total protein concentration of the beads was determined for each bead ratio. (**C**) The colocalisation of αSyn and p-αSyn on the beads was confirmed using MJFR1 and MJFR-13 phospho. (**D**) The calcium influx of 0% cardiolipin liposomes was assessed after incubation of beads containing varying concentrations of αSyn and p-αSyn. (**E**) The calcium influx into liposomes containing 20% cardiolipin was assessed after addition of beads with varying concentrations of αSyn and p-αSyn. Graphs show four biological repeats, bars represent the mean and SD.

4.4. Discussion

4.4.1. Phosphorylated αSyn induced dysfunction

Within this chapter, I aimed to decipher which species of αSyn are more involved in the toxicity observed in PD patient cells by comparing different isoforms. To achieve this, I utilized a model of αSyn seeding in healthy control iDNLs and induced αSyn associated dysfunctions. Fibrillar phosphorylated αSyn was more toxic to iDNLs than wildtype αSyn and oligomeric forms of αSyn. Fibrillar p-αSyn induced mitochondrial dysfunction and Lewy Body-like aggregate formation within healthy control cells, unlike the wildtype αSyn fibrils.

While wildtype αSyn fibrils have been shown to induce toxicity and Lewy body formation in other models they did not show the same effects in these experiments. However, this does not lead us to conclude that wildtype αSyn fibrils are not pathogenic. In this regard, it is crucial to note that this study was conducted under a specific concentration regime and time frame that allowed us to detect differences in toxicity among various αSyn aggregates without causing significant cell death. If higher concentrations had been used or longer incubation was performed, toxicity would likely have been observed across all αSyn species, aligning with findings from other studies. Cellular dysfunction was measured only 48 hours after addition of aggregates, whereas other studies measure dysfunction up to three weeks for cellular models, and one month for animal models (Chung et al., 2019; Mahul-Mellier et al., 2020). This research was intentionally designed to assess the induced toxicity of different αSyn species to determine if different species exert a more pronounced influence on disease progression or manifest toxicity via diverse mechanisms. By using low concentrations of seeds and early time points to measure toxicity, I aimed to model the early stages of αSyn dysfunction, effectively simulating the initial phases of disease. This approach allows us to capture the

subtle onset of pathological changes and provides insights into how different αSyn species may contribute to the pathogenesis of the disease.

Future experiments would involve characterising the oligomer and fibril preparations to determine any structural differences between the species and WT and phosphorylated aggregates. As protein structure hugely influence's function, a direct link could be made by using other methodologies such as electron microscopy and atomic force microscopy to determine in-depth structural properties. Further, the use of fluorescence microscopy to quantify mitochondrial dysfunction, gives rise to limitations as colocalised events could be due to resolution limits within the microscope. To strengthen this data, additional mitochondrial function assays could be undertaken e.g. oxygen consumption rate measurement and ATP assays.

Additionally, an important point to note is that I previously found SNCA to have reduced mitophagy compared to Control 1 (Figure 3.21). However, in this chapter when I induced dysfunction in a healthy control, an increase in mitophagy was observed. This could be attributed to the healthy control possessing greater capacity to clear out the dysfunctional mitochondria as a result of p-αSyn 7d, a process that is dysregulated in the SNCA patient cells. Additionally, SNCA iDNLs have dealt with increased αSyn for a prolonged amount of time, and therefore will not mount a response in the same way that healthy control cells will upon the addition of PFFs in a short timeframe.

4.4.2. Uptake and processing of αSyn species

To elucidate the mechanisms of p-αSyn fibrillar toxicity, I investigated individual steps in the specific pathway to dysfunction. There was no difference in uptake between p-αSyn and αSyn by healthy control iDNLs. Whether αSyn was inside the cell or located at the membrane was not investigated by Z-stacking, and further experiments need to be carried out to confirm this. However, MSD-ELISA data show there is an increased presence of αSyn or p-αSyn in the cell lysate after seeding (Supplementary Figure 1). Therefore, the increase in toxicity was not due to there being a preferential uptake of p-αSyn into the iDNLs. I next investigated the processing of αSyn and p-αSyn by the degradation machinery of the cell. Colocalisation of αSyn and the lysosomes was used as a proxy for the degradation of αSyn. Wildtype αSyn was more efficiently trafficked to the lysosome for degradation than the non-phosphorylated form, this is indicative of a build-up of toxic p-αSyn within the cells that is not properly

processed for degradation. The dysfunction and aggregation of αSyn within cells can damage lysosomes and lead to impairment in αSyn clearance and could explain why p-αSyn is less efficiently degraded than αSyn (Bourdenx et al., 2014).

On the contrary, researchers have found the phosphorylated form of αSyn is degraded faster than a non-phosphorylated form (Zheng et al., 2019). Studies suggest that αSyn is degraded via the ubiquitin-proteasome pathway, and phosphorylated αSyn in Lewy Bodies is preferentially ubiquitinated and therefore a target of degradation (Kawahata & Fukunaga, 2020). However, due to the accumulation of Lewy Bodies that are not degraded, there may be a balance between phosphorylated αSyn degradation and aggregation. More in-depth studies are required to confirm the processing and degradation of different species of αSyn, with a focus on both lysosomal proteolysis and the ubiquitin-proteasome pathway.

4.4.3. Seeding propensities of αSyn and p-αSyn

One of the main mechanisms of the spreading of αSyn pathology in PD is αSyn seeding, where αSyn seeds promote the aggregation of endogenous monomeric αSyn. These findings show that p-αSyn has a higher propensity to seed monomeric αSyn aggregation than wildtype αSyn. This work is consistent with findings in a mouse model, where treatment of phosphorylated αSyn fibrils were more efficient at seeding endogenous αSyn and creating Lewy Body inclusions (Karampetsou et al., 2017). However contradictory to previous findings that wildtype αSyn can seed at a faster rate than the phosphorylated form (Ghanem et al., 2022). The literature contains a large amount conflicting evidence for the role of pSer129 αSyn specifically in seeding. It is likely that the function of pSer129 αSyn is tightly regulated by its structure and environment. Differences in preparation of phosphorylated αSyn, aggregation of αSyn into fibrils and environmental conditions have led to differences observed in fibrilization, and properties of the fibrils (Ghanem et al., 2022; Karampetsou et al., 2017; Ma et al., 2016; Schreurs et al., 2014). Therefore, I hypothesise that structural differences in the fibrils lead to the formation of heterogenous strains of p-αSyn that differ in toxicity.

4.4.4. Mitochondrial dysfunction induced by p-αSyn

Mitochondrial dysfunction was induced in cells that were seeded with p-αSyn compared to wildtype αSyn. To elucidate this mechanism further, the ability of αSyn species to damage mitochondrial membranes was assessed. The data suggests phosphorylated oligomeric species of αSyn are more potent at inducing pore formation in mitochondrial membranes

than corresponding monomers and fibrils. This is supported by the fact oligomeric species of αSyn are more potent at causing membrane permeabilization than fibrillar species (Emin et al., 2022). I observed increased membrane permeabilization of both αSyn and p-αSyn oligomeric species in cardiolipin free vesicles compared to fibrillar or monomeric αSyn, but p-αSyn is even more potent in the context of mitochondrial membranes, whereas wildtype αSyn does not differ in toxicity in the presence of cardiolipin. αSyn has been shown in the literature to interact with mitochondrial lipid cardiolipin, and the aggregates of αSyn are believed to induce mitochondrial dysfunction via this interaction (Ghio et al., 2019).

Much of the scientific literature produces αSyn protein in vitro and aggregates are prepared usually containing only one form of the protein, however in humans many conformations are present together to form heterogeneous aggregates (Narkiewicz et al., 2014). Nanospheres were coated with both αSyn and p-αSyn, to investigate what proportion of p-αSyn needs to be present within an aggregate to induce toxicity. I found that only 25% of the aggregate needs to be phosphorylated to induce enhanced mitochondrial membrane damage compared to its WT counterpart, and the amount of pSer129 αSyn present is correlated to its toxicity. This data also suggests a mechanism as to why the extent of αSyn phosphorylation is correlated with disease severity (Stewart et al., 2015).

4.5. Conclusions

In this chapter, this study has provided valuable insights into the differential roles and toxicities of various αSyn isoforms in PD pathology. The phosphorylated form of αSyn was shown to be significantly more damaging compared to WT αSyn, and both fibrillar and oligomeric species can induce toxicity through distinct mechanisms. Fibril species are key pathogenic agents to spread αSyn pathology, as they can be used to induce aggregation of endogenous αSyn by recruiting physiological monomeric αSyn. This seeded aggregation can subsequently generate can form oligomeric species that are damaging to mitochondrial membranes and induce dysfunction. It was also demonstrated how p-αSyn can render αSyn more toxic through co-aggregation. This chapter highlights a complex interplay between different species of p-αSyn and αSyn in the toxicity and dysfunction occurring in PD.

Chapter 5: Uncovering potential therapeutics to rescue αSyn dysfunction in PD patient cells.

5.1. Introduction

There is currently no cure for Parkinson's Disease, and many of the current therapeutic opportunities involve targeting αSyn to not only halt the progression of PD but also to alleviate its symptoms. Approaches to targeting αSyn include inhibiting its aggregation, enhancing its clearance from neuronal cells, or preventing its toxic spread from one cell to another. Modulating αSyn pathology offers a more direct means of influencing the diseases course and provides a measurable endpoint to evaluate the effectiveness of treatments. The recent FDA approval of amyloid clearance therapy for Alzheimer's Disease, which has shown promise in improving patient outcomes, further bolsters the hope that similar strategies targeting αSyn could yield significant benefits for individuals with PD (Christopher H. van Dyck et al., 2023; Harris, 2023).

Silencing of SNCA has been investigated to prevent protein synthesis, aggregation, and spreading of αSyn. The gene therapy approach to silence SNCA in PD was first investigated with a lentiviral shRNA which successfully silenced SNCA both in vitro in a dopaminergic cell line and in vivo in rat brains (Sapru et al., 2006). Since, various methods have been utilised to downregulate αSyn, including adeno-associated virus (AAV) vector delivery and microRNAs (miRNAs) (Hayashita-Kinoh et al., 2006; Junn et al., 2009). These studies demonstrated that the repression of αSyn enhanced dopaminergic neuron survival and reduced oxidative stress in neurons.

However, many studies have since reported that total silencing of SNCA is neurotoxic and leads to long-term adverse effects. A study reducing αSyn in a rat model reported an improvement in motor symptoms, however the SNCA reduction also led to a loss of dopaminergic neurons (Khodr et al., 2011). Reduced dopamine concentration and increased neuroinflammation have also been observed in dopaminergic neurons due to the loss of αSyn (Benskey et al., 2018). These findings indicate the essential role of endogenous αSyn in dopaminergic neurons. Although its role is not fully understood, endogenous αSyn is speculated to be involved in synaptic function and the regulation of dopamine (Cabin et al., 2002; Perez et al., 2002). This highlights the need for a balance of maintaining a level of endogenous αSyn whilst reducing αSyn overexpression and aggregation.

Previous studies have suggested that partial knockdown of αSyn instead of complete knockout is a potential option to mitigate αSyn mediated toxicity. Partial knockdown of αSyn in a SNCA triplication cell model was sufficient to increase neurite length and rescue defects in electrophysiology (Oliveira et al., 2015). A transgenic fly model of PD, which used overexpression of αSyn to induce dysfunctions, showed that reducing αSyn expression to a normal level is sufficient to rescue motor deficits whilst conferring no additional toxicity (Takahashi et al., 2015). Within this chapter, I also utilised the concept of partial knockdown of αSyn in iDNL cell lines to determine if there is a reduction in disease phenotypes.

Another therapeutic target is the pathological αSyn that is directly involved in spreading of αSyn aggregation and disease. The BRICHOS domain from Bri2 is a molecular chaperone that has been widely investigated in relation to Alzheimer's Disease (AD) and PD. It has been found to bind to Aβ42 and αSyn aggregates and modulate the aggregation process (Biverstål et al., 2020). Amyloid formation occurs when monomeric protein forms a nucleus through primary nucleation, elongation of the nucleus then forms a fibril (Figure 5.1) (Michaels et al., 2023). Additionally, several secondary processes of aggregation can occur including secondary nucleation. This involves an amyloid fibril providing a surface for nucleation events to take place and allows aggregation kinetics to occur at a much faster rate than primary nucleation (Tö et al., 2018). BRICHOS directly binds to the surface of αSyn fibrils but not monomers and inhibits subsequent secondary nucleation (Figure 6.1) (Adam et al., 2024). The process of secondary nucleation dominates in cell to cell seeding, allowing seeds of αSyn to spread throughout the brain (Luk et al., 2009; Luk, V. Kehm, et al., 2012). Additionally, secondary nucleation has been shown to be the primary driver of oligomer and aggregate formation (Xu et al., 2024). This highlights the potential of BRICHOS in inhibiting αSyn aggregation and the spread of disease.

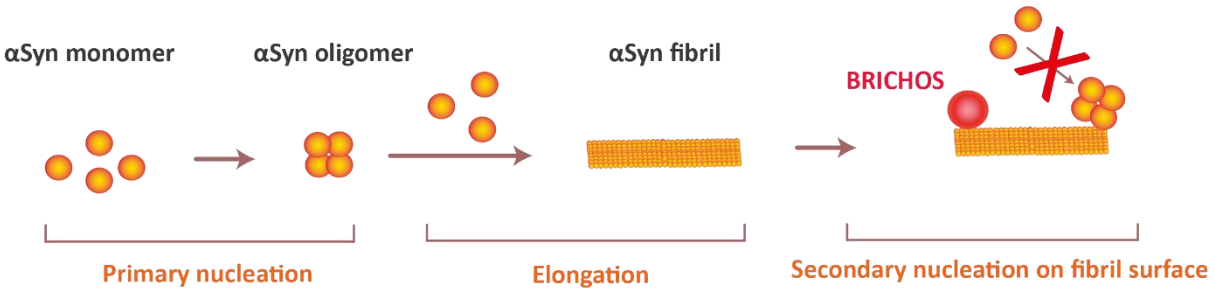

Figure 5.1. Schematic of how BRICHOS works to inhibit secondary nucleation. αSyn aggregation occurs through a process of primary nucleation, where monomeric αSyn forms nuclei that aggregate

into oligomers. The process of elongation then forms an amyloid fibril. A secondary process of aggregation is secondary nucleation, where monomeric αSyn can aggregate on the fibril surface and form oligomers. BRICHOS binds to the αSyn fibrils and prevents secondary nucleation at the fibril surface.

The use of BRICHOS has been investigated in reducing disease related secondary processes including seeding of αSyn and Aβ and alleviating symptoms in both PD and AD respectively. The BRICHOS R221E mutant has been widely used as it forms stable monomers and is more effective at suppressing Aβ toxicity than WT BRICHOS (Chen et al., 2020). Treatment of hippocampal mouse brain slices with Aβ42 induces neurotoxicity presented by electrophysiology readings, this neurotoxic effect is rescued with the addition of BRICHOS (Chen et al., 2020). Similarly, neurotoxicity induced by αSyn can be rescued by the addition of BRICHOS (Adam et al., 2024). Improvements in cognition and reduction in Aβ pathology were observed in Aβ knock-in mice after intravenous injections of BRICHOS (Manchanda et al., 2023). This data presents the molecular chaperone BRICHOS as a potential therapeutic to halt disease progression and improve cognition in protein misfolding diseases, however BRICHOS efficacy in human models is limited and more work needs to be done to determine if it would be a good candidate for clinical trials. Within this chapter, I will observe whether the phenotypes observed in PD patient cells can be reversed by the different therapeutic techniques mentioned here.

5.2. Aims and Objectives

The aims of this chapter are to try and rescue disease phenotype in PD iDNLs back to the level of control cells. The objectives are:

- To partially knockdown αSyn levels in iDNLs and assess the formation of Lewy Body-like aggregates.
- To inhibit seed-induced monomer recruitment in order to slow down secondary aggregation, then determine disease-associated mitochondrial dysfunction and the formation of Lewy body-like aggregates.

5.3. Results

5.3.1. Knockdown of SNCA reduces phosphorylated αSyn specifically in SNCA triplication cells.

I have observed a corelation between the presence of αSyn and the dysfunction in PD iDNLs. To understand if this dysfunction can be reversed, SNCA knockdown in Control 1 and SNCA

iDNLs was carried out by Dr Francesco Capriglia. Levels of αSyn and p-αSyn before and after knockdown were assessed by MSD ELISA in both Control 1 and SNCA (Figure 5.2). It was found that after knockdown, both Control 1 and SNCA had a significant decrease in the amount of αSyn present within the cells, 30% and 72% reduction respectively, which suggests the partial knockdown of αSyn was successfully achieved. The levels of p-αSyn were significantly reduced by 80% in SNCA after knockdown, however there was no difference in Control 1.

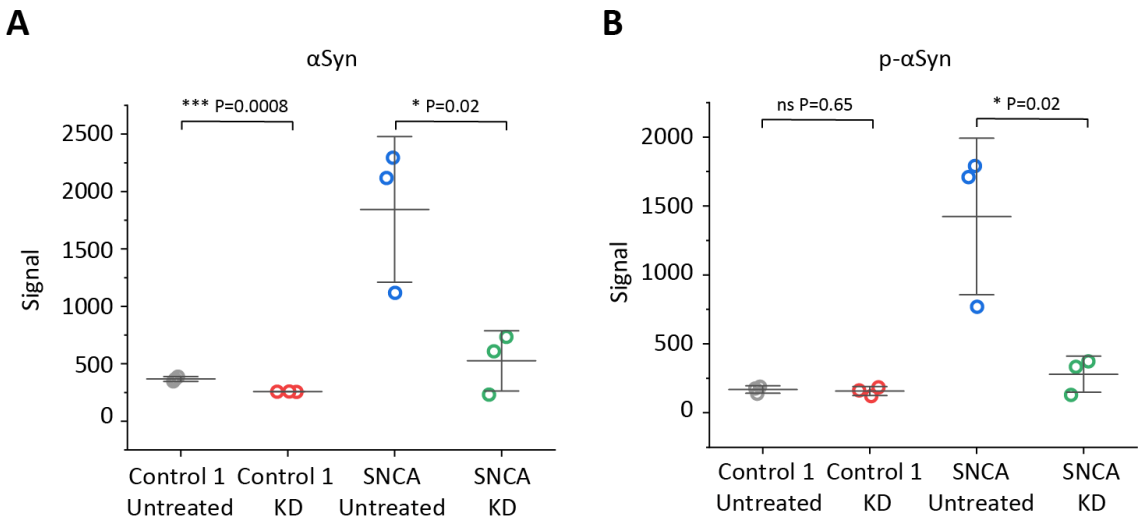

Figure 5.2. Quantification of αSyn and p-αSyn after SNCA knockdown by MSD ELISA. The levels of αSyn (**A**) and p-αSyn (**B**) were assessed by MSD ELISA in iDNLs Control 1 and SNCA before and after knockdown of SNCA. Each data point represents one biological replicate, bars represent mean ±SD. Statistical significance was determined by two sample t-test.

5.3.2. Knockdown of SNCA reduces aggregated and phosphorylated αSyn in SNCA triplication cells.

After successful reduction of the total αSyn protein levels within iDNLs, the number of different conformations of αSyn were tested. Using SiMPull the number of aggregated and phosphorylated αSyn species were quantified (Figure 5.3 A). A comparison of the levels of αSyn aggregate showed there was no significant difference between both Control 1 and SNCA before and after knockdown (Figure 5.3 B). There was a significant reduction in pSer129 αSyn in SNCA by 92% after knockdown, however no difference in Control 1 (Figure 5.3 C). The number of aggregates that were also phosphorylated was reduced by 96% in SNCA after knockdown, but no significant reduction was observed in Control 1 (Figure 5.3 D). When the

fold change of αSyn before and after knockdown was calculated, there was a significant reduction in all αSyn species in SNCA, but no difference observed in Control 1 (Figure 5.3 E-G). This data shows that knockdown of SNCA reduces pathogenic species of αSyn in PD cell lines but does not change αSyn in healthy control cell lines.

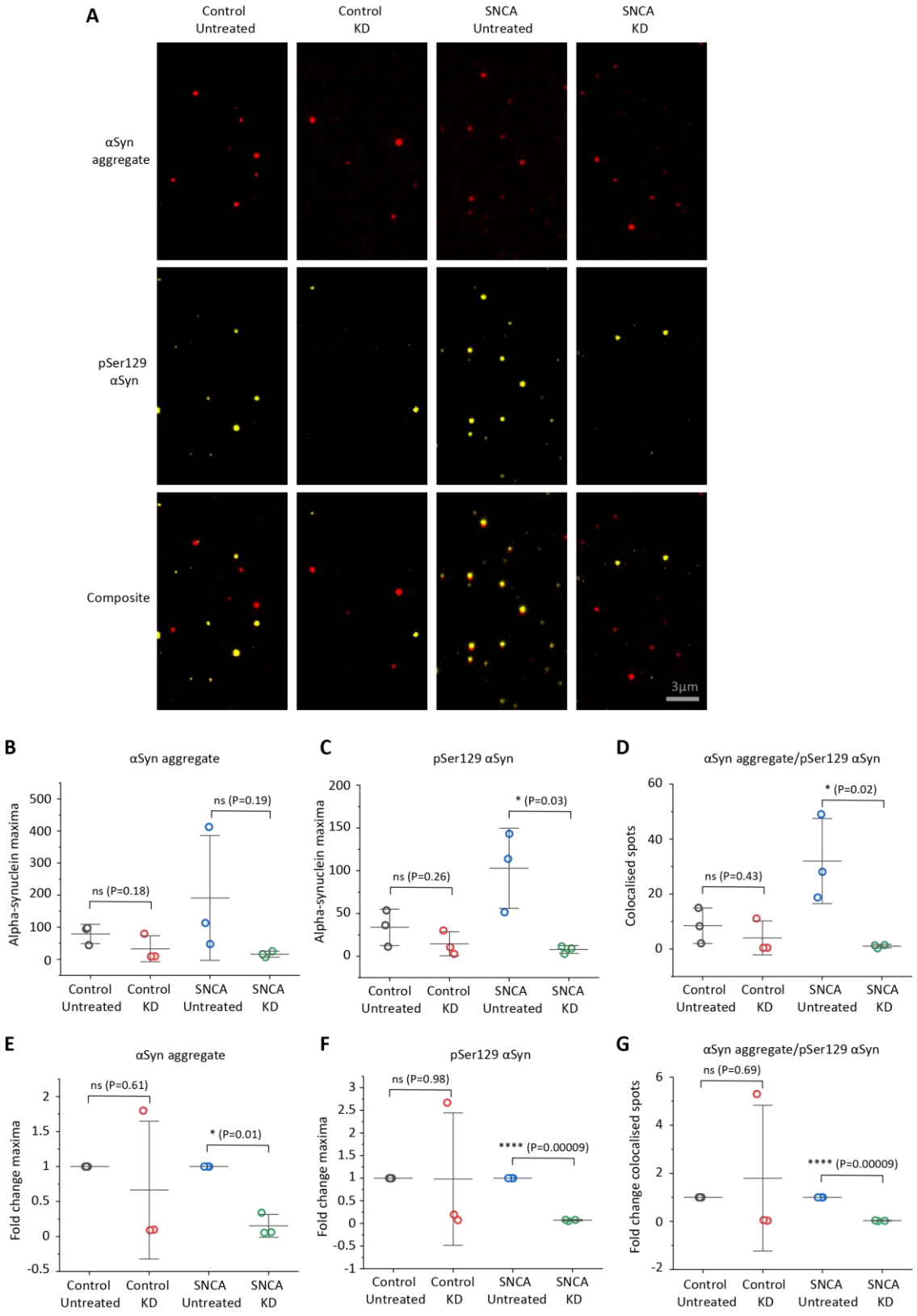

Figure 5.3. The number of αSyn aggregate, phosphorylated αSyn, and phosphorylated aggregates is reduced after SNCA knockdown specifically in SNCA triplication but not Control 1. (**A**) Representative images of αSyn aggregate and pSer129 αSyn in Control Untreated cells, Control knockdown, SNCA untreated cells and SNCA knockdown. The number of αSyn aggregate (**B**), pSer129 αSyn (**C**) and

colocalised spots (**D**) were quantified. The fold change of αSyn aggregate (**E**), pSer129 αSyn (**F**) and colocalised spots (**G**) was plotted. Graphs show three biological replicates, bars show mean ±SD. Statistical significance was determined by either two sample t-test or paired t-test.

5.3.3. The formation of Lewy Body-like aggregates in PD cell lines is reduced after SNCA knockdown.

After confirming the knockdown was effectively reducing the amount of αSyn and p-αSyn within the iDNLs, I investigated whether knockdown could reduce the number of Lewy Body-like aggregates that were forming in SNCA iDNLs. SiMPull was carried out to probe αSyn aggregates that were colocalised with pSer129 αSyn and a Lewy Body marker.

Firstly, the interaction of mitochondrial markers with αSyn was tested by probing for TOM20 (Figure 5.4 A-F). The number of colocalised spots of αSyn aggregate and TOM20, pSer129 αSyn and TOM20, and all three channels together, showed no difference before or after knockdown in either Control 1 or SNCA (Figure 5.4 A-C). There appeared to be a reduced number of colocalised spots in SNCA, but due to variability there was no significant difference. However, when the results were normalised to either Control 1 no treatment, or SNCA no treatment, there was a significant reduction in Lewy Body-like aggregates with TOM20 in SNCA, but no difference observed in Control 1 (Figure 5.4 D-F). These results suggest reduction of αSyn levels within the cells is sufficient to reduce Lewy Body-like aggregates containing TOM20.

The presence of Lewy Body-like aggregates containing lysosomal proteins was then assessed, by probing for LAMP1 (Figure 5.4 G-L). There was an 89% reduction in LAMP1 colocalised with αSyn aggregate in SNCA, and no difference was observed in Control 1 (Figure 5.4 G, J). Phosphorylated αSyn colocalised with LAMP1 did not change in both Control 1 and SNCA as a result of knockdown (Figure 5.4 H, K). The number of αSyn species containing aggregated, phosphorylated αSyn and LAMP1 remained unaltered after knockdown in both Control 1 and SNCA (Figure 5.4 I, L). This data shows that SNCA knockdown reduces αSyn aggregate and LAMP1 interactions, but not phosphorylated αSyn and LAMP1 interactions.

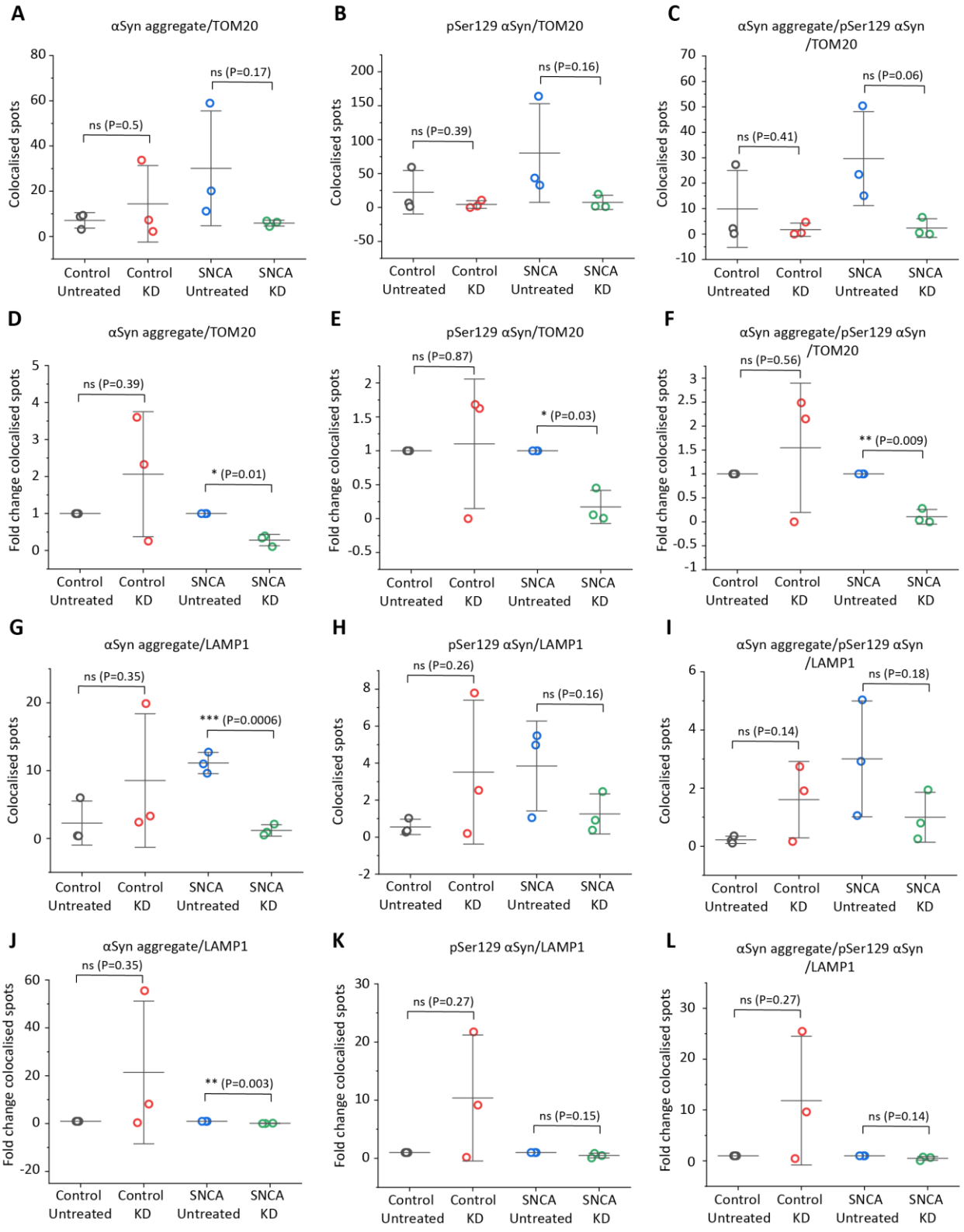

Figure 5.4. The number of TOM20 and LAMP1 containing Lewy Bodies is decreased after SNCA knockdown in SNCA but not Control 1. The number of Lewy body-like aggregates forming after before and after knockdown were assessed in Control 1 and SNCA. Colocalisation of αSyn aggregate and TOM20 (**A**), pSer129 αSyn and TOM20 (**B**), and colocalisation of αSyn aggregate, pSer129 αSyn and TOM20 (**C**) were quantified. The fold change after SNCA knockdown of colocalised αSyn

aggregate and TOM20 (**D**), pSer129 αSyn and TOM20 (**E**), and αSyn aggregate, pSer129 αSyn and TOM20 was (**F**) determined. The colocalisation of LAMP1 with αSyn aggregate (**G**), pSer129 αSyn (**H**), and both αSyn aggregate and pSer129 αSyn (**I**) was assessed. The fold change of LAMP1 colocalised with αSyn aggregate (**J**), pSer129 αSyn (**K**), and both αSyn aggregate and pSer129 αSyn (**L**) after SNCA knockdown was compared between Control 1 and SNCA cells. Graphs show three biological replicates, bars represent the mean ±SD. Statistical significance was determined by either two sample t-test or paired t-test.

Another Lewy Body marker, Ubiquitin, was assessed for presence within Lewy Body-like aggregates before and after SNCA knockdown. The number of αSyn species interacting with ubiquitin were not significantly different before and after knockdown in either Control 1 or SNCA (Figure 5.5 A-C). Due to the variability between biological replicates, the fold change of Lewy Bodies before and after knockdown in each replicate was calculated. The fold change after SNCA knockdown shows there is a significant reduction of 81% Lewy Body-like aggregates containing ubiquitin in SNCA after knockdown, and no difference in Control 1 after knockdown (Figure 5.5 D-F).

Finally, p62 containing Lewy Body-like aggregates were assessed before and after knockdown. There was no significant difference in αSyn aggregates containing p62 for both Control 1 and SNCA (Figure 5.5 G). There was a significant reduction in p62 colocalised with pSer129, and both pSer129 αSyn and αSyn aggregate, by 94% and 96% respectively (Figure 5.5 H-I). The fold change in Lewy Body-like aggregates after knockdown was significantly reduced in SNCA but not Control 1 (Figure 5.5 J-L). Overall, this data shows that knockdown of SNCA in a PD patient cell line was sufficient to reduce the number of Lewy Body-like aggregates that were formed.

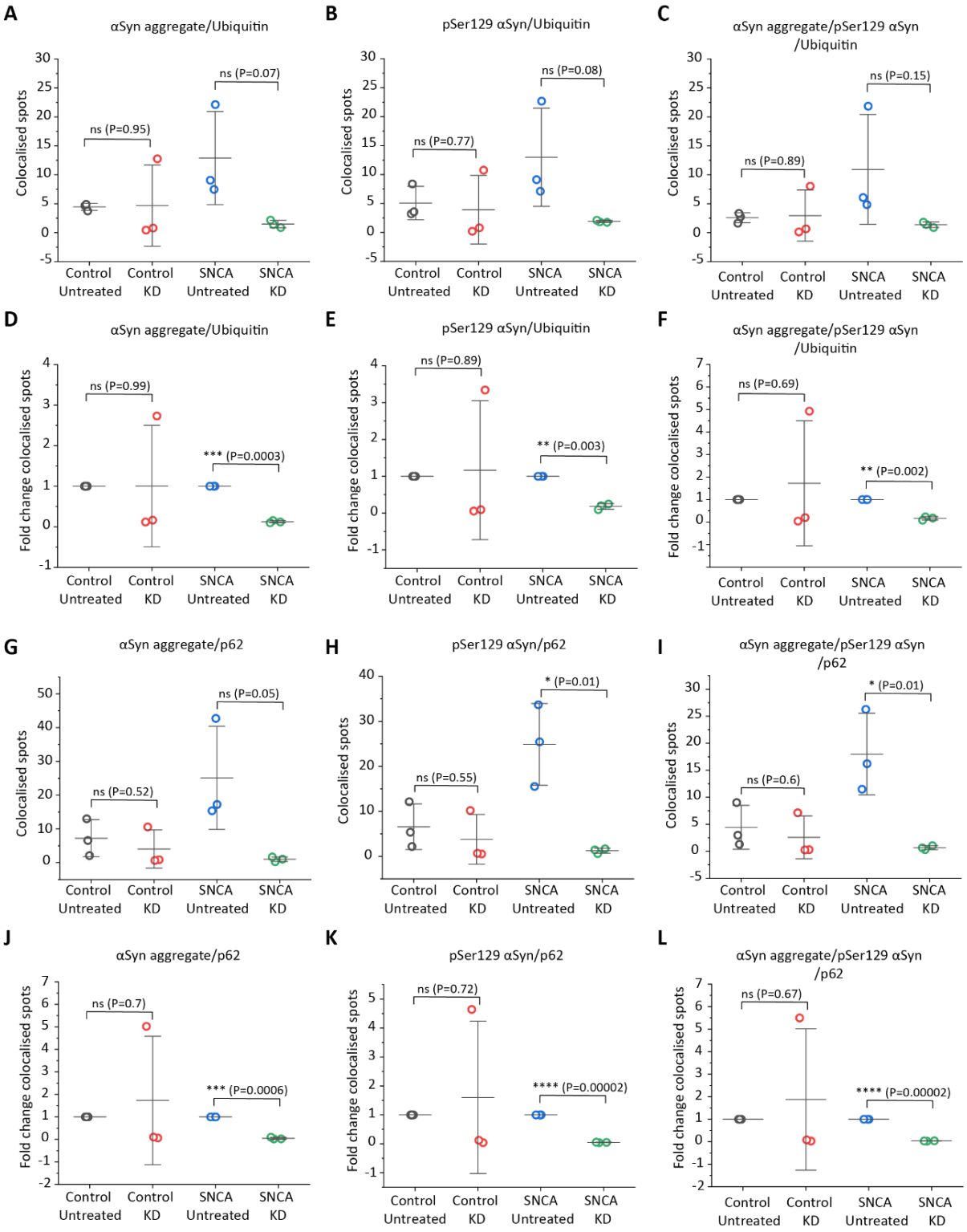

Figure 5.5. The number of Lewy Bodies containing p62 and ubiquitin is reduced in SNCA but not control after SNCA knockdown. Control and SNCA were treated with SNCA shRNA, and the formation of Lewy bodies was assessed. Number of Lewy Bodies containing ubiquitin and αSyn aggregate (**A**), pSer129 αSyn (**B**), and αSyn aggregate and pSer129 αSyn (**C**). Fold change of Lewy Bodies containing ubiquitin and αSyn aggregate (**D**), pSer129 αSyn (**E**), and αSyn aggregate and pSer129 αSyn (**F**) after SNCA knockdown. Number of Lewy bodies containing p62 and αSyn

aggregate (**G**), pSer129 αSyn (**H**), and αSyn aggregate and pSer129 αSyn (**I**). Fold change of Lewy bodies containing p62 and αSyn aggregate (**J**), pSer129 αSyn (**K**), and αSyn aggregate and pSer129 αSyn (**L**). Graphs show three biological replicates, bars represent mean ± SD. Statistical significance was determined by either two sample t-test or paired t-test.

5.3.4. Rescuing the toxic effects of p-αSyn seeds with by suppressing secondary nucleation in iDNLs

As previously observed in Chapter 4, seeding control iDNLs with phosphorylated species of αSyn is sufficient to cause mitochondrial dysfunction and Lewy Body formation in a normal healthy cell. The aim of this section is to understand if a reagent can be used to alleviate the effects of αSyn seeding. If there is a reagent that can inhibit αSyn seeding, then it has great potential as a therapeutic to patients who already display αSyn dysfunction and Lewy Body formation. The BRICHOS R221E monomer is used within this section, to investigate whether it can alleviate mitochondrial dysfunction and Lewy Body formation after αSyn seeding. This BRICHOS R221E monomer has been shown to suppress secondary nucleation and subsequent oligomer generation of recombinant αSyn in vitro (Adam et al., 2024).

To determine if BRICHOS R221E monomer could reduce the toxic p-αSyn aggregates formed when seeding healthy control iDNLs with αSyn species, the seeding was repeated. This time, cells were seeded with αSyn or p-αSyn fibrils, as well as with αSyn or p-αSyn fibrils in the presence of BRICHOS R221E monomer. The goal was to assess whether BRICHOS R221E could mitigate the toxicity associated with p-αSyn aggregation and therefore protect against the resulting cellular dysfunction. BRICHOS R221E monomer only was used as a negative control. The levels of αSyn and p-αSyn in the iDNL lysate were assessed by MSD ELISA when adding αSyn species with or without BRICHOS (Figure 5.6 A-B). No difference was observed in levels of αSyn and p-αSyn in the presence or absence of BRICHOS. Similarly, when the levels of αSyn and p-αSyn were assessed in the media of iDNLs, no significant difference was observed (Figure 5.6 C-D). The data suggests a trend towards lower αSyn levels with the addition of BRICHOS to either αSyn or p-αSyn fibrils, however due to variability this difference is not significant.

Next, I evaluated the proportion of αSyn and p-αSyn released by the iDNLs relative to the total αSyn within the cells. The αSyn or p-αSyn in the media was normalised to the total αSyn in the lysate (Figure 5.6 E-F). There appeared to be no difference in the levels of αSyn in the media. Interestingly, there was a 24% reduction of p-αSyn in the media when seeded with p-

αSyn and BRICHOS, compared to seeding without BRICHOS. This result shows that in the case of p-αSyn, the addition of BRICHOS significantly lowers the proportion of αSyn that is released from the cells. Given that the release of p-αSyn is a consistent phenotype observed across PD cell lines, and using BRICHOS this phenotype can be reversed, suggests its potential as a therapeutic strategy for reducing the pathological spread of p-αSyn in PD.

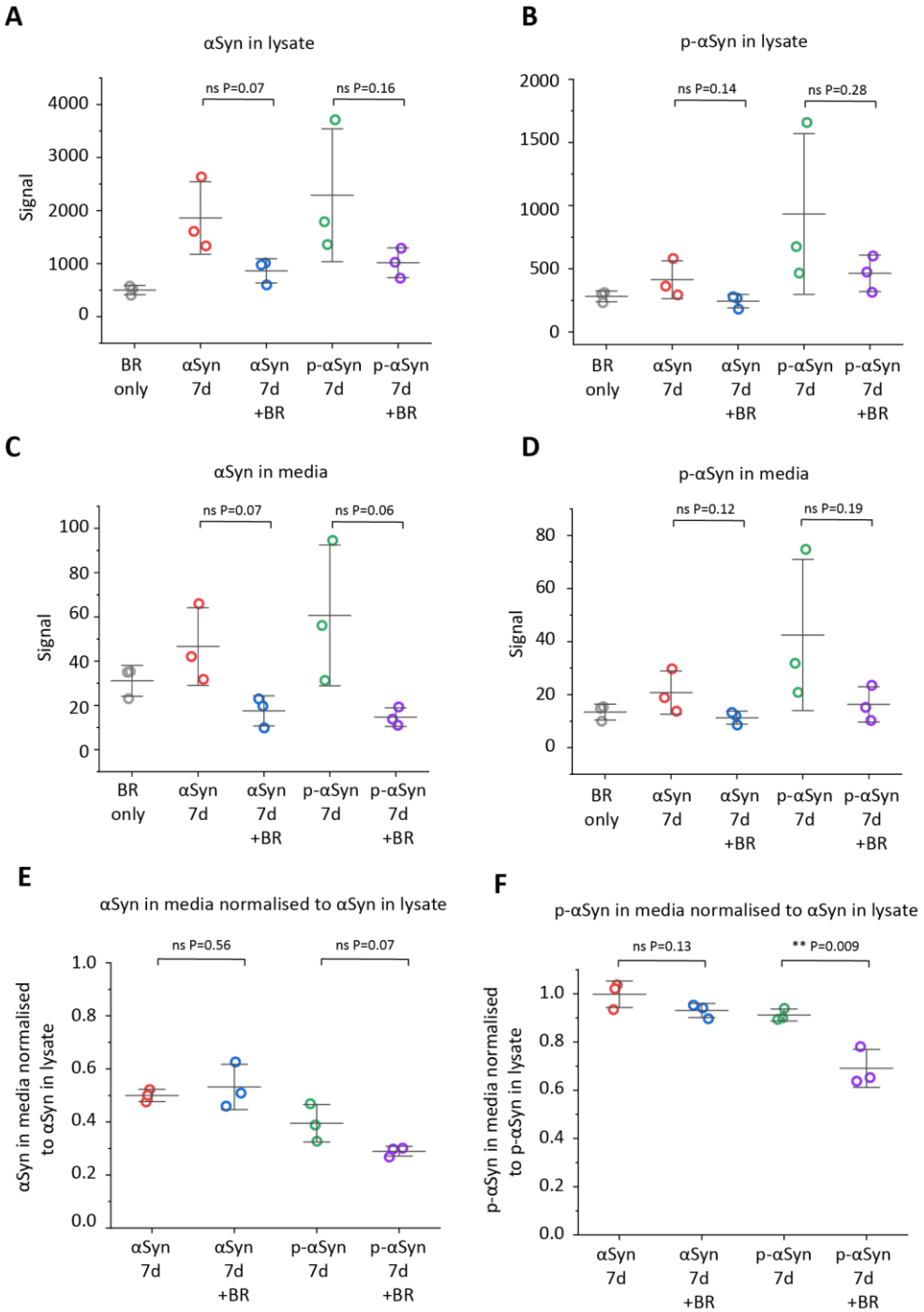

Figure 5.6. BRICHOS reduces the proportion of p-αSyn released from control cells as a result of p-αSyn seeding. Control cells were seeded with αSyn and p-αSyn in the presence and absence of BRICHOS and total αSyn and p-αSyn levels were assessed. The total αSyn in lysate (**A**) and total p-

αSyn in lysate (**B**) were assessed. The levels of αSyn (**C**) and p-αSyn (**D**) released into the media was determined. The proportion of total αSyn that was released into the media was determined for αSyn (**E**) and p-αSyn (**F**) by normalising αSyn in p-αSyn in the media to total αSyn in lysate. Graphs show three biological replicates, bars represent mean ± SD. Statistical significance was determined by two sample t-test.

5.3.5. BRICHOS treatment alleviates mitochondrial dysfunction associated with p-αSyn seeding.

Chapter 4 shows that seeding phosphorylated αSyn fibrils in healthy control iDNLs is sufficient to cause mitochondrial dysfunction. Here I determined whether this mitochondrial dysfunction could be reversed by the addition of BRICHOS with αSyn and p-αSyn fibrils (Figure 5.7). The results from the Chapter 4 of seeding iDNLs with αSyn and p-αSyn fibrils were combined with results from this chapter of seeding iDNLs with αSyn BRICHOS and p-αSyn fibrils with BRICHOS, to determine if BRICHOS influences mitochondrial function. This comparison allowed us to evaluate whether BRICHOS could mitigate the mitochondrial dysfunction induced by these αSyn species.

The number of mitochondria per cell was calculated, and there was no significant difference when cells were seeded with αSyn fibrils and the addition of BRICHOS, however for cells seeded with p-αSyn fibrils there was a reduction in the number of mitochondria per cell after BRICHOS treatment (Figure 5.7 A). The number of lysosomes per cell was calculated and there was a significant reduction in lysosome number after seeding with p-αSyn fibrils in the presence of BRICHOS (Figure 5.7 B). The reduction of mitochondria and lysosomes due to BRICHOS treatment, restores the levels of these organelles to similar levels observed in healthy control untreated cells. There was no difference observed as a result of adding BRICHOS to cells seeded with αSyn fibrils. The amount of mitophagy was measured in the control iDNLs after treatment with αSyn and BRICHOS. Although there was no difference in mitophagy detected with the addition of BRICHOS in cells seeded with either αSyn fibrils or p-αSyn fibrils, there was a trend towards a reduction in mitophagy after seeding cells with p-αSyn fibrils and BRICHOS (P=0.05) (Figure 5.7 C).

Overall, these results suggest BRICHOS is rescuing the mitochondrial and lysosomal dysfunction observed after seeding with the toxic species p-αSyn fibrils. To confirm these results further, future experiments include running all the conditions (αSyn fibrils, αSyn fibrils

+ BRICHOS, p-αSyn fibrils, p-αSyn fibrils + BRICHOS) in the same experiment and increasing the number of biological replicates.

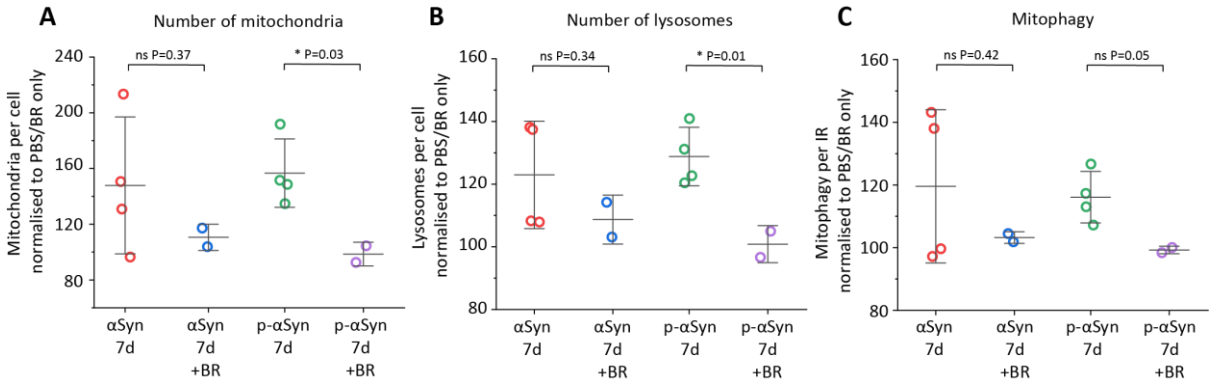

Figure 5.7 BRICHOS rescues mitochondrial dysfunction associated with p-αSyn. Mitochondrial and lysosomal dysfunction was assessed as a result of seeding with αSyn 7d and p-αSyn 7d in the presence and absence of BRICHOS. The data was normalised to a negative control, either PBS only or BRICHOS only. The number of mitochondria per cell (**A**), lysosomes per cell (**B**), and mitophagy per image region (**C**) was calculated. The data from αSyn 7d and p-αSyn 7d is taken from Chapter 4 seeding and combined with αSyn 7d + BRICHOS and p-αSyn + BRICHOS in Chapter 5. For αSyn 7d and p-αSyn 7d four biological replicates were done, and for αSyn 7d + BRICHOS and p-αSyn 7d + BRICHOS two biological replicates were done. The bars represent mean ± SD. Statistical significance was determined by two sample t-test.

5.3.6. BRICHOS rescues Lewy Body-like aggregate formation containing VDAC1 and p62 when seeded with p-αSyn.

The effect of BRICHOS on reducing Lewy Body-like aggregates was then assessed. Control cells were seeded with αSyn and p-αSyn fibrils in Chapter 4 and the induced dysfunctions were measured. In this chapter I measured if BRICHOS influences the number of Lewy Body-like aggregates forming.

Colocalisation of mitochondrial marker VDAC1 with αSyn was assessed (Figure 5.8 A-C). There was a reduction in the number of αSyn aggregate colocalised to VDAC1 after treatment with BRICHOS for both αSyn and p-αSyn (Figure 5.8 A). There is a significant reduction in the number of pSer129 αSyn colocalised with VDAC1 after p-αSyn treatment with BRICHOS, but no difference is observed after αSyn treatment (Figure 5.8 B). Similarly, there a reduction in aggregated phosphorylated αSyn with VDAC1 after p-αSyn seeding in the presence of BRICHOS, but no difference observed in cells seeded with αSyn (Figure 5.8 C).

The ability of BRICHOS to reduce Lewy Body-like aggregates containing typical Lewy Body marker p62 (Figure 5.8 D-F). There was a reduction in Lewy Body-like aggregates after adding BRICHOS to cells seeded with p-αSyn but not αSyn. This is consistent across p62 colocalised with aggregate αSyn, phosphorylated αSyn and aggregated phosphorylated αSyn.

Lastly, the number of ubiquitin containing Lewy Bodies was quantified as a result of αSyn seeding (Figure 5.8 G-I). No difference was observed in the number of aggregated αSyn colocalised with ubiquitin in either αSyn or p-αSyn fibril seeded cells and the addition of BRICHOS (Figure 5.8 G). When assessing the presence of pSer129 αSyn and ubiquitin, there was a higher number of these species when seeded with p-αSyn which was reduced when BRICHOS was added (Figure 5.8 H). The presence of aggregated phosphorylated αSyn colocalised with ubiquitin showed no change after the addition of BRICHOS in both αSyn 7d and p-αSyn fibril seeded cells (Figure 5.8 I).

These results suggest that BRICHOS does play a role in reducing Lewy Body-like aggregates that form as a result of p-αSyn seeding. BRICHOS does not cause a difference after seeding with αSyn fibrils, since there is no difference in Lewy Body-like aggregates forming when adding αSyn fibrils compared to PBS only, for the concentration used in this study (Figure 4.4 and Figure 4.5).

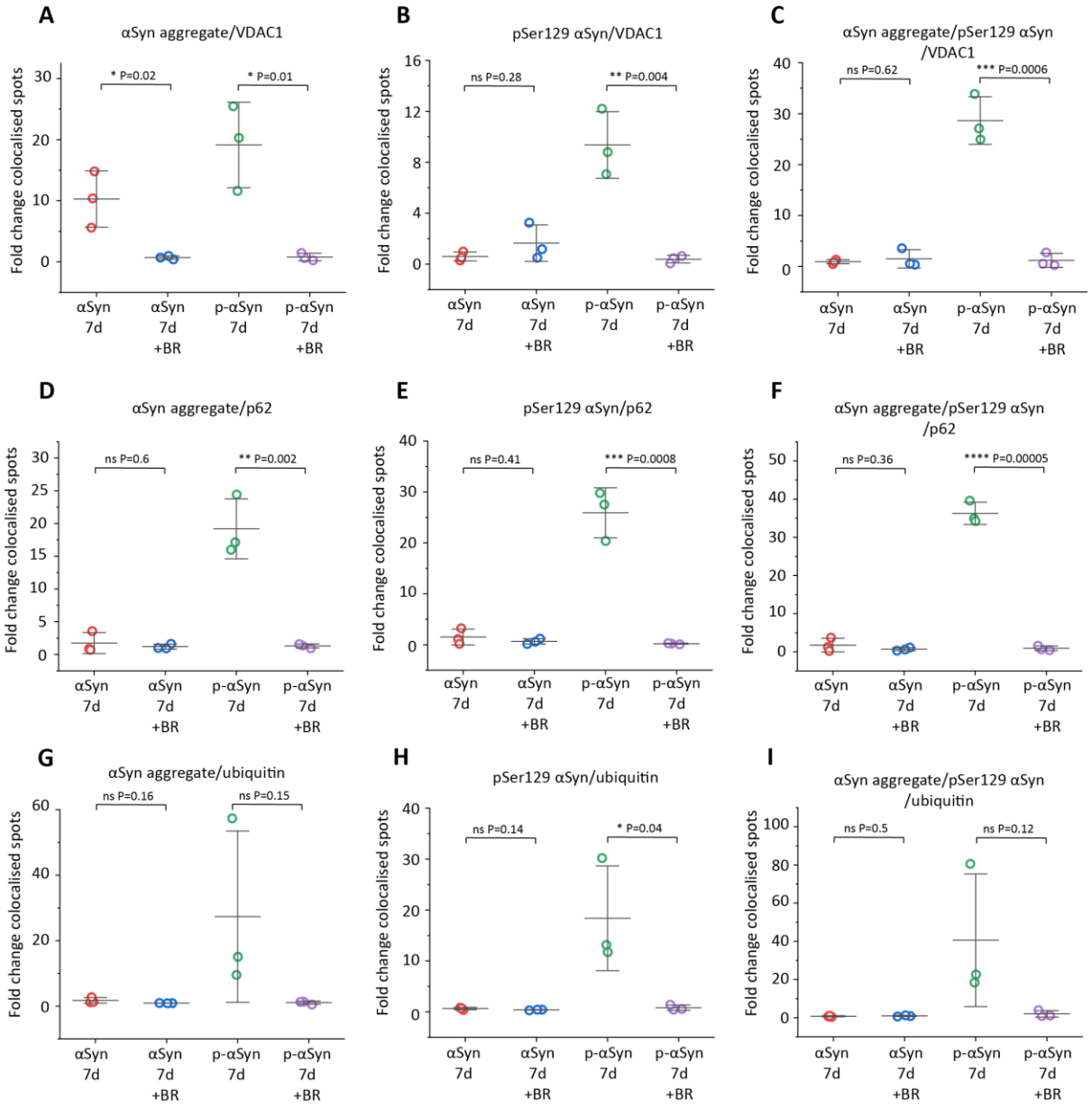

Figure 5.8. Treatment with BRICHOS reduces the number of Lewy Body like aggregates when cells were seeded with p-αSyn. After control cells were seeded with either αSyn or p-αSyn, the number of Lewy Body-like aggregates was assessed in the presence and absence of BRICHOS. The fold change of aggregates was calculated from a negative control, either PBS only or BRICHOS only. The fold change of VDAC1 colocalised with aggregated αSyn (**A**), phosphorylated αSyn (**B**), and aggregated phosphorylated αSyn (**C**) was calculated. The fold change of p62 colocalised with αSyn aggregate (**D**), pSer129 αSyn (**E**), and αSyn aggregate and pSer129 αSyn (**F**) was determined. The fold change of colocalised ubiquitin and αSyn aggregate (**G**), pSer129 αSyn (**H**), and αSyn aggregate and pSer129 (**I**) was assessed. Data from αSyn 7d and p-αSyn 7d is taken from Chapter 4 and combined with αSyn 7d + BR and p-αSyn 7d + BR from Chapter 5. Graphs show three biological replicates, bars represent mean ± SD. Statistical significance was determined by two sample t-test.

5.4. Discussion

5.4.1. Knockdown of αSyn as a therapeutic for PD

Partial knockdown of αSyn could be an effective therapeutic specifically for patients with triplication of SNCA. The shRNA knockdown of SNCA shown in this chapter is sufficient to reduce the number of αSyn aggregates, phosphorylated αSyn and Lewy Body-like aggregates. Endogenous αSyn is crucial for the development of Lewy body pathology, even when external αSyn preformed fibrils are applied; the absence of endogenous αSyn leads to the absence of Lewy bodies (Chen et al., 2019).

This work presents only one SNCA triplication cell line in which αSyn is present at a much higher level than control, however there is huge heterogeneity in αSyn levels between patients with PD. Lewy Body-like aggregates are not observed at a higher level in Parkin and LRRK2 patients, so it is unclear whether knockdown of SNCA would be beneficial for patients with mutations in LRRK2 and Parkin.

A key finding consistent across PD cell lines, was the increased presence of p-αSyn within the cell media (Chapter 3), which are potential seeds for disease progression. More work needs to be done to determine whether SNCA knockdown will reduce the toxic p-αSyn observed in the cell media, responsible for the spreading of αSyn aggregates from cell to cell. Many studies suggest that knockdown of αSyn will prevent the spreading of pathological species. The reduction of αSyn expression in the hippocampus of transgenic mice prevents spreading of pathological phosphorylated αSyn to various brain areas such as midbrain and cerebellum (Menon et al., 2021). Conversely, inoculation of mice with αSyn at a specific site report the spreading of αSyn by the increased presence of pathological αSyn in the form of Lewy Bodies at distal regions (Luk, V. M. Kehm, et al., 2012). These findings highlight the importance of αSyn protein levels in the pathological spreading of αSyn in disease.

In Chapter 3 it was highlighted that some PD patient derived cells exhibit both Lewy Body-like aggregate formation and mitochondrial dysfunction. Within this chapter I have observed that Lewy Body-like aggregate formation can be reduced by the knockdown of αSyn. An important experiment to complete would be to measure the mitochondrial dysfunction after knockdown of SNCA. It is unclear whether the knockdown of αSyn would be sufficient to rescue the mitochondrial dysfunction within this model. Studies in adult rats treated with

Rotenone to induce mitochondrial dysfunction by inhibition of complex I of the mitochondrial respiratory chain, show that a reduction of αSyn leads to decreased neurodegeneration and amelioration of motor symptoms (Zharikov et al., 2015). PD cellular models utilizing SK-N-SH and HEK293T cells overexpressing αSyn, showed increased mitochondrial dysfunction as a result of increased αSyn, cells displayed increased reactive oxygen species and reduced membrane potential (Qu et al., 2020). This study used a peptide-based therapeutic to increase the degradation of αSyn, this correlated with a reduction in reactive oxygen species and increased mitochondrial membrane potential. These results support the requirement for reducing αSyn levels to rescue mitochondrial dysfunction in PD models.

5.4.2. Potential of inhibiting secondary nucleation as a therapeutic for PD

As presented in Chapter 4, mitochondrial dysfunction and Lewy Body-like formation is observed as a result of seeding control cells with p-αSyn. BRICHOS has been reported to prevent secondary nucleation of αSyn, which is a primary driver of αSyn seeding and spreading from cell to cell (Adam et al., 2024). To determine if inhibiting secondary nucleation was sufficient to stop the dysfunction generated by p-αSyn seeding, cells were seeded with both p-αSyn and BRICHOS. The total αSyn and p-αSyn levels after BRICHOS treatment were assessed by MSD ELISA, no difference was observed after the addition of BRICHOS. There was a slight reduction in mean αSyn levels but due to variability it was not significant. Due to time constraints, more biological replicates could not be carried out, but a difference could potentially be observed with a higher n number.

Importantly, after p-αSyn seeding, BRICHOS treatment reduces the proportion of p-αSyn that is released into the cell media (Figure 5.6 F). This is a critical finding, as it highlights the ability of BRICHOS to reduce the amount of cell to cell spreading, and therefore could be a potential therapeutic in reducing disease progression. The increased release of p-αSyn is a phenotype observed in all PD cell lines used within this work and highlights the importance of this finding that BRICHOS can reduce the levels of p-αSyn released into the cell surroundings.

Chapter 4 outlines mitochondrial dysfunction can be induced in healthy control cells by seeding with p-αSyn. I have taken this data and compared it with the mitochondrial function after seeding with αSyn fibrils + BRICHOS and p-αSyn fibrils + BRICHOS. Due to time constraints, I did not carry out all the conditions within the same biological replicate, and future experiments will focus on this to confirm these results. I observed a reduction in

mitochondrial dysfunction in the presence of BRICHOS to cells that were seeded with p-αSyn. There was no difference in mitochondrial function in cells seeded with αSyn, but as noted in chapter 2, αSyn 7d is not sufficient to cause mitochondrial dysfunction. There is currently no literature researching the impact of BRICHOS in mitochondrial function, but if mitochondrial dysfunction is synergistic with αSyn aggregation then BRICHOS is suspected to rescue mitochondrial function.

The effects of the inhibition of secondary nucleation by BRICHOS was investigated. The ability of BRICHOS to stop nanoscopic Lewy Body-like aggregate formation because of p-αSyn seeding and spreading was investigated. After adding BRICHOS to p-αSyn seeded cells, there was a consistent reduction of Lewy Body-like aggregates containing phosphorylated αSyn and a Lewy Body marker. In p-αSyn fibril seeded cells, all Lewy Body-like aggregates containing VDAC1 and p62 were reduced as a result of BRICHOS treatment. Since secondary nucleation is the primary driver of aggregate formation, inhibiting this process is expected to lead to a reduction in Lewy body formation (Xu et al., 2024). When investigating ubiquitin containing Lewy Bodies, there was no difference in aggregated αSyn and ubiquitin, and aggregated phosphorylated αSyn with ubiquitin. This is likely due to the huge variability between biological replicates of p-αSyn 7d seeding. These results are consistent with research showing the effects of BRICHOS in mouse models of AD, Aβ precursor protein (*App*) knockin mice treated with BRICHOS exhibit reduced Aβ plaques in multiple brain regions (Manchanda et al., 2023).

When cells were seeded with αSyn 7d, there is no difference in Lewy Body formation (Figure 4.5 and Figure 4.5), and this is consistent with BRICHOS having no effect on Lewy Body formation here (Figure 5.8), except for one reduction observed in the number of αSyn aggregates colocalised with VDAC1 after the addition of BRICHOS.

Due to time constraints, data from Chapter 4 and Chapter 5 were combined to assess the influence of BRICHOS on the dysfunction caused by seeding with p-αSyn. An imperative future experiment is to carry out all the seeding conditions in one assay at the same time, direct comparison of conditions will strengthen these findings.

5.5. Conclusions

This chapter outlines two therapeutic approaches that could be used to reduce dysfunction in PD patient cells. Firstly, knockdown of SNCA is sufficient to reduce the formation of Lewy Body-like aggregates that are found in PD patient cells. Secondly, inhibiting seed induced monomer recruitment by supressing secondary nucleation effectively reduces the levels of p-αSyn that are released from healthy control cells after seeding with p-αSyn and reduces the Lewy Body-like aggregate formation and mitochondrial dysfunction associated with seeding. The reduction of Lewy Body-like aggregate formation and p-αSyn released from cells could be a critical target to prevent the spread of PD.

Chapter 6: Discussion

Parkinson's Disease (PD) is a progressive neurodegenerative disease. The main pathological hallmark of PD is the deposition of aggregated αSyn in Lewy Bodies deposited in the central nervous system (Gibb & Lees, 1988; Spillantini et al., 1997). The gold standard diagnosis of PD is detection of Lewy Bodies in postmortem tissue, but aggregates of αSyn are known to form 10 years before symptom onset, and when symptom onset occurs 50-70% of dopaminergic neurons are already lost (Lansbury & Lashuel, 2006; Wong et al., 2019). Detection of the toxic αSyn in the early stages of disease could lead to more effective therapeutics to slow the progression of the disease before the irreversible neuronal damage is done.

Within this thesis, to shed some light on this issue, a dopaminergic neuron like cell model was utilised to understand αSyn dysfunction in patients in sporadic and familial PD; this study used two sporadic lines, one SNCA triplication, one LRRK2 mutant, one Parkin mutant and their matched healthy controls. The total levels of αSyn were measured in PD patients and controls. Elevated levels of αSyn was a key feature of SNCA triplication cells, but there was no difference in αSyn levels between other PD cell lines and their matched controls. There was a large amount of heterogeneity between PD patient cells; SNCA triplication cells and one sporadic cell line had an increased number of Lewy Body-like aggregates compared to their matched controls, these Lewy Body-like aggregates were present in the other PD cell lines but not to a higher extent than their matched controls. A unique combination of the patient derived cellular model, and high-resolution imaging has revealed the formation of these nanoscopic Lewy Body-like aggregates, that have only been observed in cellular models of PD after the addition of preformed fibrils or external stressors (Mahul-Mellier et al., 2020). This spontaneous formation of Lewy Bodies observed not only supports the directly reprogrammed iDNLs validity as a model for PD but also allows us to quantify this disease relevant pathology as a marker of PD. Further development of this methodology to detect pathogenic species from human biofluids in CSF and blood could be key to generating a predictive biomarker for PD.

Although there is heterogeneity present between PD cell lines in the total levels of αSyn and the presence of Lewy body-like aggregates, one consistent phenotype that unifies familial and sporadic PD cases is the increased presence of phosphorylated αSyn in the secretome compared to the corresponding healthy controls. This increased extracellular pSer129 αSyn is

present irrespective of intracellular αSyn levels. Increased secretion of αSyn has been correlated to lysosomal dysfunction, treatment of αSyn overexpressing SH-SY5Y cells with a lysosomal inhibitor increases the release of αSyn in exosomes (Alvarez-Erviti et al., 2011). Similarly, in primary microglia when cells are overloaded with αSyn and undergo lysosome stress, increased extracellular insoluble αSyn is present in the cell media (Abe et al., 2024). These results suggest a lysosomal dysfunction in the PD cells could contribute to the increased toxic release of pSer129 αSyn. Increased extracellular levels of αSyn is also indicative of more pronounced cell to cell seeding in PD patient cells, these results implicate pSer129 αSyn in the spreading of PD (Bae et al., 2022). However, additional experiments including αSyn-SAA would need to be performed to confirm if the extracellular p-αSyn detected within the cell media are seed competent. Elevated extracellular levels of pSer129 αSyn could be of importance in diagnosing PD, the αSyn-SAA is a technique used to amplify pathogenic forms of αSyn in the CSF to distinguish PD patients from healthy controls (Siderowf et al., 2023). If pSer129 αSyn is spreading in the early presymptomatic stages of disease, detection of these species could be imperative for early diagnostics, SiMPull methodology outlined in this thesis could be integral in detecting low concentrations αSyn in biofluids.

αSyn aggregation and pathology has been linked to another integral driver of PD: mitochondrial dysfunction. It is unclear which phenomenon occurs first; whether the aggregation and accumulation of toxic species of αSyn leads to the dysregulation of mitochondria, or the production of reactive oxygen species by damaged mitochondria contributes to the accumulation of αSyn (Dias, Junn and Mouradian, 2013). I determined whether the αSyn dysfunction in the iDNL model was also correlated to mitochondrial dysfunction. The mitochondrial and lysosomal function were assessed in both PD and healthy control cells. The PD cells consistently showed an increased number of mitochondria and lysosomes, compared to corresponding healthy controls, with a trend towards reduction in mitophagy in SNCA triplication and one sporadic line. The increased number of mitochondria and lysosomes is indicative of an accumulation of dysfunctional organelles, and problems in the quality control pathways of the cell (Henrich et al., 2023). This accumulation of damaged mitochondria and lysosomes can eventually lead to cell death, which is observed as the loss of dopaminergic regions in the substantia nigra of PD patients. Mitochondrial dysfunction in these lines has been extensively measured by other Mortiboys lab members, showing an

increase in reactive oxygen species, increased in the number of mitochondria, and reduction in mitochondrial membrane potential in SNCA, sporadic, Parkin and LRRK2 cell lines (Carling et al., 2020; Schwartzentruber et al., 2020, R Hughes PhD thesis, Capriglia Unpublished). Taken together, these results highlight the putative role of mitochondrial dysfunction in both sporadic and familial PD.

PD is a complex disorder, with various genetic and environmental causes, this research aimed to provide clarity for the role of αSyn dysfunction in both sporadic and familial PD. The development of therapeutic agents to target one common mechanism that is present within all patient cells has been challenging (Frasier, Fiske and Sherer, 2022). The findings in this thesis unify sporadic and familial cases of PD and present a consistent phenotype of increased extracellular phosphorylated αSyn. This potential target could lead to more effective treatment options for all individuals irrespective of the cause of PD.

To strengthen the work outlined in this thesis, the validity of findings in specific disease mutations could be increased by the application of isogenic controls (Soldner et al., 2011). However, in sporadic cases the use of isogenic controls is not possible as there is no known genetic cause. Future work should focus on increasing the number of cell lines to increase the statistical validity of the results of this work. Additional sporadic and SNCA triplication lines should be investigated to see if this phenotype is maintained.

To confirm if the findings in PD patient-derived cellular models were consistent in human tissue, the presence of pSer129 αSyn and total αSyn was investigated using postmortem tissue from PD patients and healthy controls. This was done by Emma Garland from the lab. Immunohistochemical staining of Lewy Bodies, using pSer129 αSyn antibody, using fixed tissue found there was significantly higher Lewy Bodies in the parietal cortex and cingulate gyrus in PD patients compared to healthy controls, but no significant difference in the midbrain areas (Figure 6.1). Importantly, the mean number of Lewy bodies in the midbrain areas of PD patients are 100 times higher than healthy controls, with increased sample size a significant result is more likely.

Quantifying protein levels in homogenates is considered a more accurate method than immunohistochemical staining, and therefore brain samples were homogenated for quantification by MSD ELISA. The presence of pSer129 αSyn and total αSyn in PD and healthy

control brain homogenates was determined by MSD ELISA (Figure 6.2). There was no difference in the total αSyn present in PD and healthy controls in the frontal cortex, cingulate gyrus, or midbrain. However, there was consistently higher pSer129 αSyn levels in PD patient tissue compared to healthy controls, this was maintained in the frontal cortex, cingulate gyrus and midbrain. This suggests that the findings within PD patient cells are recapitulated in PD patient postmortem tissue. The phosphorylated αSyn observed here is present in brain homogenates from tissue, and therefore represents intracellular protein. To confirm the extracellular presence of pSer129 αSyn in humans, detection of pSer129 αSyn in CSF or selective isolation of extracellular protein from postmortem tissue would be required (Mollenhauer et al., 2012; Hong et al., 2018).

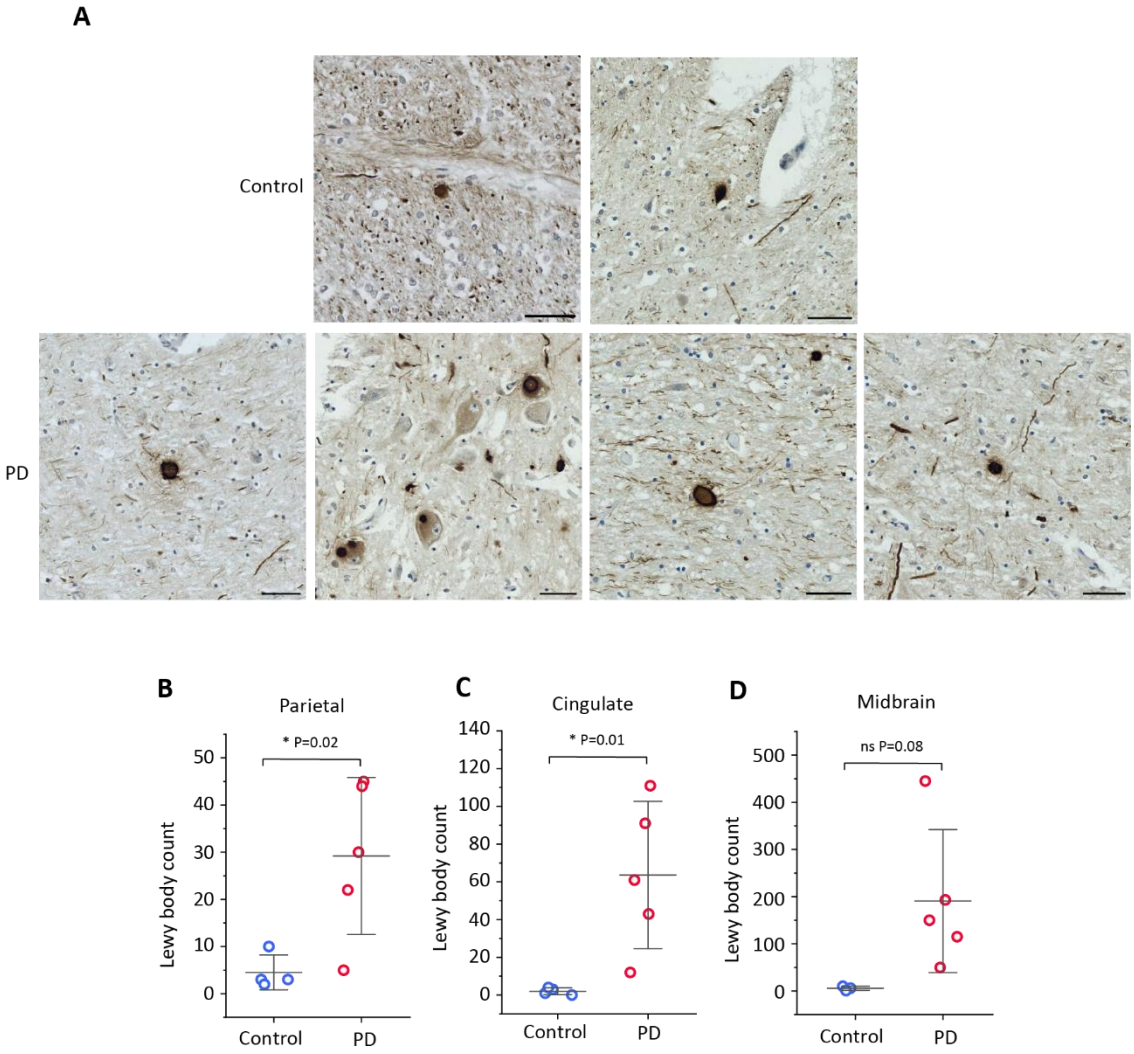

Figure 6.1. Lewy Body pathology in Parkinson´s Disease and healthy control postmortem tissue. A. Representative images of postmortem midbrain tissue staining with pSer129 αSyn to detect Lewy Bodies. **B-D**. The number of Lewy Bodies were counted in the parietal cortex (**B**), cinuglate gyrus (**C**) and midbrain (**D**). Scale bars represent 50 µm. Each data point represents a single patient or healthy

control. Bars represent mean ± SD. Statistical significance was determined using a two-sample t-test. Sample preparation and data collection by Emma Garland.

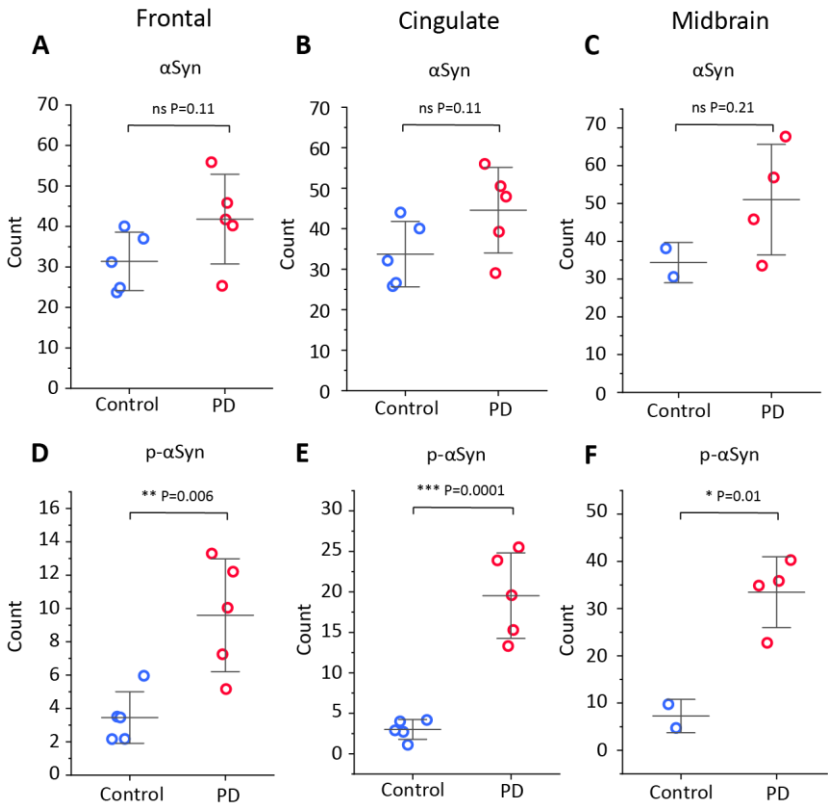

Figure 6.2. Measurement of phosphorylated and total αSyn in Parkinson´s Disease and healthy control postmortem tissue. A-C. The total αSyn in both healthy control and patient was quantified in the frontal cortex (**A**), the cingulate gyrus (**B**) and midbrain (**C**). **D-F**. The levels of pSer129 αSyn were quantified for PD patient and healthy control in the frontal cortex (**D**), cingulate gyrus (**E**), and the midbrain (**F**). Each data point represents a single patient or healthy control. Bars represent mean ± SD. Statistical significance was determined using a two-sample t-test. Sample preparation was done by Emma Garland.

After confirming that αSyn dysfunction and mitochondrial damage was occurring within PD patient iDNLs, I aimed to understand the pathogenic mechanisms that contribute to disease progression. To determine which species of αSyn are toxic and elucidate the pathogenic mechanisms occurring within cells, healthy control iDNLs were treated with various species of αSyn including WT αSyn and p-Ser129 αSyn and different aggregation states of 48 h which represents oligomeric species, and 7 d containing fibrillar species. It was found that pSer129 αSyn fibrillar species induced a PD like phenotype in healthy controls, by causing mitochondrial dysfunction and the formation of Lewy Body-like aggregates. This was not

observed after treatment with other species of αSyn. I aimed to decipher the exact mechanisms of dysfunction by pSer129 αSyn fibrils.

Conformational differences are known to affect the uptake and/or degradation of αSyn, when primary cortical neurons were treated with αSyn PFFs containing missense mutations E46K and H50Q there was increased intracellular αSyn, compared to WT αSyn PFFs and other missense mutations (Guan et al., 2020). In this thesis, the uptake of in vitro formed αSyn species was measured, to determine if cells had a preferential uptake of p-αSyn fibrils, which led to more aggregates within the cells responsible for the increased toxicity. No difference was observed in the uptake of phosphorylated and non-phosphorylated αSyn (Figure 6.3). This suggests increased toxicity of p-αSyn fibrils is not due to increased cellular uptake.

Additionally, the cellular processing of both αSyn and p-αSyn fibrils was investigated, by probing interactions between the protein and degradation machinery including lysosomes. The results suggest that αSyn fibrils are processed by the cell at a faster rate than p-αSyn fibrils, as it is trafficked to the lysosome at a faster rate than the phosphorylated form (Figure 6.3). A slower degradation is also implicated in αSyn missense mutation A53T pathology, which consistently shows increased αSyn aggregation and Lewy Body formation (Bennett et al., 1999; Lee et al., 2002). This could explain why phosphorylated αSyn builds up and is deposited within Lewy Bodies. Some contradictory studies suggest that phosphorylated αSyn is preferentially degraded (Zheng et al., 2019). This preferential degradation could represent physiological conditions in healthy cells, however overload of phosphorylated αSyn aggregates in disease could inhibit normal functioning of this pathway (Ebrahimi-Fakhari et al., 2012). Taken together, the data indicates a fine balance in phosphorylated αSyn concentration between physiological and diseased conditions.

Next, the seeding ability of αSyn and p-αSyn fibrils was assessed, by incubating the seeds with monomeric wildtype αSyn and following the aggregation kinetics. Phosphorylated αSyn seeds proved more effective at seeding the aggregation of monomeric WT αSyn, indicative by a reduction in half-time. This could suggest that once the aggregates are taken up by cells, phosphorylated αSyn fibril seeds aggregation of endogenous protein faster than WT αSyn fibrils and could explain the formation of Lewy Body-like aggregates observed exclusively in the phosphorylated αSyn treated cells (Figure 6.3). These results are contradictory to some research studies, that suggest WT αSyn aggregates at a faster rate than phosphorylated αSyn

(Schreurs et al., 2014). This could be due to differences in the preparation of phosphorylated αSyn, and the aggregation conditions. Fibril morphological differences are present within the p-αSyn fibrils presented in this work and the highlighted research article, this work shows shorter more fragmented fibrils, whereas Schreurs et al. shows phosphorylated αSyn forming longer fibrils. Shorter fibrils are known to be more toxic than longer fibrils due to increased fibril ends to induce aggregation and elongation (Cascella et al., 2021).

This thesis shows that when healthy iDNLs are treated with toxic αSyn species, mitochondrial dysfunction is induced. To probe the mechanisms for dysfunction and to understand if there is a direct interaction between αSyn and mitochondria, the ability of αSyn aggregate species to permeabilize mitochondrial mimicking membranes *in vitro* was observed. The presence of both WT αSyn and phosphorylated αSyn oligomers was sufficient to cause membrane permeabilization of non-specific lipid membranes, no membrane damage by monomers or fibrils was observed. This has been shown widely in the literature and is one of the known pathological mechanisms for αSyn toxicity (Musteikytė et al., 2021). To mirror a mitochondrial membrane preparation in vitro, the lipid cardiolipin was introduced in the model membrane which is exclusive to the mitochondria. The phosphorylated oligomers were more damaging to mitochondrial mimicking membranes than non-phosphorylated oligomers by inducing greater membrane permeabilization, which was attributed to a direct interaction between phosphorylated αSyn and cardiolipin (Figure 6.3). These findings are consistent with the previously published work suggesting phosphorylated αSyn preferentially binds to mitochondrial membranes (Wang et al., 2019). I propose a direct relationship between the addition of phosphorylated fibrils and mitochondrial dysfunction. Importantly, although WT αSyn aggregates are toxic to mitochondrial membranes, the addition of 25% phosphorylated αSyn into the aggregate renders them even more toxic to the mitochondrial membrane, toxicity to the membrane increases when co-aggregates contain 75% p-αSyn. This suggests that during the aggregation process, if phosphorylated αSyn recruits WT αSyn to form co-aggregates, it can induce higher mitochondrial membrane toxicity than a pure WT αSyn aggregate.

Overall, the results of this thesis outline a complex interplay of phosphorylated αSyn and αSyn oligomers and fibrils in contributing to the toxicity observed in PD (Figure 6.3). Increased extracellular pSer129 αSyn is present in PD cell media, indicative of increased secretion of

pSer129 αSyn by the cells. pSer129 αSyn released by the cell can then be taken up by a neighbouring cell, with no difference observed in the uptake of WT αSyn and pSer129 αSyn by the cells. However, within the cell, pSer129 αSyn fibril seeds are more effective at promoting seeded aggregation of monomeric αSyn than non-phosphorylated αSyn seeds. The pSer129 αSyn fibril seeds provide a surface for endogenous monomeric αSyn to aggregate on and accelerate the formation of Lewy Body-like aggregates within the cell. I have shown that the presence of endogenous αSyn is essential for this αSyn induced dysfunction to occur, as knockdown of αSyn prevents the formation of Lewy Body-like aggregates. This seed induced aggregation can lead to the formation of various αSyn aggregates within the cell, including oligomeric species. Oligomeric species of pSer129 αSyn are the key drivers of mitochondrial dysfunction, by preferentially binding to cardiolipin at the mitochondrial membrane to induce pore formation. This research underscores the dual role of αSyn species: fibrillar forms are pivotal in seeded aggregation, leading to the formation of Lewy body-like aggregates, while oligomeric species are central to the direct mitochondrial dysfunction that underpins PD pathology.

Although this thesis has shown a knockdown of αSyn reduces the pathological phenotype in PD patient cells, this is not a viable therapeutic for patients due to the importance of the physiological functions of αSyn. Physiological αSyn is plays an important role in synaptic vesicle release and recycling through interactions with proteins such as VAMP2 involved in SNARE complex formation, and physiological phosphorylated αSyn is an important mediator of αSyn protein interactions at the synapse with a key role in regulating neurotransmitter release (Burré et al., 2010; Parra-Rivas et al., 2023). Although αSyn and phosphorylated αSyn are essential for normal cellular function, their intrinsically disordered nature makes them aggregation prone, and facilitates the formation of toxic aggregates (Ma et al., 2016). I have shown different conformations of phosphorylated αSyn to be toxic, including both oligomeric and fibrillar species. Therefore, therapeutics targeting the pathogenic mechanisms of αSyn dysfunction, such as αSyn seeding, might be an effective and feasible option rather than targeting specific aggregated conformations of αSyn.

Within this thesis, it was also examined whether inhibiting the recruitment of physiological monomers to form pathological aggregates – species responsible for organelle damage and further disease progression through cell-to-cell seeding – could be a viable treatment strategy.

Specifically, the ability of the molecular chaperone domain BRICHOS to rescue αSyn-induced dysfunction was invesitgated. BRICHOS works by binding to αSyn fibril surfaces and preventing secondary nucleation from new pathological aggregates (Adam et al., 2024). Targeting this mechanism will prevent endogenous αSyn from aggregating on the fibril surface and prevent the formation of Lewy Body-like aggregates and oligomeric species that are cytotoxic (Xu et al., 2024). In the patient-derived cellular model, I sought to understand if BRICHOS could prevent the p-αSyn fibril induced toxicity. The addition of BRICHOS in cells seeded with p-αSyn fibrils was sufficient to prevent the formation of Lewy Body-like aggregates and mitochondrial dysfunction caused by phosphorylated αSyn and reduce the levels of secreted phosphorylated αSyn (Figure 6.3). This highlights the importance of phosphorylated αSyn seeding in the pathology of PD. Although the results show BRICHOS rescues phosphorylated αSyn dysfunction and no difference is observed in WT αSyn, it does not suggest that BRICHOS cannot prevent WT αSyn secondary nucleation and induced dysfunction. Previous literature has highlighted the importance of BRICHOS in preventing secondary nucleation of αSyn, reducing the oligomeric population of αSyn and the rescuing fibril associated neurotoxicity (Adam et al., 2024). BRICHOS-type molecules, which specifically target the toxic mechanisms responsible for recruiting physiological αSyn to form pathological aggregates, represent promising therapeutic targets. These molecules can potentially inhibit the spread of toxic aggregates without interfering with the physiological αSyn that is essential for normal cellular function, making them an attractive option for disease-modifying therapies in conditions like Parkinson's Disease.

Overall, this thesis highlights a complex mechanism of phosphorylated αSyn dysfunction in the formation of Lewy bodies and mitochondrial dysfunction. A therapeutic target is proposed, using inhibiting secondary nucleation to reduce the pathogenic effects of phosphorylated αSyn in PD patients.

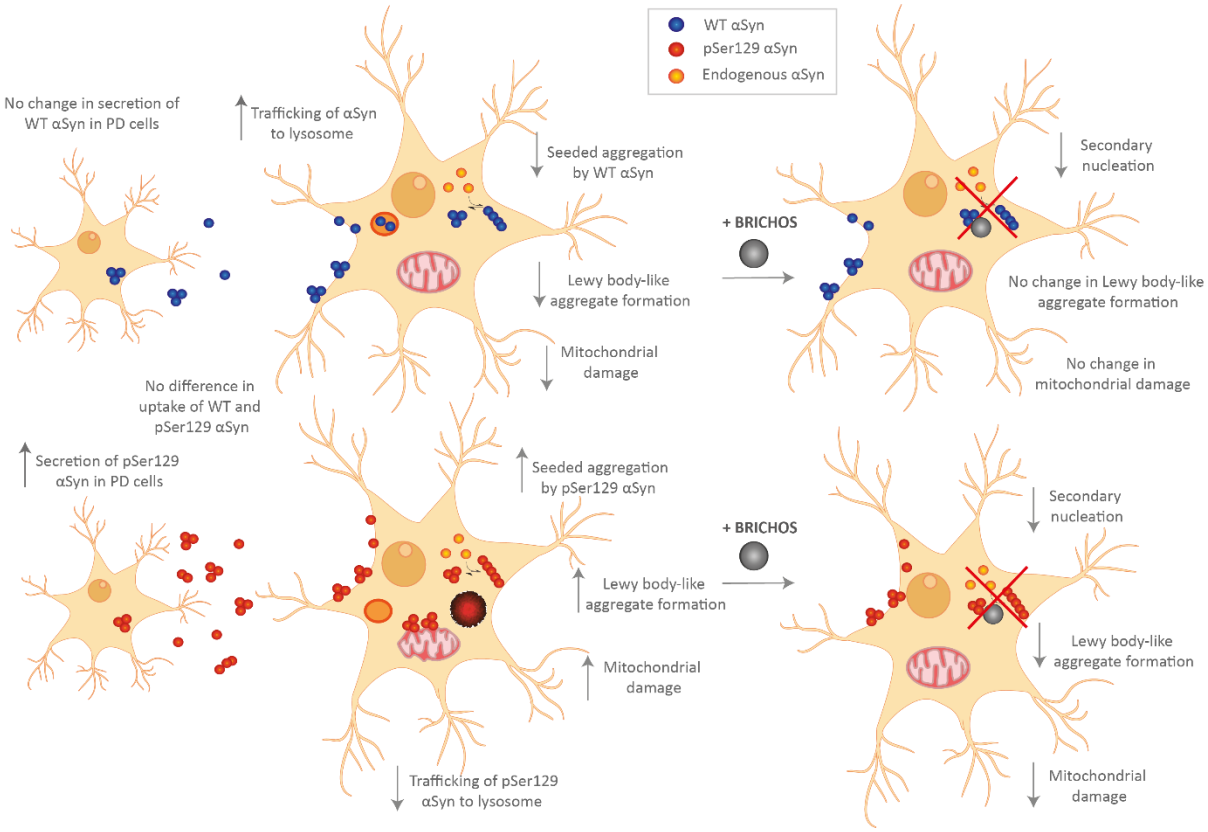

Figure 6.3. Proposed mechanisms of αSyn dysfunction in PD patient cells. Schematic of the proposed mechanisms of αSyn and p-αSyn toxicity in PD. PD patient cells secrete higher amount of pSer129 αSyn (red) into the cell media than healthy controls. There is no difference between the amount of WT αSyn (blue) secreted in PD and healthy control cells. Both WT αSyn and pSer129 αSyn can be taken up by neighbouring cells. Once inside the cell, WT αSyn is trafficked to the lysosome faster than pSer129 αSyn. pSer129 αSyn more effectively seeds the aggregation of endogenous monomeric αSyn (orange), to form new oligomeric and fibrillar aggregates. Within the cell the pSer129 αSyn aggregates promote Lewy Body-like formation and mitochondrial dysfunction. This phenotype is not observed with WT αSyn. Cells treated with BRICHOS (grey) and pSer129 αSyn show reduced dysfunction. BRICHOS binds to αSyn seeds and prevent secondary nucleation. This prevents the formation of new aggregate on the surface of the seeds and prevents Lewy Body-like aggregate formation and mitochondrial dysfunction. No difference was observed in cells treated with WT αSyn and BRICHOS. ↑ Indicates an increase ↓ Indicates a decrease.

References

Aarsland, D. *et al.* (2003) 'Prevalence and characteristics of dementia in Parkinson disease: an 8-year prospective study', *Archives of neurology*, 60(3), pp. 387–392. doi:https://doi.org/10.1001/ARCHNEUR.60.3.387.

Abe, T. *et al.* (2024) 'Lysosomal stress drives the release of pathogenic α-synuclein from macrophage lineage cells via the LRRK2-Rab10 pathway', *iScience*, 27(2), p. 108893. doi :https://doi.org/10.1016/J.ISCI.2024.108893.

Adam, L. *et al.* (2024) 'Specific inhibition of α-synuclein oligomer generation and toxicity by the chaperone domain Bri2 BRICHOS', *Protein Science*, 33(8). doi:https://doi.org/10.1002/PRO.5091.

Adamcik, J. and Mezzenga, R. (2018) 'Amyloid Polymorphism in the Protein Folding and Aggregation Energy Landscape', *Angewandte Chemie International Edition*, 57(28), pp. 8370–8382. doi: https://doi.org/10.1002/ANIE.201713416.

Akdemır, Ü.Ö., Bora Tokçaer, A. and Atay, L.Ö. (2021) 'Dopamine transporter SPECT imaging in Parkinson's disease and parkinsonian disorders', *Turkish Journal of Medical Sciences*, 51(2), p. 400. doi: https://doi.org/10.3906/SAG-2008-253.

Alberts, B. *et al.* (2002) 'The Shape and Structure of Proteins'. *Molecular Biology of the Cell*, doi: https://www.ncbi.nlm.nih.gov/books/NBK26830/

Alvarez-Erviti, L. *et al.* (2011) 'Lysosomal dysfunction increases exosome-mediated alpha-synuclein release and transmission', *Neurobiology of Disease*, 42(3), p. 360. doi: https://doi.org/10.1016/J.NBD.2011.01.029.

Anderson, J.P. *et al.* (2006) 'Phosphorylation of Ser-129 Is the Dominant Pathological Modification of α-Synuclein in Familial and Sporadic Lewy Body Disease', *Journal of Biological Chemistry*, 281(40), pp. 29739–29752. doi: https://doi.org/10.1074/JBC.M600933200.

Angius, F. *et al.* (2023) 'Combined measure of salivary alpha-synuclein species as diagnostic biomarker for Parkinson's disease', *Journal of Neurology 2023*, 1, pp. 1–9. doi: https://doi.org/10.1007/S00415-023-11893-X.

Appel-Cresswell, S. *et al.* (2013) 'Alpha-synuclein p.H50Q, a novel pathogenic mutation for Parkinson's disease', *Movement disorders : official journal of the Movement Disorder Society*, 28(6), pp. 811–813. doi: https://doi.org/10.1002/MDS.25421.

Bae, E.J. *et al.* (2022) 'TNF-α promotes α-synuclein propagation through stimulation of senescence-associated lysosomal exocytosis', *Experimental & Molecular Medicine*, 54(6), p. 788. doi: https://doi.org/10.1038/S12276-022-00789-X.

Baena-Montes, J.M., Avazzadeh, S. and Quinlan, L.R. (2021) 'α-synuclein Pathogenesis in Hipsc Models of parkinson's Disease', *Neuronal Signaling*, 5(2), pp. 1–10. doi: https://doi.org/10.1042/NS20210021/229008.

Bajaj, N., Hauser, R.A. and Grachev, I.D. (2013) 'Clinical utility of dopamine transporter single photon emission CT (DaT-SPECT) with (123I) ioflupane in diagnosis of parkinsonian syndromes', *Journal of Neurology, Neurosurgery & Psychiatry*, 84(11), pp. 1288–1295. doi: https://doi.org/10.1136/JNNP-2012-304436.

Baldacci, F. *et al.* (2020) 'The path to biomarker-based diagnostic criteria for the spectrum of neurodegenerative diseases HHS Public Access', *Expert Rev Mol Diagn*, 20(4), pp. 421–441. doi: https://doi.org/10.1080/14737159.2020.1731306.

Bartels, T., Choi, J.G. and Selkoe, D.J. (2011) 'α-Synuclein occurs physiologically as a helically folded tetramer that resists aggregation', *Nature 2011 477:7362*, 477(7362), pp. 107–110. doi: https://doi.org/10.1038/nature10324.

Beitz, J.M. (2014) 'Parkinson's disease: A review', *Frontiers in Bioscience - Scholar*, 6 S(1), pp. 65–74. doi: https://doi.org/10.2741/S415/PDF.

Bennett, C.M. *et al.* (1999) 'Degradation of-Synuclein by Proteasome', *Journal of Biological Chemistry* [Preprint]. doi: http://www.jbc.org

Benskey, M.J. *et al.* (2018) 'Silencing alpha synuclein in mature nigral neurons results in rapid neuroinflammation and subsequent toxicity', *Frontiers in Molecular Neuroscience*, 11. doi: https://doi.org/10.3389/FNMOL.2018.00036/FULL.

Bisi, N. *et al.* (2021) 'α-Synuclein: An All-Inclusive Trip Around its Structure, Influencing Factors and Applied Techniques', *Frontiers in Chemistry*, 9, p. 666585. doi: https://doi.org/10.3389/FCHEM.2021.666585/BIBTEX.

Biverstål, H. *et al.* (2020) 'Functionalization of amyloid fibrils via the Bri2 BRICHOS domain', *Scientific reports* [Preprint]. doi: https://doi.org/10.1038/s41598-020-78732-1.

Bose, A., Petsko, G.A. and Studer, L. (2022) 'Induced pluripotent stem cells: a tool for modeling Parkinson's disease', *Trends in Neurosciences*, 45(8), pp. 608–620. doi: https://doi.org/10.1016/J.TINS.2022.05.001.

Boström, E. *et al.* (2024) 'Safety, Tolerability, and Pharmacokinetics of Single Doses of Exidavnemab (BAN0805), an Anti-α-Synuclein Antibody, in Healthy Western, Caucasian, Japanese, and Han Chinese Adults', *The Journal of Clinical Pharmacology*, 2024(0), pp. 1–11. doi: https://doi.org/10.1002/JCPH.6103.

Bourdenx, M. *et al.* (2014) 'Lysosomes and α-synuclein form a dangerous duet leading to neuronal cell death', *Frontiers in Neuroanatomy*, 8, p. 108133. doi: https://doi.org/10.3389/FNANA.2014.00083.

Braak, H. *et al.* (1999) 'Extensive axonal Lewy neurites in Parkinson's disease: a novel pathological feature revealed by α-synuclein immunocytochemistry', *Neuroscience Letters*, 265(1), pp. 67–69. doi: https://doi.org/10.1016/S0304-3940(99)00208-6.

Braak, H. *et al.* (2003) 'Staging of brain pathology related to sporadic Parkinson's disease', *Neurobiology of Aging*, 24(2), pp. 197–211. doi: https://doi.org/10.1016/S0197-4580(02)00065-9.

Brichta, L. and Greengard, P. (2014) 'Molecular determinants of selective dopaminergic vulnerability in Parkinson's disease: An update', *Frontiers in Neuroanatomy*, 8(DEC), p. 122879. doi: https://doi.org/10.3389/FNANA.2014.00152/BIBTEX.

Brighina, F. *et al.* (2019) 'G2019S Variation in LRRK2: An Ideal Model for the Study of Parkinson's Disease?' *Frontiers in human neuroscience*. doi: https://doi.org/10.3389/fnhum.2019.00306.

Buell, A.K. *et al.* (2014) 'Solution conditions determine the relative importance of nucleation and growth processes in α-synuclein aggregation', *Proceedings of the National Academy of Sciences of the United States of America*, 111(21), pp. 7671–7676. doi: https://doi.org/10.1073/PNAS.1315346111/-/DCSUPPLEMENTAL/PNAS.1315346111.SAPP.PDF.

Burré, J. *et al.* (2010) 'α-Synuclein Promotes SNARE-Complex Assembly in vivo and in vitro', *Science (New York, N.Y.)*, 329(5999), p. 1663. doi: https://doi.org/10.1126/SCIENCE.1195227.

Byers, B. *et al.* (2011) 'SNCA Triplication Parkinson's Patient's iPSC-derived DA Neurons Accumulate a-Synuclein and Are Susceptible to Oxidative Stress'.*PLoS One*. doi: https://doi.org/10.1371/journal.pone.0026159.

Cabin, D.E. *et al.* (2002) 'Synaptic Vesicle Depletion Correlates with Attenuated Synaptic Responses to Prolonged Repetitive Stimulation in Mice Lacking α-Synuclein', *The Journal of Neuroscience*, 22(20), p. 8797. doi: https://doi.org/10.1523/JNEUROSCI.22-20-08797.2002.

Candelise, N. *et al.* (2019) 'Seeding variability of different alpha synuclein strains in synucleinopathies', *Annals of Neurology*, 85(5), pp. 691–703. doi: https://doi.org/10.1002/ANA.25446.

Carling, P.J. *et al.* (2020) 'Deep phenotyping of peripheral tissue facilitates mechanistic disease stratification in sporadic Parkinson's disease', *Progress in Neurobiology*, 187, p. 101772. doi: https://doi.org/10.1016/J.PNEUROBIO.2020.101772.

Cascella, R. *et al.* (2021) 'The release of toxic oligomers from α-synuclein fibrils induces dysfunction in neuronal cells', *Nature Communications 2021 12:1*, 12(1), pp. 1–16. doi: https://doi.org/10.1038/s41467-021-21937-3.

Chai, C. and Lim, K.-L. (2013) 'Genetic Insights into Sporadic Parkinson's Disease Pathogenesis', *Current Genomics*, 14(8), p. 486. doi: https://doi.org/10.2174/1389202914666131210195808.

Chen, C. *et al.* (2023) 'Parkinson's disease neurons exhibit alterations in mitochondrial quality control proteins', *Npj Parkinson´s Disease* [Preprint]. doi: https://doi.org/10.1038/s41531-023-00564-3.

Chen, G. *et al.* (2020) 'Augmentation of Bri2 molecular chaperone activity against amyloid-β reduces neurotoxicity in mouse hippocampus in vitro'. *Communications biology*. 32(3) doi: https://doi.org/10.1038/s42003-020-0757-z.

Chen, Y. *et al.* (2019) 'Engineering synucleinopathy-resistant human dopaminergic neurons by CRISPR-mediated deletion of the SNCA gene', *The European journal of neuroscience*, 49(4), pp. 510–524. doi: https://doi.org/10.1111/EJN.14286.

Chiti, F. and Dobson, C.M. (2017) 'Protein Misfolding, Amyloid Formation, and Human Disease: A Summary of Progress Over the Last Decade', *https://doi.org/10.1146/annurev-biochem-061516-045115*, 86, pp. 27–68. doi: https://doi.org/10.1146/ANNUREV-BIOCHEM-061516-045115.

Choi, M.L. *et al.* (2022) 'Pathological structural conversion of α-synuclein at the mitochondria induces neuronal toxicity', *Nature Neuroscience 2022 25:9*, 25(9), pp. 1134–1148. doi: https://doi.org/10.1038/s41593-022-01140-3.

Christopher H. van Dyck *et al.* (2023) 'Lecanemab in Early Alzheimer's Disease', *New England Journal of Medicine*, 388(17), pp. 1630–1632. doi: https://doi.org/10.1056/NEJMC2301380.

Chung, H.K. *et al.* (2019) 'Modeling α-Synuclein Propagation with Preformed Fibril Injections', *Journal of Movement Disorders*, 12(3), p. 139. doi: https://doi.org/10.14802/JMD.19046.

Cohen, S.I.A. *et al.* (2012) 'From Macroscopic Measurements to Microscopic Mechanisms of Protein Aggregation'. *Journal of molecular biology*, 421(2-3), pp 160-71. doi: https://doi.org/10.1016/j.jmb.2012.02.031.

Cohen, S.I.A. *et al.* (2013) 'Proliferation of amyloid-β42 aggregates occurs through a secondary nucleation mechanism', *Proceedings of the National Academy of Sciences of the United States of America*, 110(24), pp. 9758–9763. doi: https://doi.org/10.1073/PNAS.1218402110/-/DCSUPPLEMENTAL.

Concha-Marambio, L. *et al.* (2023) 'Seed amplification assay for the detection of pathologic alpha-synuclein aggregates in cerebrospinal fluid', *Nature Protocols 2023 18:4*, 18(4), pp. 1179–1196. doi: https://doi.org/10.1038/s41596-022-00787-3.

Concha-Marambio, L., Shahnawaz, M. and Soto, C. (2019) 'Detection of misfolded α-synuclein aggregates in cerebrospinal fluid by the protein misfolding cyclic amplification platform', *Methods in Molecular Biology*, 1948, pp. 35–44. doi: https://doi.org/10.1007/978-1-4939-9124-2_4/FIGURES/2.

Cornejo-Olivas, M.R. *et al.* (2015) 'A Peruvian family with a novel PARK2 mutation: Clinical and pathological characteristics', *Parkinsonism & related disorders*, 21(5), pp. 444–448. doi: https://doi.org/10.1016/J.PARKRELDIS.2015.01.005.

Corti, O., Lesage, S. and Brice, A. (2011) 'What genetics tells us about the causes and mechanisms of Parkinson's disease', *Physiological reviews*, 91(4), pp. 1161–1218. doi: https://doi.org/10.1152/PHYSREV.00022.2010.

Cremades, N., Chen, S.W. and Dobson, C.M. (2017) 'Structural Characteristics of α-Synuclein Oligomers', *International review of cell and molecular biology*, 329, pp. 79–143. doi: https://doi.org/10.1016/BS.IRCMB.2016.08.010.

Cykowski, M.D. *et al.* (2017) 'Clinical Significance of TDP-43 Neuropathology in Amyotrophic Lateral Sclerosis', *Journal of Neuropathology and Experimental Neurology*, 76(5), p. 402. doi: https://doi.org/10.1093/JNEN/NLX025.

Dahlstrand, J., Lardelli, M. and Lendahl, U. (1995) 'Nestin mRNA expression correlates with the central nervous system progenitor cell state in many, but not all, regions of developing central nervous system', *Developmental Brain Research*, 84(1), pp. 109–129. doi: https://doi.org/10.1016/0165-3806(94)00162-S.

Danzer, K.M. *et al.* (2012) 'Exosomal cell-to-cell transmission of alpha synuclein oligomers', *Molecular Neurodegeneration*, 7(1), p. 42. doi: https://doi.org/10.1186/1750-1326-7-42.

Day, J.O. and Mullin, S. (2021) 'The Genetics of Parkinson's Disease and Implications for Clinical Practice', *Genes 2021,* 12(7), p. 1006. doi: https://doi.org/10.3390/GENES12071006.

Dear, A.J. *et al.* (2020) 'Identification of on- and off-pathway oligomers in amyloid fibril formation', *Chemical Science*, 11(24), pp. 6236–6247. doi: https://doi.org/10.1039/C9SC06501F.

Decressac, M. *et al.* (2012) 'Progressive neurodegenerative and behavioural changes induced by AAV-mediated overexpression of α-synuclein in midbrain dopamine neurons', *Neurobiology of disease*, 45(3), pp. 939–953. doi: https://doi.org/10.1016/J.NBD.2011.12.013.

Devi, L. *et al.* (2008) 'Mitochondrial Import and Accumulation of α-Synuclein Impair Complex I in Human Dopaminergic Neuronal Cultures and Parkinson Disease Brain', *The Journal of Biological Chemistry*, 283(14), p. 9089. doi: https://doi.org/10.1074/JBC.M710012200.

Devine, Michael J *et al.* (2011) 'Parkinson's disease induced pluripotent stem cells with triplication of the α -synuclein locus', *Nature Communications*, 23;2;440. doi: https://doi.org/10.1038/ncomms1453.

Dezsi, L. and Vecsei, L. (2017) 'Monoamine Oxidase B Inhibitors in Parkinson's Disease', *CNS & Neurological Disorders - Drug Targets*, 16(4). doi: https://doi.org/10.2174/1871527316666170124165222.

Diagnosing Parkinson's: Medical History & Physical Exam (2017). https://parkinsonsdisease.net/diagnosis/diagnosis-medical-history-physical-exam

Dias, V., Junn, E. and Mouradian, M.M. (2013) 'The Role of Oxidative Stress in Parkinson's Disease', *Journal of Parkinson's disease*, 3(4), p. 461. doi: https://doi.org/10.3233/JPD-130230.

Doherty, K.M. *et al.* (2013) 'Parkin Disease: A Clinicopathologic Entity?', *JAMA Neurology*, 70(5), pp. 571–579. doi: https://doi.org/10.1001/JAMANEUROL.2013.172.

Dorsey, E.R. and Bloem, B.R. (2018) 'The Parkinson Pandemic—A Call to Action', *JAMA Neurology*, 75(1), pp. 9–10. doi: https://doi.org/10.1001/JAMANEUROL.2017.3299.

Drouin-Ouellet, J. *et al.* (2022) 'Age-related pathological impairments in directly reprogrammed dopaminergic neurons derived from patients with idiopathic Parkinson's disease', *Stem Cell Reports*, 17(10), pp. 2203–2219. doi: https://doi.org/10.1016/j.stemcr.2022.08.010.

Duffy, M.F. *et al.* (2018) 'Quality over quantity: Advantages of using alpha-synuclein preformed fibril triggered synucleinopathy to model idiopathic Parkinson's disease', *Frontiers in Neuroscience*, 621(12), p. 402212. doi: https://doi.org/10.3389/FNINS.2018.00621/BIBTEX.

Ebrahimi-Fakhari, D., McLean, P.J. and Unni, V.K. (2012) 'Alpha-synuclein's degradation in vivo: Opening a new (cranial) window on the roles of degradation pathways in Parkinson disease', *Autophagy*, 8(2), p. 281. doi: https://doi.org/10.4161/AUTO.8.2.18938.

Elfarrash, S. *et al.* (2019) 'Organotypic slice culture model demonstrates inter-neuronal spreading of alpha-synuclein aggregates', *Acta Neuropathologica Communications*, 7(1). doi: https://doi.org/10.1186/S40478-019-0865-5.

Emin, D. *et al.* (2022) 'Small soluble α-synuclein aggregates are the toxic species in Parkinson's disease', *Nature Communications 2022 13:1*, 13(1), pp. 1–15. doi: https://doi.org/10.1038/s41467-022-33252-6.

Emmanouilidou, E. *et al.* (2010) 'Cell-Produced α-Synuclein Is Secreted in a Calcium-Dependent Manner by Exosomes and Impacts Neuronal Survival', *The Journal of Neuroscience*, 30(20), p. 6838. doi: https://doi.org/10.1523/JNEUROSCI.5699-09.2010.

Eusebi, P. *et al.* (2017) 'Diagnostic utility of cerebrospinal fluid α-synuclein in Parkinson's disease: A systematic review and meta-analysis', *Movement Disorders*, 32(10), pp. 1389–1400. doi: https://doi.org/10.1002/MDS.27110.

Farrer, M. *et al.* (2001) 'Lewy bodies and parkinsonism in families with parkin mutations', *Annals of Neurology*, 50(3), pp. 293–300. doi: https://doi.org/10.1002/ANA.1132.

Fauvet, B. and Lashuel, H.A. (2015) 'Semisynthesis and Enzymatic Preparation of Post-translationally Modified α-Synuclein', *Methods in Molecular Biology*, 1345, pp. 3–20. doi: https://doi.org/10.1007/978-1-4939-2978-8_1/FIGURES/6.

Fields, C.R., Bengoa-Vergniory, N. and Wade-Martins, R. (2019) 'Targeting Alpha-Synuclein as a Therapy for Parkinson's Disease', *Frontiers in Molecular Neuroscience*, 12, p. 496177. doi: https://doi.org/10.3389/FNMOL.2019.00299/BIBTEX.

Flagmeier, P. *et al.* (2016) 'Mutations associated with familial Parkinson's disease alter the initiation and amplification steps of α-synuclein aggregation', *Proceedings of the National Academy of Sciences of the United States of America*, 113(37), pp. 10328–10333. doi: https://doi.org/10.1073/PNAS.1604645113/-/DCSUPPLEMENTAL.

Flagmeier, P. *et al.* (2017) 'Ultrasensitive Measurement of Ca2+ Influx into Lipid Vesicles Induced by Protein Aggregates', *Angewandte Chemie International Edition*, 56(27), pp. 7750–7754. doi: https://doi.org/10.1002/ANIE.201700966.

Frasier, M., Fiske, B.K. and Sherer, T.B. (2022) 'Precision medicine for Parkinson's disease: The subtyping challenge', *Frontiers in Aging Neuroscience*, 14, p. 1064057. doi: https://doi.org/10.3389/FNAGI.2022.1064057/BIBTEX.

Froula, J.M. *et al.* (2019) 'Defining-synuclein species responsible for Parkinson's disease phenotypes in mice'. *Journal of biology chemistry*, 594(27), pp. 10392-10406. doi: https://doi.org/10.1074/jbc.RA119.007743.

Fusco, G. *et al.* (2017) 'Structural basis of membrane disruption and cellular toxicity by a-synuclein oligomers', *Science*, 358(6369), pp. 1440-1443. doi: https://www.science.org

Gai, W.P. *et al.* (2000) 'In Situ and in Vitro Study of Colocalization and Segregation of α-Synuclein, Ubiquitin, and Lipids in Lewy Bodies', *Experimental Neurology*, 166(2), pp. 324–333. doi: https://doi.org/10.1006/EXNR.2000.7527.

Gallardo, J., Escalona-Noguero, C. and Sot, B. (2020) 'Role of α-Synuclein Regions in Nucleation and Elongation of Amyloid Fiber Assembly', *ACS Chemical Neuroscience*, 11(6), pp. 872–879. doi: https://doi.org/10.1021/ACSCHEMNEURO.9B00527/ASSET/IMAGES/MEDIUM/CN9B00527_M002.GIF.

Galvagnion, C. *et al.* (2015) 'Lipid vesicles trigger α-synuclein aggregation by stimulating primary nucleation', *Nature Chemical Biology 2015 11:3*, 11(3), pp. 229–234. doi: https://doi.org/10.1038/nchembio.1750.

Galvin, J.E., Lee, V.M.Y. and Trojanowski, J.Q. (2001) 'Synucleinopathies: Clinical and Pathological Implications', *Archives of Neurology*, 58(2), pp. 186–190. doi: https://doi.org/10.1001/ARCHNEUR.58.2.186.

Gandhi, K.R. and Saadabadi, A. (2023) 'Levodopa (L-Dopa)', *PNDR: Psychologists' Neuropsychotropic Drug Reference*, pp. 185–189. doi: https://doi.org/10.4324/9781315825748-35.

Ganguly, U. *et al.* (2021) 'Alpha-Synuclein as a Biomarker of Parkinson's Disease: Good, but Not Good Enough', *Frontiers in Aging Neuroscience*, 13, p. 702639. doi: https://doi.org/10.3389/FNAGI.2021.702639/BIBTEX.

Garcia-Reitböck, P. *et al.* (2010) 'SNARE protein redistribution and synaptic failure in a transgenic mouse model of Parkinson's disease', *Brain*, 133(7), p. 2032. doi: https://doi.org/10.1093/BRAIN/AWQ132.

Gaspar, R. *et al.* (2021) 'Secondary nucleation of monomers on fibril surface dominates α-synuclein aggregation and provides autocatalytic amyloid amplification', *Quarterly Reviews of Biophysics*, 50, pp. 1–12. doi: https://doi.org/10.1017/S0033583516000172.

Gatto, N. *et al.* (2021) 'Directly converted astrocytes retain the ageing features of the donor fibroblasts and elucidate the astrocytic contribution to human CNS health and disease', *Aging Cell*, 20(1), p. e13281.doi: https://doi.org/10.1111/ACEL.13281.

Geertsma, H.M. *et al.* (2024) 'A topographical atlas of α-synuclein dosage and cell type-specific expression in adult mouse brain and peripheral organs', *npj Parkinson's Disease 2024 10:1*, 10(1), pp. 1–14. doi: https://doi.org/10.1038/s41531-024-00672-8.

Ghanem, S.S. *et al.* (2022) 'α-Synuclein phosphorylation at serine 129 occurs after initial protein deposition and inhibits seeded fibril formation and toxicity', *Proceedings of the National Academy of Sciences of the United States of America*, 119(15). doi: https://doi.org/10.1073/PNAS.2109617119/-/DCSUPPLEMENTAL.

Ghio, S. *et al.* (2019) 'Cardiolipin Promotes Pore-Forming Activity of Alpha-Synuclein Oligomers in Mitochondrial Membranes', *ACS chemical neuroscience*, 10(8), pp. 3815–3829. doi: https://doi.org/10.1021/ACSCHEMNEURO.9B00320.

Gibb, G. and Lees, A.J. (1988) 'The relevance of the Lewy body to the pathogenesis of idiopathic Parkinson's disease', *Neurosurgery, and Psychiatry*, 51, pp. 745–752. doi: https://doi.org/10.1136/jnnp.51.6.745

Goetz, C.G. *et al.* (2008) 'Movement Disorder Society-Sponsored Revision of the Unified Parkinson's Disease Rating Scale (MDS-UPDRS): Scale presentation and clinimetric testing results', *Movement Disorders*, 23(15), pp. 2129–2170. doi: https://doi.org/10.1002/mds.22340.

Guan, Y. *et al.* (2020) 'Pathogenic Mutations Differentially Regulate Cell-to-Cell Transmission of α-Synuclein', *Frontiers in Cellular Neuroscience*, 14, p. 542430. doi: https://doi.org/10.3389/FNCEL.2020.00159/BIBTEX.

Guo, M. *et al.* (2020) 'Microglial exosomes facilitate α-synuclein transmission in Parkinson's disease', *Brain*, 143(5), p. 1476. doi: https://doi.org/10.1093/BRAIN/AWAA090.

Gustafsson, G. *et al.* (2018) 'Secretion and Uptake of α-Synuclein Via Extracellular Vesicles in Cultured Cells', *Cellular and Molecular Neurobiology*, 38(8), p. 1539. doi: https://doi.org/10.1007/S10571-018-0622-5.

Haehner, A. *et al.* (2009) 'Prevalence of smell loss in Parkinson's disease--a multicenter study', *Parkinsonism & related disorders*, 15(7), pp. 490–494. doi: https://doi.org/10.1016/J.PARKRELDIS.2008.12.005.

Harris, E. (2023) 'Alzheimer Drug Lecanemab Gains Traditional FDA Approval', *JAMA*, 330(6), pp. 495–495. doi: https://doi.org/10.1001/JAMA.2023.12548.

Hattori, N. and Mizuno, Y. (2015) 'Mitochondrial Dysfunction in Parkinson's Disease', *Experimental Neurobiology*, 24(2), p. 103. doi: https://doi.org/10.5607/EN.2015.24.2.103.

Hayashita-Kinoh, H. *et al.* (2006) 'Down-regulation of α-synuclein expression can rescue dopaminergic cells from cell death in the substantia nigra of Parkinson's disease rat model', *Biochemical and Biophysical Research Communications*, 341(4), pp. 1088–1095. doi: https://doi.org/10.1016/J.BBRC.2006.01.057.

Henrich, M.T. *et al.* (2023) 'Mitochondrial dysfunction in Parkinson's disease – a key disease hallmark with therapeutic potential', *Molecular Neurodegeneration 2023 18:1*, 18(1), pp. 1–20. doi: https://doi.org/10.1186/S13024-023-00676-7.

Heras-Garvin, A. *et al.* (2019) 'Anle138b modulates α-synuclein oligomerization and prevents motor decline and neurodegeneration in a mouse model of multiple system atrophy', *Movement disorders : official journal of the Movement Disorder Society*, 34(2), pp. 255–263. doi: https://doi.org/10.1002/MDS.27562.

Hobson, P. and Meara, J. (2004) 'Risk and incidence of dementia in a cohort of older subjects with Parkinson's disease in the United Kingdom', *Movement Disorders*, 19(9), pp. 1043–1049. doi: https://doi.org/10.1002/MDS.20216.

Hobson, P. and Meara, J. (2018) 'Mortality and quality of death certification in a cohort of patients with Parkinson's disease and matched controls in North Wales, UK at 18 years: a community-based cohort study', *BMJ Open*, 8, p. 18969. doi: https://doi.org/10.1136/bmjopen-2017-018969.

Hoerter, J.E. and Ellis, S.R. (2023) 'Biochemistry, Protein Synthesis', *StatPearls* https://www.ncbi.nlm.nih.gov/books/NBK545161/

Holden, S.K. *et al.* (2018) 'Progression of MDS-UPDRS Scores Over Five Years in De Novo Parkinson Disease from the Parkinson's Progression Markers Initiative Cohort', *MOVEMENT DISORDERS CLINICAL PRACTICE*, 5(1), pp. 47–53. doi: https://doi.org/10.1002/mdc3.12553.

Hong, W. *et al.* (2018) 'Diffusible, highly bioactive oligomers represent a critical minority of soluble Aβ in Alzheimer's disease brain', *Acta neuropathologica*, 136(1), p. 19. doi: https://doi.org/10.1007/S00401-018-1846-7.

Hryc, C.F. *et al.* (2023) 'Structural insights into cardiolipin replacement by phosphatidylglycerol in a cardiolipin-lacking yeast respiratory supercomplex', *Nature Communications 2023 14:1*, 14(1), pp. 1–13. doi: https://doi.org/10.1038/s41467-023-38441-5.

Hu, Z.X. *et al.* (2011) 'A study of six point mutation analysis of LRRK2 gene in Chinese mainland patients with Parkinson's disease', *Neurological Sciences*, 32(4), pp. 741–742. doi: https://doi.org/10.1007/S10072-010-0453-8/METRICS.

Iannielli, A. *et al.* (2022) 'Modeling native and seeded Synuclein aggregation and related cellular dysfunctions in dopaminergic neurons derived by a new set of isogenic iPSC lines with SNCA multiplications', *Cell Death & Disease 2022 13:10*, 13(10), pp. 1–16. doi: https://doi.org/10.1038/s41419-022-05330-6.

Ip, C.W. *et al.* (2017) 'AAV1/2-induced overexpression of A53T-α-synuclein in the substantia nigra results in degeneration of the nigrostriatal system with Lewy-like pathology and motor impairment: a new mouse model for Parkinson's disease', *Acta neuropathologica communications*, 5(1), p. 11. doi: https://doi.org/10.1186/S40478-017-0416-X/FIGURES/6.

Jankovic, J. (2008) 'Parkinson's disease: clinical features and diagnosis', *J Neurol Neurosurg Psychiatry*. 79(4), pp. 368-76. doi: https://doi.org/10.1136/jnnp.2007.131045.

Jankovic, J. *et al.* (2018) 'Safety and Tolerability of Multiple Ascending Doses of PRX002/RG7935, an Anti–α-Synuclein Monoclonal Antibody, in Patients With Parkinson Disease: A Randomized Clinical Trial', *JAMA Neurology*, 75(10), p. 1206. doi: https://doi.org/10.1001/JAMANEUROL.2018.1487.

Jao, C.C. *et al.* (2004) 'Structure of membrane-bound α-synuclein studied by site-directed spin labelling', *Proceedings of the National Academy of Sciences of the United States of America*, 101(22), pp. 8331–8336. doi: https://doi.org/10.1073/PNAS.0400553101/SUPPL_FILE/00553FIG8.PDF.

Jiang, H. *et al.* (2012) 'Parkin controls dopamine utilization in human midbrain dopaminergic neurons derived from induced pluripotent stem cells', *Nature Communications*. doi: https://doi.org/10.1038/ncomms1669.

Junn, E. *et al.* (2009) 'Repression of-synuclein expression and toxicity by microRNA-7'. *Proceedings of the National Academy of Sciences of the United States of America,* 106(31), pp. 13052-7. doi: https://doi.org/10.1073/pnas.0906277106

Kalia, L. V. *et al.* (2015) 'Clinical Correlations With Lewy Body Pathology in LRRK2-Related Parkinson Disease', *JAMA Neurology*, 72(1), pp. 100–105. doi: https://doi.org/10.1001/JAMANEUROL.2014.2704.

Karampetsou, M. *et al.* (2017) 'Phosphorylated exogenous alpha-synuclein fibrils exacerbate pathology and induce neuronal dysfunction in mice', *Scientific Reports 2017 7:1*, 7(1), pp. 1–18. doi: https://doi.org/10.1038/s41598-017-15813-8.

Karpowicz, R.J. *et al.* (2017) 'Selective imaging of internalized proteopathic -synuclein seeds in primary neurons reveals mechanistic insight into transmission of synucleinopathies', *Journal of Biological Chemistry*, 292(32), pp. 13482–13497. doi: https://doi.org/10.1074/jbc.M117.780296.

Kawahata, I. and Fukunaga, K. (2020) 'Degradation of Tyrosine Hydroxylase by the Ubiquitin-Proteasome System in the Pathogenesis of Parkinson's Disease and Dopa-Responsive Dystonia', *International Journal of Molecular Sciences*, 21(11). doi: https://doi.org/10.3390/IJMS21113779.

Kay, D.M. *et al.* (2008) 'Genetic association between α-synuclein and idiopathic Parkinson's disease', *American Journal of Medical Genetics, Part B: Neuropsychiatric Genetics*, 147(7), pp. 1222–1230. doi: https://doi.org/10.1002/AJMG.B.30758.

Khandogin, J. and Brooks, C.L. (2007) 'Linking folding with aggregation in Alzheimer's β-amyloid peptides', *Proceedings of the National Academy of Sciences of the United States of America*, 104(43), pp. 16880–16885. doi: https://doi.org/10.1073/PNAS.0703832104/SUPPL_FILE/03832TABLE1.PDF.

Khodr, C.E. *et al.* (2011) 'An alpha-synuclein AAV gene silencing vector ameliorates a behavioral deficit in a rat model of Parkinson's disease, but displays toxicity in dopamine neurons'. doi: https://doi.org/10.1016/j.brainres.2011.04.036.

Khounlo, R. *et al.* (2021) 'Membrane Binding of α-Synuclein Stimulates Expansion of SNARE-Dependent Fusion Pore', *Frontiers in Cell and Developmental Biology*, 9, p. 663431. doi: https://doi.org/10.3389/FCELL.2021.663431/BIBTEX.

Khurana, R. *et al.* (2003) 'A General Model for Amyloid Fibril Assembly Based on Morphological Studies Using Atomic Force Microscopy', *Biophysical Journal*, 85(2), p. 1135. doi: https://doi.org/10.1016/S0006-3495(03)74550-0.

Kim, K.T. (2022) 'Lumbar puncture: considerations, procedure, and complications', *Encephalitis*, 2(4), p. 93. doi: https://doi.org/10.47936/ENCEPHALITIS.2022.00045.

Kim, S. *et al.* (2021) 'Dysregulation of mitochondria-lysosome contacts by GBA1 dysfunction in dopaminergic neuronal models of Parkinson's disease', *Nature Communications 2021 12:1*, 12(1), pp. 1–14. doi: https://doi.org/10.1038/s41467-021-22113-3.

Kirik, D. *et al.* (2002) 'Parkinson-Like Neurodegeneration Induced by Targeted Overexpression of α-Synuclein in the Nigrostriatal System', *The Journal of Neuroscience*, 22(7), p. 2780. doi: https://doi.org/10.1523/JNEUROSCI.22-07-02780.2002.

Kluge, A. *et al.* (2024) 'Detecting Misfolded α-Synuclein in Blood Years before the Diagnosis of Parkinson's Disease', *Movement Disorders* [Preprint]. doi: https://doi.org/10.1002/MDS.29766.

Kobayashi, S. *et al.* (2015) 'Dependence pH and proposed mechanism for aggregation of Alzheimer's disease-related amyloid-b(1-42) protein', *Journal of Molecular Structure*, 1094, pp. 109–117. doi: https://doi.org/10.1016/j.molstruc.2015.03.023.

Koller, W.C. (2018) 'Table 1, The clinical diagnostic criteria for Parkinson's disease, based on the Movement Disorder Society guidelines', *Neurology*, 43(2), pp. S1-11. doi: https://doi.org/10.15586/CODONPUBLICATIONS.PARKINSONSDISEASE.2018.CH6.

Krüger, R. *et al.* (1998) 'Ala30Pro mutation in the gene encoding alpha-synuclein in Parkinson's disease', *Nature genetics*, 18(2), pp. 106–108. doi: https://doi.org/10.1038/NG0298-106.

Krzystek, T.J. *et al.* (2021) 'Differential mitochondrial roles for α-synuclein in DRP1-dependent fission and PINK1/Parkin-mediated oxidation', *Cell Death & Disease 2021 12:9*, 12(9), pp. 1–16. doi: https://doi.org/10.1038/s41419-021-04046-3.

Kuang, Y. *et al.* (2024) 'A skin-specific α-Synuclein seeding amplification assay for diagnosing Parkinson's disease', *npj Parkinson's Disease 2024 10:1*, 10(1), pp. 1–12. doi: https://doi.org/10.1038/s41531-024-00738-7.

Kumar, S.T. *et al.* (2020) 'How specific are the conformation-specific α-synuclein antibodies? Characterization and validation of 16 α-synuclein conformation-specific antibodies using well-characterized preparations of α-synuclein monomers, fibrils and oligomers with distinct structures and morphology', *Neurobiology of Disease*, 146, p. 105086. doi: https://doi.org/10.1016/J.NBD.2020.105086.

Kumfor, F., Halliday, G.M. and Piguet, O. (2017) 'Clinical Aspects of Alzheimer's Disease', *Advances in Neurobiology*, 15, pp. 31–53. doi: https://doi.org/10.1007/978-3-319-57193-5_2.

Kuusisto, E., Parkkinen, L. and Alafuzoff, I. (2003) 'Morphogenesis of Lewy Bodies: Dissimilar Incorporation of-Synuclein, Ubiquitin, and p62', *Journal of Neuropathology and Experimental Neurology*, 62(12). doi: https://academic.oup.com/jnen/article/62/12/1241/2610054

Lang, A.E. *et al.* (2022) 'Trial of Cinpanemab in Early Parkinson's Disease', *New England Journal of Medicine*, 387(5), pp. 408–420. doi: https://doi.org/10.1056/NEJMOA2203395/SUPPL_FILE/NEJMOA2203395_DATA-SHARING.PDF.

Lansbury, P.T. and Lashuel, H.A. (2006) 'A century-old debate on protein aggregation and neurodegeneration enters the clinic', *Nature*, 443(7113), pp. 774–779. doi: https://doi.org/10.1038/NATURE05290.

Lapasset, L. *et al.* (2011) 'Rejuvenating senescent and centenarian human cells by reprogramming through the pluripotent state', *Genes & Development*, 25(21), pp. 2248–2253. doi: https://doi.org/10.1101/GAD.173922.111.

Lee, H.-J. *et al.* (2008) 'Assembly-dependent endocytosis and clearance of extracellular-synuclein', *The International Journal of Biochemistry & Cell Biology*, 40, pp. 1835–1849. doi: https://doi.org/10.1016/j.biocel.2008.01.017.

Lee, H.J., Patel, S. and Lee, S.J. (2005) 'Intravesicular Localization and Exocytosis of α-Synuclein and its Aggregates', *Journal of Neuroscience*, 25(25), pp. 6016–6024. doi: https://doi.org/10.1523/JNEUROSCI.0692-05.2005.

Lee, J.G. *et al.* (2016) 'Unconventional secretion of misfolded proteins promotes adaptation to proteasome dysfunction in mammalian cells', *Nature cell biology*, 18(7), p. 765. doi: https://doi.org/10.1038/NCB3372.

Lee, M.K. *et al.* (2002) 'Human α-synuclein-harboring familial Parkinson's disease-linked Ala-53 → Thr mutation causes neurodegenerative disease with α-synuclein aggregation in transgenic mice', *Proceedings of the National Academy of Sciences of the United States of America*, 99(13), pp. 8968–8973. doi: https://doi.org/10.1073/PNAS.132197599/SUPPL_FILE/1975SUPPORTINGMETHODS.HTML.

Lesage, S. *et al.* (2006) 'LRRK2 G2019S as a Cause of Parkinson's Disease in North African Arabs ', *New England Journal of Medicine*, 354(4), pp. 422–423. doi: https://doi.org/10.1056/NEJMC055540/SUPPL_FILE/NEJM_LESAGE_422SA1.PDF.

Lesage, S. *et al.* (2013) 'G51D α-synuclein mutation causes a novel parkinsonian-pyramidal syndrome', *Annals of neurology*, 73(4), pp. 459–471. doi: https://doi.org/10.1002/ANA.23894.

Lesage, S. *et al.* (2020) 'Genetic and Phenotypic Basis of Autosomal Dominant Parkinson's Disease in a Large Multi-Center Cohort', *Frontiers in Neurology*, 11, p. 682. doi: https://doi.org/10.3389/FNEUR.2020.00682/FULL.

Levin, J. *et al.* (2022) 'Safety, tolerability and pharmacokinetics of the oligomer modulator anle138b with exposure levels sufficient for therapeutic efficacy in a murine Parkinson model: A randomised,

double-blind, placebo-controlled phase 1a trial', *EBioMedicine*, 80. doi: https://doi.org/10.1016/J.EBIOM.2022.104021.

Lin, L. *et al.* (2016) 'Molecular Features Underlying Neurodegeneration Identified through In Vitro Modeling of Genetically Diverse Parkinson's Disease Patients', *Cell Reports*, 15(11), pp. 2411–2426. doi: https://doi.org/10.1016/j.celrep.2016.05.022.

Lin, M.T. and Beal, M.F. (2006) 'Mitochondrial dysfunction and oxidative stress in neurodegenerative diseases', *Nature 2006 443:7113*, 443(7113), pp. 787–795. doi: https://doi.org/10.1038/nature05292.

Lindsay, R.J. *et al.* (2021) 'Effects of pH on an IDP conformational Ensemble Explored by Molecular Dynamics Simulation', *Biophysical chemistry*, 271, p. 106552. doi: https://doi.org/10.1016/J.BPC.2021.106552.

Ludtmann, M.H.R. *et al.* (2018) 'α-synuclein oligomers interact with ATP synthase and open the permeability transition pore in Parkinson's disease', *Nature Communications*, 9(1). doi: https://doi.org/10.1038/S41467-018-04422-2.

Luk, K.C. *et al.* (2009) 'Exogenous α-synuclein fibrils seed the formation of Lewy body-like intracellular inclusions in cultured cells', *Proceedings of the National Academy of Sciences of the United States of America*, 106(47), pp. 20051–20056. doi: https://doi.org/10.1073/PNAS.0908005106/SUPPL_FILE/0908005106SI.PDF.

Luk, K.C., Kehm, V.M., *et al.* (2012) 'Intracerebral inoculation of pathological α-synuclein initiates a rapidly progressive neurodegenerative α-synucleinopathy in mice', *The Journal of Experimental Medicine*, 209(5), p. 975. doi: https://doi.org/10.1084/JEM.20112457.

Luk, K.C., Kehm, V., *et al.* (2012) 'Pathological α-synuclein transmission initiates Parkinson-like neurodegeneration in nontransgenic mice', *Science*, 338(6109), pp. 949–953. doi: https://doi.org/10.1126/SCIENCE.1227157/SUPPL_FILE/LUK.SM.PDF.

Luth, E.S. *et al.* (2014) 'Soluble, Prefibrillar α-Synuclein Oligomers Promote Complex I-dependent, Ca2+-induced Mitochondrial Dysfunction', *The Journal of Biological Chemistry*, 289(31), p. 21490. doi: https://doi.org/10.1074/JBC.M113.545749.

Ma, M.R. *et al.* (2016) 'Phosphorylation induces distinct alpha-synuclein strain formation', *Scientific Reports 2016 6:1*, 6(1), pp. 1–11. doi: https://doi.org/10.1038/srep37130.

Madsen, D.A. *et al.* (2021) 'Interaction between Parkin and α-Synuclein in PARK2-Mediated Parkinson's Disease', *Cells*, 10(2), pp. 1–30. doi: https://doi.org/10.3390/CELLS10020283.

Mahul-Mellier, A.L. *et al.* (2020) 'The process of Lewy body formation, rather than simply α-synuclein fibrillization, is one of the major drivers of neurodegeneration', *Proceedings of the National Academy of Sciences of the United States of America*, 117(9), pp. 4971–4982. doi: https://doi.org/10.1073/PNAS.1913904117/SUPPL_FILE/PNAS.1913904117.SD04.XLSX.

Di Maio, R. *et al.* (2016) 'α-Synuclein binds TOM20 and inhibits mitochondrial protein import in Parkinson's disease', *Science translational medicine*, 8(342), p. 342ra78. doi: https://doi.org/10.1126/SCITRANSLMED.AAF3634.

Manchanda, S. *et al.* (2023) 'Intravenous treatment with a molecular chaperone designed against beta-amyloid toxicity improves Alzheimer's disease pathology in mouse models'. doi: https://doi.org/10.1016/j.ymthe.2022.08.010.

Maraganore, D.M. *et al.* (2006) 'Collaborative Analysis of α-Synuclein Gene Promoter Variability and Parkinson Disease', *JAMA*, 296(6), pp. 661–670. doi: https://doi.org/10.1001/JAMA.296.6.661.

Maroteaux, L., Campanelli, J.T. and Scheller, R.H. (1988) 'Synuclein: A Neuron-Specific Protein Localized to the Nucleus and Presynaptic Nerve Terminal', *The Journal of Neuroscience*, 8(8), pp. 2804–2815. doi: https://doi.org/ 10.1523/JNEUROSCI.08-08-02804.1988

Maroteaux, L. and Scheller, R.H. (1991) 'The rat brain synucleins; family of proteins transiently associated with neuronal membrane', *Molecular Brain Research*, 11(3–4), pp. 335–343. doi: https://doi.org/10.1016/0169-328X(91)90043-W.

Marrone, L. *et al.* (2018) 'Generation of iPSCs carrying a common LRRK2 risk allele for in vitro modeling of idiopathic Parkinson's disease'. *Proceedings of the National Academy of Sciences of the United States of America*, 13(3), doi: https://doi.org/10.1371/journal.pone.0192497.

Masliah, E. *et al.* (2011) 'Passive Immunization Reduces Behavioral and Neuropathological Deficits in an Alpha-Synuclein Transgenic Model of Lewy Body Disease', *PLOS ONE*, 6(4), p. e19338. doi: https://doi.org/10.1371/JOURNAL.PONE.0019338.

Massano, J. and Bhatia, K.P. (2012) 'Clinical Approach to Parkinson's Disease: Features, Diagnosis, and Principles of Management', *Cold Spring Harbor Perspectives in Medicine*, 2(6). doi: https://doi.org/10.1101/CSHPERSPECT.A008870.

Mbefo, M.K. *et al.* (2010) 'Phosphorylation of Synucleins by Members of the Polo-like Kinase Family ', *Journal of Biological Chemistry*, 285, pp. 2807–2822. doi: https://doi.org/10.1074/jbc.M109.081950.

McFarthing, K. *et al.* (2022) 'Parkinson's Disease Drug Therapies in the Clinical Trial Pipeline: 2022 Update', *Journal of Parkinson's Disease*, 12(4), p. 1073. doi: https://doi.org/10.3233/JPD-229002.

Meder, D. *et al.* (2019) 'The role of dopamine in the brain - lessons learned from Parkinson's disease', *NeuroImage*, 190, pp. 79–93. doi: https://doi.org/10.1016/J.NEUROIMAGE.2018.11.021.

Menon, S. *et al.* (2021) 'Viral alpha-synuclein knockdown prevents spreading synucleinopathy', *Brain,* 3(4).doi: https://doi.org/10.1093/braincomms/fcab247.

Meyer, K. *et al.* (2014) 'Direct conversion of patient fibroblasts demonstrates non-cell autonomous toxicity of astrocytes to motor neurons in familial and sporadic ALS', *Proceedings of the National Academy of Sciences of the United States of America*, 111(2), pp. 829–832. doi: https://doi.org/10.1073/PNAS.1314085111.

Mezey, E. *et al.* (1998) 'Alpha synuclein is present in Lewy bodies in sporadic Parkinson's disease', *Molecular Psychiatry 1998 3:6*, 3(6), pp. 493–499. doi: https://doi.org/10.1038/sj.mp.4000446.

Michaels, T.C.T. *et al.* (2020) 'Dynamics of oligomer populations formed during the aggregation of Alzheimer's Aβ42 peptide', *Nature Chemistry 2020 12:5*, 12(5), pp. 445–451. doi: https://doi.org/10.1038/s41557-020-0452-1.

Michaels, T.C.T. *et al.* (2023) 'Amyloid formation as a protein phase transition', *Nature Reviews Physics 2023 5:7*, 5(7), pp. 379–397. doi: https://doi.org/10.1038/s42254-023-00598-9.

Miller, D.W. *et al.* (2004) 'α-synuclein in blood and brain from familial Parkinson disease with SNCA locus triplication', *Neurology*, 62(10), pp. 1835–1838. doi: https://doi.org/10.1212/01.WNL.0000127517.33208.F4.

Mohamed, N.-V. *et al.* (2021) 'Midbrain organoids with an SNCA gene triplication model key features of synucleinopathy', *Brain communications*, 25;3(4). doi: https://doi.org/10.1093/braincomms/fcab223.

Mollenhauer, B. *et al.* (2012) 'α-Synuclein in human cerebrospinal fluid is principally derived from neurons of the central nervous system', *Journal of Neural Transmission*, 119(7), pp. 739–746. doi: https://doi.org/10.1007/S00702-012-0784-0/FIGURES/3.

Muntau, A.C. *et al.* (2014) 'Innovative strategies to treat protein misfolding in inborn errors of metabolism: Pharmacological chaperones and proteostasis regulators', *Journal of Inherited Metabolic Disease*, 37(4), pp. 505–523. doi: https://doi.org/10.1007/S10545-014-9701-Z.

Musteikytė, G. *et al.* (2021) 'Interactions of α-synuclein oligomers with lipid membranes', *Biochimica et Biophysica Acta (BBA) - Biomembranes*, 1863(4), p. 183536. doi: https://doi.org/10.1016/J.BBAMEM.2020.183536.

Nakamura, K., Nemani, Venu M., *et al.* (2011) 'Direct membrane association drives mitochondrial fission by the Parkinson disease-associated protein α-synuclein', *Journal of Biological Chemistry*, 286(23), pp. 20710–20726. doi: https://doi.org/10.1074/JBC.M110.213538/ATTACHMENT/07CA9743-609D-40C9-BFCA-1AFA7B2CB0C0/MMC1.ZIP.

Nakamura, K., Nemani, Venu M, *et al.* (2011) 'Direct Membrane Association Drives Mitochondrial Fission by the Parkinson Disease-associated protein alpha-synuclein'. Journal of biological chemistry, 10;286(23), pp. 20710-26. doi: https://doi.org/10.1074/jbc.M110.213538.

Narkiewicz, J., Giachin, G. and Legname, G. (2014) 'In vitro aggregation assays for the characterization of α-synuclein prion-like properties', *Prion*, 8(1), p. 19. doi: https://doi.org/10.4161/PRI.28125.

Natalwala, A. *et al.* (2022) 'An Isogenic Collection of Pluripotent Stem Cell Lines With Elevated α-Synuclein Expression Validated for Neural Induction and Cortical Neuron Differentiation', *Frontiers in*

Cell and Developmental Biology, 10, p. 898560. doi: https://doi.org/10.3389/FCELL.2022.898560/BIBTEX.

Nemani, V.M. *et al.* (2010) 'Increased Expression of Alpha-Synuclein Reduces Neurotransmitter Release by Inhibiting Synaptic Vesicle Reclustering After Endocytosis', *Neuron*, 65(1), p. 66. doi: https://doi.org/10.1016/J.NEURON.2009.12.023.

Nikolcheva, T. *et al.* (2023) 'A study to evaluate the efficacy and safety of intravenous prasinezumab in participants with early Parkinson's disease (PADOVA): Rationale, design, and baseline data'. *Roche.*

O'Hara, D.M. *et al.* (2020) 'LRRK2 and α-Synuclein: Distinct or Synergistic Players in Parkinson's Disease?', *Frontiers in Neuroscience*, 14, p. 541220. doi: https://doi.org/10.3389/FNINS.2020.00577/BIBTEX.

Olgiati, S. *et al.* (2015) 'Early-onset parkinsonism caused by alpha-synuclein gene triplication: Clinical and genetic findings in a novel family', *Parkinsonism & Related Disorders*, 21(8), pp. 981–986. doi: https://doi.org/10.1016/J.PARKRELDIS.2015.06.005.

Oliveira, L. *et al.* (2015) 'Elevated alpha-synuclein caused by SNCA gene triplication impairs neuronal differentiation and maturation in Parkinson's patient-derived induced pluripotent stem cells', *Cell Death and Disease*, 6. doi: https://doi.org/10.1038/cddis.2015.318.

Ou, Z. *et al.* (2021) 'Global Trends in the Incidence, Prevalence, and Years Lived With Disability of Parkinson's Disease in 204 Countries/Territories From 1990 to 2019', *Frontiers in Public Health*, 9, p. 776847. doi: https://doi.org/10.3389/FPUBH.2021.776847/FULL.

Pagano, G. *et al.* (2022) 'Trial of Prasinezumab in Early-Stage Parkinson's Disease', *The New England journal of medicine*, 387(5), pp. 421–432. doi: https://doi.org/10.1056/NEJMOA2202867.

Pagano, G. *et al.* (2024) 'Prasinezumab slows motor progression in rapidly progressing early-stage Parkinson's disease', *Nature medicine*, 30(4), pp. 1096–1103. doi: https://doi.org/10.1038/S41591-024-02886-Y.

Palakurthi, B. and Preetham Burugupally, S. (2019) 'brain sciences Review Postural Instability in Parkinson's Disease: A Review'. doi: https://doi.org/10.3390/brainsci9090239.

.

Parra-Rivas, Leonardo A. *et al.* (2023) 'Serine-129 phosphorylation of α-synuclein is an activity-dependent trigger for physiologic protein-protein interactions and synaptic function', *Neuron*, 111(24), pp. 4006-4023.e10. doi: https://doi.org/10.1016/J.NEURON.2023.11.020.

Parres-Gold, J. *et al.* (2020) 'Real-time Characterization of Cell Membrane Disruption by α-Synuclein Oligomers in Live SH-SY5Y Neuroblastoma Cells', *ACS chemical neuroscience*, 11(17), p. 2528. doi: https://doi.org/10.1021/ACSCHEMNEURO.0C00309.

Payne, T. *et al.* (2024) 'Multimodal assessment of mitochondrial function in Parkinson's disease', *Brain*, 147(1), p. 267. doi: https://doi.org/10.1093/BRAIN/AWAD364.

Perez, R.G. *et al.* (2002) 'A Role for-Synuclein in the Regulation of Dopamine Biosynthesis'. *Journal of neuroscience,* 15;22(8), pp. 3090-9. doi: https://doi.org/ DOI: 10.1523/JNEUROSCI.22-08-03090.2002

Pérez-López, F.R. *et al.* (2009) 'Effects of the Mediterranean diet on longevity and age-related morbid conditions', *Maturitas*, 64(2), pp. 67–79. doi: https://doi.org/10.1016/J.MATURITAS.2009.07.013.

Periquet, M. *et al.* (2003) 'Parkin mutations are frequent in patients with isolated early-onset parkinsonism', *Brain*, 126(6), pp. 1271–1278. doi: https://doi.org/10.1093/BRAIN/AWG136.

Pfisterer, U. *et al.* (2011) 'Direct conversion of human fibroblasts to dopaminergic neurons', *Proceedings of the National Academy of Sciences of the United States of America*, 108(25), pp. 10343–10348. doi: https://doi.org/10.1073/PNAS.1105135108/SUPPL_FILE/PNAS.201105135SI.PDF.

Pickrell, A.M. and Youle, R.J. (2015) 'The Roles of PINK1, Parkin and Mitochondrial Fidelity in Parkinson's Disease', *Neuron*, 85(2), p. 257. doi: https://doi.org/10.1016/J.NEURON.2014.12.007.

Polinski, N.K. (2021) 'A Summary of Phenotypes Observed in the In Vivo Rodent Alpha-Synuclein Preformed Fibril Model', *Journal of Parkinson's Disease*, 11(4), p. 1555. doi: https://doi.org/10.3233/JPD-212847.

Polymeropoulos, M.H. *et al.* (1997) 'Mutation in the α-synuclein gene identified in families with Parkinson's disease', *Science*, 276(5321), pp. 2045–2047. doi: https://doi.org/10.1126/SCIENCE.276.5321.2045/ASSET/B8D7EAD8-394A-404C-83B7-CADE1B02415A/ASSETS/GRAPHIC/SE2775400004.JPEG.

Qu, J. *et al.* (2020) 'Specific Knockdown of α-Synuclein by Peptide-Directed Proteasome Degradation Rescued Its Associated Neurotoxicity', *Cell Chemical Biology*, 27(6), pp. 751-762.e4. doi: https://doi.org/10.1016/J.CHEMBIOL.2020.03.010.

Ramalingam, N. *et al.* (2023) 'Dynamic physiological α-synuclein S129 phosphorylation is driven by neuronal activity', *npj Parkinson's Disease 2023 9:1*, 9(1), pp. 1–15. doi: https://doi.org/10.1038/s41531-023-00444-w.

Reinhardt, P. *et al.* (2013) 'Genetic Correction of a LRRK2 Mutation in Human iPSCs Links Parkinsonian Neurodegeneration to ERK-Dependent Changes in Gene Expression', *Cell Stem Cell*, 12(3), pp. 354–367. doi: https://doi.org/10.1016/J.STEM.2013.01.008.

Risiglione, P. *et al.* (2021) 'Alpha-Synuclein and Mitochondrial Dysfunction in Parkinson's Disease: The Emerging Role of VDAC', *Biomolecules,* 11(5), p.718. doi: https://doi.org/10.3390/biom11050718.

Rodrigues, M. *et al.* (2022) 'Structure-specific amyloid precipitation in biofluids', *Nature Chemistry 2022 14:9*, 14(9), pp. 1045–1053. doi: https://doi.org/10.1038/s41557-022-00976-3.

Ross, C.A. and Poirier, M.A. (2004) 'Protein aggregation and neurodegenerative disease', *Nature Medicine 2004 10:7*, 10(7), pp. S10–S17. doi: https://doi.org/10.1038/nm1066.

Rossi, P. *et al.* (2000) 'Acute challenge with apomorphine and levodopa in Parkinsonism', *European neurology*, 43(2), pp. 95–101. doi: https://doi.org/10.1159/000008142.

Rusilowicz-Jones, E. V. *et al.* (2021) 'Benchmarking a highly selective USP30 inhibitor for enhancement of mitophagy and pexophagy', *Life science alliance*, 5(2). doi: https://doi.org/10.26508/LSA.202101287.

Salles, P., Tirapegui, J.M. and Chaná-Cuevas, P. (2024) 'Genetics of Parkinson's disease: Dominant forms and GBA', *Neurology perspectives*, 4(3). doi: https://doi.org/10.1016/J.NEUROP.2024.100153.

Sampson, T.R. *et al.* (2016) 'Gut Microbiota Regulate Motor Deficits and Neuroinflammation in a Model of Parkinson's Disease', *Cell*, 167(6), p. 1469. doi: https://doi.org/10.1016/J.CELL.2016.11.018.

Sánchez-Danés, A. *et al.* (2012) 'Disease-specific phenotypes in dopamine neurons from human iPS-based models of genetic and sporadic Parkinson's disease', *EMBO Mol Med*, 5, p. 11. doi: https://doi.org/10.1002/emmm.201200215.

Sanderson, J.B. *et al.* (2020) 'Analysis of α-synuclein species enriched from cerebral cortex of humans with sporadic dementia with Lewy bodies', *Brain Communications*, 2(1). doi: https://doi.org/10.1093/BRAINCOMMS/FCAA010.

Sapru, M.K. *et al.* (2006) 'Silencing of human α-synuclein in vitro and in rat brain using lentiviral-mediated RNAi', *Experimental Neurology*, 198(2), pp. 382–390. doi: https://doi.org/10.1016/J.EXPNEUROL.2005.12.024.

Satake, W. *et al.* (2009) 'Genome-wide association study identifies common variants at four loci as genetic risk factors for Parkinson's disease', *Nature GeNetics*, 41. doi: https://doi.org/10.1038/ng.485.

Schade, S. *et al.* (2017) 'Acute Levodopa Challenge Test in Patients with de novo Parkinson's Disease: Data from the DeNoPa Cohort', *Movement Disorders Clinical Practice*, 4(5), pp. 755–762. doi: https://doi.org/10.1002/MDC3.12511.

Schenck, C.H., Bundlie, S.R. and Mahowald, M.W. (1996) 'Delayed emergence of a parkinsonian disorder in 38% of 29 older men initially diagnosed with idiopathic rapid eye movement sleep behaviour disorder', *Neurology*, 46(2), pp. 388–393. doi: https://doi.org/10.1212/WNL.46.2.388.

Schreurs, S. *et al.* (2014) 'In vitro phosphorylation does not influence the aggregation kinetics of WT α-synuclein in contrast to its phosphorylation mutants', *International journal of molecular sciences*, 15(1), pp. 1040–1067. doi: https://doi.org/10.3390/IJMS15011040.

Schwartzentruber, A. *et al.* (2020) 'Oxidative switch drives mitophagy defects in dopaminergic parkin mutant patient neurons', *Scientific reports*, 10(1). doit: https://doi.org/10.1038/S41598-020-72345-4.

Shahmoradian, S.H. *et al.* (2019) 'Lewy pathology in Parkinson's disease consists of crowded organelles and lipid membranes', *Nature neuroscience*, 22(7), pp. 1099–1109. doi: https://doi.org/10.1038/S41593-019-0423-2.

Shahnawaz, M. *et al.* (2017) 'Development of a Biochemical Diagnosis of Parkinson Disease by Detection of α-Synuclein Misfolded Aggregates in Cerebrospinal Fluid', *JAMA neurology*, 74(2), pp. 163–172. doi: https://doi.org/10.1001/JAMANEUROL.2016.4547.

Shahnawaz, M. *et al.* (2020) 'Discriminating α-synuclein strains in Parkinson's disease and multiple system atrophy', *Nature 2020 578:7794*, 578(7794), pp. 273–277. doi: https://doi.org/10.1038/s41586-020-1984-7.

Shi, S. *et al.* (2013) 'Establishing quantitative real-time quaking-induced conversion (qRT-QuIC) for highly sensitive detection and quantification of PrPSc in prion-infected tissues', *Acta neuropathologica communications*, 1(1). doi: https://doi.org/10.1186/2051-5960-1-44.

Shrigley, S. *et al.* (2018) 'Simple Generation of a High Yield Culture of Induced Neurons from Human Adult Skin Fibroblasts', *JoVE (Journal of Visualized Experiments)*, 2018(132), p. e56904. doi: https://doi.org/10.3791/56904.

Siderowf, A. *et al.* (2023) 'Assessment of heterogeneity among participants in the Parkinson's Progression Markers Initiative cohort using α-synuclein seed amplification: a cross-sectional study', *The Lancet Neurology*, 22(5), pp. 407–417. doi: https://doi.org/10.1016/S1474-4422(23)00109-6.

Singh Dolt, K., Hammachi, F. and Kunath, T. (2017) 'Modeling Parkinson's disease with induced pluripotent stem cells harboring α-synuclein mutations', *Brain Pathology*, 27(4), p. 545. doi: https://doi.org/10.1111/BPA.12526.

Singleton, A.B. *et al.* (2003) 'Synuclein Locus Triplication Causes Parkinson's Disease'. *Science,* 31;203(5646), p. 841. doi: https://doi.org/ 10.1126/science.1090278

Smith, W.W. *et al.* (2005) 'Alpha-synuclein phosphorylation enhances eosinophilic cytoplasmic inclusion formation in SH-SY5Y cells', *The Journal of neuroscience : the official journal of the Society for Neuroscience*, 25(23), pp. 5544–5552. doi: https://doi.org/10.1523/JNEUROSCI.0482-05.2005.

Soldner, F. *et al.* (2011) 'Generation of isogenic pluripotent stem cells differing exclusively at two early onset parkinson point mutations', *Cell*, 146(2), pp. 318–331. doi: https://doi.org/10.1016/j.cell.2011.06.019.

Spillantini, M.G. *et al.* (1997) 'α-Synuclein in Lewy bodies', *Nature 1997 388:6645*, 388(6645), pp. 839–840. doi: https://doi.org/10.1038/42166.

St Martin, J.L. *et al.* (2007) 'Dopaminergic neuron loss and up-regulation of chaperone protein mRNA induced by targeted over-expression of alpha-synuclein in mouse substantia nigra', *Journal of neurochemistry*, 100(6), pp. 1449–1457. doi: https://doi.org/10.1111/J.1471-4159.2006.04310.X.

Stefanis, L. (2012) 'α-Synuclein in Parkinson's Disease', *Cold Spring Harbor Perspectives in Medicine*, 2(2). doi: https://doi.org/10.1101/CSHPERSPECT.A009399.

Steiner, J.A., Angot, E. and Brundin, P. (2011) 'A deadly spread: cellular mechanisms of α-synuclein transfer', *Cell Death and Differentiation*, 18(9), p. 1425. doi: https://doi.org/10.1038/CDD.2011.53.

Stephens, A.D., Zacharopoulou, M. and Kaminski Schierle, G.S. (2019) 'The Cellular Environment Affects Monomeric α-Synuclein Structure', *Trends in Biochemical Sciences*, 44(5), pp. 453–466. doi: https://doi.org/10.1016/J.TIBS.2018.11.005.

Stewart, T. *et al.* (2015) 'Phosphorylated α-synuclein in Parkinson's disease: correlation depends on disease severity', *Acta neuropathologica communications*, 3(1), p. 7. doi: https://doi.org/10.1186/S40478-015-0185-3/FIGURES/3.

Strodel, B. (2021) 'Energy Landscapes of Protein Aggregation and Conformation Switching in Intrinsically Disordered Proteins', *Journal of molecular biology*, 433(20). doi: https://doi.org/10.1016/J.JMB.2021.167182.

Stuendl, A. *et al.* (2016) 'Induction of α-synuclein aggregate formation by CSF exosomes from patients with Parkinson's disease and dementia with Lewy bodies', *Brain*, 139(2), pp. 481–494. doi: https://doi.org/10.1093/BRAIN/AWV346.

Suhr, S.T. *et al.* (2010) 'Mitochondrial Rejuvenation After Induced Pluripotency', *PLOS ONE*, 23;5(11). doi: https://doi.org/10.1371/journal.pone.0014095.

Sui, X. *et al.* (2019) 'Hyposmia as a Predictive Marker of Parkinson's Disease: A Systematic Review and Meta-Analysis', *BioMed Research International*, 2019. doi: https://doi.org/10.1155/2019/3753786.

Taguchi, K. *et al.* (2016) 'Brain region-dependent differential expression of alpha-synuclein', *The Journal of comparative neurology*, 524(6), pp. 1236–1258. doi: https://doi.org/10.1002/CNE.23901.

Taguchi, K. *et al.* (2019) 'Expression of α-synuclein is regulated in a neuronal cell type-dependent manner', *Anatomical Science International*, 94(1), p. 11. doi: https://doi.org/10.1007/S12565-018-0464-8.

Takahashi, H. *et al.* (1994) 'Familial juvenile parkinsonism: clinical and pathologic study in a family', *Neurology*, 44(3 Pt 1), pp. 437–441. doi: https://doi.org/10.1212/WNL.44.3_PART_1.437.

Takahashi, K. *et al.* (2007) 'Induction of Pluripotent Stem Cells from Adult Human Fibroblasts by Defined Factors', *Cell*, 30;131(5), pp. 861-72. doi: https://doi.org/10.1016/j.cell.2007.11.019

Takahashi, K. and Yamanaka, S. (2006) 'Induction of Pluripotent Stem Cells from Mouse Embryonic and Adult Fibroblast Cultures by Defined Factors', *Cell*, 126(4), pp. 663–676. doi: https://doi.org/10.1016/j.cell.2006.07.024.

Takahashi, M. *et al.* (2015) 'Normalization of Overexpressed Î±-Synuclein Causing Parkinson's Disease By a Moderate Gene Silencing With RNA Interference', *Molecular Therapy*, 4, p. e241. doi: https://doi.org/10.1038/mtna.2015.14.

Tan, Y.Y., Jenner, P. and Chen, S. Di (2022) 'Monoamine Oxidase-B Inhibitors for the Treatment of Parkinson's Disease: Past, Present, and Future', *Journal of Parkinson's Disease*, 12(2), p. 477. doi: https://doi.org/10.3233/JPD-212976.

Tanudjojo, B. *et al.* (2021) 'Phenotypic manifestation of α-synuclein strains derived from Parkinson's disease and multiple system atrophy in human dopaminergic neurons', *Nature Communications 2021 12:1*, 12(1), pp. 1–16. doi: https://doi.org/10.1038/s41467-021-23682-z.

Tenreiro, S. *et al.* (2014) 'Phosphorylation Modulates Clearance of Alpha-Synuclein Inclusions in a Yeast Model of Parkinson's Disease', *PLoS Genetics*, 10(5). doi: https://doi.org/10.1371/JOURNAL.PGEN.1004302.

Terroba Chambi, C. *et al.* (2017) 'Diagnostic Value of Combined Acute Levodopa Challenge and Olfactory Testing to Predict Parkinson's Disease', *Movement Disorders Clinical Practice*, 4(6), pp. 824–828. doi: https://doi.org/10.1002/MDC3.12517.

Theodore, S. *et al.* (2008) 'Targeted overexpression of human alpha-synuclein triggers microglial activation and an adaptive immune response in a mouse model of Parkinson disease', *Journal of neuropathology and experimental neurology*, 67(12), pp. 1149–1158. doi: https://doi.org/10.1097/NEN.0B013E31818E5E99.

Tian, C. *et al.* (2013) 'Characterization of Induced Neural Progenitors from Skin Fibroblasts by a Novel Combination of Defined Factors', *Scientific Reports 2013 3:1*, 3(1), pp. 1–7. doi: https://doi.org/10.1038/srep01345.

Tö, M. *et al.* (2018) 'Secondary nucleation in amyloid formation', *Chem. Commun*, 54, p. 8667. doi: https://doi.org/10.1039/c8cc02204f.

Uversky, V.N. (2015) 'Intrinsically disordered proteins and their (disordered) proteomes in neurodegenerative disorders', *Frontiers in Aging Neuroscience*, 7(MAR), p. 132731. doi: https://doi.org/10.3389/FNAGI.2015.00018/BIBTEX.

Valente, E.M. *et al.* (2004) 'Hereditary early-onset Parkinson's disease caused by mutations in PINK1', *Science (New York, N.Y.)*, 304(5674), pp. 1158–1160. doi: https://doi.org/10.1126/SCIENCE.1096284.

Varela, J.A. *et al.* (2018) 'Optical Structural Analysis of Individual α-Synuclein Oligomers', *Angewandte Chemie*, 130(18), pp. 4980–4984. doi: https://doi.org/10.1002/ANGE.201710779.

Verma, M., Vats, A. and Taneja, V. (2015) 'Toxic species in amyloid disorders: Oligomers or mature fibrils', *Annals of Indian Academy of Neurology*, 18(2), p. 138. doi: https://doi.org/10.4103/0972-2327.144284.

Vivacqua, G. *et al.* (2016) 'Abnormal Salivary Total and Oligomeric Alpha-Synuclein in Parkinson's Disease'. doi: https://doi.org/10.1371/journal.pone.0151156.

Vlaar, T. *et al.* (2018) 'Association of Parkinson's disease with industry sectors: a French nationwide incidence study', *European journal of epidemiology*, 33(11), pp. 1101–1111. doi: https://doi.org/10.1007/S10654-018-0399-3.

Volpicelli-Daley, L.A. *et al.* (2011) 'Exogenous α-synuclein fibrils induce Lewy body pathology leading to synaptic dysfunction and neuron death', *Neuron*, 72(1), pp. 57–71. doi: https://doi.org/10.1016/J.NEURON.2011.08.033.

Volpicelli-Daley, L.A. *et al.* (2016) 'How can rAAV-α-synuclein and the fibril α-synuclein models advance our understanding of Parkinson's disease?', *Journal of Neurochemistry*, pp. 131–155. doi: https://doi.org/10.1111/JNC.13627.

Wagner, J. *et al.* (2013) 'Anle138b: a novel oligomer modulator for disease-modifying therapy of neurodegenerative diseases such as prion and Parkinson's disease', *Acta neuropathologica*, 125(6), pp. 795–813. doi: https://doi.org/10.1007/S00401-013-1114-9.

Wang, Lijuan *et al.* (2015) 'Cerebrospinal fluid alpha-synuclein as a biomarker for Parkinson's disease diagnosis: a systematic review and meta-analysis', *The International journal of neuroscience*, 125(9), pp. 645–654. doi: https://doi.org/10.3109/00207454.2014.961454.

Wang, X., Becker, K., Levine, N., Zhang, M., Lieberman, Andrew P., *et al.* (2019) 'Pathogenic alpha-synuclein aggregates preferentially bind to mitochondria and affect cellular respiration', *Acta neuropathologica communications*, 7(1), p. 41. doi: https://doi.org/10.1186/S40478-019-0696-4/FIGURES/8.

Ward, J.J. *et al.* (2004) 'Prediction and Functional Analysis of Native Disorder in Proteins from the Three Kingdoms of Life', *Journal of Molecular Biology*, 337(3), pp. 635–645. doi: https://doi.org/10.1016/j.jmb.2004.02.002.

Van De Warrenburg, B.P.C. *et al.* (2001) 'Clinical and pathologic abnormalities in a family with parkinsonism and parkin gene mutations', *Neurology*, 56(4), pp. 555–557. doi: https://doi.org/10.1212/WNL.56.4.555.

Wegrzynowicz, M. *et al.* (2019) 'Depopulation of dense α-synuclein aggregates is associated with rescue of dopamine neuron dysfunction and death in a new Parkinson's disease model', *Acta neuropathologica*, 138(4), pp. 575–595. doi: https://doi.org/10.1007/S00401-019-02023-X.

Weihofen, A. *et al.* (2019) 'Development of an aggregate-selective, human-derived α-synuclein antibody BIIB054 that ameliorates disease phenotypes in Parkinson's disease models', *Neurobiology of disease*, 124, pp. 276–288. doi: https://doi.org/10.1016/J.NBD.2018.10.016.

Weinreb, P.H. *et al.* (1996) 'NACP, a protein implicated in Alzheimer's disease and learning, is natively unfolded', *Biochemistry*, 35(43), pp. 13709–13715. doi: https://doi.org/10.1021/BI961799N/ASSET/IMAGES/LARGE/BI961799NF00003.JPEG.

West, A.B. *et al.* (2005) 'Parkinson's disease-associated mutations in leucine-rich repeat kinase 2 augment kinase activity', *Proceedings of the National Academy of Sciences of the United States of America*, 102(46), pp. 16842–16847. doi: https://doi.org/10.1073/PNAS.0507360102.

Whetten-Goldstein, K. *et al.* (1997) 'The burden of Parkinson's disease on society, family, and the individual', *Journal of the American Geriatrics Society*, 45(7), pp. 844–849. doi: https://doi.org/10.1111/J.1532-5415.1997.TB01512.X.

Winner, B. *et al.* (2011) 'In vivo demonstration that α-synuclein oligomers are toxic', *Proceedings of the National Academy of Sciences of the United States of America*, 108(10), pp. 4194–4199. doi: https://doi.org/10.1073/PNAS.1100976108/SUPPL_FILE/PNAS.201100976SI.PDF.

Wong, Y.C. *et al.* (2019) 'Neuronal vulnerability in Parkinson disease: Should the focus be on axons and synaptic terminals?', *Movement Disorders*, 34(10), pp. 1406–1422. doi: https://doi.org/10.1002/MDS.27823.

Wood, S.J. *et al.* (1999) 'Synuclein Fibrillogenesis Is Nucleation- Implications for the pathogenesis of Parkinson's disease'. *Journal of biological chemistry,* 9;274(28), pp. 19509-12. doi: https://doi.org/ 10.1074/jbc.274.28.19509.

Wooten, G.F. *et al.* (2004) 'Are men at greater risk for Parkinson's disease than women?', *Journal of Neurology, Neurosurgery & Psychiatry*, 75(4), pp. 637–639. doi: https://doi.org/10.1136/JNNP.2003.020982.

Xu, C.K. *et al.* (2024) 'α-Synuclein oligomers form by secondary nucleation', *Nature Communications 2024 15:1*, 15(1), pp. 1–11. doi: https://doi.org/10.1038/s41467-024-50692-4.

Xu, Y. *et al.* (2018) 'DNAJC5 facilitates USP19-dependent unconventional secretion of misfolded cytosolic proteins', *Cell Discovery 2018 4:1*, 4(1), pp. 1–18. doi: https://doi.org/10.1038/s41421-018-0012-7.

Xue, W.F. *et al.* (2009) 'Fibril Fragmentation Enhances Amyloid Cytotoxicity', *The Journal of Biological Chemistry*, 284(49), p. 34272. doi: https://doi.org/10.1074/JBC.M109.049809.

Yamaguchi, K.I. *et al.* (2005) 'Seeding-dependent Propagation and Maturation of Amyloid Fibril Conformation', *Journal of Molecular Biology*, 352(4), pp. 952–960. doi: https://doi.org/10.1016/J.JMB.2005.07.061.

Yang, W. *et al.* (2020) 'Current and projected future economic burden of Parkinson's disease in the U.S.', *npj Parkinson's Disease 2020 6:1*, 6(1), pp. 1–9. doi: https://doi.org/10.1038/s41531-020-0117-1.

Zafar, S. and Yaddanapudi, S.S. (2023) 'Parkinson Disease', *StatPearls*, 8, pp. 1–13. https://www.ncbi.nlm.nih.gov/books/NBK470193/

Zarbiv, Y. *et al.* (2014) 'Lysine residues at the first and second KTKEGV repeats mediate α-Synuclein binding to membrane phospholipids', *Neurobiology of disease*, 70, pp. 90–98. doi: https://doi.org/10.1016/J.NBD.2014.05.031.

Zarranz, J.J. *et al.* (2004) 'The new mutation, E46K, of alpha-synuclein causes Parkinson and Lewy body dementia', *Annals of neurology*, 55(2), pp. 164–173. doi: https://doi.org/10.1002/ANA.10795.

Zhang, X. *et al.* (2010) 'Pax6 is a human neuroectoderm cell fate determinant', *Cell stem cell*, 7(1), p. 90. doi: https://doi.org/10.1016/J.STEM.2010.04.017.

Zharikov, A.D. *et al.* (2015) 'ShRNA targeting α-synuclein prevents neurodegeneration in a Parkinson's disease model', *Journal of Clinical Investigation*, 125(7), pp. 2721–2735. doi: https://doi.org/10.1172/JCI64502.

Zheng, W. *et al.* (2019) 'Phosphorylation dependent α-synuclein degradation monitored by in-cell NMR', *Chemical Communications*, 55(75), pp. 11215–11218. doi: https://doi.org/10.1039/C9CC05662A.

Zhou, B. *et al.* (2015) 'The Diagnostic and Differential Diagnosis Utility of Cerebrospinal Fluid alpha-synuclein Levels in Parkinson's Disease: A Meta-Analysis'. *Parkinson's Disease.* doi: https://doi.org/10.1155/2015/567386.

Zhou, J. *et al.* (2020) 'Effects of sedimentation, microgravity, hydrodynamic mixing and air–water interface on α-synuclein amyloid formation', *Chemical Science*, 11(14), pp. 3687–3693. doi: https://doi.org/10.1039/D0SC00281J.

Zimmermann, M.R. *et al.* (2022) 'Mechanism of secondary nucleation from the direct observation of Aβ42 aggregation at the single fibril level', *Biophysical Journal*, 121(3), p. 443a. doi: https://doi.org/10.1016/j.bpj.2021.11.556.

Supplementary Figures

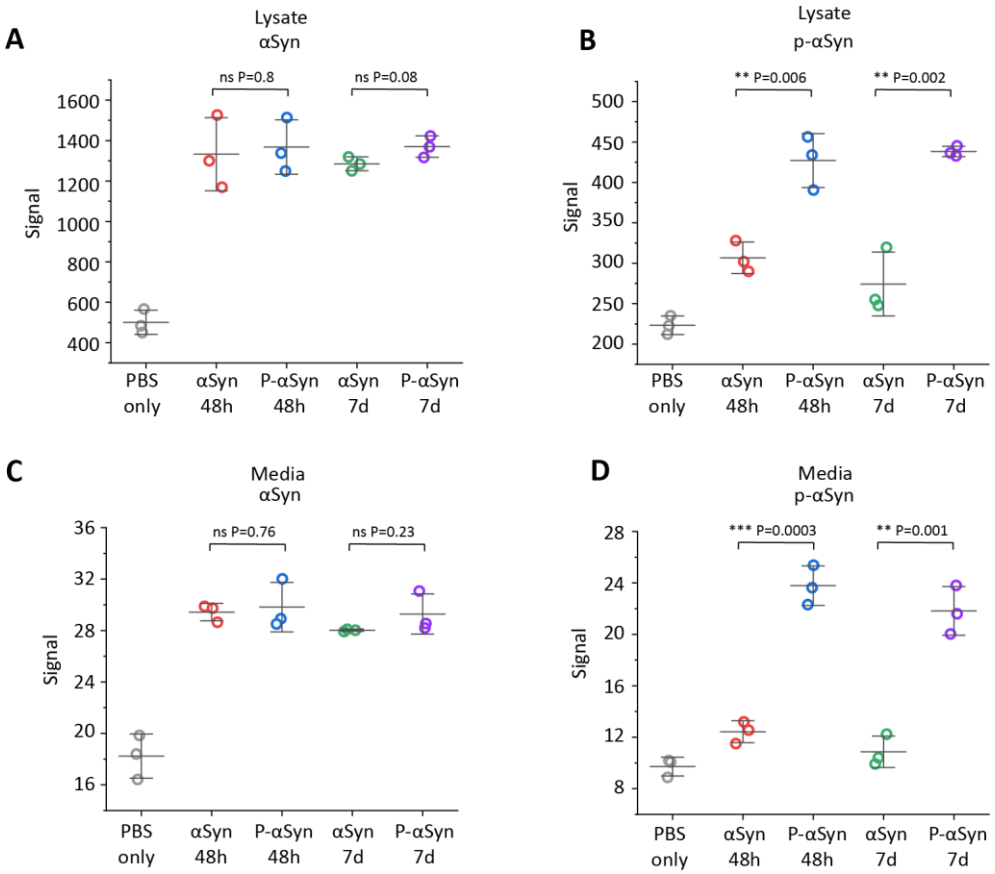

Supplementary Figure 1. MSD-ELISA quantification of αSyn and p-αSyn in lysate and media after seeding. After seeding iDNLs with either PBS, αSyn 48h, p-αSyn 48h, αSyn 7d or p-αSyn 7d, amount of αSyn (A) and p-αSyn (B) in the lysate and αSyn (C) and p-αSyn (D) in the cell media was quantified. Graphs show three biological replicates, bars represent mean ±SD.

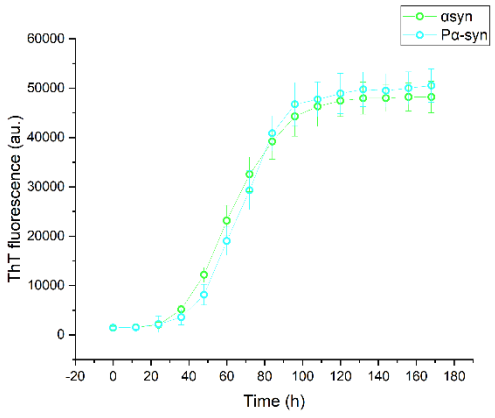

Supplementary Figure 2. In vitro aggregation curve of αSyn and p-αSyn over time. Thioflavin T fluorescence measures the aggregation of monomeric αSyn (green) and p-αSyn over time. Graph shows mean ±SD.